Conversion of Oxygenates over Zeolite Catalysts: Structure-Activity Relations

Holm, Martin Spangsberg

Publication date:
2011

Document Version
Publisher's PDF, also known as Version of record

Conversion of Oxygenates over Zeolite Catalysts: Structure-Activity Relations

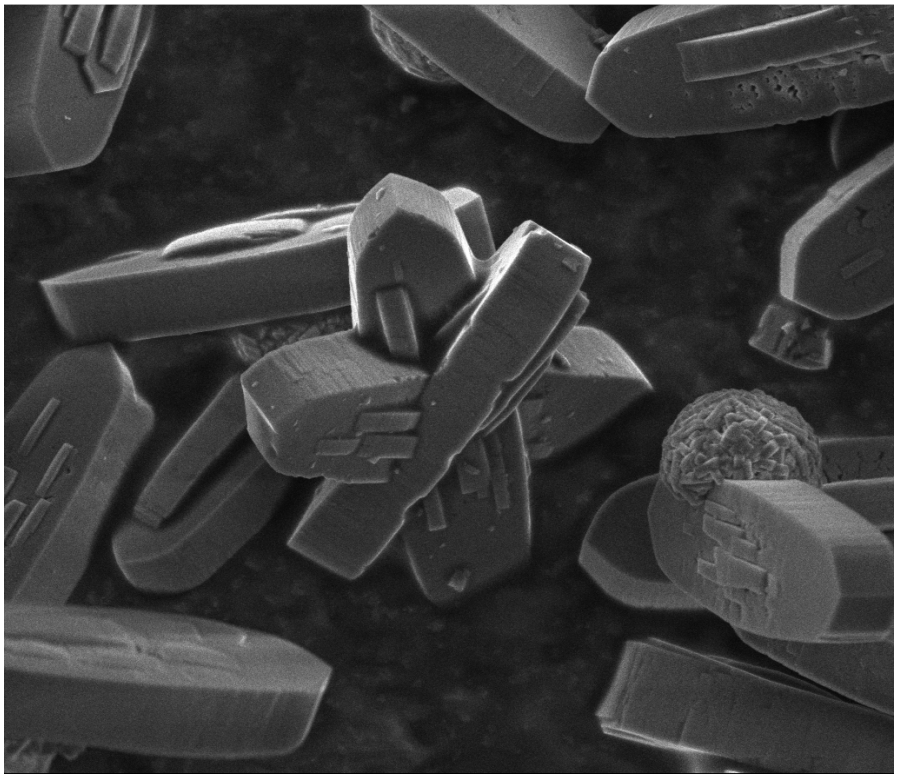

Martin Spangsberg Holm

Ph.D. Thesis
Department of Chemistry
Technical University of Denmark

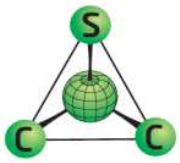

Conversion of Oxygenates over Zeolite Catalysts: Structure-Activity Relations

Martin Spangsberg Holm

February 2011
Ph.D. Thesis
Department of Chemistry
Technical University of Denmark

Danish National Research Foundation´s
Center for Sustainable and Green Chemistry

0.0 Preface

This thesis is submitted in candidacy to the PhD degree from the Technical University of Denmark (DTU). My employment at DTU as a PhD student started in February 2008 under the supervision of Professor Claus Hviid Christensen in the Center for Sustainable and Green Chemistry (CSG). Professor Christensen left DTU in the summer of 2008 and supervision was kindly taken over by Professor Rasmus Fehrmann. My work was therefore finished in the Centre for Catalysis and Sustainable Chemistry (CSC). My PhD study was financed partly by the Danish National Research Foundation, the Department of Chemistry at DTU and Haldor Topsoe A/S. It has undoubtedly been advantageous for my PhD study to be scientifically related to Haldor Topsoe A/S and in particular to senior scientist Finn Joensen.

The results presented here have not been accomplished by me alone. The work was done in collaboration with other students and/or scientists and they are recognized in the list of authors on the respective papers included in the thesis.
It has been a great pleasure to have PhD student Uffe Vie Mentzel as a colleague. Informal but fruitful scientific discussions were possible on a daily basis and planning and execution of scientific work was done in a humorous yet professional manner. The opportunity to work with Esben Taarning was a truly fortunate turn of events. We entered the project with complementary backgrounds and Esben demonstrated an incredible insight into the organic chemistry related to the project and repeatedly generated brilliant ideas.

Martin Spangsberg Holm, February, 2011

0.1 Abstract

English

Zeolites have found application within the petrochemical industry for decades. This thesis explores the possibilities of using zeolite catalysts in the emerging bio-refinery field. For fuels and chemicals derived from renewable resources to be able to compete with fossil counterparts the invention of a vast array of transformation processes are needed. This thesis explores the possibilities of using zeolites as catalysts for biomass utilization.

Mesoporosity in zeolites is important to optimize the catalytic performance and the generation of mesoporous catalysts is a research area of increasing interest. We have investigated to what extent mesoporosity can be controlled and maximized by using base treatment, or desilication, in combination with carbon-templating. In addition, we have introduced a novel protocol in which organic bases are used as an alternative to mineral bases. Interestingly, the introduction of mesoporosity by desilication does not only modify the porosity of the sample but also the acidity. By using FT-IR it was possible to follow these acidity changes as a function of desilication severity.

Converting biomass into a suitable liquid usable in the transportation sector (Biomass-to-Liquid) has long been a goal. Bio-oil can be produced by a short heat treatment of lignocellulosic material. The liquid bio-oil is easier to handle than solid material - but is not suitable as a universal energy carrier. To this end, zeolites have been tested in catalytic deoxygenation of bio-oil with the aim of producing hydrocarbons which can be blended into gasoline, however the zeolite catalyst unfortunately deactivates extremely fast. Bio-oil is a complex mixture of more than 300 compounds and it is thus difficult to identify the specific reason for this deactivation. Therefore, we investigated a series of representative model-compounds to rationalize the reactivity of individual species. In relation to this study, we discovered that higher alcohols are in fact better suited than methanol for the zeolite-catalyzed conversion at methanol-to-gasoline (MTG) -like reaction conditions.

The production of commodity chemicals rather than fuels could represent an economically attractive utilization of the strategic biomass resource. By using Lewis acidic zeolite and zeotype catalysts we were able to convert C_3-sugars into a potential platform chemical, namely lactic acid (methyl lactate). Dealuminated zeolite Y and Sn-Beta (tin incorporated in zeolite Beta) gave near quantitative yield of methyl lactate from C_3-sugars. Sn-Beta further proved applicable in the transformation of hexoses into methyl lactate. A reaction path involving retro aldol- and aldol condensations of the sugars is proposed to rationalize the results.

Dansk

Zeolitter er i årtier blevet anvendt som katalysatorer til rafrinering af fossile ressourcer. Megen forskning bliver på nuværende tidspunkt foretaget inden for udnyttelsen af biomasse, der tiltænkes at kunne skabe et alternativ til fossile brændsler. Denne indsats kan beskrives ved fællesbetegnelsen ”bio-refinery”. Hvis kemikalier og brændstoffer lavet fra biomasse skal være i stand til at konkurrere med de fossile analoger, er det nødvendigt at opbygge et helt arsenal af omdannelsesprocesser, nøjagtigt som det er tilfældet i traditionelle rafinaderier. Denne afhandling undersøger muligheden for at bruge zeolitkatalysatorer indenfor biomasse udnyttelse.

Mesoporøsitet i zeolitter er yderst vigtigt for ydeevnen af en zeolit katalysator og dette videnskabelige felt er i rivende udvikling. Vi har undersøgt i hvilken grad mesoporøsitet kan kontrolleres ved at kombinere basebehandling, desilicering, og kulstof-templating. Endvidere, har vi beskrevet en ny protokol til desilicering af zeolitter hvor organiske baser frem for uorganiske er den aktive agent. Denne nye fremgangsmåde rummer både ulemper og fordele, som vi har forsøgt kortlagt. Det viser sig at desilicering ikke kun skaber mesoporøsitet men samtidigt modificerer surheden af katalysatoren. Studier med FT-IR gjorde det muligt, at følge disse ændringer som funktion af behandlingsstyrken.

Et af de erklærede mål inden for biomasseudnyttelse er at blive i stand til at omdanne biomasse til et flydende brændsel velegnet til anvendelse i transportsektoren. Halm kan ved en kortvarig varmebehandling omdannes til bio-olie. Bio-olie er ikke en anvendelig energibærer, men det er fordelagtigt at transportere denne frem for det faste materiale. En anvendelsesstrategi for bio-olien er at opgradere denne katalytisk ved hjælp af zeolitter. Produktet er forskellige typer af kulbrinter, som teoretisk set kan blandes i konventionel benzin som et ”grønt” tilsætningsstof. Den zeolit-katalyseret omdannelse deaktiverer dog katalysatoren ekstremt hurtigt og fordi bio-olien indeholder mere end 300 forskellige komponenter er det vanskeligt at afgøre, hvilke der er ansvarlige for dette. For at klarlægge problemet har vi derfor konverteret en serie af repræsentative modelmolekyler som er tilsted i bio-olie. I den forbindelse opdagede vi, at højere alkoholer besidder væsentlige fordele sammenlignet med methanol når omdannet ved reaktionsbetingelser brugt for Methanol-to-Gasoline reaktionen.

Brændsler har en forholdsvis lav salgsværdi og det kan derfor være økonomisk attraktivt at omdanne biomassen til kemikalier i stedet. Ved at anvende Lewis sure zeolit-katalysatorer viste vi, at det er muligt at konvertere C_3-sukre til mælkesyrederivater. Mælkesyre er et attraktivt molekyle at skabe fordi det har talrige anvendelsesmuligheder både direkte ved tilsætning i kosmetik, mad og lignende men især gennem videre raffinering. De to katalysatorer dealumineret zeolit Y og Sn-Beta (tin inkorporeret i BEA strukturen) producerede mælkesyre-metyl-ester med høj selektivitet. Videre undersøgelser viste at Sn-Beta tilmed var istand til at katalyserede omdannelsen af C_6-sukre til mælkesyre derivater. Reaktionsveje involverende retro aldol- og aldol kondenseringsreaktioner er foreslået for at rationalisere observationerne.

0.2 Table of contents

0.3 Aim of thesis

The aim of the PhD was to pursue and describe new zeolite modification techniques and find application for zeolites in novel catalytic reactions. Catalysis with zeolites represented the core element of this thesis. My experimental work included zeolite synthesis, characterization and catalytic testing. To individually perform all three aspects was a clear advantage which made it possible to obtain a broad understanding of structure-activity relations within zeolite catalysis.

The thesis is organized into three main sections: One, a general introduction to the relevant subjects. Second, the results divided into three parts. Each of these parts are introduced by a description of the more specifically related literature and our initial thoughts and goals prior to the studies. The results are presented in the form of published papers or manuscripts in preparation. The focus of the individual parts is catalyst modification by desilication (Part 1), bio-gasoline production (Part 2) and lactic acid synthesis (Part 3). The third section is a general discussion of the obtained results supplemented by considerations which did not find their way into the respective papers.

My specific contributions to the individual studies are stated in the authorship declarations in section 4.3.

0.4 Abbreviations

ACI	The accessibility index
DHA	Dihydroxy acetone
DME	Dimethyl ether
DOE	Department of Energy (US)
EFAL	Extra framework aluminum
FT-IR	Fourier transformed infrared spectroscopy
GC-FID	Gas chromatography and a flame ionization detector
GC-MS	Gas chromatography coupled with mass spectrometry
GLA	Glyceraldehyde
HPLC	High performance liquid chromatography
LHSV	Liquid Hourly Space Velocity
MPV	Meerwein-Ponndorf-Verley
MPVO	Meerwein-Ponndorf-Verley reduction and Oppenauer oxidation
MTG	Methanol-to-Gasoline
MTH	Methanol-to-Hydrocarbons
MTO	Methanol-to-Olefins
MTP	Methanol-to-Propylene
PE	Poly ethylene
PET	Poly ethylene terephthalate
PLA	Poly lactic acid
SDA	Structure directing agent
SEM	Scanning electron microscopy
WHSV	Weight hourly space velocity
XRPD	X-Ray powder diffraction

1.0 Introduction and background

1.1 Biomass utilization

Incentives and scope

The incorporation of biomass-derived resources in the supply of energy and chemicals to our modern society has become increasingly important in recent times. Several incentives for biomass utilization exist, with perhaps reduction of CO_2 emissions and the desire for independence of foreign oil import being among the most cited reasons.[1] Interestingly, we are today reviving strategies for biomass utilization which, at least to some extent, have been invented and/or discussed some thirty years ago when the world experienced the previous energy crisis.[2,3,4] Due to decreasing fossil fuels prices compared to biomass derived substrates, such as sugars, the use of biomass was abandoned then. However, the economic balance between fossil resources and biomass is now changing. The tipping economical balance is accompanied by an increased environmental anxiety of the public and renewed political concerns about global warming which altogether results in that utilization of biomass is once again gaining priority. Biomass utilization offers at least a supplementary source of energy and chemicals and can thus relieve the import of fossil resources. One of the advantages of using biomass is that this vast resource is not solely located in specific regions of the world and the implementation strategies can vary depending on local conditions such as weather, demand, wages, soil quality, soil availability as well as local human expertise.

Biomass is currently the only viable non-fossil source for liquid hydrocarbons that can be used as an additive to conventional liquid transportation fuels. One such example produced in large scale is bioethanol which can be obtained through fermentation.[5] The potential for biomass utilization is very large, however the practical implementation is technical complex and politically sensitive due to a number of reasons. The most obvious complication is the potential competition of biofuel production versus food production on the same land, but also protection of biodiversity, soil degradation issues, fluctuating price of fossil fuels as well as the willingness to seriously abate CO_2 emissions no matter the high expense are important issues.[6] The US DOE (Department of Energy) and Department of Agriculture have made an estimate which concludes that more than 1 billion tons/year of lignocellulosic material could be sustainably produced within the US before the mid of this century. This, however, is not enough to meet the fuel requirement and only covers perhaps around 1/3 the need but it could theoretically suffice to replace the fossil compounds used in the production of chemicals.[7,8] Similar studies have been conducted in Europe, they predict that biomass utilization can suffice to meet the current goal of bioenergy introduction by 2030 but biomass resources was considered to be insufficient in covering the total energy demand.[9] While several important assumptions need to be considered when interpreting these numbers the consumption of transportation fuels in itself equals a demand of such a gigantic magnitude that it is difficult to imagine biomass derived fuels to be more than a modest additive.

It is important to consider that fuels are sold mainly based on their energy content and density. This means that it is difficult for oxygenated biomass to compete with the reduced hydrocarbons. The energy content of dry biomass can be compared to other sources by using the boe (barrels of oil energy equivalents) unit - 1 metric ton of dry biomass equals around 3,15 boe.[10] However, if the dry biomass requires multiple complicated conversion steps before it reaches a suitable form usable as

transportation fuel much of this chemical energy will inevitably be lost. Given that chemicals are generally sold on a mass basis this could provide an advantageous strategy for biomass utilization. The production of chemicals which resemble the starting point of biomass with respect to molecular functionalities could perhaps even require fewer processing steps while producing a higher value product.

Composition of biomass

Compared to fossil feedstocks biomass is compositionally very different. Oil is a highly stable, reduced and energy dense substance. Even though it consists of numerous components over time a vast processing industry has been created to separate and catalytically convert the individual components into useful starting materials for further upgrading or isolation of applicable liquids such as gasoline.

The most abundant volume of biomass is lignocellulosic material such as wood or straw. Figure 1.1 shows the structure of cellulose, hemicelluloses, and lignin which are the major components of lignocellulose. Cellulose is a linear polysaccharide of D-glucose. The percentage of cellulose in for example wood differs depending of the specific material but typically makes up around 40%. The abundance of hemicellulose is approximately 30% of the matter. Hemicellulose is a branched amorphous polysaccharide made up of several different sugar monomers mainly the hexoses glucose, galactose and mannose and the pentoses xylose and arabinose. Finally lignin is present in amounts around 25%. Lignin is a polymer that consists of branched phenyl propane units predominantly linked by ether bonds. Additionally, minor amounts of extractable organics and inorganic salts are present in lignocellulose.

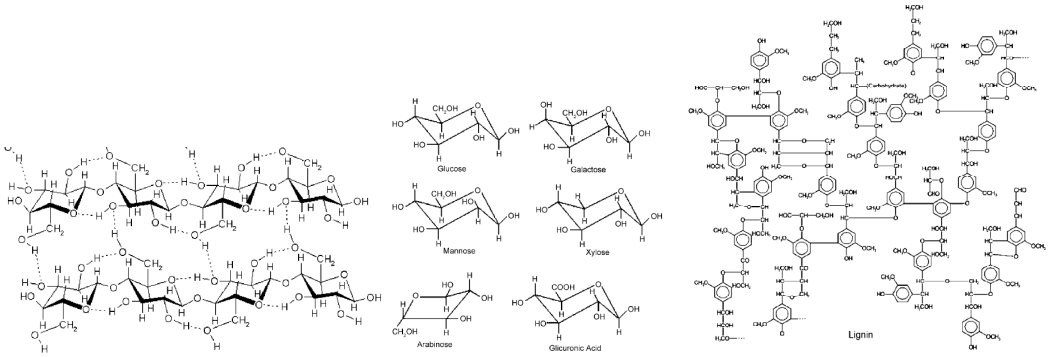

Figure 1.1. Cellulose polysaccharide (left), monomers in hemicellulose (middle) and lignin (right). Reproduced from Ref. 2.

Through mechanical and/or chemical treatment it is possible to roughly separate the individual three major components based on differences in the rate of hydrolysis by steam explosion, base stability etc. thus allowing for the very different components to be utilized through separate dedicated processes.[11] Alternatively crops such as rape, sunflower or sugar cane, and sugar beet can be grown which contain either large amounts of oils or readily available mono- and disaccharides. However, in these cases the risk of utilizing only part of the crop exists while transforming edible fractions into fuels/chemicals. Fast growing energy crops containing only lignocellose are thus projected to be a favored crop for biofuel production.[12]

Biorefinery concept

Much like what is the case for current oil refineries the utilization of biomass will require a dedicated and flexible processing apparatus. In strong contrast to fossil resources biomass is most often highly oxygenated, it has a low energy density and are potentially solid.
The challenges of utilizing biomass can be described through the biorefinery concept. A biorefinery uses mechanical, chemical, or biochemical processes to produce value-added products from a biomass resource and can for illustrative reasons conveniently be divided into phase I to III. A phase I biorefinery is able to convert a single biomass-derived resource or class of compounds into a single main product while a phase II biorefinery will be able to produce multiple products though still from a single source. Finally a phase III biorefinery will be able to utilize multiple resources and simultaneously produce a variety of products which could include fuels, power, chemicals and food products.[13]

The biorefinery-concept brings forward the need to consider whether bulk products such as fuels, commodity chemicals or simply heat and power are optimally produced from a given biomass resource. Since grain, oils, sugar, cellulose or lignin could serve as the starting material numerous strategies could make economical (and chemical) sense. Given the large heterogeneity of biomass derived molecules for example different oxidation levels and functionalizations it is interesting and rather important to discuss where in the value chain biomass derived products could most beneficially be introduced. Undoubtedly, commodity and especially fine chemicals represent high value products in contrast to the simple generation of heat and power through combustion or the production of lower value transportation fuels. Scientific breakthroughs or politically motivated subsidies can change the aim fundamentally. Therefore the invention of a multitude of transformation processes is required in order to be able to utilize the available biomass in a flexible and sensible way.

Direct and indirect "green" substitution

The majority of chemicals, which are used in producing the multitude of everyday tools, clothing, wrappings etc. originate from fossil sources. Interestingly, relatively few molecular building blocks including syngas (CO and H_2), methanol, ethylene, propylene, butadiene, benzene, toluene and xylene make up the common starting materials in the complicated value chain. If biomass aims to substitute the use of fossil resources a key difference will therefore be whether it is transformed into one of the existing basic building blocks or whether new chemicals are targeted.[14] As mentioned, biomass derived compounds generally are highly functionalized and carry little resemblance to the classical fossil building blocks. It is thus important to distinguish between direct and indirect substitution strategies. In a direct strategy biomass is converted into identical chemicals replacing compounds derived from fossil sources whereas an indirect substitution would produce a different chemical which could fulfill the same function as the traditionally fossil derived product. It is clear that both advantages and disadvantages exist when targeting an "old" or alternatively a new platform molecule. If biomass would be converted selectively into for example cumene, a known market already exists including a unit price and therefore the economical potential of the process could be evaluated. It would however also make the production highly vulnerable to price fluctuations of the specific chemical.

Lactic acid as a platform chemical

The term "platform chemical" is used to describe a compound which has a suitable chemistry to allow multiple transformations into numerous useful products. Lactic acid (Figure 1.2) is chosen as an example of a platform molecule since it was a target molecule in the studies presented in part 3 of this thesis. Known transformations of lactic acid include dehydration, decarbonylation, reduction etc.

which form useful products that can be further upgraded or sold in a niche application directly.[15] Besides being subject to chemical conversions, lactic acid is also used as a direct additive in food and cosmetic products and is already produced on a large scale today.[16] In a similar way several other bio derived molecules have been evaluated for potential as platform molecules by the US Department of Energy (DOE).[17] Clearly, the potential of a given molecule is a combination of several aspects including substrate/precursor availability and limitations, the current ease of production, toxicity, upgrading possibilities, and marked evaluations. Both chemical and biological conversions are considered and the comprehensive list of molecules reveals that not a single superior compound stands out as an obvious choice.

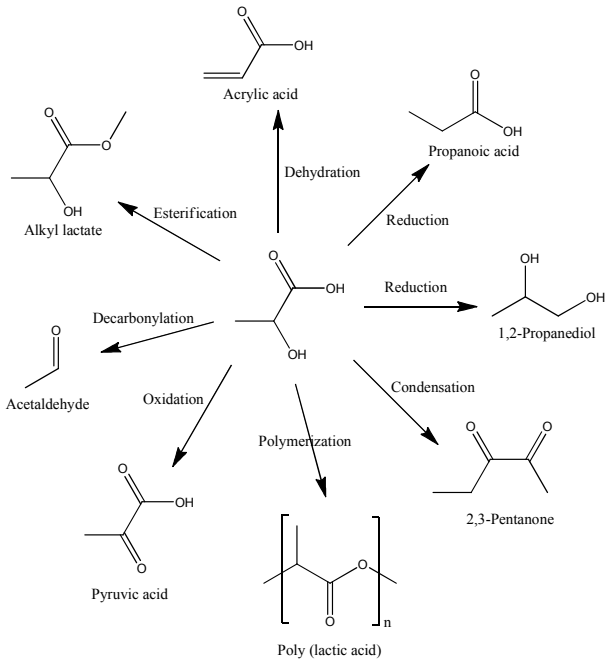

Figure 1.2. Known conversion strategies for lactic acid.

A particularly interesting example of the use of bio-molecules is as monomers for polymerization. As shown in Figure 1.2 lactic acid can be polymerized into PLA (poly lactic acid) which has somewhat similar properties to conventional plastics such as PE (polyethylene) and PET (polyethylene terephthalate). The main advantage which has received significant attention is the fact that PLA is non-toxic and biodegradable.[18] Replacing conventional plastic with PLA can thus serve to minimize current waste disposal problems and PLA has, in fact, been adopted for use in surgical and pharmaceutical applications where the devices are not intended to be removed.[19] This example serves to show that depending on the intended use of PLA products, it can be a superior choice even if it does not outperform conventional products in all property aspects.

1.2 Zeolites

Structure and composition

Zeolites are naturally occurring microporous aluminosilicates made up of tetrahedrally coordinated silicon atoms bridged by oxygen which gives the framework an overall composition of SiO_2. The

organization of the framework forms pores and channels extending throughout the entire crystal giving rise to the microporosity (actually nanoporosity). The number of "approved" zeolite structures approach 200 which shows the great diversity of frameworks that in fact exists. Continuously, new frameworks are being discovered although some of the structures require sophisticated synthesis conditions to crystallize.[20] The zeolite frameworks are conveniently divided into small, medium, and large pore structures with 8, 10 or 12 T-atoms (silicon atoms if pure silicate) in the pore opening. Figure 1.3 shows the framework dimensions of the MFI structure which along with zeolite Beta are the zeolites primarily used in the work presented in this thesis.

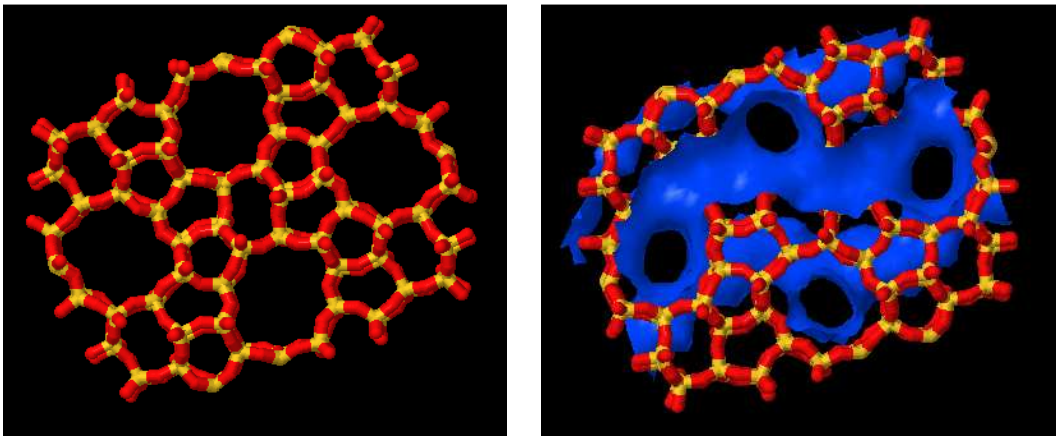

Figure 1.3. Framework of the MFI structure. Pore dimensions (left), channel system highlighted (right). From Ref. 20.

The pore dimensions of zeolites are in the range of small organic molecules typically between 4-8 Å. The pore dimensions thus deny access to the interior of the crystal for molecules with a dynamic diameter larger than this. Therefore it is important to distinguish between externally accessible sites versus internal sites and their relative abundance. Naturally this is determined by the framework structure and the crystal size but typically the majority of T-atoms are present within the crystal e.i. "behind" the microporosity. An example would be a MFI crystal with a size of 1 μm where less than 0.5% of the T-positions are located externally.[21]

Replacement of a silicon atom with trivalent aluminum leads to a charge deficit of the framework which requires compensation by a cation located nearby in the adjacent channel or cavity. If this cation is a proton, the zeolite becomes a strong solid Brønsted acid as schematically shown in Figure 1.4. The strength of the corresponding site depends on the specific zeolite structure.

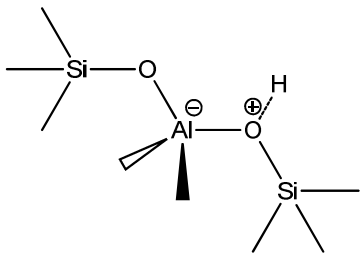

Figure 1.4. Schematic presentation of Brønsted acidity in zeolites.

Due to the fact that the majority of the total surface area is present within the zeolite shape selective catalysis arises since only molecules small enough to enter the zeolite pores will be able to reach the catalytically active site.

Channels need not only to progress in one direction within the zeolite. Structures are in addition to the size of pore openings grouped according to the connectivity of their channels making either 1-, 2- or 3- dimensional networks. As one might expect, a channel system connected 3-dimensionally offers far better molecular transport than a framework of lower order. The channels are not always circularly shaped nor do they necessarily run straight through the crystal (a sinusoidal channel shape in the MFI structure can be seen in Figure 1.3) and various types of channel intersections exist. This forms differently shaped cavities (or nanoreactors) within the structure which are indeed important since steric restrictions within the zeolite can direct selectivity and/or can define the lifetime of the catalyst. The crystallinity of the zeolite makes it possible to define unique atom positions within the repeating framework. It is important whether aluminum preferably incorporates in distinct framework positions since the microenvironment around the site will be different depending on whether a site is located in a channel vs. within a cavity. A remarkable difference thus exists between the various zeolite structures (particularly when applied in catalysis) and it is hard to predict specific reactivity, diffusivity, and adsorption behavior of the individual structures.

Application

Zeolites have found application within several areas due to their high temperature stability, molecular sieving property, adsorption affinity, ion-exchange ability or the strong acidity of the solid material.[22] Depending on the hydrophobicity/hydrophilicity of the zeolite framework drying or purification by for example moisture adsorption or removal of organics by selective adsorption can be done. Per volume, zeolites are mostly used in non-catalytic applications such as laundry detergent; but if considering marked values the catalytic applications are the most important.[23]. Zeolites constitute the backbone of hydrocarbon conversion in oil refineries where major application of especially zeolite Y (FAU structure) include FCC (fluid catalytic cracking) and hydrocracking of heavy oil fractions.[24,25] Although the application of zeolites is predominant within the petrochemical industry new areas are emerging where zeolites are used to study broad aspects of science as cell-adhesion behavior[26], drug delivery[27] and as hosts for dyes in light harvesting[28].

Zeolite synthesis

Synthetic zeolites are typically synthesized under hydrothermal conditions i.e. in an aqueous solution at high temperature and pressures. Sources of silicon and aluminum are dissolved or suspended in water along with a structure directing agent (SDA) and an alkali hydroxide is added as a mineralizer to catalyze the breaking and formation of T-O-T bonds. The homogenized zeolite gel is transferred to an autoclave as presented in Figure 1.5. The gel is heated and the zeolite crystallizes from the amorphous substrates typically within days. Frequently, the zeolite product is metastable under the synthesis conditions which means that the nature of the specific product is kinetically controlled. This is the reason why *exact* synthesis conditions need to be monitored/reported since slight variations can lead to the co-formation of an additional zeolitic phase or simply lead to synthesis failure. Indeed the synthesis of a particular zeolite can include the initial formation of (traces of) a different phase. Alternatively, if the synthesis is not stopped timely (over-run) the zeolite product may transform into a denser phase such as quartz.

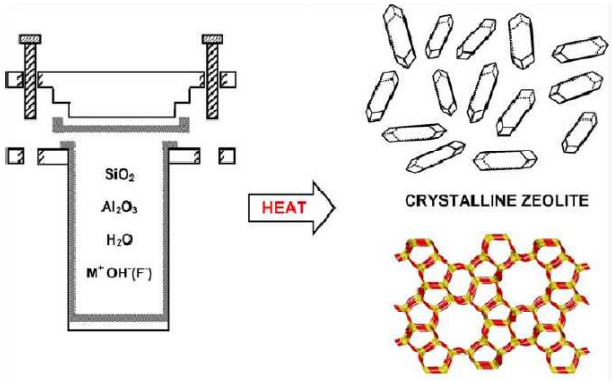

Figure 1.5. Schematic presentation of hydrothermal zeolite synthesis. Figure from Ref. 29.

The crystallization can be divided into several stages first an induction period; where substrates mix, reorganize and/or dissolution takes place but still no crystalline material can yet be detected. Second the nucleation; here precursor species organize into simple ordered structures that form countless seeds within the gel. Third the growth period, here the zeolite structure increases in size by polymerization condensation reactions that occur on the surface of the seeds. The crystal growth phase continues until all of the amorphous materials are transformed into the crystalline zeolite structure. The division into these three phases is presented in Figure 1.6. Here it can be seen that the initial gel can dissolve and re-precipitate as an equilibrated gel that contains local order directed by the organic SDA cation but lacks the long range ordering of the zeolite framework. Leaving the homogenized gel for a given period of time at a temperature below crystallization temperature is called ageing of the gel. Ageing can have a pronounced effect on the final product. From the assumption that the crystal growth rate is equal for all crystals at all times; the final average crystal size will be dictated by the number of nucleation events. Ageing the gel forming what is described as the equilibrated gel in Figure 1.6 would then be expected to increase the number of nucleations and thus lead to a larger number of smaller crystals.

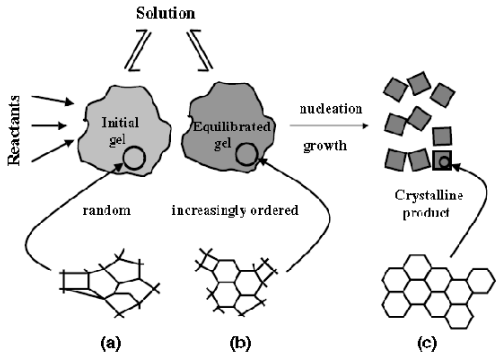

Figure 1.6. Schematic presentation of the course of zeolite synthesis. Figure from Ref. 29.

Seeding is another common trick which has been used intensively in the synthesis of the catalysts used in this thesis. The aim of seeding is to circumvent the primary nucleation and make crystals grow directly by condensation polymerization on the seeds surfaces. Several fates can undergo seeds when added to a synthesis gel. This include inertness (if the seeds become surface passivated), total dissolution, fragmentation into siliceous building blocks or finally seeding by growth. Typically relatively large amounts of seeds are used perhaps 5 wt.% (based on silicon) simply to see an effect.

In conclusion, if seeding occurs according to the aim the particular structure can have a kinetic advantage which minimizes "contamination" by other phases and the crystallization time required.
The mineralizer most commonly used is the hydroxide ion thus dictating that synthesis is conducted at high pH. Interestingly, also the fluoride ion has been proven suitable though typically larger crystals are formed through the fluoride route. Crystallizing zeolites at neutral or slightly acidic conditions is useful to incorporate hetero atoms which would otherwise form insoluble precipitates at high pH values. Flouride mediated synthesis (near) neutral pH has specifically been the case for synthesis of Sn-Beta[30,31,32] although examples of hydroxide mediated synthesis of Sn-MFI[33,34], Sn-MTW[35] and Sn-MEL[36] have been published.

1.3 Desilication

Diffusion in zeolites

For decades diffusivity or mass transport in zeolite catalysts has been the subject of research since it profoundly affects the applicability of the materials.[37,38] The close resemblance in size of a reactant/adsorbant and the zeolite channels can induce strong restrictions in intracrystalline mass transport typically beyond what could be predicted based on temperature and concentration gradients. For this reason, the rates of diffusion within a zeolite crystal can be orders of magnitude lower than molecular or Knudsen diffusion and are commonly denoted configurational diffusion.[39] Further, diffusivity of straight chain molecules deviate compared to their branched isomer again depending on the specific channel size and shape. Additional restraints in diffusion within a zeolite can be cases where two molecules are unable to pass each other within a channel ("single-file" diffusion) which limits the overall molecular progression.[40] Interestingly, the restricted diffusion can be used as an advantage. This can be exemplified by the selectivity obtained from toluene disproportionation over zeolite ZSM-5 that forms benzene and xylene. Of the three isomers *p*-xylene is the desired product and since *p*-xylene has the highest diffusion rate within the zeolite an increase in crystal size increases the selectivity towards this product. In this way diffusion rates rather than the thermodynamic equilibrium controls selectivity.[41] Strong restrictions in mass transport can negatively affect catalytic application of the zeolite catalyst. This leads to the outer most shell is the only part of the crystal that is effectively utilized as illustrated in Figure 1.7 by an increasing Thiele modulus.

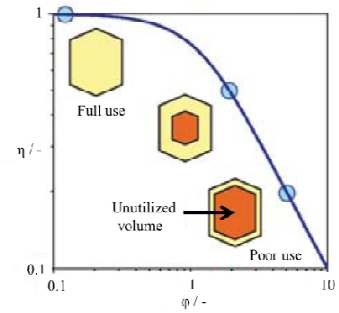

Figure 1.7. Decreasing utilization of a zeolite crystal as a function of an increasing Thiele modulus. Adapted from Ref. 42.

However, the unique selectivity of zeolites is often caused by the narrow pore dimensions. Consequently, it is not desirable to completely diminish the shape selectivity. As described in detail in the review in section 2.5 a compromise that relieves the diffusion restrains while maintaining shape selectivity are often sought. Interestingly, Ryoo and co-workers have recently developed a synthesis

procedure that forms zeolite nanosheets with a thickness of only approximately 1 unit cell. This likely will show very little steric hindrance and could thus open entirely new fields of application or act as an ideal reference since it has no (or marginal) intracrystalline diffusion limitations.[43] Nevertheless a potent approach when trying to find a balance between full utilization of the crystal volume while still maintaining satisfactory selectivity is the introduction of mesoporosity into the individual crystals.

Mesoporosity and zeolites

Figure 1.8 gives a schematic presentation of a multilevel porosity which can be integrated into zeolites. Mesopores are defined as pores with a diameter between 2-50 nm. and pores larger than 50 nm. are called macropores. Figure 1.8 shows how the inherent microporosity of the zeolite can be supplemented by additional auxiliary pore systems. The preparation of mesoporous zeolites are done through a variety of strategies best described as top-down or bottom-up approaches. These either manipulate the crystallization process (top-down) or treat the crystals after synthesis has terminated (bottom-up). Two widely known examples of the above are carbon-templating of the crystals e.g. letting the material crystallize occluded within a porous matrix or performing a demetalization treatment e.g. dealumination of the crystals post synthesis.[42]

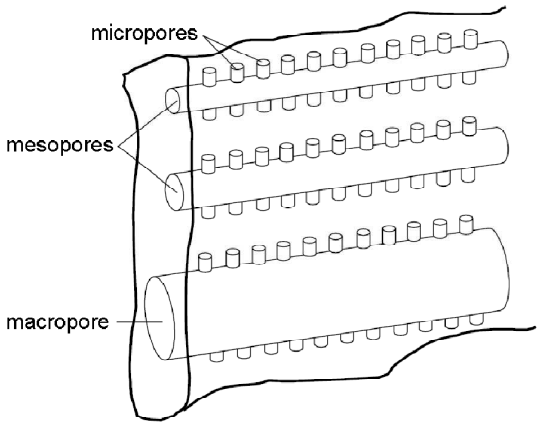

Figure 1.8. Schematic presentation of the various levels of porosity in a zeolite. Figure from Ref. 39,44.

In section 2.5 numerous examples reporting an improved catalytic performance with respect to selectivity, activity, lifetime, and/or stability of mesoporous zeolites have been reviewed. The beneficial effect arises from improved mass transport through the auxiliary pore system while simultaneously creating additional pore openings and thereby shortening the effective diffusion path length.[42,45]

Mesoporous zeolites are used in industry today. Probably the prime example is dealuminated Y zeolite forming USY (Ultra Stable Y) which is a workhorse in the petrochemical industry used for cracking large hydrocarbons into the gasoline range. However, also dealumination of mordenite has been studied extensively. During dealumination, aluminium is extracted from the zeolite framework and as a result a new level of porosity appears in the individual crystals. Since each aluminium atom incorporated into the framework gives rise to an acidic site, dealumination will not only lead to the introduction of porosity but also inevitably modifies the acidity of the sample.

Structures and desilication agents

Desilication i.e. base treatment is a post synthesis treatment able to form mesoporosity in zeolites. Early examples of "base treatment" of zeolites exist in literature[46,47,48] but within the last decade or so greater attention has been dedicated to this post-treatment. This interest correlates with promising results showing significant beneficial catalytic improvements of desilicated samples.[49] Yet another attractive thing about desilication is the relative ease with which the treatment can be performed i.e. submersion of the zeolite into dilute sodium hydroxide at moderate temperatures. The simplicity of the treatment along with promising results could pave the road for industrial use of desilciation when compared to many other complex and expensive preparation routes. In effect, silicon is selectively dissolved from the zeolite crystal leading to the formation of an auxiliary mesoporous network within the individual crystals. Figure 1.9 gives a recent example of high resolution STEM (scanning transmission electron microscopy) analysis of mesopores formed in ZSM-5 by desilication. Impressively, the mesopores within the crystals can be clearly seen. But why does the dissolution process form beautiful mesopores instead of simple random crystal degradation?

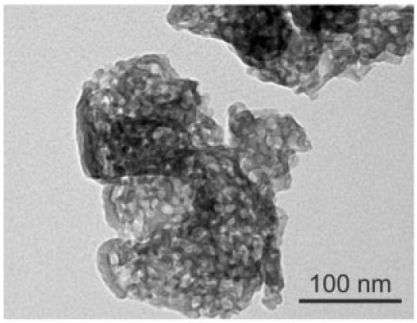

Figure 1.9. High resolution STEM image of mesoporosity in ZSM-5 obtained by desilication. Figure from Ref. 50.

Aluminium incorporated into the framework carries a negative charge and is therefore believed to direct the desilication process through charge repulsion of the hydroxide ion.[51] Consequently, the amount of aluminium present in the zeolite framework is critically important to evaluate the feasibility of desilciation.[52] It has been observed that at low Si/Al ratios only very modest desilication occurrs whereas in highly silicious zeolites a pronounced dissolution takes place. A window for optimal desilication for ZSM-5 could thus be defined within Si/Al ratios between 25 and 50.[51] This indicates that the rate of hydrolyzation of Si-O bond in the proximity of aluminum is reduced. Alternatively, since hydroxide is (most commonly) used as mineralizer in zeolite synthesis and desilication conditions actually resemble synthesis conditions i.e. a hot, basic aqueous media this could allow for reincorporation of aluminium.[51]

Several zeolite structures e.g. MFI[53,54], BEA[55,56], MTW[57,58], MEL[59], FER[60,61], MOR[60,62],CHA[63] and even 0-dimensional octadecasil[64] can be desilicated using quite similar treatment conditions. Bases other than sodium hydroxide have also been tested and showed that LiOH and KOH are potent for desilciation but NH_4OH and hydrofluoric acid lead to poor pore formation or non-selective dissolution, respectively.[65] Several examples are known that apply sodium carbonate in desilcation while also organic bases have been investigated[66,67,50] including the results presented in section 2.4.[68] One would suspect that isomorphous substitution of silicon with other trivalent elements capable of producing Brønsted acidity in zeolites e.g. Ga^{+3}, Fe^{+3} or B^{3+} would have similar attributes as aluminium. To some extend this appears to be the case.[69]

By increasing the base concentration while keeping the volume and mass of treated zeolite constant one can produce zeolites with increasing mesoporosity. Such a sample series is very interesting to study in catalysis in order to isolate the catalytic effect of porosity. Further this approach allows for potential side effects (formation of extra framework aluminium, crystal collapse etc.) to be characterized systematically. Not surprisingly the desilication treatment can be performed too harshly. This is typically seen as a decrease in crystallinity of the treated sample or through low yields of recovered zeolite post treatment. Indeed a relatively large amount (≥25%) of the zeolite is commonly dissolved even in a careful desilication. This should be considered when thinking about applicability of desilication.[66,70] However, since amorphous silica dissolves before crystalline material this could account for some of the mass loss and could improve sample quality (and hence catalytic performance) without the formation of mesoporosity. Additionally, most reports compare newly prepared mesoporous material to reference samples based on sample weight. A mesoporous sample is likely to take up a larger reactor volume compared to a conventional dense sample. This could to some extend negate parts of the improved performance if reactor volume is the limiting factor rather than catalyst weight.

1.4 The Methanol-to-Hydrocarbons reaction

Discovery of the Methanol-to-Gasoline process

The methanol-to-gasoline (MTG) reaction was discovered by serendipity in the 1970's and published in 1976-77 by researchers employed at Mobil Oil.[71,72] The process is able to form long chain hydrocarbons from a single carbon source, namely methanol. This route has received substantial interest for the production of a synthetic fuel since it the only alternative to Fischer-Tropsch diesel. Interestingly, the array of products obtained from MTG includes practically all possible isomers of the C_1-C_{10} hydrocarbons. The shape selectivity of the MFI structure is the reason for the relatively sharp cut off in products at 10 carbon atoms. Conveniently, this product range correlates closely with what is used as conventional gasoline. Steam reforming of natural gas or gasification of coal can produce synthesis gas (CO and H_2) which among numerous applications can be used to synthesize methanol. The MTG process, including a methanol synthesis step from syn gas, was chosen over Fischer-Tropsch diesel synthesis for exploitation of vast off shore natural gas resources in New Zealand approximately 30 years ago. A production facility that supplied approximately one third of the gasoline need for the country was thus operating in the mid-1980s. It was eventually taken offline when the oil prices declined after the oil crisis.[73] Gasoline is not produced by MTG technology today but by modifying the catalyst and the process conditions the selectivity in methanol conversion can be pushed towards olefins which has led to the commercial processes MTO (Methanol-to-Olefins) and MTP (Methanol-to-Propylene) operated by UOP/Hydro and Lurgi, respectively.[74,75]

Today, the once again rising oil prices has sparked enhanced interest in the family of methanol conversion processes partly because it can be implemented in a "clean" Coal-to-Liquid strategy where biomass could potentially be co-gasified. However, particularly the production of gasoline is problematic since the percentage of aromatic compounds inevitably present in MTG derived gasoline is rather high compared to current health regulations.[76] However, this does not mean that MTG products could not act as a "green" or "domestic" component added to conventional gasoline in the future.[77]

Process overview

The MTH process is comprised of multiple reaction steps including alkylation, oligomerization, aromatization, isomerization, and cracking of the hydrocarbon products all catalyzed by strong Brønsted acidic sites in the zeolite catalyst. Figure 1.10 provides a simplified overview of the selectivity of the process starting with the dehydration of methanol to dimethyl ether (DME) and water.

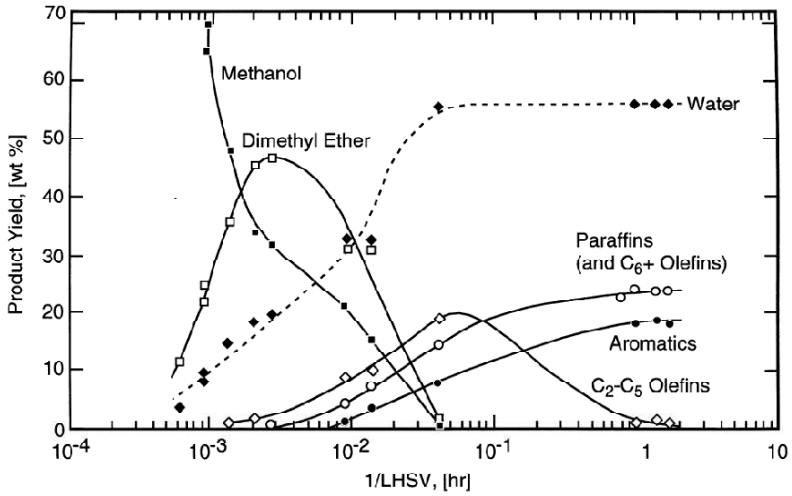

Figure 1.10. Product selectivity as a function of the reciprocal liquid hourly space velocity (LHSV) (space time). Figure from Ref. 73.

Analyzing Figure 1.10 from left to right (left corresponding to large and right to low feed rates) it can be inferred that initially the acidic zeolite catalyzes the methanol-DME equilibrium and at prolonged contact times olefins start to form. A further increase of the catalyst to methanol ratio leads to the production of paraffins and aromatics at the expense of the olefins. Importantly, no reaction conditions exist where full conversion of methanol/DME is obtained and solely olefins are formed showing that aromatic compounds are inevitably formed.

The key reaction step in the MTH process is the coupling of the C_1 specie (methanol) to higher hydrocarbons thus forming new C-C bonds. The mechanism has been intensively discussed in the literature but general consensus now exists that the methanol incorporation proceeds through a "Hydrocarbon Pool Mechanism". An early presentation of this mechanism is given in Figure 1.11 as published by Dahl et al. They suggested that methanol was added to existing hydrocarbon species present in the zeolite and therefore ruling out (or at least marginalizing) direct methanol-methanol C-C bond forming.[78]

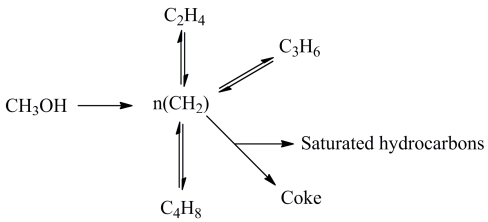

Figure 1.11. Early schematic presentation of the hydrocarbon pool mechanism. Adapted from Ref. 78.

Later an elegant way of extending the mechanism; "the dual cycle concept" was proposed by Bjørgen et al.[79] The aromatic hydrocarbon pool species present within the zeolite are able to split off small olefins after being alkylated by methanol. Olefins are also formed by chain prolongation of a short olefin followed by cracking. From isotopic labeling studies Bjørgen et al. observed a very close similarity in ^{13}C content between ethene and the aromatics which lead them to suggest the grouping of the reactions into the two catalytic cycles presented in Figure 1.12.

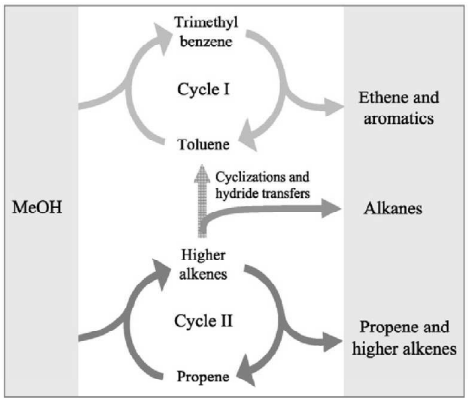

Figure 1.12. Methanol incorporation explained through the dual cycle concept. Figure from Ref. 79.

Figure 1.12 shows the two cycles in which methanol alkylates either aromatic methyl benzenes producing poly methyl benzene or alternatively olefins which prolong the carbon chain. The alkylated benzenes dissociate predominantly ethene (and depending on the reaction conditions propene) whereas the higher olefins crack into two shorter (non-ethene) olefins. Since aromatic compounds are a significant product of the reaction the aromatic molecules that escape the zeolite are replenished through cyclization and aromatization of the olefins while simultaneously forming paraffins.

Catalyst deactivation

The zeolite catalyst deactivates through gradual carbon deposition (coking) eventually blocking access of the reactants to the acidic sites. Figure 1.13 presents a working MTG catalyst operated in plug flow mode with the reactant entering at the left and products exiting to the right.

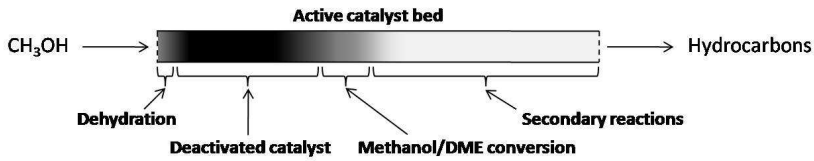

Figure 1.13. Schematic presentation of a working ZSM-5 catalyst during methanol conversion. Reproduced from Ref. 80.

The catalyst shown in Figure 1.13 resembles a visual inspection of a ZSM-5 catalyst stopped approximately halfway into deactivation. At the top of the catalyst bed (left) methanol is dehydrated and further down a deactivated black (coked) zone is building. The lower gray part of the catalyst is responsible for secondary reactions. As a function of time the methanol conversion front progresses through the catalyst bed directly below the deactivated zone. This deactivation profile can be compared to a gradual loss of catalytic material which results in a selective change from an initial production of relatively high amounts of paraffinic and aromatic compounds and gradually shifting towards an increased olefin yield. The deactivated zeolite can be regenerated by combustion of the

deposited carbon typically done in a flow of air at temperatures above ~450 °C. Regenerating the catalyst leads to recovery of the initial activity although numerous conversion-regeneration cycles of the catalyst eventually leads to irreversible dealumination of the zeolite i.e. a depletion of the catalytically active acidic sites.[81]

1.5 Experimental

XRPD

X-ray diffraction on zeolites is a convenient tool to identify a zeolite structure and ensure phase purity. More complex applications such as deriving models of unknown frameworks based on a diffraction pattern can also be performed. This makes X-ray diffraction a key analytical technique within zeolite science.

Diffraction occurs when an incident radiation interacts with an ordered solid and the wavelength of the electron magnetic radiation (or electrons, neutrons) is in the same order as the distance between the crystal planes *d*. Most often, the zeolite is analyzed in the form of a powder and the obtained powder X-ray diffractogram can be used as a "fingerprint" unique to the particular crystalline phase.

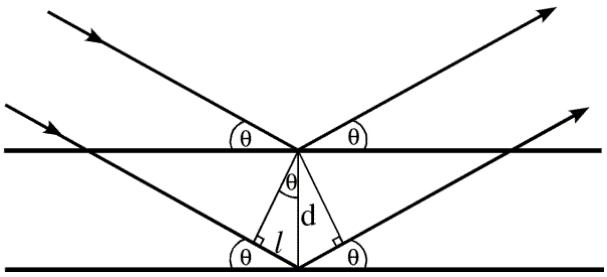

Figure 1.14. Schematic presentation of diffraction in a solid having a lattice spacing *d*.

Braggs law shows that constructive interference will only happen if the extra distance traveled by the lower incoming beam equals an integer of the wavelength. Figure 1.14 gives this distance as two times *l* which can be rewritten into 2*d* sinθ.

$$n\lambda = 2d \sin\theta$$

Different distances (*d* values) belong to the individual lattice planes and thus each planes will give a characteristic deflection. In the case of a zeolite powder countless orientations of the individual crystals are present and give rise to diffraction rings. The well-known powder diffractograms are obtained as a slice of the ring plotted as the distance from the center and out (2θ) versus the intensity. Evidently, the position of the diffractions gives information regarding size and shape of the unit cell while the diffraction intensity is derived from the specific atom and its location within the unit cell.[82]

N_2-sorption

A key parameter for any catalyst is the surface area accessible for reactants. A conventional way of measuring this is by low temperature (77 K) adsorption of N_2. This technique is based on stepwise adsorption of N_2 initially building a submono layer - as the N_2 pressure above the sample increases multilayer formation begins. Since the desorption energy of nitrogen desorbing from the surface vs. nitrogen desorbing from a multilayer is different it is possible to derive at which point a monolayer is

reached. By exploiting that each nitrogen molecule occupies 0.16 nm^2, the surface area of the catalyst can be calculated. However, capillary condensation can complicate the picture since as soon as this occurs a pore volume rather than the surface area is measured.[83]
For dedicated literature describing gas adsorption in micro- and mesoporous zeolites the reader is referred to expert literature.[84]

Scanning electron microscopy (SEM)

SEM is an analytical technique exploiting the physical events that occur when a beam of electrons is directed onto a specimen. Figure 1.15 schematically shows the various phenomena.

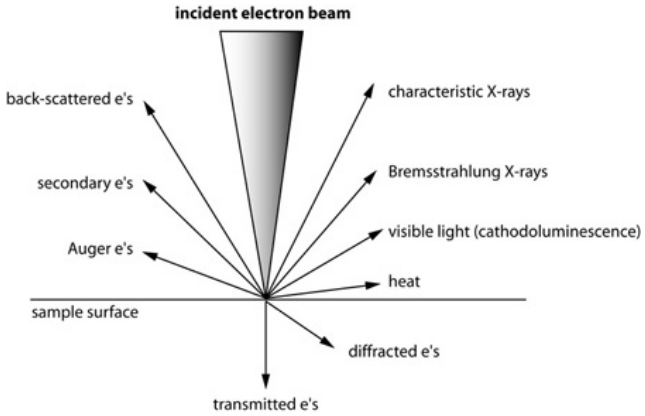

Figure 1.15. High energy electron beam hitting a surface and inducing several phenomena. Figure from Ref. 85.

A typical SEM micrograph of a sample can be obtained by systematically scanning the surface with a focused e-beam accelerated to 5-20 KeV. A micrograph can be obtained by simultaneously detecting the produced secondary or backscattered electrons. The two images obtained are not identical since secondary electrons have such a low energy (perhaps 10-50 eV.) that they are only able to escape the top layer of the sample while backscattered electrons with higher energy can come from further within the material. However, the low escape depth is ideal in order to map surface morphology of a sample.[86] Further, depending on the acceleration voltage of the incident electron beam the interaction volume and thus the volume from which electrons can originate will increase. A Monte Carlo simulation showing this is presented in Figure 1.16.

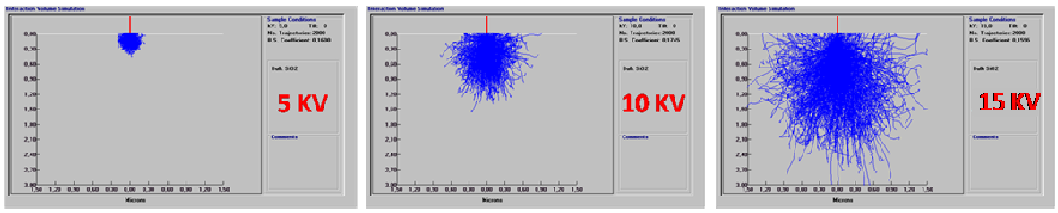

Figure 1.16. Monte Carlo simulations of high energy electrons interaction with bulk SiO_2. Note that the scale on Y-axis is identical in the three examples.

Clearly if high resolution SEM is desired electrons accelerated to the lowest possible level should be applied.

Characteristic X-rays and Auger electrons produced upon impact can be used to obtain information about the elemental composition of the sample. By using high electron energy (100-200 KeV) and thin specimens the electrons can penetrate the sample and thus operate in transmission mode i.e. move into the vast field of TEM (transmission electron microscopy).
Since an electron beam bombards the sample local surface charging can be a problem and for zeolites a conductive coating of for example carbon is required to obtain good SEM images.

NH_3-temperature programmed desorption

Temperature programmed desorption of ammonia is a standard procedure to characterize the acidity of zeolites. The principle behind the analysis is based on the strong acid-base adsorption in-between ammonia and the acidic sites of the zeolite (assuming that the zeolite is in its proton form). If an ammonia saturated sample is gradually heated; ammonia will desorb at a temperature dictated by the strength of the acidic site. If physisorbed ammonia is removed prior to heating the quantity of acidic sites in the sample can be evaluated by assuming that exactly one molecule will desorb from each acidic site.
The analysis is composed of three steps. Initially adsorbed species (water, hydrocarbons from the air etc.) in the zeolite are removed in a flow of inert gas at elevated temperature. Next the zeolite is saturated with ammonia and loosely bound ammonia is removed by keeping the sample at for example 100 °C for 2 hours. The analysis itself is initiated by applying a heating ramp which in our case typically was 10 °C/min. Meanwhile the ammonia is quantified as it desorbs. Quantification is conveniently done by a thermal conductivity detector (TCD) but desorbed ammonia could also be collected and titrated.
Ammonia does not discriminate between Lewis and Brønsted acidity and usually the resolution of the bands are relatively poor likely due to re-adsorption and transport phenomena within the sample. NH_3-TPD however, is an excellent tool to quantify the total acidity of zeolites. The data can then be supplemented by information from other complementary characterization technique such as FT-IR that can provide a Brønsted/Lewis ratio of the total acidity.

FT-IR

Infrared spectroscopy exploits the electromagnetic radiation (see Figure 1.17) where the energy is sufficient to excite vibrational states of chemical bonds. Bonds that have a dipole moment that can change over time absorb infrared radiation in a quantized process. This means that a particular bond will give rise to only absorptions that match their respective stretching or bending modes of vibration. Infrared spectroscopy is a powerful characterization tool to obtain direct information about the acidity of zeolites. The analysis can be performed in transmission mode where the zeolite is pressed into a self-supporting wafer and the radiation is directed perpendicular to the sample with the detector directly behind. Water and organics from the atmosphere are always adsorbed in the zeolite meaning that the analysis needs to be performed in vacuum (or dried in a flow of inert gas) for the zeolite surface and catalytic sites to be vacant. If this is the case silanol and bridging hydroxyl groups are seen as isolated bands in the 3000-3800 cm^{-1} region while framework Si-O vibrations are located at lower wavenumbers of typically 600-1200 cm^{-1}. The specific absorption frequencies of the bridging hydroxyls cannot be used to derive information about the acid strength of the sites - for this probe molecules are needed. By allowing a probe molecule to coordinate to a site the acid strength can be indirectly found as the magnitude of the frequency shift in the probe vibration. If the probe molecule is dosed (or desorbed) gradually the affinities towards the individual sites can also be identified.

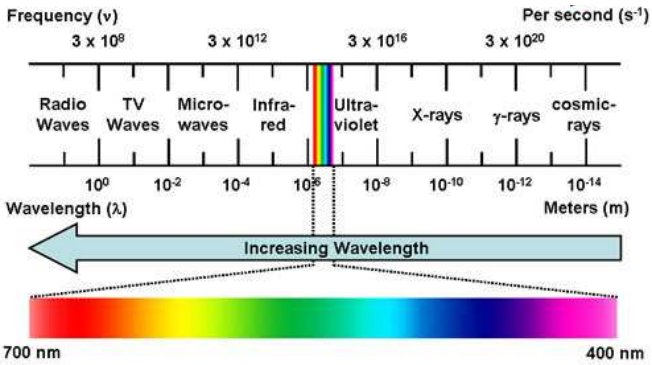

Figure 1.17. Overview of the grouping of electromagnetic radiation. Figure from Ref. 87.

The detection (strength as well as presence) of Lewis acidity in a zeolite sample is done in a similar way since these sites have on visible bonds. Conveniently, coordination of a probe to a Lewis or Brønsted acidic site induces a characteristic band which makes it possible to derive qualitative information about the sample. By knowing the respective extinction coefficients of these dedicated bands it is possible to calculate a Lewis/Brønsted ratio of the acidity in the sample. Quantification of the acidity in zeolite samples (given as mmol/$g_{zeolite}$) is rather difficult but it is however possible by careful experimentation. Naturally, various probe molecules can be used depending on the functionality under investigation. In the case of characterizing Sn-Beta samples cyclohexanone proved suitable[88] but otherwise pyridine or CO are good choices with a large literature describing thorough experiments.

GC-FID and GC-MS

Gas chromatography (GC) was used in almost all aspect of the work presented within this thesis. Gas chromatography separates compounds based on their volatility and retention in a capillary column while a gas serves as the mobile phase. When dealing with small organic reactant and products; gas chromatography is nicely suited for quantification (GC-FID) and identification (GC-MS) but other equipment combinations such as GC-FTIR could serve the same purpose. The detection of the individual compounds eluting are done by combustion in a hydrogen flame in the FID (flame ionization detector) or by electron ionization followed by mass spectrometric analysis in the MS unit. The signal in the FID arises from the ions produced during analyte combustion and hence inorganic compounds will give (almost) no signal. Individual compounds have a unique response factor meaning that a dedicated calibration curve for each is in principle required. High contents of oxygen will lower the sensitivity in the FID but for hydrocarbons the response can be assumed proportional to the carbon content. Compound identification by GC-MS is based on the fragmentation pattern of the molecule after electron ionization. The molecule will undergo characteristic uni-molecular decomposition reaction and the instrument is able to detect the resulting positively charged species. By comparing the "fingerprint" fragmentation pattern to a vast library of known compounds likely molecular structures are identified. This library search is possible because the fragmentation patterns are surprisingly similar independent of variations in-between instruments and laboratory practice. If the molecule is commercially available the gas chromatographic retention time can support the qualified "guess" made from a library search.[89]

HPLC

High Performance Liquid Chromatography is a complementary technique to gas chromatography. The separation principle is similar; expect the mobile phase is liquid in HPLC. The sample is injected into the mobile carrier and separation is based upon selective interaction/retention with a solid column material. HPLC is obviously well suited for analytes which are non-volatile or heat sensitive but columns functionalized with materials ranging from C_{18}-chains to acid functionalities exist and are able to separate almost any analyte. Detection of analytes can be done with a variety of detectors and often HPLC systems are equipped with more than one. Detectors can be designed to complement the weakness of the other or serve as quantification and identification when combined. Common examples for liquid chromatographic systems include UV-VIS, fluorescence, refractive index, electrochemical detection, or an interface to MS. Liquid chromatography can also be operated in preparative scale when the intention is not qualitative sampling but rather complete separation of compounds present in a reaction mixture.

1.6 References

[1] http://tpmlivewire.talkingpointsmemo.com/2010/06/tpmtv-latest-videos-jon-stewart-8-presidents-said-well-get-off-foreign-oil----fool-me-8-times-am-i-a.php

[2] M. Stöcker, *Microp. Mesop. Mater.*, 29, (1999), 3-48.

[3] E. S. Lipinsky, *Science*, 199, (**1978**), 644-651.

[4] E. S. Lipinsky, *Science*, 212, (**1981**), 1465-1471.

[5] J. R. Regalbuto, *Science*, 325, (**2009**), 822-824.

[6] D. L. Klass, Biomass for Renewable Energy and Fuels, Encyclopedia of Energy, Volume 1. (**2004**) Elsevier Inc.

[7] Biomass as Feedstock for a Bioenergy and Bioproducts Industry: The Technical Feasibility of a Billion-Ton Annual Supply (feedstockreview.ornl.gov/pdf/billion_ton_vision.pdf).

[8] D. R. Dodds, R. A. Gross, *Science*, 318, (**2007**), 1250-1251.

[9] Tobias Wiesenthal, Aphrodite Mourelatou, Jan-Erik Petersen, Peter Taylor, How much bioenergy can Europe produce without harming the environment?, European Environmental Agency, Report No. 7/**2006**

[10] G. W. Huber, S. Iborra, A. Corma, *Chem. Rev.*, 106, (**2006**), 4044-4098.

[11] K. Olofsson, M. Bertilsson, G. Lidèn, *Biotechnology for Biofuels*, 1, (**2008**), 1-14.

[12] R. H. Sims, A. Hastings, B. Schlamadinger, G. Taylors, P. Smith, *Glob. Change Biol.*, 12, (**2005**), 2054-2076.

[13] J. H. Clark, F. E. I. Deswarte, *Introduction to Chemicals from Biomass*, Wiley, (**2008**).

[14] C. H. Christensen, J. Rass-Hansen, C. C. Marsden, E. Taarning, K. Egeblad, *ChemSusChem*, 1, (**2008**), 283-289.

[15] Y. Fan, C. Zhou, X. Zhu, *Catal. Rev.*, 51, (**2009**), 293-324.

[16] E. T. H. Vink, K. R. Rabago, D. A. Glassner, P. R. Gruber, *Polym. Degrad. Stab.*, 80, (**2003**), 403-419.

[17] T. Werpy, P. Petersen, *Top Value Added Chemicals from Biomass*. Volume I: Results of Screening for Potential Candidates from Sugars and Synthesis Gas (www1.eere.energy.gov/biomass/pdfs/35523.pdf).

[18] J. Lunt, *Polym. Degrad. Stab.*, 59, (**1998**), 145-152.

[19] S-H. Hyon, K. Jamshidi, Y. Ikada, *Biomaterials*, 18, (**1997**), 1503-1508.

[20] http://www.iza-structure.org/databases/

[21] J. P. Gilson, E. G. Derouane, *J. Catal.*, 88, (**1984**), 538-541.

[22] http://www.zeolyst.com

[23] J. A. Rabo, M. W. Schoonover, *Appl. Catal. A*, 222, (**2001**), 261-275.

[24] T. Maesen, *Introduction to Zeolite Science and Practice*, 3rd revised edition, Chap. 1, 1-12.

[25] W. Vermeiren, J-P. Gilson, *Top. Catal.*, 52, (**2009**), 1131-1161.

[26] N. S. Kehr, K. Riehemann, J. El-Gindi, A. Schäfer, H. Fuchs, H-J. Galla, L. de Cola, *Adv. Funct. Mater.*, 20, (**2010**), 2248-2254.

[27] P. Horcajada, C. Marquez-Alvarez, A. Ramila, J. Perez-pariente, M. Vallet-Regi, *Solid State Sci.*, 8, (**2006**), 1459-1465.

[28] S. Megelski, G. Calzaferri, *Adv. Funct. Mater.*, 1 1, (**2001**), 277-286.

[29] C. S. Cundy, P. A. Cox, *Microp. Mesop. Mater.*, 82, (**2005**), 1-78.

[30] M. Renz, T. Blasco, A. Corma, V. Fornes, R. Jensen, L. Nemeth, *Chem. Eur. J.*, 8, (**2002**), 4708-4717.

[31] N. K. Mal, A. V. Ramaswamy, *Chem. Commun.*, (**1997**), 425-426.

[32] S. V. Valencia, A. C. Corma, US Patent 6306364, (**2001**).

[33] P. Fejes, J. B. Nagy, K. Kovacs, G. Vanko, *Appl. Catal. A*, 145, (**1996**), 155-184.

[34] N. K. Mal, V. Ramaswamy, P. R. Rajamohanan, A. V. Ramaswamy, *Microporous Mater.*, 12, (**1997**), 331-340.

[35] N. K. Mal, A. Bhaumik, V. Ramaswamy, A. A. Belhekar, A. V. Ramaswamy, *Stud. Surf. Sci. Catal.*, 94, (**1995**), 317-324.

[36] N. K. Mal, V. Ramaswamy, S. Ganapathy, A. V. Ramaswamy, *Appl. Catal. A*, 125, (**1995**), 233-245.

[37] D. M. Ruthven, *Stud. Surf. Sci. Catal.*, Zeolites: a refined tool for designing catalytic sites, (**1995**), 223-233.

[38] D. M. Ruthven, *Introduction to Zeolite Science and Practice*, 3rd revised edition, Chap. 21, 737-785.

[39] S. van Donk, A. H. Janssen, J. H. Bitter, K. P. de Jong, *Catal. Rev.*, 45, (**2003**), 297-319.

[40] K. Hahn, J. Kärger, V. Kukla, *Phys. Rev. Lett.*, 76, (**1996**), 2762-2765.

[41] N. Y. Chen, W. W. kaeding, F. G. Dwyer, *J. Am. Chem. Soc.*, 101, (**1979**), 6783-6784.

[42] J. Perez-Ramirez, C. H. Christensen, K. Egeblad, C. H. Christensen, J. C. Groen, *Chem. Soc. Rev.*, 37, (**2008**), 2530-2542.

[43] M. Choi, K. Na, J. Kim, Y. Sakamoto, O. Terasaki, R. Ryoo, *Nature*, 461, (**2009**), 246-250.

[44] R. Mann, *Catal. Today*, 18, (**1993**), 509-528.

[45] A. Corma, *Chem. Rev.*, (**1997**), 97, 2373-2419.

[46] A. Cizmek, B. Subotic, R. Aiello, F. Crea, A. Nastro, C. Tuoto, *Microporous. Mater.*, 4, (**1995**), 159-168.

[47] R. M. Dessau, E. W. Valyocsik, N. H. Goeke, *Zeolites*, 12, (**1992**), 776-779.

[48] G. Lietz, K. H. Schnabel, C. Peuker, T. Gross, W. Storek, J. Völter, *J. Catal.*, 148, (**1994**), 562-568.

[49] M. S. Holm, E. Taarning, K. Egeblad, C. H. Christensen, *Catal. Today*, (**2011**), accepted.

[50] J. Perez-Ramirez, D. Verboekend, A. Bonillo, S. Abello, *Adv. Funct. Mater.*, 19, (**2009**), 1-8.

[51] J. C. Groen, L. A. A. Peffer, J. A. Moulijn, J. Perez-Ramirez, *Chem. Eur. J.*, 11, (**2005**), 4983-4994.

[52] J. C. Groen, J. A. Moulijn, J. Perez-Ramirez, *J. Mater. Chem.*, 16, (**2006**), 2121-2131.

[53] M. Ogura, S. Shinomiya, J. Tateno, Y. Nara, E. Kikuchi, M. Matsukata, *Chem. Lett.*, (**2000**), 882-883.

[54] M. Ogura, S. Shinomiya, Y. Tateno, Y. Nara, M. Nomura, E. Kikuchi, M. Matsakata, *Appl. Catal. A.*, 219, (**2001**), 33-43.

[55] M. S. Holm, M. K. Hansen, C. H. Christensen, *Eur. J. Inorg. Chem.*, (**2009**), 1194-1198.

[56] J. C. Groen, S. Abello, L. A. Villaescusa, J. Perez-Ramirez, *Microp. Mesop. Mater.*, 114, (**2008**), 93-102.

[57] X. Wei, P. G. Smirniotis, *Microp. Mesop. Mater.*, 97, (**2006**), 97-106.

[58] L. Mokrzycki, B. Sulikowski, Z. Olejniczak, *Catal. Lett.*, 127, (**2009**), 296-303.

[59] X. Li, C. Wang, S. Liu, W. Xin, Y. Wang, S. Xie, L. Xu, *J. Mol. Catal. A-Chem*, in press.

[60] J. C. Groen, L. A. A. Peffer, J. A. Moulijn, J. Perez-Ramirez, *Microp. Mesop. Mater.*, 69, (**2004**), 29-34.

[61] A. Bonilla, D. Baudouin, J. Perez-Ramirez, *J. Catal.*, 265, (**2009**), 170-180.

[62] J. C. groen, T. Sano, J. A. Moulijn, J. Perez-Ramirez, *J. Catal.*, 251, (**2007**), 21-27.

[63] L. Sommer, D. Mores, S. Svelle, M. Stöcker, B. M. Weckhuysen, U. Olsbye, *Microp. Mesop. Mater.*, 132, (**2010**), 384-394.

[64] J. Perez-Ramirez, S. Abello, L. A. Villaescusa, A. Bonilla, *Angew. Chem. Int. Ed.*, 47, (**2008**), 7913-7917.

[65] J. C. Groen, J. A. Moulijn, J. Perez-Ramirez, *Ind. Eng. Chem. Res.*, 46, (**2007**), 4193-4201.

[66] C. Doremieux-Morin, A. Ramsaran, R. Le Van Mao, P. Batamack, L. Heeribout, V. Semmer, G. Denes, J. Fraissard, *Catal. Lett.*, 34, (**1995**), 139-149.

[67] S. Abello, A. Bonilla, J. Perez-Ramirez, *Appl. Catal. A.*, 364, (**2009**), 191-198.

[68] M. S. Holm, M. K. Hansen, C. H. Christensen, *Eur. J. Inorg. Chem.*, (**2009**), 1194-1198.

[69] J. C. Groen, R. Caicedo-Realpe, S. Abello, J. Perez-Ramirez, *Mater. Lett.*, 63, (**2009**), 1037-1040.

[70] R. Chal, C. Gerardin, M. Bultu, S. van Donk, *ChemCatChem*, 3, (**2011**), 67-81.

[71] C. D. Chang, A. J. Silvestri, *J. Catal.*, 47, (**1977**), 249-259.

[72] S. L. Meisel, J. P. McCullough, C. H. Lechthaler, P. B. Weisz, *Chemtech*, 6, (**1976**), 86.

[73] M. Stöcker, *Microp. Mesop. Mater.*, 29, (**1999**), 3-48.

[74] www.uop.com

[75] T. Mokrani, M. Scurrell, *Catal. Rev.*, 51, (**2009**), 1-145.

[76] Haw J. F.; Marcus, D. M. *Nanotechnology in Catalysis*; Plenum Publisher: New York, (**2004**), Vol. 1, Chapter 13.

[77] www.nma.org/

[78] I. M. Dahl, S. Kolboe, *J. Catal.*, 149, (**1994**), 458-464.

[79] M. Bjørgen, S. Svelle, F. Joensen, J. nerlov, S. Kolboe, F. Bonino, L. Palumbo, S. Bordiga, U. Olsbye, *J. Catal.*, 249, (**2007**), 195-207.

[80] U. V. Mentzel, PhD. Dissertation, *Towards a methanol economy: Zeolite catalyzed production of synthetic fuels*, (**2010**), Department of Chemistry, Technical University of Denmark.

[81] S. E. Voltz, J. J. Wise, *Development studies on conversion of methanol and related oxygenates to gasoline*, Final report, Mobil research and development corporation, Paulsboro, NJ, (**1976**), US ERDA contract No E (49-18)-1773.

[82] L. E. Smart, E. A. Moore, *Solid State Chemistry*, 3rd edition, (**2005**), Taylor & Francis Group

[83] I. Chorkendorff, J. W. Niemantsverdriet, *Concepts of Modern Catalysis and Kinetics*, (**2003**), Wiley-VCH.

[84] J. C. Groen, PhD. Dissertation, *Mesoporous Zeolites Obtained by Desilication*, Faculty of Applied Sciences, (**2007**), Delft University of technology, Netherlands.

[85] http://serc.carleton.edu/research_education/geochemsheets/electroninteractions.html (accessed 08-02-2011)

[86] P. J. Goodhew, J. Humphreys, R. Beanland, *Electron Microscopy and Analysis*, 3rd edition, (**2001**), Taylor & Francis

[87] http://www.chemicalconnection.org.uk/chemistry/topics/view.php?topic=3&headingno=5&lang=en (accessed 24-02-2011)

[88] A. Corma, M. E. Domine, S. Valencia, *J. Catal.*, 215, (**2003**), 294-304.

[89] K. Robards, P. R. Haddad, P. E. Jackson, *Principles and Practice of Modern Chromatographic Methods*, (**2002**), Elsevier Science.

2.0 Results

Part 1

2.1 Aim and idea preceding the studies within desilication

Several strategies can be employed to produce a zeolite catalyst with a hierarchical porosity.[1,2] The mesoporous zeolite materials can be categorized into nanosized crystals, widepore zeolites (pore dimensions exceeding 1 nm), composite materials (zeolite regimes in/on an amorphous mesoporous support) and simply mesoporous single crystals.[3] Interestingly, by far the majority of reports on mesoporosity shows it is in fact beneficial for a given catalytic test reaction. When this is not the case it can often be explained by thorough characterization of the sample. Still, it is relatively difficult to compare the catalytic performance of two materials prepared in different laboratories even if the catalysts are tested in the same reaction due to variations in reaction conditions (catalyst loading, temperature, acidity etc.). Further, since researchers often emphasize on the material preparation; careful catalytic experimentation can lack priority. The majority of reports that deal with mesoporosity compare a reference sample with a mesoporous counterpart. This key comparison is very important but can suffer from a simplification of the unique mesoporosity in the sample by stating that either a zeolite is mesoporous or not. Mesoporosity in zeolite crystals can be of different nature i) in the form of isolated internal "pockets" not sufficiently interconnected ii) located preferentially in the outer most layers of the crystal or iii) can vary in average size, shape or size/shape distribution or iv) other. Naturally this will affect the effective diffusivity within the zeolite and thereby the catalytic performance of the sample.

Inspired by the above considerations, we set out to investigate to which extend the mesoporosity can be controlled/maximized. These results are presented in **section 2.2**.

It is well known that as a function of desilication-severity the formed mesopores increase in average size. By starting with a mesoporous MFI sample prepared by carbon-templating we sought to combine the relatively large mesopores made by this approach with smaller pores originating from a modest desilication. The goal was to create the world's most mesoporous zeolite (or simply an ultra-porous sample).

It is a challenge within the field of mesoporous zeolites to prepare a suitable reference sample. A reference sample that differs only in the absence of mesoporosity is required to safely claim that the catalytic improvement can in fact be ascribed to porosity. Correspondingly, a series of samples containing increasing levels of mesoporosity can provide excellent information of the diffusivity effect in catalysis but this requires that the introduction of mesoporosity is the only (most significant) change within the series. This prompted us to investigate whether this could in fact be claimed for a series of samples created by desilication. The results are presented in **section 2.3**. We chose to use FT-IR supplemented by probe molecules (CO and collidine) on a series of desilicated samples which had previously been tested as catalysts in the MTG reaction.

So far the most commonly used bases in desilication are sodium hydroxide or sodium carbonate yielding a mesoporous zeolite in the sodium form. This is a lesser problem if desilication is done on the calcined zeolite directly, because then it is (likely) already in sodium form. However, desilication with an excess of organic base could leave the zeolite charge compensated by the organic cation. The organic cation could then be combusted and thereby tentatively produce the active proton form directly thus circumventing an ion-exchange procedure with for example NH_4NO_3 that is otherwise required for the sodium analogue. In addition to this overall simplification of the desilication protocol we wanted to understand the versatility of desilication. **Section 2.4** presents our results from desilication of zeolite Beta with tetramethyl ammonium hydroxide.

A large number of innovative approaches that produce hierarchical zeolites are published and this area of zeolite research is expanding quickly. The subject of material preparation was recently reviewed.[3,4] As discussed in section 1.3, a comparison of catalytic data from various reports can be rather difficult. In addition, since negative results are very seldom published it is challenging to evaluate the limitations for hierarchical zeolite application. Based on this concern we have tried to give an overview of the catalytic reactions in which mesoporous materials have been tested in as of today. The review is presented as **section 2.5.** The collection of data accompanied by our interpretation and grouping is intended to assist researchers in choosing a suitable catalytic reaction as model reaction whether it is an identical or complementary approach. By doing so, this could allow for a synergistic understanding of the performance of mesoporous materials in catalysis. Hopefully comparing porosities obtained from different protocols will be possible and the effect of mesoporosity in zeolites can reach the 'next level' of understanding with respect to selectivity gain, increased conversion capacity, resistance towards deactivation etc.

[1] R. Chal, C. Gerardin, M. Bultu, S. van Donk, *ChemCatChem*, 3, (**2011**), 67-81.

[2] Y. Tao, H. Kanoh, L. Abrams, K. Kaneko, *Chem. Rev.*, 106, (**2006**), 896-910.

[3] J. Perez-Ramirez, C. H. Christensen, K. Egeblad, C. H. Christensen, J. C. Groen, *Chem. Soc. Rev.*, 37, (**2008**), 2530-2542.

[4] S. van Donk, A. H. Janssen, J. H. Bitter, K. P. De Jong, *Catal. Rev.*, 45, (**2003**), 297-319.

DOI: 10.1002/ejic.200800781

Enhancing the Porosity of Mesoporous Carbon-Templated ZSM-5 by Desilication

Martin S. Holm,[a,b] Kresten Egeblad,[a] Peter N. R. Vennestrøm,[a] Christian G. Hartmann,[a] Marina Kustova,[b] and Claus H. Christensen*[b]

Keywords: ZSM-5 / Zeolites / Desilication / Carbon-templating / Mesoporous materials

A tunable desilication protocol applied on a mesoporous ZSM-5 zeolite synthesized by carbon-templating is reported. The strategy enables a systematic manufacture of zeolite catalysts with moderate to very high mesoporosities. Coupling carbon-templating and desilication thus allow for more than a doubling of the original mesopore volume and mesopore surface area. The porosity effect arising from various treatment times and base amounts in the media has been thoroughly mapped. Initially, small mesopores are created, and as desilication strength increases the average mesopore size enhances. Crystallinity of the treated samples is retained, and electron microscopy indicates solely intracrystalline mesoporosity.

Introduction

Zeolites are crystalline microporous aluminosilicates that have found a multitude of industrial applications as, e.g. sorbents, ion-exchangers, and catalysts. The widespread application of zeolites in industry can be attributed to the inherent micropore system of molecular dimensions, which allows for shape-selective catalysis. Moreover, they are often thermally highly stable materials, which possess remarkably high surface areas. These properties make zeolites particularly useful for catalytic applications, and the use of zeolites as catalysts has indeed received significant attention.[1,2] However, molecular transport to the catalytically active micropore system in the bulk of the crystals may become a limiting factor for their activity in some catalytic applications.[3] Recently, several preparative strategies have been developed with the aim of producing zeolite materials that overcome this diffusion limitation.[4,5] The strategies pursued so far include increasing the width of the zeolite micropores,[6–9] decreasing the size of the zeolite crystals,[10–14] and the introduction of an auxiliary mesopore system in addition to the inherent micropore system.[15–18] The latter two classes of materials can be classified as hierarchical in terms of porosity because they have bi- or trimodal pore-size distributions, and the preparation of such materials by use of mesopore templates was reviewed very recently.[19] For the preparation of zeolites with intracrystalline hierarchical porosity, two main approaches appear to be the most promising,[20] namely carbon-templating[21–23] and desilication.[24–27]

In carbon-templating, porous zeolite crystals are produced by removal of auxiliary carbon particles encapsulated in the zeolite crystals during growth. In desilication, conventional purely microporous zeolite crystals are treated with dilute aqueous base to preferentially dissolve silica species from the zeolite crystals. Here, we show that the porosity of carbon-templated mesoporous zeolite crystals can be tuned, as well as increased by more than a factor of two, by subjecting the already mesoporous material to a desilication procedure. Coupling of these two procedures have in fact been attempted earlier, however, with limited success.[28] The process of desilication corresponds to a partial dissolution of the zeolite framework. Therefore, it is important either to use a limited amount of a base or to restrict the time during which the process is allowed to proceed.[29]

Results and Discussion

A mesoporous carbon-templated ZSM-5 zeolite was subjected to various desilication treatments as listed in Table 1.

Physico-chemical properties of the resulting materials from N_2 physisorption, XRD and NH_3-TPD measurements are included. First of all, it can be seen that the microporosity is preserved after desilication since the micropore volumes of the samples are not affected by the treatments. Moreover, it can be seen that the parent carbon-templated sample has a considerable mesopore volume of ca. 0.3 mL/g.

[a] Center for Sustainable and Green Chemistry, Department of Chemistry, Technical University of Denmark, Building 206, 2800 Lyngby, Denmark
[b] Haldor Topsoe A/S, Nymøllevej 55, 2800 Lyngby, Denmark
E-mail: chc@topsoe.dk

Supporting information for this article is available on the WWW under http://www.eurjic.org or from the author.

Table 1. Textural data from N_2 adsorption/desorption experiments on the parent and desilicated samples.[a]

Sample	Base amount [mmol/g]	Time [min]	S_{BET} [m^2/g]	S_{meso} [m^2/g]	V_{meso} [mL/g]	V_{micro} [mL/g]	D[101][b] [Å]	Acidity[c] [mmol/g]
Parent	–	–	408	117	0.30	0.11	677	0.164
1	3	30	408	162	0.37	0.11	595	0.180
2	5	30	422	195	0.47	0.10	513	0.206
3	7.5	30	478	222	0.63	0.11	494	0.235
4	10	30	478	232	0.72	0.10	460	0.272
5	15	30	503	234	0.75	0.11	386	0.293
6	8	5	295	142	0.33	0.06	–	–
7	8	10	466	241	0.64	0.10	–	–
8	8	15	443	210	0.66	0.10	–	–
9	8	20	456	208	0.70	0.11	–	–
10	8	30	450	201	0.73	0.11	–	–
11	8	70	445	181	0.65	0.11	–	–

[a] Samples 1–5 were desilicated in a 0.1 M solution and samples 6–11 in a 0.2 M solution. $V_{meso} = V_{ads,P/P0 = 0.99} - V_{micro}$. V_{micro} from t-plot. S_{meso} from BJH. Surface area of pores 17–3000 Å. [b] Scherrer equation. [c] NH_3-TPD. NH_3 desorbed at 175 °C for 2 h.

This porosity corresponds to a moderate mesopore surface area S_{meso} of 117 m^2/g due to rather large mesopores centered around ca. 20–30 nm. The physisorption isotherms obtained from samples treated with different volumes of 0.1 M NaOH solutions for 30 min (samples 1–5) are shown in Figure 1(a). In Figure 1(a) it can be seen that the mesopore volume of the samples increases with increasing desilication strength. Moreover, closer inspection of Figure 1(a) reveals that a hysteresis loop starts to develop at a relative pressure of 0.45 at low treatment strengths (samples 1 and 2). This is attributed to the formation of new smaller mesopores, initially with a diameter below 10 nm as is evident from the BJH-derived pore-size distribution given in Figure 1(b).

The sizes of the created mesopores are in excellent agreement with previously published data on desilication of purely microporous ZSM-5 samples.[30,31] Interestingly, because the mesopores initially formed are smaller than the inherent mesopore system present, these results indicate that it is possible to create a hierarchical zeolite with a multi-level mesoporosity by coupling the carbon-templating and desilication protocols. As the desilication strength is increased, these smaller mesopores grow larger, as can be seen by the disappearance of the mesopores below 10 nm (samples 3 and 4) and simultaneous growth of pore volume attributed to pores around 15 nm. Thus, the observed increase in mesopore volumes apparent from Table 1 does not only originate from an increase in the pore sizes of already existing mesopores, but also from newly generated mesopores. The generation of mesopores can also be tuned by variation of the reaction time as evident from the physisorption data presented in Table 1 for samples 6–11. It can be seen, that the mesopore volume as well as the mesopore surface area of the parent mesoporous sample are doubled after only 10 min (sample 7). Moreover, it can be seen that further extending the desilication time only marginally increases the mesopore volume, and an extreme time has a detrimental effect on the mesopore surface area (sample 11). This is attributed to the pore size distribution extending significantly into the macropore region. Key sorption isotherms and the respective BJH-derived mesopore diameters are given in the Supporting Information (Figure S1). Figure 2 shows the XRD patterns of the parent sample along with samples 1–5 illustrating the preserved crystallinity and phase purity of the treated samples. In ac-

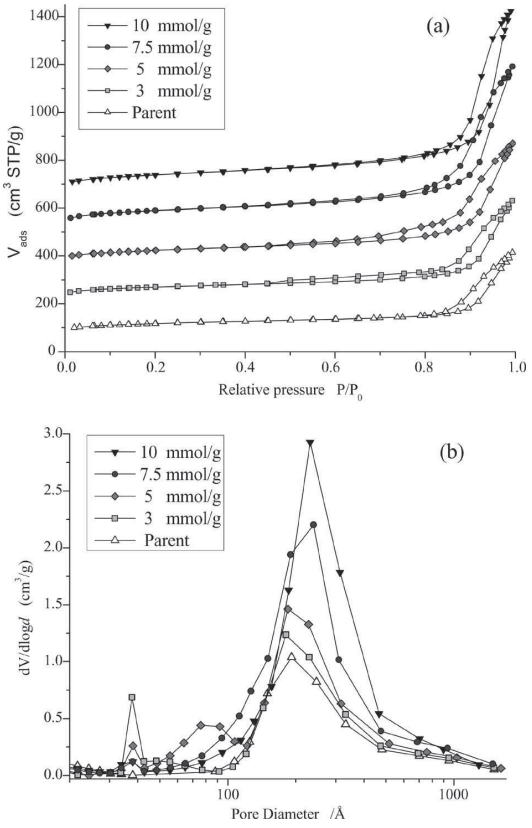

Figure 1. (a) N_2 adsorption/desorption isotherms of the parent along with samples 1–4. Isotherms of samples 1–4 are offset by 150 for illustrative reasons. (b) BJH-derived pore-size distributions.

cordance with results obtained after desilication of conventional zeolite samples, the intensity of the reflections gradually decrease as the desilication strength is increased.[32,33]

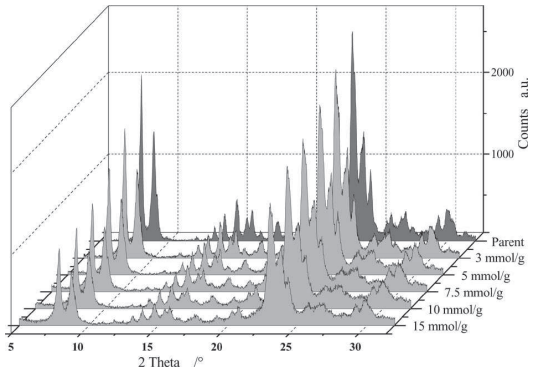

Figure 2. XRD diffractograms of parent sample and samples 1–5 desilicated for 30 min with increasing desilication strength.

The effective average crystal diameter calculated by the Scherrer equation reveal a gradual decrease in crystal diameter. The D[101] deflection was chosen for Table 1. Table S1 (Supporting Information) contains effective crystal sizes derived from other deflections. By analyzing the XRD results in relation to imaging obtained from SEM and TEM analysis, it appears unlikely that the desilicated crystals dismantle to produce interparticle mesoporosity. The observed decrease in the average crystal size could alternatively be explained by the formation of an increasing number of intracrystalline domains bordering a mesopore within the single crystal. From NH_3-TPD an acidity of 0.164 mmol/g was measured for the parent sample after desorption of NH_3 at 175 °C for 2 h. This acidity correlates to the anticipated Si/Al ratio of approximately 45 when compared to a calibration curve from ZSM-5 zeolites of known acidities, thus indicating complete aluminium incorporation from the gel during crystallization. Furthermore, it can be seen from Table 1 (samples 1–5) that the total acidity of the materials increase as a function of the desilication, as would be expected from the selective silicon extraction. Figure 3 presents the NH_3 desorption curves obtained after desorption of weakly bound NH_3 at 100 °C for 1 h and at 175 °C for 2 h. A continuing increase in total acidity and nearly a doubling for the most severely treated zeolites is apparent in both cases. In Figure 3(b) it can be seen that a significant contribution to the acidity orginates from a shoulder on the low-temperature side of the desorption maximum at ca. 365 °C. As the treatment strength increases, the shoulder intensifies, which is possibly due to partial (extra) framework aluminum species generated during the desilication.

Figure 4 gives representative SEM and TEM images of the parent and desilicated samples. SEM was used to verify the homogeneity of the parent material with respect to crystal size and porosity, and to visually monitor the effect of the desilication treatments. In Figure 4(a) a SEM image of the parent sample is shown. It can be seen that the crystals

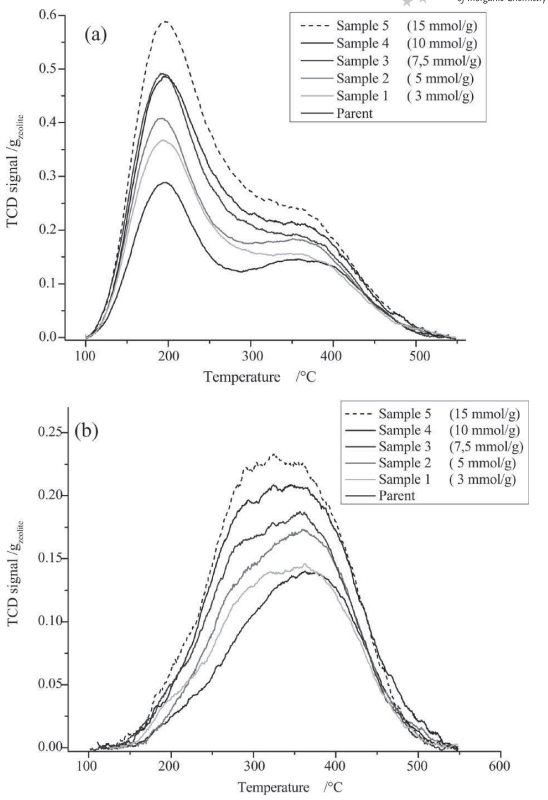

Figure 3. NH_3 desoprtion curves of parent sample and samples 1–5. Weakly bound NH_3 desorbed in He at (a) 100 °C for 1 h and (b) at 175 °C desorbing for 2 h.

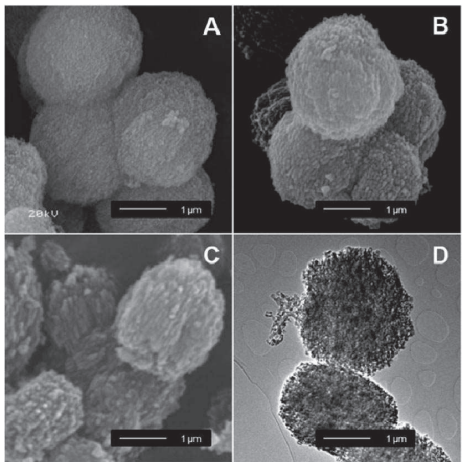

Figure 4. (a)–(c) SEM images of the parent sample, sample 7 (desilicated 10 min.) and sample 10 (desilicated 30 min), respectively. (d) TEM image of sample 10 (desilicated 30 min).

exhibit the well-known sponge-like morphology characteristic of mesoporous carbon-templated MFI zeolites.[34] Overview images of the parent sample confirmed that the crystals were similar in size (2–3 μm long) and that the vast majority of them exhibited this morphology. Figures 4(b) and (c) show SEM images of desilicated samples obtained after 10 min (sample 7) and 30 min (sample 10) treatment times, respectively. From these images, it is evident that desilication leads to a gradual "roughening" of the crystals, which appear to be more and more rugged as the desilication time is increased. TEM analyses also revealed the sponge-like morphology of the crystals as evident from the highly contrasted image of the 30 min desilicated samples shown in Figure 4(d).

Conclusions

We have shown that the porosity of carbon-templated mesoporous ZSM-5 may be enhanced by a factor of at least two by desilication of such a sample in terms of mesopore surface area as well as mesopore volume. Two types of desilication protocols were applied for tuning the porosity of the carbon-templated mesoporous sample: variation in the volume of hydroxide solution and variation in reaction time. Pore-size distribution plots revealed that at lower desilication strengths both newly generated smaller mesopores (initally centered below 10 nm) as well as mesopores already present in the sample (centered around ca. 20–30 nm) contributed to the mesopore volume. With increased desilication strength, these smaller mesopores grew larger, eventually, after excessive desilication, into the macropore region. The method applied here could easily be extended to other zeolite structure types, and it therefore provides a useful and easy approach for systematically generating highly mesoporous zeolite samples.

Experimental Section

A mesoporous ZSM-5 sample was prepared by carbon-templating according to a modified literature procedure.[35] A nominal Si/Al ratio of 45 was used in the gel. Briefly, 2 g of carbon black pearls 2000 was impregnated with a fresh solution of aluminium isopropoxide in tetrahydrofuran (0.084 g in 6 mL) and left to dry overnight. Then the carbonaceous material was impregnated with a mixture of tetrapropylammonium hydroxide (3.44 g, 40 wt.-%), aqueous sodium hydroxide (0.1 g in 0.5 g H_2O) and ethanol (3.03 g), and left to dry overnight. The material was impregnated with tetraethyl orthosilicate (3.87 g) and left to dry overnight before being crystallized at 180 °C for 5 d. The carbon matrix was removed by calcination at 550 °C in static air for 20 h reached at a ramp of ca. 2 °C/min. The proton form of the zeolites was obtained by threefold ion-exchange in a 1 M NH_4NO_3 solution and calcination at 550 °C in static air for 4 h. The sample was subjected to different desilication procedures by immersion of the zeolite samples in aqueous sodium hydroxide solutions at 65 °C for various periods of time. After reaction, the desilicated samples were collected by filtration and washed thoroughly with water. Nitrogen physisorption measurements were conducted with a micromeretics ASAP 2020. Powder X-ray diffraction (XRD) patterns of the parent and desilicated samples were recorded with a Bruker AXS powder diffractometer. Scanning electron micrographs (SEM) were recorded with a JEOL JSM 5900 equipped with an LaB_6 filament. Prior to measurements, the samples were sputter-coated with Au for 40 s by using a Polaron SC 7620. Transmission electron microscopy (TEM) images and selected area diffraction (SAD) were recorded with a JEM 2000 FX with an accelerating voltage of 300 kV, as described previously.[36] NH_3-TPD measurements were performed with a Micromeritics Autochem II equipped with a TCD detector. Samples were transformed into proton form prior to NH_3-TPD analysis through a similar procedure as described above for the parent material. Dry weight of the samples was found after evacuation at 300 °C for 1 h. Weakly bound ammonia was desorbed prior to measurement at 100 °C in an He flow of 25 mL/min for 1 h or at 175 °C in an He flow of 50 mL/min for 2 h, respectively.

Supporting Information (see footnote on the first page of this article): N_2 physisorption isotherms and crystal-size measurements (calculated by use of the Scherrer equation from X-ray data).

Acknowledgments

The Center for Sustainable and Green Chemistry is sponsored by the Danish National Research Foundation. The authors thank Bodil F. Holten for technical assistance.

[1] A. Corma, *Chem. Rev.* **1995**, *95*, 559.
[2] A. Corma, *Chem. Rev.* **1997**, *97*, 2373.
[3] M. Hartmann, *Angew. Chem. Int. Ed.* **2004**, *43*, 5880.
[4] Y. Tao, H. Kanoh, L. Abrams, K. Kaneko, *Chem. Rev.* **2006**, *106*, 896.
[5] J. C. Groen, C. H. Christensen, K. Egeblad, C. H. Christensen, J. Pérez-Ramírez, *Chem. Soc. Rev.* **2008**, accepted.
[6] M. E. Davis, C. Saldarriaga, C. Montes, J. Garces, C. Crowder, *Nature* **1988**, *331*, 698.
[7] C. C. Freyhard, M. Tsapatsis, R. F. Lobo, K. J. Balkus, *Nature* **1996**, *381*, 295.
[8] T. Wessels, C. Baerlocher, L. B. McCusker, E. J. Creyghton, *J. Am. Chem. Soc.* **1999**, *121*, 6242.
[9] A. Corma, M. Diaz-Cabanas, J. Martinez-Triguero, F. Rey, J. Rius, *Nature* **1992**, *418*, 514.
[10] L. Tosheva, V. P. Valtchev, *Chem. Mater.* **2005**, *17*, 2494.
[11] P. A. Jacobs, E. G. Derouane, J. Weitkamp, *J. Chem. Soc., Chem. Commun.* **1981**, 591.
[12] M. A. Camblor, A. Corma, S. Valencia, *Microporous Mesoporous Mater.* **1998**, *25*, 59.
[13] C. Madsen, C. J. H. Jacobsen, *Chem. Commun.* **1999**, 673.
[14] W.-C. Li, A.-H. Lu, R. Palkovits, W. Schmidt, B. Spliethoff, F. Schüth, *J. Am. Chem. Soc.* **2005**, *127*, 12595.
[15] C. J. H. Jacobsen, C. Madsen, J. Houzvicka, I. Schmidt, A. Carlsson, *J. Am. Chem. Soc.* **2000**, *122*, 7116.
[16] M. Ogura, S. H. Shinomiya, J. Tateno, Y. Nara, E. Kikuchi, M. Matsukata, *Chem. Lett.* **2000**, 882.
[17] F.-S. Xiao, L. Wang, C. Yin, K. Lin, Y. Di, J. Li, R. Xu, D. S. Su, R. Schlögl, T. Yokoi, T. Tatsumi, *Angew. Chem. Int. Ed.* **2006**, *45*, 3090.
[18] H. Wang, T. Pinnavaia, *Angew. Chem. Int. Ed.* **2006**, *45*, 7603.
[19] K. Egeblad, C. H. Christensen, M. Kustova, C. H. Christensen, *Chem. Mater.* **2008**, *20*, 946.
[20] K. Egeblad, C. H. Christensen, M. Kustova, C. H. Christensen, "Mesoporous Zeolite Crystals", in *Zeolites: From Model Materials to Industrial Catalysts* (Eds.: J. Cejka, J. Perez-Pariente, W. J. Roth), Transworld Research Network, Kerala, India, **2008**, pp. 391–442.
[21] M. Y. Kustova, P. Hasselriis, C. H. Christensen, *Catal. Lett.* **2004**, *96*, 205.

[22] X. Wei, P. G. Smirniotis, *Microporous Mesoporous Mater.* **2005**, *89*, 170.
[23] Y. Tao, H. Kanoh, K. Kaneko, *J. Phys. Chem. B* **2003**, *107*, 10974.
[24] J. C. Groen, L. A. A. Peffer, J. A. Moulijn, J. Pérez-Ramírez, *Chem. Eur. J.* **2005**, *11*, 4983.
[25] J. C. Groen, J. A. Moulijn, J. Pérez-Ramírez, *J. Mater. Chem.* **2006**, *16*, 2121.
[26] M. Bjørgen, F. Joensen, M. S. Holm, U. Olsbye, K.-P. Lillerud, S. Svelle, *Appl. Catal. A* **2008**, *345*, 43.
[27] Y. Tao, H. Kanoh, K. Kaneko, *Adsorption* **2006**, *12*, 309.
[28] Y. H. Chou, C. S. Cundy, A. A. Garforth, V. L. Zholobenko, *Microporous Mesoporous Mater.* **2006**, *89*, 78.
[29] J. C. Groen, L. A. A. Peffer, J. A. Moulijn, J. Pèrez-Ramirez, *Colloids Surf., A* **2004**, *241*, 53.
[30] J. C. Groen, W. Zhu, S. Brouwer, S. J. Huynink, F. Kapteijn, J. A. Moulijn, J. Pérez-Ramírez, *J. Am. Chem. Soc.* **2007**, *129*, 355.
[31] M. Ogura, S. Shinomiya, J. Tateno, M. Nomura, E. Kikuchi, M. Matsukata, *Appl. Catal. A* **2001**, *219*, 33.
[32] Y. Song, X. Zhu, T. Song, Q. Wang, L. Xu, *Appl. Catal. A* **2006**, *302*, 69.
[33] J. S. Jung, J. W. Park, G. Seo, *Appl. Catal. A* **2005**, *288*, 149.
[34] K. Zhu, K. Egeblad, C. H. Christensen, *Eur. J. Inorg. Chem.* **2007**, 3955.
[35] M. Y. Kustova, A. L. Kustov, C. H. Christensen, *Stud. Surf. Sci. Catal.* **2005**, *158*, 255.
[36] K. Egeblad, M. Kustova, S. K. Klitgaard, K. Zhu, C. H. Christensen, *Microporous Mesoporous Mater.* **2007**, *101*, 214.

Received: August 5, 2008
Published Online: October 22, 2008

Supplementary information for the manuscript:

Enhancing the Porosity of Mesoporous Carbon-templated ZSM-5 by Desilication

Martin S. Holm, Kresten Egeblad, Peter N. R. Vennestrøm, Christian G. Hartmann, Marina Kustova, Claus H. Christensen

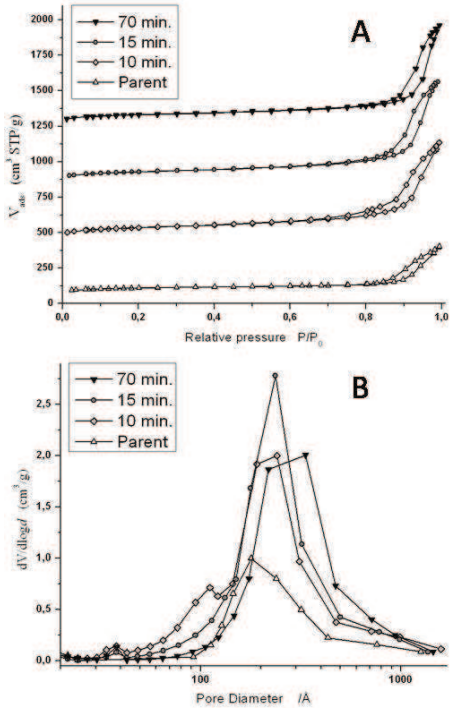

Figure s1. (a) N_2-sorption isotherms for sample 6-11. Isotherms moved 400 units respectively for illustrative reasons. (b) BJH derived pore size distributions.

Table S1. Average crystal size calculated from the Scherrer equation.

Sample	D[101] (Å)	D[200] (Å)	D[111] (Å)	D[103] (Å)	D[113] (Å)	D[151] (Å)	D[303] (Å)	D[313] (Å)
Parent	677	430	>1000	675	525	431	486	413
1	595	380	>1000	483	421	334	446	337
2	513	352	885	457	422	284	412	319
3	494	315	>1000	349	489	295	242	326
4	460	293	815	370	506	352	398	306
5	386	286	308	424	417	130	337	289

Applied Catalysis A: General 356 (2009) 23–30

Contents lists available at ScienceDirect

Applied Catalysis A: General

journal homepage: www.elsevier.com/locate/apcata

Assessing the acid properties of desilicated ZSM-5 by FTIR using CO and 2,4,6-trimethylpyridine (collidine) as molecular probes

Martin Spangsberg Holm [a,b], Stian Svelle [c], Finn Joensen [b], Pablo Beato [b], Claus Hviid Christensen [a,b], Silvia Bordiga [d], Morten Bjørgen [e,*]

[a] Center for Sustainable and Green Chemistry, Department of Chemistry, Building 206, Technical University of Denmark, DK-2800 Lyngby, Denmark
[b] Haldor Topsøe, Nymøllevej 55, DK-2800 Lyngby, Denmark
[c] Innovative Natural Gas Processes and Products (inGAP), Department of Chemistry, University of Oslo, P.O. Box 1033 Blindern, N-0315 Oslo, Norway
[d] Department of Inorganic, Physical and Materials Chemistry, NIS Centre of Excellence, and Centro di Riferimento INSTM, University of Turin, I-10125 Torino, Italy
[e] Department of Chemistry, Norwegian University of Science and Technology, N-7491 Trondheim, Norway

ARTICLE INFO

Article history:
Received 31 August 2008
Received in revised form 13 November 2008
Accepted 26 November 2008
Available online 11 December 2008

Keywords:
MFI
MTG
MTH
NaOH treatment
Mesoporous
Lewis acidity

ABSTRACT

A series of desilicated ZSM-5 catalysts previously shown to have improved catalytic performance in the MTG (methanol-to-gasoline) reaction [M. Bjørgen, F. Joensen, M.S. Holm, U. Olsbye, K.-P. Lillerud, S. Svelle, Appl. Catal. A 345 (2008) 43] was subjected to thorough examination using FTIR. Clearly, defects represented by internal Si-OH sites are removed upon NaOH treatment. In a parallel manner, free Si-OH sites increase in concentration and the results point to a selective mechanism for formation of mesopores as the framework dissolution preferentially takes place at defective sites in the crystallites. The acid properties of the desilicated materials were investigated by applying CO and collidine (2,4,6-trimethylpyridine) as molecular probes. Monitoring the induced frequency shifts upon CO adsorption at liquid N_2 temperature revealed that the desilication procedure did not alter the acid strength of the Brønsted sites significantly. This weakens the explanation linking improved catalytic behaviour, such as increase in both catalyst activity and hydrogen transfer activity, to modified Brønsted acid strength. Simultaneous to the mesopore formation resulting from the desilication, strong Lewis acid sites were generated, presumably from dislodged framework aluminium. Collidine, which is too bulky to enter the micropore system of ZSM-5, could access Lewis acidity, suggesting that these sites were predominantly generated on the external surface or in the newly created mesopores. Additionally, by first saturating the zeolite surface with collidine and subsequently adsorbing CO, we show that barely any Lewis acidity was uncoordinated post-collidine saturation while the Brønsted acidity continuously was protected behind the micropore system. It is hypothesized from the present study that the desilication procedure can lead to a slight dealumination of the samples while forming Lewis acidity preferentially at the crystal surface.

1. Introduction

Zeolites are crystalline aluminosilicates built from corner-sharing TO_4 tetrahedra, where T represents Al or Si. The zeolite crystal structures are such that regularly shaped channels, or pores, of molecular dimensions run through the materials. The H-ZSM-5 (MFI structure code) zeolite is a medium sized pore system with channel dimensions defined by 10 T-atoms (Si or Al). The pore system consists of straight channels (5.1 Å × 5.5 Å) that are intersected by zig–zag channels (5.3 Å × 5.6 Å), thus creating a three-dimensional microporous network [1].

It is the presence of these micropores that has paved the way for the successful application of zeolites in catalysis, but the same pore system also imposes severe diffusion constraints in catalytic applications. As outlined in three fairly recent reviews [2–4] several different approaches have been followed to improve catalyst performance by improving the diffusion properties by the introduction of mesopores in addition to the micropores inherent to the crystal structures. Among these techniques, we find dealumination with steam and acid leaching [2], various carbon templating routes [2,4], and post-synthesis treatment of the zeolite crystals in alkaline media such as NaOH solutions [3].

The potential of the post-synthesis treatments with NaOH, or desilication, has been highlighted by a series of publications by Groen and co-workers, where the effects of many treatment parameters, such as NaOH concentration, treatment time, temperature, and elemental composition on the mesoporosity

* Corresponding author. Tel.: +47 73 59 48 46; fax: +47 73 55 08 77.
E-mail address: morten.bjorgen@chem.ntnu.no (M. Bjørgen).

0926-860X/$ – see front matter © 2008 Elsevier B.V. All rights reserved.
doi:10.1016/j.apcata.2008.11.033

generation have been studied extensively for H-ZSM-5 [5–11]. In addition to the reports on H-ZSM-5, Wei and Smirniotis [12] studied the desilication of H-ZSM-12 (MTW) and observed the formation of intracrystalline mesopores and, as a consequence, improved diffusivity of bulky hydrocarbons. Groen et al. investigated the effects of NaOH treatment on zeolite H-mordenite (MOR) [13]. For this material, substantial mesopore development was also found, along with an improved catalytic performance in benzene alkylation which was attributed to improved mass transport. Interestingly, very recently a desilication study on zeolite beta was published. It is revealed that surprisingly mild treatment conditions lead to mesopore formation but with a substantial loss of crystallinity in the desilicated material [14]. A few other examples on the effects of desilication on the catalytic properties of the zeolites may be found in the literature [15–21], but as mesopore creation by zeolite desilication has received increased attention only recently, most reports focus on the characterization of the materials by sorption techniques, X-ray diffraction, and electron microscopy, and, in a few cases, diffusion measurements [10,12,15].

FTIR spectroscopy is a commonly used technique for characterization of heterogeneous catalysts, and it has proven to be very useful for the characterization of zeolite catalysts, yet only a minority of the abovementioned reports employ FTIR as a characterization tool [7,9,12,13,15,19,20]. In most of these publications, the spectra covering the OH stretching regions of the zeolites are reported and typically reductions in the bands corresponding to internal silanol groups involved in extensive hydrogen bonding and increases in the bands corresponding to isolated silanol groups are observed (vide infra) [7,9,13,20]. Also, pyridine adsorption has been employed in some cases to quantify the relative amounts of Brønsted and Lewis acid sites [12,15,19]. Hence, the use of FTIR spectroscopy on desilicated zeolites is limited, and in particular, the use of probe molecules, which may give valuable information, is virtually absent. This report is focused on spectroscopic characterization of an H-ZSM-5 zeolite that has been submitted to such post-synthesis treatment in dilute NaOH solutions. A catalyst sample with relatively large crystals of approximately 15 μm and a significant concentration of crystal defects, and therefore a fairly short catalyst lifetime, was specifically chosen in order to monitor structural changes occurring during a catalytic improvement process. CO was employed as a probe molecule to study the acidic properties of the material, and 2,4,6-trimethyl pyridine (collidine), which is too bulky to diffuse into the H-ZSM-5 micropores, was used to study the mesopore formation and accessibility to active sites. This approach of using molecular probes of different sizes has previously been shown to provide valuable information regarding the location of the catalytically active sites in various zeolites [22]. In a previous study [23], we reported the catalytic improvements of desilicated H-ZSM-5 in the well known and industrially relevant methanol-to-gasoline (MTG) reaction [24–26]. The catalyst lifetime, quantified as the total conversion capacity, increased by a factor of 3.3 as a result of the NaOH treatment. Also the product selecitivites were altered substantially and the selectivity towards the gasoline fraction (C_{5+} hydrocarbons) was at best increased by a factor of 1.7. Hydrogen transfer reactions became faster, leading to more aromatic and paraffinic products. In this report, we present extensive spectroscopic characterization of the same catalysts and attempt to correlate the spectroscopy with the improved catalytic properties. By using the abovementioned probe molecules, the formation of mesopores is confirmed and it is shown that the acid strength of the Brønsted sites is unaltered by the treatment and that Lewis acid sites, mainly located on the external surface of the zeolite crystals, are formed as a consequence of desilication.

2. Experimental

H-ZSM-5 was synthesized and modified by NaOH treatment according to previously given procedures [23]. The obtained samples are designated H-ZSM-5-PARENT (parent sample, no NaOH treatment), H-ZSM-5-0.05M (treated with 0.05 M NaOH for 2× 4 h at 75 °C), and H-ZSM-5-0.20M (treated with 0.20 M NaOH for 2× 4 h at 75 °C). These specific samples were transferred into proton form by threefold ion-exchange in 1 M NH_4NO_3 followed by calcination and characterized by N_2-sorption, elemental analysis (ICP-AES), NH_3-TPD, XRD, FTIR (without probe molecules) and for catalytic properties in the MTG reaction in the previous study [23]. In this study, transmission FTIR spectra of the samples in proton form (compressed into self-supporting wafers) were recorded at 2 cm^{-1} resolution using an in-house designed quartz cell (NaCl windows) for operations down to liquid N_2 temperatures (i.e. a nominal temperature of −196 °C). Prior to the experiments, the samples were pretreated for 1 h at 450 °C in vacuum. 2,4,6-trimethylpyridine (collidine) was adsorbed in situ on the samples at room temperature whereas CO was adsorbed after cooling the sampleholder with liquid N_2. The spectra were recorded by a BioRad FTS 80 spectrometer, equipped with a MCT detector. Peak fitting (Fig. 3 only) was performed using the Origin 7.5 peak fitting module and Gaussian line shapes. The center of the bands was located by second order derivative analysis and a close inspection of the obtained residuals.

3. Results and discussion

3.1. FTIR spectra of the pretreated zeolites

In our previous work on alkaline treatment of H-ZSM-5, the key issue was the effects on catalytic properties in the methanol-to-gasoline reaction [23]. A rather thorough physical characterization of the samples based on powder XRD, DRIFTS, N_2 adsorption, and elemental analysis was also reported. In the present contribution, the same set of samples has been studied. The parent zeolite, denoted H-ZSM-5-PARENT, was treated with 0.05 M or 0.20 M NaOH solution giving the samples H-ZSM-5-0.05M and H-ZSM-5-0.20M, respectively. XRD confirmed phase purity and retention of crystallinity after alkaline treatment. Elemental analysis (ICP-AES) revealed the following overall Si/Al ratios: 46 (H-ZSM-5-PARENT), 39 (H-ZSM-5-0.05M) and 27 (H-ZSM-5-0.20M) which confirm the preferred silicon extraction occurring during desilication [9]. N_2 adsorption measurements showed an increase in BET surface area from 313 to 372 (H-ZSM-5-0.05M) and 419 m^2/g (H-ZSM-5-0.20M) as a consequence of the NaOH treatment, and the adsorption data also indicated mesopore formation. The catalytic studies demonstrated that the total conversion capacity of the catalyst (defined as grams of methanol converted per gram of catalyst before complete deactivation) increased by a factor of 3.3 for the most severely treated sample (H-ZSM-5-0.20M). The treatment also led to higher initial activities and a substantial increase in the rate of hydrogen transfer reactions, in particular for H-ZSM-5-0.20M. The obtained results can be rationalized by improved diffusivity resulting from mesopore formation, but the treatment may well change the acid properties of the catalysts, which in turn also can account for higher initial activities and faster hydrogen transfer reactions. Possible changes in acid strength were not addressed at that time, and detailed acidity characterizations of alkaline treated zeolites have not been presented earlier.

In our previous contribution on alkaline treatment of H-ZSM-5, DRIFTS (Diffuse Reflectance Infrared Fourier Transform Spectroscopy) spectra (recorded at room temperature) of the three samples where presented and discussed [23]. In the present study

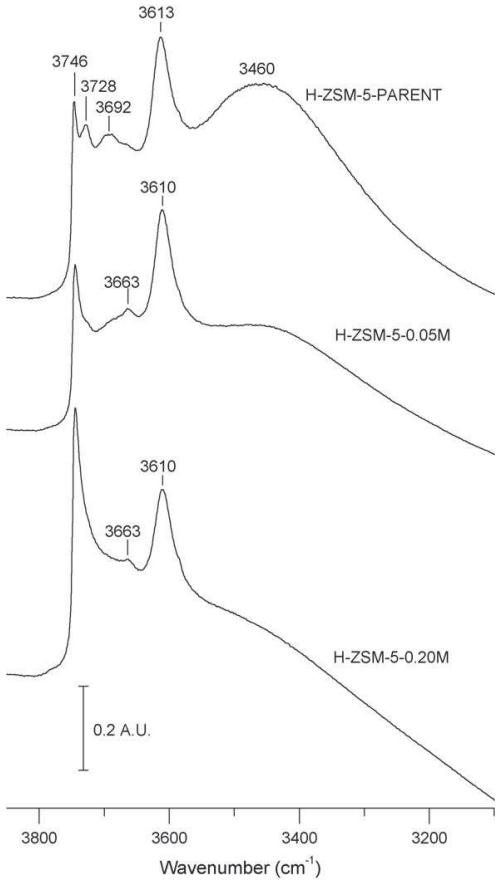

Fig. 1. FTIR spectra (only the ν(OH) region shown) of dehydrated H-ZSM-5-PARENT, H-ZSM-5-0.05M and H-ZSM-5-0.20M. For clarity, the spectra have been shifted along the ordinate. The spectra were recorded at room temperature.

we have chosen to work in transmission mode due to the practical simplicity of performing low temperature (liquid N_2) experiments with this set-up. The transmission spectra of the pretreated zeolites (dehydrated by heating in vacuum) presented here are very similar to the already published DRIFTS spectra and the different features will only be discussed briefly. Fig. 1 shows the ν(OH) modes of the three samples (the intensities have been normalized using the framework overtone at 2010 cm^{-1}). The parent sample has five well-separated bands with the following assignments—(i) 3746 cm^{-1}: virtually isolated Si–OH groups located on the external surface of the zeolite; (ii) 3728 cm^{-1}: weakly perturbed Si–OH sites predominantly located inside the zeolite structure (vide infra). The distinct separation of this peak from the 3746 cm^{-1} peak is normally not observed and is most likely resulting from the relatively large crystal dimensions (an average of 15 μm) and thus the low contribution from external Si–OH sites (3746 cm^{-1}); (iii) 3692 cm^{-1}: same assignment as (ii); (iv) 3613 cm^{-1}: strong Brønsted acid Al(OH)Si sites, hereafter denoted $OH_{Brønsted}$; (v) 3460 cm^{-1}: a variety of internally located Si–OH groups involved in relatively strong hydrogen bonds, *e.g.* so-called silanol nests in which dangling oxygens around a T-site vacancy are saturated by protons. Notice that a zeolite crystal completely free from bulk defects will only have a Si–OH contribution from the external surface where the lattice is terminated (giving the sharp absorption peak at 3746 cm^{-1}). Thus, the remaining Si–OH components located at lower frequencies in Fig. 1 represent various imperfections in the zeolite framework.

As seen from Fig. 1, the NaOH treatment induces some rather clear changes in the ν(OH) region: the 3746 cm^{-1} band increases in intensity relative to the peak representing the $OH_{Brønsted}$ sites (3613/3610 cm^{-1}). The intensity of this peak has previously been correlated with the external surface area and thus the average crystal size of the zeolite [27,28]. Based on this statement, one may claim that the NaOH treatment leads to a substantial reduction in crystallite size. This can, however, not be the case as the SEM images showed no change in crystallite size or morphology after treatment [23]. It is also clear from Fig. 1 that the different Si–OH contributions at the lower frequencies, the 3460 cm^{-1} band in particular, are substantially reduced, implying that the Si–OH sites become more homogeneous and to a much larger extent unperturbed. This means that the defects either are healed (i.e. dissolved Si or Al species are re-inserted into the vacancies originally creating Si–OH nests) or that the defects simply are eroded by NaOH, thus creating an extensive internal surface (e.g. mesopores) that effectively appears like the ordinary external surface with isolated virtually unperturbed Si–OH sites. This latter notion is illustrated in Scheme 1. Scheme 1a represents a crystallite of the parent sample with several internal Si–OH defects in addition to the Si–OH groups located on the external surface. Scheme 1b represents a crystal in which mesopores have been formed and most internal defects have been removed upon alkaline treatment. Thus, Scheme 1 gives a simplified representation of how the number of internal defects may be dramatically reduced whereas the number of unperturbed Si–OH groups may increase when the zeolite is subjected to NaOH desilication. The stability of mordenite towards alkali treatment has previously been addressed, though in a different context [29]. Decreased alkali resistance was observed for defect rich crystals when compared to crystals with a perfect framework.

The NaOH treatment also generates extra lattice Al–OH groups, giving rise to the rather small component at 3663 cm^{-1} seen for the treated samples. The 3746 cm^{-1} peak of H-ZSM-5-0.20M also has a barely discernible high frequency shoulder around 3780 cm^{-1} which previously has been associated with the ^{27}Al NMR resonance of octahedral extra framework Al [30]. Others have linked the 3780 cm^{-1} band in the beta zeolite to tri-coordinated Al connected to the framework [31]. In any case, these observations point to incipient dealumination as a result of the alkaline treatment and based on elemental analyses of the filtrate and pyridine adsorption experiments, Ogura et al. indeed found a minor dealumination of H-ZSM-5 upon the NaOH treatment [15]. The 3663 cm^{-1} band is also known to appear after steam treatment of ZSM-5 [32–34]. Extraction of framework Al is often accompanied by generation of Lewis acidity and this will be further elaborated in Section 3.2.

The FTIR spectra of the dehydrated H-ZSM-5 samples are valuable for following the major changes in surface OH groups and dealumination resulting from the NaOH treatment. The limitation is, however, the complete lack of information concerning possible changes in the acid strength, generation of Lewis acidity, the site localization (internally vs. externally) and accessibility. Such information may be decisive for understanding the observed changes in catalytic behaviour of the samples.

3.2. Acid strength measured by FTIR using CO as molecular probe

The acid strength of zeolites is intimately linked to their catalytic properties with respect to activity, deactivation rate and product selectivity. As already mentioned, in our previous work on the MTG reaction we found that the initial activity and, in particular, the hydrogen transfer activity could be improved substantially by NaOH treatment. An increased hydrogen transfer

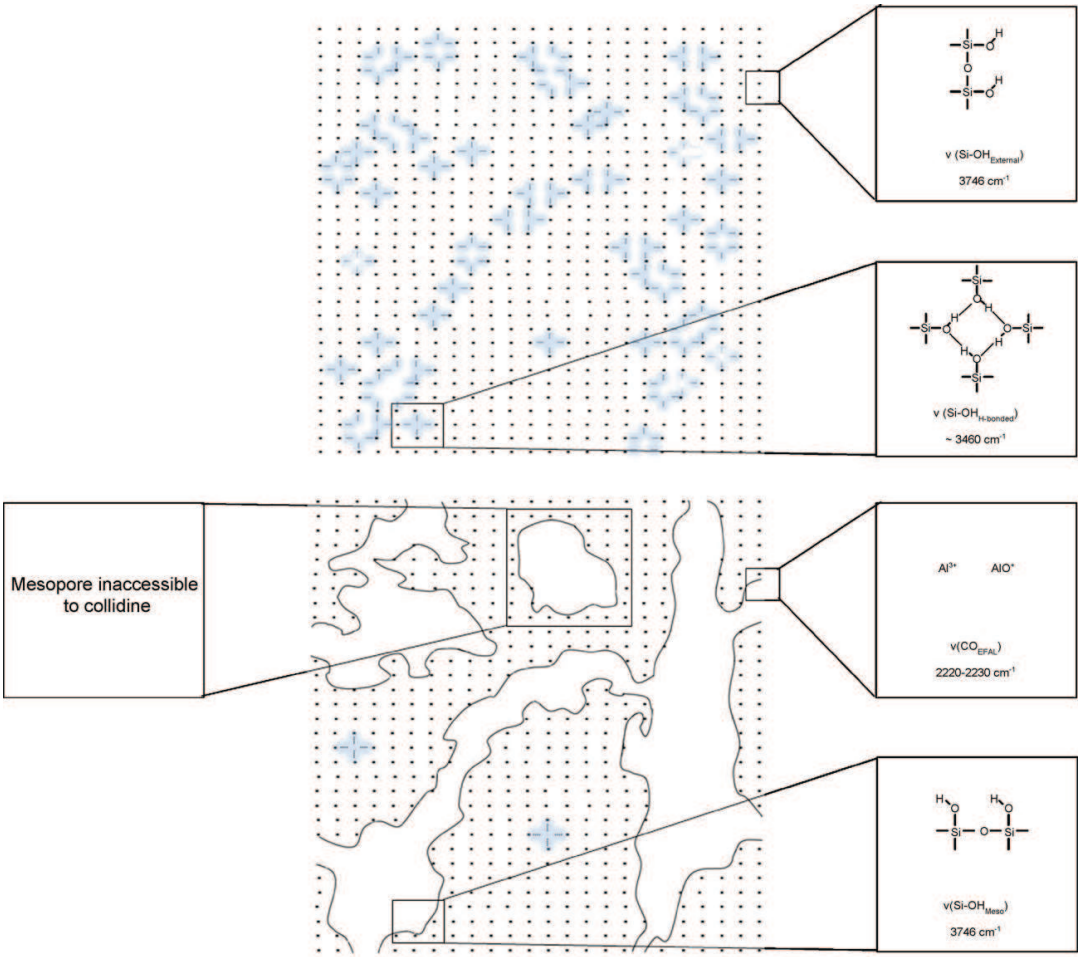

Scheme 1. Schematic illustration of a possible route to mesopore formation following desilication. (a) Structural defects distributed throughout the zeolite. (b) Mesopore formation as a consequence of preferential framework dissolution near crystal defects. Aluminium based Lewis acidic sites are detected mainly in mesopores/external surface where it is accessible to collidine.

activity gives higher yields of saturated aliphatics and aromatics, and less alkenes in the product stream. Several previous reports have suggested a link between hydrogen transfer activity and zeolite acid strength [35,36]. Likewise, also cracking reactions are suggested to be promoted by increasing acid strength [37]. Thus, a possible explanation for our previous observations is an increased acid strength of the $OH_{Brønsted}$ sites.

The acid strength of solid acids, such as protonated zeolites, has to be measured indirectly by assessing the interaction strength between an adsorbed basic probe and the solid [38]. For this purpose, temperature programmed desorption of basic molecules is routinely employed, but the major drawbacks are relatively poor resolution and that Brønsted and Lewis sites are indistinguishable. Here, we have studied the relative interaction strengths between CO and the acid sites of the three zeolites by FTIR spectroscopy. CO is a weakly basic probe molecule which is adsorbed end-on through the carbon on polarizing sites that in our case are represented by protons. The OH···CO acid/base adducts that are formed upon adsorption will feature perturbed ν(O–H) and ν(C≡O) modes and accordingly their vibrational frequencies will be shifted. The O–H bond will be weakened and the vibrational frequency will thus shift towards lower frequencies (red-shifted). On the other hand, the CO triple bond will be strengthened by electron donation from the slightly antibonding 5σ orbital and the vibrational frequency will therefore be blue-shifted. The magnitude of these frequency shifts is proportional to the OH/CO interaction strength, and thus proportional to the Brønsted acid strength of the zeolite. As opposed to CO, strongly basic probe molecules such as pyridine will induce proton transfer from a wide range of OH groups and thus not have the same ability to discriminate between sites of different acidity.

After having recorded the spectra presented in Fig. 1, the samples were cooled to liquid N_2 temperature (−196 °C nominal) and the CO coverage on the zeolites was changed stepwise. Fig. 2 shows the obtained series of spectra 1–11 in the ν(OH) region (left part) and in the ν(CO) region (right part) for the three samples. Spectrum 11 represents the highest CO coverage for all three samples. The spectra are all presented as difference plots, i.e. the spectra of the corresponding pretreated zeolites have been subtracted from spectra 1 to 11. Thus, positive contributions in Fig. 2 represent peaks that are growing as a result of CO adsorption, whereas negative contributions represent peaks that are reduced in intensity upon CO adsorption. The grey bold-drawn spectrum at intermediate CO loading (spectrum 5 in each series) represents the

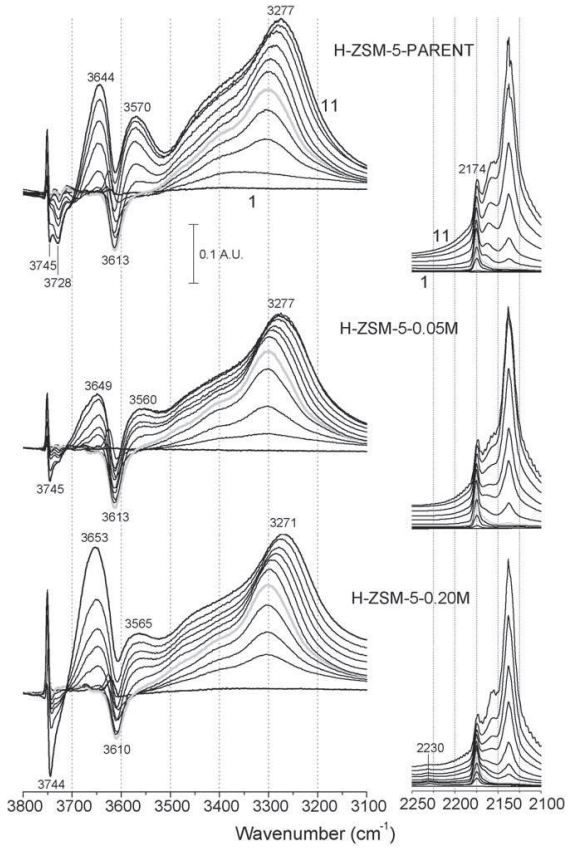

Fig. 2. FTIR difference spectra of dehydrated H-ZSM-5-PARENT, H-ZSM-5-0.05M and H-ZSM-5-0.20M following CO adsorption at −196 °C. Left panel: the ν(OH) region; right panel: the ν(CO) region. The CO coverage increases successively from spectra 1 to 11 in each series.

highest CO pressure where the weakly acidic Si-OH sites still are virtually unperturbed. At this CO pressure, the major part of the $OH_{Brønsted}$ sites have been consumed, i.e. formed adducts with CO. Notice that the sharp positive contribution at the highest frequency (3750 cm^{-1} for all three samples) is related to a temperature effect and should not be considered as a feature arising from the interaction between the zeolites and CO. A small blue-shift upon cooling has also been reported earlier [39].

For all three samples, the strongly acidic $OH_{Brønsted}$ sites are consumed first (at the lowest CO pressures), giving the negative band at 3613 cm^{-1} (3610 cm^{-1} for H-ZSM-5-0.20M) in Fig. 2. The formation of $OH_{Brønsted}\cdots CO$ adducts leads to a red-shift of the $\nu(OH)_{Brønsted}$ mode to 3300 cm^{-1} at intermediate CO loadings (spectrum 5) for all three samples. This equals a frequency shift of around −310 cm^{-1}. A significant enhancement in acid strength as a result of the NaOH treatment would have increased the red-shift of the entire band or generated a downside shoulder below 3300 cm^{-1} if only certain sites were affected. The magnitude of this shift (310 cm^{-1}) is representative for H-ZSM-5 [38] and the acid strength distribution of the $OH_{Brønsted}$ sites seems to be unaffected by the increasing NaOH treatment. The high frequency shoulder around 3450–3400 cm^{-1} is ascribed to perturbed OH groups of extra framework Al originally absorbing at 3663 cm^{-1} (Fig. 1). The OH groups represented by this band have previously been reported to red-shift 220–200 cm^{-1} upon CO adsorption [34,35,40]. A further increase in CO pressure (spectra 6–11) progressively shifts the $\nu(OH_{Brønsted})$ frequency to 3280–3270 cm^{-1} due to multilayered CO adsorption [41]. The increasing CO pressure also leads to erosion of the ν(OH) vibrations of the weakly acidic Si-OH components at the higher frequencies and for the parent sample two clearly distinct negative bands appear at 3745 and 3728 cm^{-1} whereas the two corresponding bands with maxima at 3644 and 3570 cm^{-1} grow in a parallel manner. These features are somewhat similar for the NaOH treated samples, but the band seen at 3570 cm^{-1} for the parent sample becomes considerably less prominent. This is most likely because the 3570 cm^{-1} band predominantly represents the Si-OH groups originally located in the 3730–3690 cm^{-1} frequency range (Fig. 1), and as we have seen these sites nearly vanish upon NaOH treatment.

The spectra representing the ν(CO) mode are displayed in the right part of Fig. 2. Starting from the lowest CO coverages, a component is clearly visible at 2174 cm^{-1} for all three samples. A blue-shift of 36 cm^{-1} compared to the free molecule (ν(CO) liquid-like 2138 cm^{-1}) confirms the expected strong polarization of CO by the adsorbing sites. The component at 2174 cm^{-1} is ascribed to CO adsorbed on the $OH_{Brønsted}$ sites, and the blue-shift of the ν(CO) mode is identical for the three samples due to their very similar acid strengths. Higher CO pressures lead to interactions between CO and Si-OH groups, giving a component with a maximum around 2160 cm^{-1}. Finally, the formation of a condensed phase (liquid-like CO) results in the growth of a strong absorption at 2138 cm^{-1}. The most severely treated sample (H-ZSM-5-0.20M) also shows a rather weak component at 2230 cm^{-1} not discernible for the parent sample and only barely visible for H-ZSM-5-0.05M upon magnification. This band is commonly attributed to CO adsorbed on strong Lewis acidic sites. The 2230 cm^{-1} band is weak, but it should be kept in mind that the extinction coefficient of CO has been suggested to be diminished by the adsorption on Lewis sites compared to adsorption on $OH_{Brønsted}$. This decrease in extinction coefficient is explained by the enhanced electron donation from CO to the Lewis site which in turn will reduce the dynamic dipole moment and thereby also the extinction of the IR light. The ratio between the two extinction coefficients ($\varepsilon(CO_{Lewis})/\varepsilon(CO_{Brønsted})$) has been reported to be as high as 0.32 [42], and the concentration of Lewis sites relative to the concentration of Brønsted sites may therefore not be negligible. Fig. 3 shows a magnification (spectrum 5 from H-ZSM-5-0.20) of the peak with a maximum at 2230 cm^{-1}. Obviously, this band is composed of at least two components and peak fitting suggest two maxima at 2230 and 2220 cm^{-1}. The sum of the two components gives a curve which is superimposed on the recorded data (dotted curve). Moreover, neither the residuals nor the second order derivative analysis indicated any further significant contributions. Two maxima around 2230 and 2220 cm^{-1} have been reported previously, but their exact assignments are still uncertain [33]. It is generally accepted that the Lewis sites in zeolites are associated with extra framework Al species. It is likely that the presence of such species affects the catalytic properties of the zeolite. The exact structure of these extra framework Al species is, however unknown, but the neutral species AlOOH and $Al(OH)_3$, $(Al(OH)_3)_2$ and oxoaluminium cations such as AlO^+, $Al(OH)_2^+$ and $Al(OH)^{2+}$ have been proposed. In our case, we obviously have (at least) two Lewis sites with a significant different ability to polarize CO (Fig. 3). Based on FTIR and quantum chemical modelling, Brand et al. suggested that the bands at 3787 and 3666 cm^{-1} (close to our observed bands at 3782 and 3663 cm^{-1}) can be assigned to terminal and bridging OH groups in dimeric $(Al(OH)_3)_2$ species. Also, Fleisher et al. found that the ^1H NMR chemical shift of the bridging protons in the $(Al(OH)_3)_2$ species is in the range assigned to OH groups associated with extra framework Al species [43].

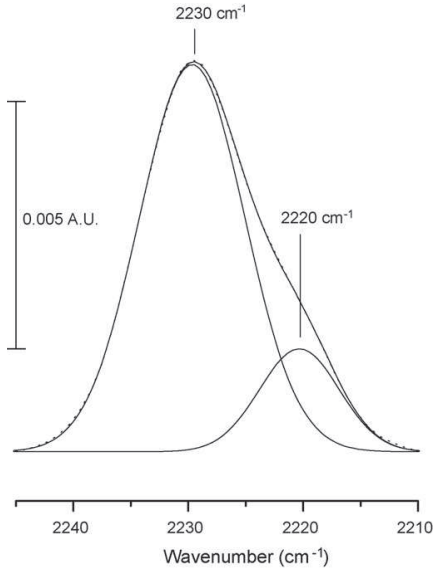

Fig. 3. Magnification and peak analysis of the ν(CO) band generated from interaction of CO with the strong Lewis acid sites present in sample H-ZSM-5-0.20M. The dotted curve represents the sum of the two peak components and is superimposed on the recorded spectrum.

The exact role of Lewis sites in zeolites is still debated, but it has been claimed for a while that they may increase the Brønsted acidity through so-called Brønsted–Lewis synergisms. Li et al. reported very recently that the preferred Lewis acid sites in dealuminated Y zeolite ($Al(OH)_3$ and $Al(OH)^{2+}$ species) may coordinate to the oxygen nearest the framework Al and enhance the Brønsted acidity of the zeolite [44]. In contrast to this, other recent works have stated that Lewis sites are not necessarily increasing the Brønsted acid strength through the above-mentioned synergism, but rather by stabilizing the conjugated base (negatively charged deprotonated zeolite) by hydrogen bonding and electrophilic interaction with the framework oxygen atom [45]. Other more subtle effects may also come into play when reactant molecules are present, and Brunner et al. showed by MAS NMR that the enhanced activity for hexane cracking obtained by a mild hydrothermal dealumination of ZSM-5 is not due to an enhanced Brønsted acidity, but rather due to the interaction of hexane with a bridging OH group and extra framework Al species [46]. Thus, apart from possibly increasing the Brønsted acidity, it also seems likely that Lewis sites indeed may facilitate hydride abstraction and thus promote hydrogen transfer reactions by providing positive charge. As the NaOH treatment also leads to some change in overall Si/Al ratio it is, however, difficult to confidently assess the exact role (if any) of the Lewis sites from the present results.

3.3. The localization of acid sites studied by FTIR and 2,4,6-trimethylpyridine (collidine) as molecular probe

The CO experiments have provided information about the acid strength and the presence of Lewis acid sites in the samples. However, as CO is a small probe molecule it does not give any information about the localization of the different sites in the ZSM-5 samples. Sterically demanding probe molecules, such as alkylated benzenes and pyridines, which are unable to penetrate certain parts of the microporous system in zeolites, have been used earlier for probing the accessibility of different sites in zeolites [47,48]. Due to the sterically restrictive micro channels of ZSM-5, it is unlikely that traditional polyaromatic coke species can be formed inside these channels and the external surface of H-ZSM-5 has previously been suggested to be the culprit for the catalyst deactivation in the MTG reaction [49]. It may therefore be of interest to examine the external acidity and the possible changes thereof as a result of NaOH treatment. Furthermore, it is also of interest to study the localization of the Lewis acid sites that are generated during the NaOH treatment. Thus, we have employed collidine, which is expected not to enter the internal voids of H-ZSM-5, as a probe molecule in order to characterize the external sites of the crystals.

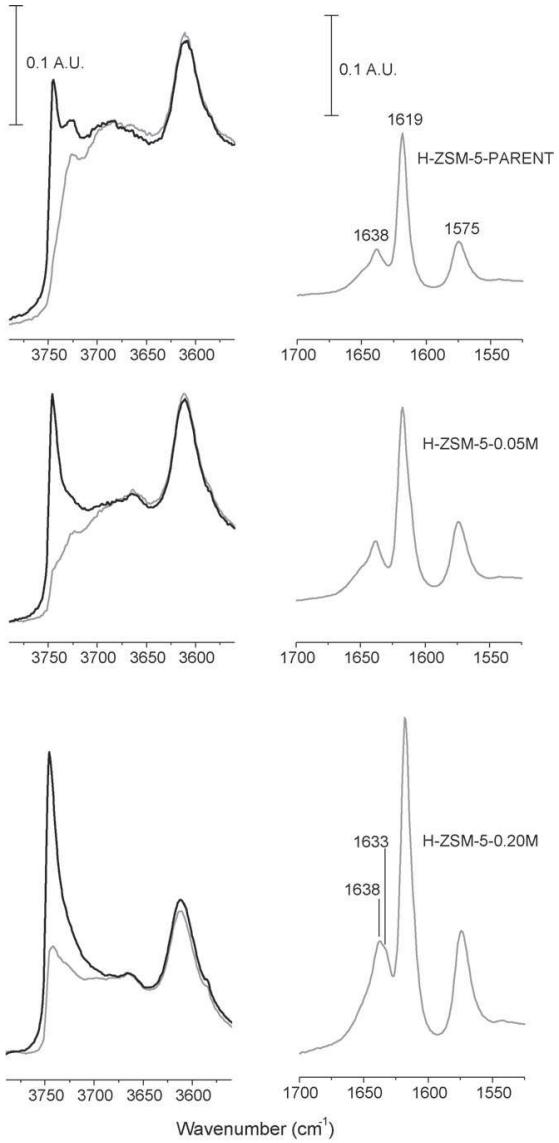

Fig. 4. FTIR spectra of dehydrated H-ZSM-5-PARENT, H-ZSM-5-0.05M and H-ZSM-5-0.20M. Left panel: spectra of the samples in the ν(OH) region before (black curves) and after (grey curves) collidine saturation. Right panel: difference spectra of the collidine saturated samples in the region covering the ring modes of collidine. The spectra were recorded at room temperature.

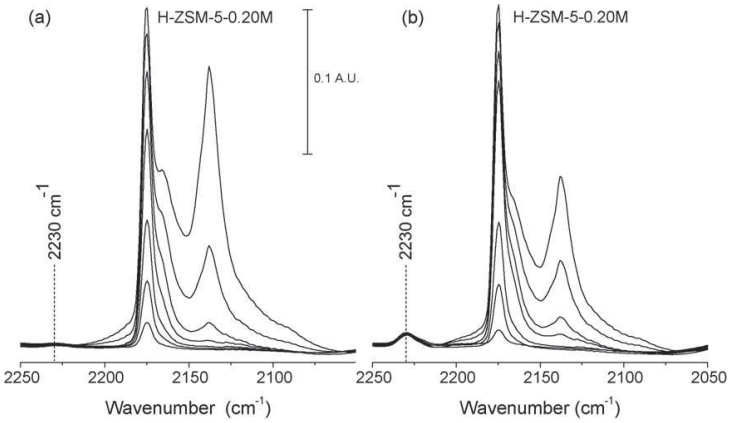

Fig. 5. FTIR difference spectra of CO adsorption at −196 °C on: (a) dehydrated H-ZSM-5-0.20M saturated by collidine, and (b) dehydrated H-ZSM-5-0.20M.

Collidine vapour was allowed to saturate the pretreated samples in the FTIR cell at room temperature. Fig. 4 presents the spectra of the pretreated zeolites (black spectra) and after collidine adsorption (grey spectra) for the three samples. The left part of Fig. 4 illustrates the effect of collidine adsorption on the ν(OH) region, whereas the right part represents the different vibration modes of collidine (difference spectra). For the parent sample, the 3746 cm^{-1} band is strongly reduced in intensity upon collidine dosage. This is in compliance with previous reports which have assigned this band to Si-OH sites located on the external surface of the crystals. The remaining bands of the parent sample are virtually unaffected, implying that the corresponding sites are located inside the micropore system. The desilicated samples act in a similar way as the parent sample in the ν(OH) region, but interestingly, a substantial part of the free Si-OH sites (3746 cm^{-1}) is not accessible for collidine. This tendency increases with treatment strength and is most pronounced for H-ZSM-5-0.20M. This supports our assumption that a significant part of the Si–OH sites that are created by the NaOH treatment is localized in mesopores, and not on the actual external surface where they would have been accessed by collidine instantaneously (Scheme 1). Why some of the sites located in the mesopores are difficult to reach for collidine cannot be confidently assessed. However, one possibility is that a part of the mesoporous system is located inside the zeolite crystals and is surrounded by a micoporous system, consequently making them unavailable for collidine as indicated in Scheme 1. The high frequency ν(OH) region of the desilicated samples also show that upon collidine dosage, the otherwise invisible/hidden peak at 3727 cm^{-1} appear, proving that these sites are still present after NaOH treament and that they are the major cause of the 3746 cm^{-1} tailing. The collidine experiments can also give us some information regarding the localization of the extralattice Al–OH species. The 3663 cm^{-1} band maintains its intensity and shape after collidine adsorption. From this information one can naturally not conclude that these sites are not distributed throughout the crystal with a minor part at the surface, analogue to the ordinary Brønsted sites, but it is clear that these sites are not only a surface phenomena since the majority of them are not able to interact with collidine.

In the region representing collidine vibrations (right part of figure), the bands at 1619 and 1575 cm^{-1} represent collidine adsorbed on Si-OH sites. Collidine adsorbed on Brønsted sites gives the band at 1638 cm^{-1} [50]. Also here, the three samples behave somewhat similar but some differences should be underlined. The H-ZSM-5-0.20M sample shows a distinct low frequency shoulder to the 1638 cm^{-1} band. This is most likely due to adsorption on external Lewis acid sites, which should give absorption at 1633 cm^{-1} [50]. A further exploration of these Lewis sites was facilitated by CO adsorption on the collidine saturated samples. Fig. 5a shows the spectra of the H-ZSM-5-0.20M sample in the CO stretching region. CO is adsorbed (at liquid N_2 temperature) subsequent to collidine saturation. Fig. 5b is included for comparison and shows the same region of the H-ZSM-5-0.20M sample after only CO adsorption. Clearly, the 2230 cm^{-1} band in Fig. 5a, representing CO on Lewis acid sites, has virtually vanished as a consequence of collidine saturation. From the characteristic bands in Fig. 5b, e.g. the Brønsted absorption at 2174 cm^{-1} it is apparent that CO has full access to the bulk crystal after collidine dosage. These observations allow us to conclude that the Lewis acid sites that are represented by the 2230 cm^{-1} absorption of CO are predominantly generated on the external surface of the desilicated sample (Scheme 1) where they may be accessed by bulky molecules such as collidine.

The direct effect of surface based Lewis acidity in the MTG reaction is at present unclear. However, this acidity may be significant since the surface sites are excluded from shape selective restraints which in turn could affect product selectivity as well as surface deactivation by coke formation.

4. Conclusions

The improved catalytic activity previously observed for a ZSM-5 zeolite treated with NaOH is possibly related to mesopore formation and changes in acidity occuring during such a treatment. This study shows that the zeolite defects represented by internal Si–OH sites (e.g. silanol nests) are removed upon NaOH treatment. In a parallel manner, free Si–OH sites, typically located on the external surface of the zeolite crystals, increase in concentration. A closer examination, carried out by using a sterically demanding probe molecule (collidine), suggested that a significant part of these sites may be located in mesoporous domains that are surrounded by a microporous framework, thus making the sites inaccessible for the sterically demanding probe molecule. Furthermore, our results point to a selective mechanism for formation of mesopores as the framework dissolution preferentially takes place at defective sites in the crystallites. It is also shown that the acid strength of the ordinary Si(OH)Al Brønsted sites, as measured by FTIR and CO adsorption at liquid N_2 temperature, is virtually unaffected by the alkaline leaching procedure. However, both CO and collidine adsorption reveals

incipient dealumination, leading to strong Lewis acidity. The major part of the thus created Lewis sites can be accessed by collidine, implying that the sites are located on the external surface of the zeolite crystals.

The suggested Brønsted–Lewis acid synergism is thus unlikely to be the cause of the improved lifetime and higher HTI observed in the desilicated samples.

References

[1] C. Baerlocher, W.M. Meier, D.H. Olson, Atlas of Zeolite Framework Types, Elsevier, Amsterdam, 2001, p. 184.
[2] M. Hartmann, Angew. Chem. Int. Ed. 43 (2004) 5880.
[3] J.C. Groen, J.A. Moulijn, J. Pérez-Ramírez, J. Mater. Chem. 16 (2006) 2121.
[4] K. Egeblad, C.H. Christensen, M. Kustova, C.H. Christensen, Chem. Mater. 20 (2008) 946.
[5] J.C. Groen, J.A. Moulijn, J. Pérez-Ramírez, Ind. Eng. Chem. Res. 46 (2007) 4193.
[6] J.C. Groen, L.A.A. Peffer, J.A. Moulijn, J. Pérez-Ramírez, Colloid Surf. A 241 (2004) 53.
[7] J.C. Groen, J.C. Jansen, J.A. Moulijn, J. Pérez-Ramírez, J. Phys. Chem. B 108 (2004) 13062.
[8] J.C. Groen, T. Bach, U. Ziese, A.M. Paulaime-van Donk, K.P. de Jong, J.A. Moulijn, J. Pérez-Ramírez, J. Am. Chem. Soc. 127 (2005) 10792.
[9] J.C. Groen, J.A. Moulijn, J. Pérez-Ramírez, Micropor. Mesopor. Mater. 87 (2005) 153.
[10] J.C. Groen, W. Zhu, S. Brouwer, S.J. Huynink, F. Kapeijn, J.A. Moulijn, J. Pérez-Ramírez, J. Am. Chem. Soc. 129 (2007) 355.
[11] J.C. Groen, L.A.A. Peffer, J.A. Moulijn, J. Pérez-Ramírez, Chem. Eur. J. 11 (2005) 4983.
[12] X. Wei, P.G. Smirniotis, Micropor. Mesopor. Mater. 97 (2006) 97.
[13] J.C. Groen, T. Sano, J.A. Moulijn, J. Pérez-Ramírez, J. Catal. 251 (2007) 21.
[14] J.C. Groen, S. Abelló, L.A. Villaescusa, J. Pérez-Ramírez, Micropor. Mesopor. Mater. 114 (2008) 93.
[15] M. Ogura, S.-Y. Shinomiya, J. Tateno, Y. Nara, M. Nomura, E. Kikuchi, M. Matsukata, Appl. Catal. A 219 (2001) 33.
[16] L. Su, L. Liu, J. Zhuang, H. Wang, Y. Li, W. Shen, Y. Xu, X. Bao, Catal. Lett. 91 (2003) 155.
[17] Y. Song, C. Sun, W. Shen, L. Lin, Catal. Lett. 109 (2006) 21.
[18] J.S. Jung, J.W. Park, G. Seo, Appl. Catal. A 288 (2005) 149.
[19] Y. Song, X. Zhu, Y. Song, Q. Wang, L. Xu, Appl. Catal. A 302 (2006) 69.
[20] G. Lietz, K.H. Schnabel, Ch. Peuker, Th. Gross, W. Storek, J. Völter, J. Catal. 148 (1994) 562.
[21] D. Ohayon, R. Le Van Mao, D. Ciaravino, H. Hazel, A. Cochennec, N. Rolland, Appl. Catal. A 217 (2001) 241.
[22] T. Montanari, M. Bevilacqua, G. Busca, Appl. Catal. A 307 (2006) 21.
[23] M. Bjørgen, F. Joensen, M.S. Holm, U. Olsbye, K.-P. Lillerud, S. Svelle, Appl. Catal. A 345 (2008) 43.
[24] C.D. Chang, Catal. Rev. 25 (1983) 1.
[25] J. Topp-Jørgensen, Stud. Surf. Sci. Catal. 36 (1988) 293.
[26] M. Støcker, Micropor. Mesopor. Mater. 29 (1999) 3.
[27] G. Qin, L. Zheng, Y. Xie, C. Wu, J. Catal. 95 (1985) 609.
[28] B.-L. Su, V. Norberg, Zeolites 19 (1997) 65.
[29] B. Lu, T. Tsuda, Y. Oumi, K. Itabashi, T. Sano, Micropor. Mesopor. Mater. 76 (2004) 1.
[30] I. Kiricsi, C. Flego, G. Pazzuconi, W.O. Parker, R. Millini, C. Perego, G. Bellussi, J. Phys. Chem. 98 (1994) 4627.
[31] A. Vimont, F. Thibault-Starzyk, J.C. Lavelley, J. Phys. Chem. B 104 (2000) 286.
[32] S.M. Campbell, D.M. Biddy, J.M. Coddington, R.F. Howe, R.H. Meinhold, J. Catal. 161 (1996) 338.
[33] H.V. Brand, A. Redondo, P.J. Hay, J. Mol. Catal. A 121 (1997) 45.
[34] J. Szanyi, M.T. Paffett, Micropor. Mater. 7 (1996) 201.
[35] A. Platon, W.J. Thomson, Catal. Lett. 101 (2005) 15.
[36] C.J.A. Mota, P.M. Esteves, M.B. deAmorim, J. Phys. Chem. 100 (1996) 12418.
[37] O. Bortnovsky, P. Sazama, B. Wichterlova, Appl. Catal. A 287 (2005) 203.
[38] C. Pazé, S. Bordiga, C. Lamberti, M. Salvalaggio, A. Zecchina, J. Phys. Chem. B 101 (1997) 4740.
[39] S. Bordiga, P. Ugliengo, A. Damin, C. Lamberti, G. Spoto, A. Zecchina, G. Spanò, R. Buzzoni, L. Dalloro, F. Rivetti, Top. Catal. 15 (2001) 43.
[40] A. Zecchina, S. Bordiga, G. Spoto, D. Scarano, G. Petrini, G. Leofanti, M. Padovan, C.O. Arean, J. Chem. Soc., Faraday Trans. 88 (1992) 2959.
[41] A. Zecchina, C.O. Areán, G.T. Palomino, F. Geobaldo, C. Lamberti, G. Spoto, S. Bordiga, Phys. Chem. Chem. Phys. 1 (1999) 1649.
[42] F. Wakabayashi, J.N. Kondo, K. Domen, C. Hirose, J. Phys. Chem. 99 (1995) 10573.
[43] U. Fleischer, W. Kutzelnigg, A. Bleiber, J. Sauer, J. Am. Chem. Soc. 115 (1993) 7833.
[44] S. Li, A. Zheng, Y. Sul, H. Zhang, L. Chen, J. Yang, C. Ye, F. Deng, J. Am. Chem. Soc. 129 (2007) 11161.
[45] C.J.A. Mota, D.L. Bhering, N. Rosenbach, Angew. Chem. Int. Ed. 43 (2004) 3050.
[46] E. Brunner, H. Ernst, D. Freude, T. Fröhlich, M. Hunger, H. Pfeifer, J. Catal. 127 (1991) 34.
[47] S.H. Baeck, K.M. Lee, W.Y. Lee, Catal. Lett. 52 (1998) 221.
[48] N.S. Nesterenko, F. Thibault-Starzyk, V. Montouillout, V.V. Yushchenko, C. Fernandez, J.-P. Gilson, F. Fajula, I.I. Ivanova, Kinet. Catal. 47 (2006) 40.
[49] M. Bjørgen, S. Svelle, F. Joensen, J. Nerlov, S. Kolboe, F. Bonino, L. Palumbo, S. Bordiga, U. Olsbye, J. Catal. 249 (2007) 195.
[50] F. Thibault-Starzyk, A. Vimont, J.-P. Gilson, Catal. Today 70 (2001) 227.

DOI: 10.1002/ejic.200801194

"One-Pot" Ion-Exchange and Mesopore Formation During Desilication

Martin Spangsberg Holm,*[a,b] Martin Kalmar Hansen,[a] and Claus Hviid Christensen*[b]

Keywords: Zeolites / Mesoporous materials / Desilication / Ion exchange

A desilication protocol using tetramethylammonium hydroxide was applied to zeolite beta. The new route presented here integrates the desilication and ion-exchange post-treatment steps allowing for a subsequent ion-exchange step to be avoided. It is shown that the acidic and highly mesoporous zeolite is obtained directly upon calcination. Thus, careful choice of base and post-treatment conditions lead to the fabrication of a hierarchical *meso-* and microporous structure with completely retained crystallinity.

Introduction

Zeolites are microporous crystalline materials composed of tetrahedral oxides of silicon and aluminum. The framework is formed through corner sharing of the oxygen atoms giving rise to a multitude of structures.[1] The micropore diameters of the zeolite structures are in the range of small organic molecules, which cause the molecular sieves ability and allow for shape selective catalysis. Slow molecular transport through the microporous channels may however limit the applicability of zeolites as catalysts.[2] Various strategies for introducing mesoporosity are now available to overcome this limitation by producing hierarchical zeolite materials.[3] Well known protocols include dealumination,[4] templating[5] and desilication.[6] Recently, several studies in which desilication is applied to the widely used high-silica zeolite ZSM-5 have been published.[7] Additional zeolite structures e.g. beta,[8] ZSM-12[9] and mordenite[10] have also been investigated. Sodium hydroxide and/or sodium carbonate[11] are the typical bases applied, although lithium hydroxide and potassium hydroxide have proven useful as well.[12] Adjustment of temperature, amount of base, and duration of the treatment are effective tools for controlling the extent of mesopore formation. However, even surprisingly mild conditions applied in attempts to desilicate zeolite beta with a mineral base were unable to create mesoporosity without seriously deteriorating the crystal structure.[8] In addition, use of mineral bases causes ion-exchange of the zeolite into the alkali form. This highlights two inherent shortcomings of the use of strong inorganic bases in the desilication protocol.Here, we use tetramethylammonium hydroxide (TMAOH in the following) as the desilicating agent, and show that it leads to several interesting advantages. A "one-pot" desilication and ion-exchange procedure as reported here gives a procedure in which a subsequent ion-exchange step transforming the zeolite into proton form is avoided. This is possible since the charge compensating TMA^+ ions in the zeolite framework decomposes during calcination to give the proton form. TMAOH was specifically chosen as the organic base due to its inherent strong basicity and the relative small size of the TMA^+ cation. Mesopore formation using TMAOH was studied as a function of treatment time, temperature, and base amount. The extent of the simultaneous ion-exchange was monitored by NH_3-TPD and FT-IR.

[a] Center for Sustainable and Green Chemistry, Department of Chemistry, Technical University of Denmark, Building 206, 2800 Lyngby, Denmark
[b] Haldor Topsoe A/S, Nymøllevej 55, 2800 Lyngby, Denmark
E-mail: chc@topsoe.dk

Results and Discussion

A zeolite beta was synthesized by the fluoride route with a nominal Si/Al ratio of 35. This aluminum content has previously been identified as within the optimal range for desilication of ZSM-5.[13] The crystalline zeolite beta was initially ion-exchanged into the sodium form to allow the transformation from Na-form into H-form to occur during post-treatment. The series of desilications were performed according to the conditions listed in Table 1. The desilication conditions were chosen to investigate the effect on mesopore formation arising from temperature, time and TMAOH amount present.

Figure 1 presents the XRPD diffractograms of the parent sample along with the most severely desilicated samples chosen from Table 1. The parent sample is identified as highly crystalline zeolite beta which is also supported by a t-plot derived micropore volume of 0.202. Further it is seen from Figure 1, that all samples desilicated using TMAOH (samples 4, 7, 11) preserve crystallinity. A mild treatment using NaOH as the desilication agent instead of TMAOH was included for comparison (sample 12). In contrast to samples 1–11, sample 12 has lost almost all crystallinity as

Table 1. Treatment conditions and physical-chemical data.

Sample	TMA media [mmol/g]	Time [h]	Temp. [°C]	TMA^+/Na^+ ratio[a]	S_{BET} [m^2/g]	S_{meso} [m^2/g]	V_{meso} [mL/g] ($P_{0.99} - V_{micro}$)	V_{micro} [mL/g]	Acidity[b] [mmol/g]	Exchange level[c]
Parent	–	–	–	–	539	66	–	0.202	0.21	–
1	10	1/2	65	20	551	93	≈ 0	0.205	0.21	0.82
2	10	2	65	20	561	114	0.076	0.198	0.24	0.91
3	10	4	65	20	585	125	0.150	0.201	0.24	1.00
4	10	6	65	20	599	140	0.173	0.197	0.24	1.02
5	10	2	50	20	531	95	≈ 0	0.194	0.22	0.82
6	10	2	80	20	601	141	0.193	0.196	0.24	1.07
7	10	2	100	20	696	266	0.364	0.186	0.28	1.10
8	2.5	2	65	5	540	106	0.034	0.193	0.23	0.97
9	5	2	65	10	563	118	0.084	0.197	0.23	1.04
10	20	2	65	40	560	107	0.083	0.200	0.24	0.86
11	50	2	65	100	559	106	0.045	0.203	0.23	0.71
12	10 (NaOH)	1/2	65	–	787	489	0.304	0.081	–	–

[a] Approximate value assuming one sodium ion per Al atom and a zeolite with Si/Al ratio of 35. [b] NH_3-TPD of the ion-exchanged material. [c] Ratio between the integrated area of the NH_3-desorption curve before and after ion-exchange.

seen from Figure 1, which is also indicated by a diminished micropore volume of only 0.081 mL/g. This is in agreement with results published recently on desilication of zeolite beta using NaOH.[8] The mesopore formation using TMAOH progresses slower than what is typically observed for desilication using NaOH.[8,14] Extending treatment time from 1/2 hour to as much as 6 h allows for continuous mesopore evolution as can be seen from the textural data in Table 1 (samples 1–4). A gradual increase in the mesopore volume V_{meso} and the mesopore surface area S_{meso} are thus observed as a function of treatment time. Isotherms and the BJH-derived pore size distributions for samples parent, 1–4, and 12 are given in Figure 2. Sorption data from sample 12 which was desilicated by NaOH are included in Figure 2. The isotherms from sample 12 do neither resemble a type I isotherm as is typical seen for a microporous materials nor one for a combined micro- and mesoporous material as can be seen for the TMAOH-desilicated samples. This observation correlates well with the results obtained from XRD analysis indicating that a partial framework collapse occur when using NaOH but can be avoided by using TMAOH.

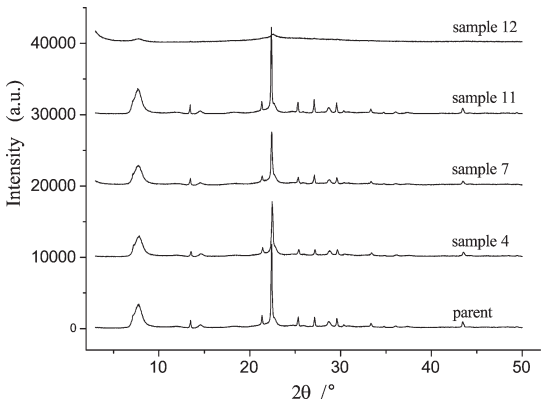

Figure 1. XRPD diffractograms of selected samples from Table 1. Diffractograms are offset by 10000 units for illustrative purposes.

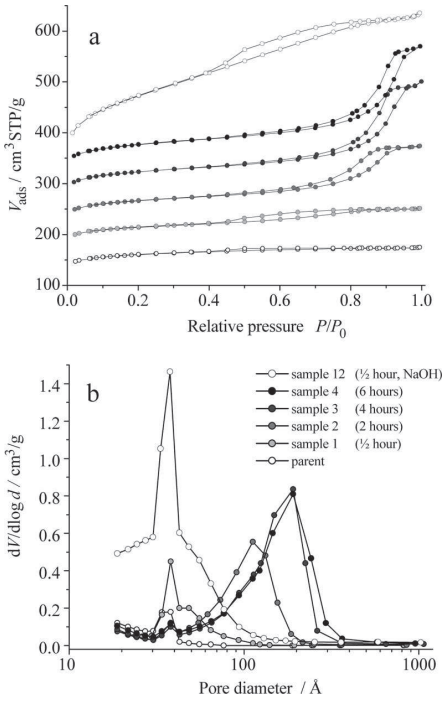

Figure 2. (a) N_2-adsorption/desorption isotherms of samples 1–4 and 12. Isotherms are offset by 50 units for illustrative purposes. (b) BJH-derived pore size distributions.

The important experimental parameters with respect to mesopore generation was systematically investigated by varying the temperature in samples 5–7 and the amount of TMAOH in samples 8–11. Interestingly, as the temperature is increased from 50 °C to 100 °C, the mesopore formation accelerates as illustrated by the isotherms in Figure 3 (a). The BJH-derived pore size distributions are shown in part b of Figure 3. From Figure 3 (b) it can be seen that pores are gradually forming within the mesopore range (2–50 nm)

and that the pore diameter increases as a function of temperature. The mesopore volume clearly increases in a similar way to as much as 0.364 mL/g for sample 7. Further analyzing the sorption data, it is interesting to note that at prolonged desilication times and at high temperatures, we observe a slight decrease in the micropore volume of up to ca. 8% (sample 7, desilicated at 100 °C), which indicate that crystallinity of these samples may be slightly reduced. This is in line with expectation since previous studies have reported similar observations on mesoporous structures.[15] Samples 2, 8–11 highlight the effect on mesoporosity when increasing the amount of TMAOH. This post-treatment parameter is very important in this new desilication protocol since we aim to quantitatively exchange Na^+ as the charge compensating cation with TMA^+ during the treatment. Sodium is present as the charge compensation cation in the starting material. In Table 1 it is shown that a TMAOH amount of 10 mmol/g leads to an approximate TMA^+/Na^+ ratio of 20. This ratio is estimated from the theoretical aluminum density in a framework with an Si/Al ratio of 35 and assuming complete initial charge compensation by sodium. Varying the TMAOH amount between 5 and 20 mmol/g during desilication (samples 2, 9, and 10) lead only to minor variations in the mesopore formation. However, a decrease and surprisingly also an increase by a factor of 4 (samples 8, and 11) both lead to a limited mesopore formation. The modest mesoporosity formed when as much as 50 mmol/g TMAOH was used could be explained by a structure stabilizing ability of the TMA^+ ion, since it resembles the template (TEA^+) typically used in the synthesis crystallizing zeolite beta.

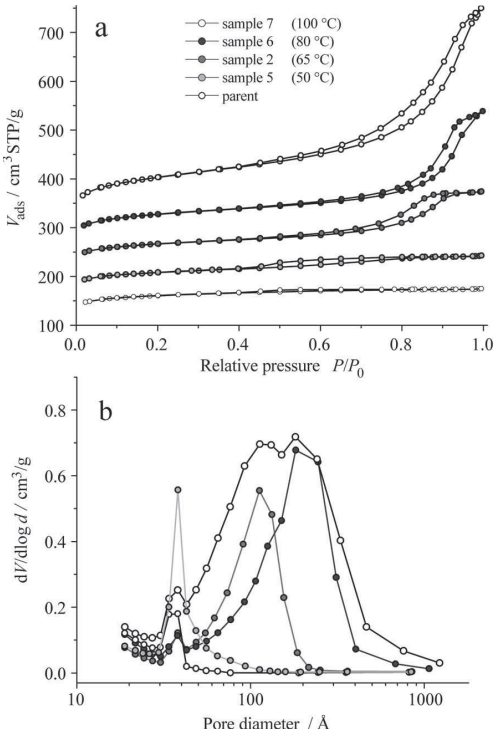

Figure 3. N_2-adsorption/desorption isotherms. (a) Increasing treatment temperature. (b) BJH-derived pore size distributions. Isotherms in (a) are offset by 50 units in relation to the previous for illustrative purposes.

NH_3-TPD was used to monitor the acidity of the zeolites. The acidity of the desilicated samples 1–11 were measured after calcination at 550 °C for 6 h in static air. Following this measurement the samples were ion-exchanged completely into H-form and the acidity measurements by NH_3-TPD were repeated. By comparing the two values, before and after ion-exchange, we were able to monitor whether the TMAOH desilication followed by calcination directly produced the protonic form of the zeolite. Figure 4 shows the NH_3-TPD curves of sample 2 before and after ion-exchange. We observe two very similar ammonia desorptions profiles both with a maximum around 345 °C corresponding to ammonia desorbing from the strong Brønsted acidic bridging hydroxy group. The integrated area under the curve corresponds to a measure of the total acidity. A slight increased is apparent after the ion-exchange in the case of sample 2. We interpreted this as the majority of the treated zeolite being transferred into proton form directly by the TMAOH desilication. However, the difference between the curves ist likely due to minor amounts of sodium still performing the charge compensation. The ratio between the integrated area of the two NH_3-desorption curves is thus a measure of the level of ion-exchange obtained directly from the TMAOH desilication. This ratio for all samples is listed in Table 1. For the most interesting samples, we observe very high exchange levels close to unity. This means that it is possible to obtain close to complete ion-exchange by combining the desilication and calcination procedures. Surprisingly, some of the most harshly desilicated samples (samples 6, 7 and 9) show an exchange level slightly above 1. This could be explained by the formation of extra framework aluminum (EFAL) as a consequence of harsh desilication which would introduce Lewis acidity.[16] Possibly

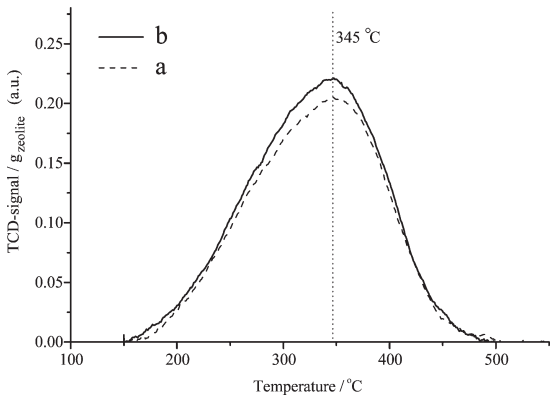

Figure 4. NH_3-TPD of (a) sample 2 after TMAOH desilication and calcination and (b) sample 2 ion-exchanged into proton form.

these extra framework aluminum species could solely contribute to the acidity before the ion-exchange due to removal during the ion-exchange procedure. Importantly, it is seen that increasing the TMAOH amount above 5 mmol/g decreases not only the mesopore surface area S_{meso} but also the level of ion-exchange obtained. This shows that huge amounts of TMAOH is not necessarily required to obtain a quantitatively ion-exchange into the proton form. We hypothesize that the ion-exchange is positively affected by a high affinity of sodium to coordinate to dissolved silicate species compared to performing the charge compensation. Further in Table 1, it is summarized that in all cases where mesoporosity is formed, an increase in total acidity is seen. This is in line with expectations from the selective silicon extraction.[14]

NH_3-TPD does not discriminate between Lewis and Brønsted acidity. However, a IR absorption at ca. 3610 cm^{-1} in the zeolite originates from the Brønsted acidic bridging hydroxy group.[17] Figure 5 presents the FT-IR absorption spectra of the parent sample in sodium and protonic form along with sample 3 which was desilicated with TMAOH and subsequently calcined. From Figure 5 it is seen that the 3610 cm^{-1} band is absent in the sodium form (a) but clearly present in the protonic form (b) of the parent sample. After the desilication process the band at 3610 cm^{-1} is reintroduced in spectrum (c) confirming that the treated zeolite indeed contains conventional Brønsted acidic sites. This information supports the previous observations that it is possible to perform the ion-exchange and mesopore formation in one synthesis step.

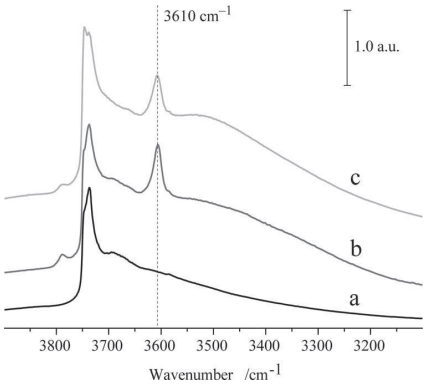

Figure 5. FT-IR absorption spectra of (a) parent sample in sodium form, (b) parent sample in protonic form and (c) sample 3 (TMAOH-desilicated and calcined). Spectra normalized to the framework overtones and offset for illustrative reasons.

Scanning electron microscopy was applied to study morphology changes in the material. For the parent zeolite a narrow crystal size distribution centered on 10 μm are found as can be seen in Figure 6A. Image 6B (sample 3) is an example of how the crystals can be partly deteriorated mainly at the top and bottom of the bipyramidal structure as a function of the desilication.

Image 6C and 6D (samples 6 and 7) reveal how increased temperature during treatment affects the crystals. Image 6C

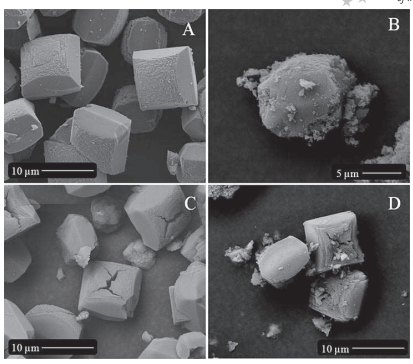

Figure 6. SEM images of the parent sample (a), sample 3 (b), sample 6 (c) and sample 7 (d).

show the presence of large cracks in the crystals. A further temperature increase to 100 °C in 6D leads to a similar behavior but additionally tends to create more crystal debris and partly destroy the original crystal morphology. It is, however, unlikely that the crystal debris is amorphous material since we observe essentially no changes in the diffractograms of these samples and only a minor decrease in micropore volume. Since we are able to introduce mesoporosity as seen in 6C before we observe substantial crystal dismantling, we interpret the micrographs as it is possible to create intra rystal mesoporosity by desilicating with TMAOH. Contributions to the overall porosity from intercrystal voids could though be substantial in cases of severe desilication conditions. Interestingly, desilicating zeolite beta initially in protonic form, i.e. without sodium present using TMAOH results only in limited mesopore formation. In this case we know that one equivalent of base is consumed to neutralize the solid acid and TMA^+ is localized near the aluminum to charge compensate the framework. However, the results obtained from varying the base amounts indicate that a slight decrease in total OH^- in the solution is unlikely to be the sole explanation for a different degree of mesopore formation. Rather this result indicates that Na^+ is needed for the hydrolysis of the Si–O–Si bond to proceed effectively, somewhat similar to the mineralizing ability during synthesis. One should note the close resemblance between typical synthesis conditions and the desilication conditions used in this study. That is a highly basic aqueous suspension of the zeolite with a tetraalkylammonium cation present. Based on this, we hypothesize that the TMA^+ ion is able to stabilize the zeolite structure during desilication. This could explain why the structure does not collapse as was seen when using NaOH.[8] Potentially also important is the fact that without sodium present during the desilication the framework will be charge compensated solely by the bulky TMA^+ ion which could increase diffusion restraints and thereby prevent or simply slow the pore formation. Considering we are trying to desilicate a structure containing a relative high amount of aluminum (Si/Al: 35) this could very well be a limiting factor.

Conclusions

In conclusion we have demonstrated how a tetraalkylammonium base is useful for desilication of zeolite beta. The procedure combines the desilication and ion-exchange steps in the direct preparation of a highly mesoporous and acidic zeolite. Further, mesopore sizes and volumes may to some extend be controlled, though not totally independent from each other. The presented study highlights the importance of proper base choice when introducing mesoporosity into zeolite structures by desilication. It shows that for specific zeolite structures, it is necessary to carefully search for the optimal base that stabilize the zeolite structure during desilication. This approach is expected to be useful for achieving hierarchical forms of other zeolites by the desilication protocol.

Experimental Section

General: Zeolite beta with a nominal Si/Al ratio of 35 was synthesized by the fluoride route using a slightly modified procedure published elsewhere.[18]

Preparation of the Synthesis Gel: Solid aluminum was dissolved in an aqueous solution (40 wt.-%) of tetraethylammonium hydroxide. After approximately one hour, a clear solution was obtained, and TEOS was slowly added over 30 min. The mixture was left for ca. 20 h with stirring at room temp. to hydrolyze TEOS and promote evaporation of ethanol, along with some water, producing a highly viscous gel. HF (40 wt.-%) was subsequently added dropwise with rapid stirring. The resulting white rigid gel with a molar oxide composition: 1 SiO_2/0.0143 Al_2O_3/0.275 $(TEA)_2O$/0.55 F was transferred to a Teflon® cup and crystallized under static conditions in a sealed stainless steel autoclave kept at 140 °C for 7 d. The crystalline zeolite was isolated by suction filtration and washed twice by re-dispersion in demineralized water. The organic template was removed by calcination at 550 °C in static air for 12 h using a heating ramp of 2 °C/min.

Typical Desilication: The zeolite (in sodium form) was suspended in hot 0.1 M aqueous TMAOH. The reaction was stopped by cooling the container in an ice bath and subsequently isolating the zeolite by suction filtration. The zeolite was washed thoroughly in demineralised water, dried at 110 °C overnight and calcined in static air at 550 °C for 6 h using a heating ramp of 2 °C/min. This calcined sample is denoted "before ion-exchange" in the text above. The proton or sodium form of the zeolite was obtained by threefold ion-exchange in a 1 M NH_4NO_3 or 1 M NaCl solution, respectively followed by calcination at 550 °C for 6 h. The proton form obtained this way is denoted "after ion-exchange" in the text above.

The samples were characterized by XRPD, N_2-sorption, FT-IR, NH_3-TPD and SEM. XRPD analysis were performed on a Bruker AXS powder diffractometer. N_2-sorption experiments were done using a Micromeritics ASAP 2020 apparatus. Prior to N_2-sorption the samples were outgassed in vacuo at 200 °C for 4 h. For FT-IR the zeolites were pressed into self supporting wafers and dehydrated at 400 °C for 2 h prior to analysis. A BioRad FTS 80 spectrometer equipped with a MCT detector was used. A Micromeretics Autochem II equipped with a TCD detector was used for NH_3-TPD experiments. Dry weights of the samples were obtained after outgassing in vacuo at 300 °C for 1 h. The NH_3 desorption curve was measured after desorption of physi-sorbed ammonia for 4 h at a temperature of 150 °C while kept in a He flow of 25 mL/ min. SEM images of the platinum/palladium-coated samples were obtained with a Philips XL 30 ESEM-FEG equipment.

Acknowledgments

The Center for Sustainable and Green Chemistry is sponsored by the Danish National Research Foundation. The authors thank Bodil F. Holten and Sven Ullmann for technical assistance.

[1] www.iza-structure.org/databases (accessed December **2008**).
[2] a) Y. Tao, H. Kanoh, L. Abrams, K. Kaneko, *Chem. Rev.* **2006**, *106*, 896; b) A. Corma, *Chem. Rev.* **1997**, *97*, 2373.
[3] J. Cejka, S. Mintova, *Catal. Rev.* **2007**, *49*, 457.
[4] A. H. Janssen, A. J. Koster, K. P. Jong, *J. Phys. Chem. B* **2002**, *106*, 11905.
[5] a) H. Wang, T. J. Pinnavaia, *Angew. Chem. Int. Ed.* **2006**, *118*, 7765; b) C. J. H. Jacobsen, C. Madsen, J. Houzvicka, I. Schmidt, A. Carlsson, *J. Am. Chem. Soc.* **2000**, *122*, 7116; c) K. Egeblad, C. H. Christensen, M. Kustova, C. H. Christensen, *Chem. Mater.* **2008**, *20*, 946; d) M. Choi, H. S. Cho, R. Srivastava, C. Venkatesan, D.-H. Choi, R. Ryoo, *Nat. Mater.* **2006**, *5*, 718.
[6] a) R. M. Dessau, E. W. Valyocsik, N. H. Goeke, *Zeolites* **1992**, *12*, 776; b) G. Lietz, K. H. Schnabel, Ch. Peuker, Th. Gross, W. Storek, J. Völter, *J. Catal.* **1994**, *148*, 562; c) D. Ohayon, R. L. V. Mao, D. Ciaravino, H. Hazel, A. Cochennec, N. Rolland, *Appl. Catal. A* **2001**, *217*, 241; d) J. C. Groen, L. A. A. Peffer, J. A. Moulijn, J. Perez-Ramirez, *Chem. Eur. J.* **2005**, *11*, 4983.
[7] a) M. Bjørgen, F. Joensen, M. S. Holm, U. Olsbye, K.-P. Lillerud, S. Svelle, *Appl. Catal. A* **2008**, *345*, 43; b) M. Ogura, S. Shinomiya, J. Tateno, M. Nomura, E. Kikuchi, M. Matsukata, *Appl. Catal. A* **2001**, *219*, 33.
[8] J. C. Groen, S. Abelló, L. A. Villaescusa, J. Pérez-Ramírez, *Microporous Mesoporous Mater.* **2008**, *114*, 93.
[9] X. Wei, P. G. Smirniotis, *Microporous Mesoporous Mater.* **2006**, *97*, 97.
[10] J. C. Groen, T. Sano, J. A. Moulijn, J. Pérez-Ramírez, *J. Catal.* **2007**, *251*, 21.
[11] R. L. V. Mao, A. Ramsaran, S. Xiao, J. Yao, V. Semmer, *J. Mater. Chem.* **1995**, *5*, 533.
[12] J. C. Groen, J. A. Moulijn, J. Pérez-Ramírez, *Ind. Eng. Chem. Res.* **2007**, *46*, 4193.
[13] J. C. Groen, J. C. Jansen, J. A. Moulijn, J. Pérez-Ramírez, *J. Phys. Chem. B* **2004**, *108*, 13062.
[14] J. C. Groen, J. A. Moulijn, J. Pérez-Ramírez, *Microporous Microporous Mater.* **2005**, *87*, 153.
[15] P. Prokesova-Fojtíková, S. Mintova, J. Cejka, N. Zilková, A. Zukal, *Microporous Microporous Mater.* **2006**, *92*, 154.
[16] M. S. Holm, S. Svelle, F. Joensen, P. Beato, C. H. Christensen, S. Bordiga, M. Bjørgen, *Appl. Catal. A*, **2008**, in press.
[17] C. Pazé, S. Bordiga, C. Lamberti, M. Salvalaggio, A. Zecchina, *J. Phys. Chem. B* **1997**, *101*, 4740.
[18] M. A. Camblor, A. Corma, S. Valencia, *J. Mater. Chem.* **1998**, *8*, 2137.

Received: December 9, 2008
Published Online: February 11, 2009

G Model
CATTOD-7186; No. of Pages 14
ARTICLE IN PRESS

Catalysis Today xxx (2011) xxx–xxx

Contents lists available at ScienceDirect

Catalysis Today

journal homepage: www.elsevier.com/locate/cattod

Catalysis with hierarchical zeolites

Martin Spangsberg Holm[a,b,c], Esben Taarning[a], Kresten Egeblad[a], Claus Hviid Christensen[a,*]

[a] Haldor Topsøe A/S, Nymøllevej 55, DK-2800 Lyngby, Denmark
[b] Center for Sustainable and Green Chemistry, Department of Chemistry, Technical University of Denmark, DK-2800 Lyngby, Denmark
[c] Centre for Catalysis and Sustainable Chemistry, Department of Chemistry, Technical University of Denmark, Anker Engelundsvej 1, 2800 Kgs, Lyngby, Denmark

ARTICLE INFO

Article history:
Received 12 October 2010
Received in revised form 9 December 2010
Accepted 8 January 2011
Available online xxx

Keywords:
Mesoporous zeolites
Hierarchical zeolites
Catalysis

ABSTRACT

Hierarchical (or mesoporous) zeolites have attracted significant attention during the first decade of the 21st century, and so far this interest continues to increase. There have already been several reviews giving detailed accounts of the developments emphasizing different aspects of this research topic. Until now, the main reason for developing hierarchical zeolites has been to achieve heterogeneous catalysts with improved performance but this particular facet has not yet been reviewed in detail. Thus, the present paper summaries and categorizes the catalytic studies utilizing hierarchical zeolites that have been reported hitherto. Prototypical examples from some of the different categories of catalytic reactions that have been studied using hierarchical zeolite catalysts are highlighted. This clearly illustrates the different ways that improved performance can be achieved with this family of zeolite catalysts. Finally, future opportunities for hierarchical zeolite catalysts are discussed, and the virtues of various preparation methods are outlined, including a discussion of possible pitfalls in the evaluation of new, potential hierarchical zeolite catalysts.

1. Introduction

During the last decade, the scientific literature on hierachical zeolites has dramatically increased, and several reviews highlighting various aspects of the recent developments have already appeared [1–7]. The term hierarchical zeolites refers to zeolites featuring at least one additional level of porosity besides the intrinsic micropore system characteristic of zeolites. In practice the term most often refers to mesoporous zeolites, i.e. hierarchical zeolites featuring additional porosity in the mesopore size region (pore diameters in the range 2–50 nm) because the major impact of auxiliary porosity on catalysis stems from porosity in this size region. Interestingly, it is difficult to trace the true origin of hierarchical zeolites, and their use as heterogeneous catalysts, since it is more or less hidden in the patent literature. However, with the current knowledge about these materials and their preparation methods there is no doubt that several early patents describe methods for preparing such zeolite materials, and also their use as heterogeneous catalysts in various reactions [8–11]. One reason that it is often not trivial to conclude when hierarchical zeolites were claimed in the patent literature is that the physical-chemical characterization reported originally does not provide direct evidence for the detailed structure of the materials studied. Thus, much of the recent interest in hierarchical zeolites can be ascribed to improved methods for visualization of the structure of these materials, and particularly to the wider availability of sufficiently elaborate electron microscopy techniques, such as high-resolution TEM and TEM tomography. With these methods, the structure of hierarchical zeolite catalysts can de deduced in impressive detail, and the observed catalytic performance can more easily be related to their structure. However, it is still necessary also to use various other physical–chemical characterization methods to establish that the structural modification of hierarchical zeolites has not lead to significant changes in other catalytically important properties of the zeolite, especially with respect to zeolite acidity. Only this way, reliable structure-activity relationships can be quantitatively established.

Here we present a review of the literature reporting the use of hierarchical zeolites as catalysts for different reaction types. The reactions types are divided into classes comprising alkylation, methanol-to-hydrocarbons (MTH) and olefin aromatization, isomerisation, cracking, condensation and other, more specific, reactions. The alkylation, isomerisation and cracking reactions share the same carbenium chemistry and could be viewed together. However, since the size of the substrates used and the operating temperature differs widely in these three categories, the effect of mesopores also differs and they are therefore treated separately.

One of the major limitations for the use of zeolites as catalysts is the limited access to the active sites within the individual crystals. This attribute serves as the material's strength (allowing for shape selectivity) as well as a weakness (mass transport limitations). It is predicted that mesoporous zeolites can contribute

* Corresponding author.
E-mail address: chc@lorc.dk (C.H. Christensen).

0920-5861/$ – see front matter © 2011 Elsevier B.V. All rights reserved.
doi:10.1016/j.cattod.2011.01.007

Please cite this article in press as: M.S. Holm, et al., Catalysis with hierarchical zeolites, Catal. Today (2011), doi:10.1016/j.cattod.2011.01.007

Table 1
Overview of the different reaction classes and the main effect of mesoporous zeolites.

Reaction type	Main observation
Alkylation reactions	Higher activity
Transalkylation reactions	Improved stability
Isomerisation reactions	Higher activity
Cracking of light substrates	No significant improvement
Cracking of heavy substrates	Substantially higher activity
MTH and aromatization reactions	Longer catalyst lifetime
Condensation reactions	Higher activity. Higher selectivity towards bulky products

to the field of catalysis in either of two ways. These hierarchical materials can potentially increase the number of reactions in which zeolites are used by allowing acceptable mass transport of larger reactants and products and allowing for reactions catalyzed by strong acidity to proceed on the mesopore surface and pore mouth. Alternatively mesoporous zeolites can simply serve by improving existing reactions/processes currently using zeolite catalysts. It is here illustrated how examples of both applications exist in literature. A summary of the major trends observed for hierarchical zeolites categorized by reaction type is shown in Table 1.

2. Alkylation reactions

Alkylations and acylations are important reactions in industry for which zeolites find use. Unfortunately, these processes are rarely operated at full potential due to mass transfer limitations within the zeolite catalysts; therefore, the advantages of applying mesoporous zeolites as catalysts for these transformations are obvious. In the literature, several reports are available dealing with mesoporous zeolites for such transformations, particular with alkylation of benzene. The general finding in these reports is the observation that mesoporous zeolites are more active for these transformations. This is expected due to shorter diffusion path length in mesoporous zeolites, however, what is perhaps not so obvious is why also an increased selectivity to monoalkylated products is observed.

2.1. Benzene alkylation

Christensen et al. [12] reported the use of mesoporous ZSM-5 prepared by carbon-templating for gas phase alkylation of benzene with ethylene (Scheme 1).

The authors used a molecular ratio of benzene:ethylene of 5.1:1, pressures from 2.5 to 5 bar and temperatures from 583 to 643 K. Undesired side reactions include the formation of di- and tri alkylated ethyl benzenes as well as numerous alkylated benzenes arising from transalkylation of the product. It was shown, that the mesoporous zeolite was significantly more active than the conventional zeolite catalyst. Moreover, it was shown that the selectivity towards ethyl benzene was significantly higher using the mesoporous zeolite and that the effect was even more pronounced at high conversions. The increased selectivtity towards the monoalkylated product, ethyl benzene, can be understood by looking at the schematic representation in Fig. 1 of the relative concentration profiles of benzene, ethylene and ethyl benzene [13].

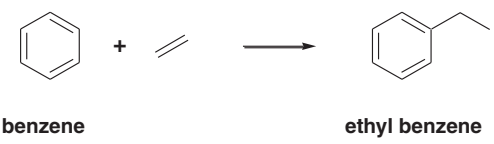

Scheme 1.

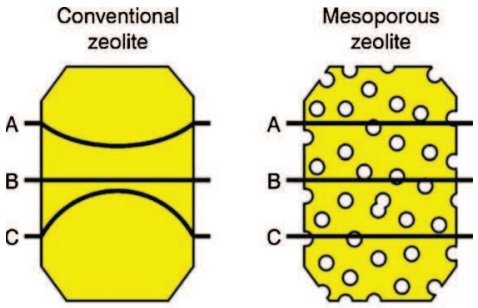

Fig. 1. Schematic of the relative concentration profiles (disregarding molecular adsorption) of benzene (A), ethylene (B) and ethyl benzene (C) in conventional and mesoporous ZSM-5 during alkylation of benzene with ethylene (figure reproduced from Ref. [13]).

The concentration profiles illustrated in Fig. 1 were derived from a classical evaluation of diffusion properties of the benzene, ethylene and ethylbenzene under actual operating conditions, showing that benzene and ethylbenzene are diffusion limited if the crystals are too large [13]. The concentrations of reactants and products in the zeolite and in the gas phase are likely different due to adsorption. However, as benzene is consumed in the alkylation reaction, a concentration gradient enriched in ethylbenzene and depleted in benzene is expected to be present in the conventional sample where diffusion restraints are pronounced. It is clear that if a relatively higher concentration of ethylbenzene exists in the interior of the crystal, this must lead to the formation higher levels of diethylbenzene. In other words, diffusion limitations in conventional crystals during alkylation of benzene with ethylene lead to higher levels of polyalkylated products than desired. On the contrary, in case of the mesoporous crystal, having a shorter average diffusion path length, the concentrations of ethylbenzene and benzene throughout the crystal will be much closer to the value strictly determined by gas phase concentration and adsorption affinity. In effect, successive alkylation of ethylbenzene is not as likely to occur in the mesoporous zeolite as in the case of the conventional one, and the monoalkylated product is predominant.

Dealumination of mordenite has been well understood for several decades but recently also base treatment (desilication) of mordenite, either alone or in combination with dealumination, has been successfully performed to obtain similar advantages.

In close relation to the previous example Groen et al. [14] compared a mesoporous mordenite catalyst obtained by desilication to a commercial sample with a smaller crystal size and higher acid density in the liquid phase benzene alkylation with ethylene. Despite the advantage with respect to crystal size and acidity, the hierarchical mordenite showed an initial higher activity in comparison with the commercial mordenite. Much more pronounced though was a remarkably slow deactivation of the mesoporous sample coupled with a slightly higher selectivity towards the desired ethyl benzene. The improved catalytic performance as discussed above was attributed to the enhanced mass transport. This report is a particularly interesting case where the authors chose to use the zeolite in the liquid phase where mass transport limitations pose much greater problems as compared to gas phase reactions. Nevertheless liquid phase reactions represent an interesting area in which mesoporous zeolites can find applications.

Three different commercially available mordenite samples were desilicated and tested in liquid phase benzene alkylation with propene producing cumene (iospropylbenzene) in a study by de Jong and co-workers [15]. The mordenite samples were outside the optimal window with respect to Si/Al ratio for desilication [16] but with an increased concentration of sodium hydroxide mesopore

Please cite this article in press as: M.S. Holm, et al., Catalysis with hierarchical zeolites, Catal. Today (2011), doi:10.1016/j.cattod.2011.01.007

formation proved possible. TEM imaging supported by additional characterization led the authors to conclude that the mesoporosity was mostly inter-particle, which lowers mass transport limitations between the nanosized particles. Indeed, for the alkylation of benzene with propylene over the alkali treated sample, an initial activity boost in the order of one magnitude was observed, while maintaining a similar cumene selectivity. The same authors [17] also used cumene synthesis to investigate whether a sequential post synthesis treatment using dealumination and desilication of commercially available mordenite could be advantageous. A comprehensive series of samples, dealuminated, desilicated or combinations thereof were prepared and compared to gain insight into the catalytic effects of Al-content, inter- and intracrystalline porosity, acid strength or the presence of extra-framework aluminum. Catalytically, the parent mordenite sample performed relatively poor, having a lower activity and selectivity towards cumene/di-isopropyl benzene as compared to reported literature values. Dealumination improved the performance only slightly, whereas a subsequent optimized desilication treatment resulted in a mesoporous catalyst having a significantly higher activity (up to 27-fold increase). Alas, the higher activity was accompanied by an increased selectivity towards di- and tri-isopropyl benzene. Interestingly, desilication of the parent sample gave an excellent combined cumene/di-isopropylenbenzene selectivity of >99% arising from suppressed propylene oligomerization which the authors attribute to the likely removal of weak Lewis acidic site present on the external surface. This observation highlights the complexity of interpreting catalytic data since mesopore formation occurs concurrently with a modification of the acidity of the samples. The use of thorough characterization methods (*e.g.* electron tomography, (MAS) NMR or FTIR using molecular probes) are thus needed in order to be able to discuss the full array of changes introduced during post synthesis treatment.

Commercial mordenite catalysts treated by desilication or dealumination have also been tested in transalkylation of alkylbenzenes (toluene and 1,2,4-trimethyl benzene) in a recent report [18]. Here an unchanged initial activity was observed; however, desilication was shown to improve the long term stability of the catalyst significantly. In line with the previous finding Yang et al. [19] tested a hierarchical beta zeolite prepared by dry gel conversion in the transalkylation of di-isopropylbenzene with benzene. The mesoporous beta sample showed a slightly lower initial activity compared to a solely microporous reference but deactivated only barely within the timeline of testing, in strong contrast to the reference. The improvements were attributed mainly to improved accessibility of the active sites and better diffusion properties in the hierarchical material.

Numerous patents from Dow Chemical [20–22] exist on the use of mesoporous (or 3-DDM) mordenite prepared by dealumination using mineral acids, and a recent review [23] highlights the catalytic properties of mesoporous mordenite in alkylation and cracking reactions. With respect to the former, mesoporous mordenite has been applied in alkylation of aromatic compounds such as biphenyl or phenol and transalkylation of alkylbenzenes. An interesting example from the open literature using mesoporous mordenite obtained by acid leaching is given by Garces and coworkers [24] The authors use the catalyst in the liquid phase alkylation of biphenyl with propylene, preferentially forming the para isomer 4,4'-diisopropylbiphenyl (DIPB). By performing the dealumination step once or twice, they elegantly introduce increasingly strong dealumination (SiO_2/Al_2O_3 ratio up to 2600) alongside mesopore formation occurring at the expense of the micropores. The best dealuminated catalyst showed a very good para selectivity of 73.5% and also had an improved stability towards deactivation. The authors discuss that the preferential removal of aluminum on the external surface could be the cause for both phenomena as non-shape selective isomerization of the products as well as pore blocking from crystal surface reactions were diminished.

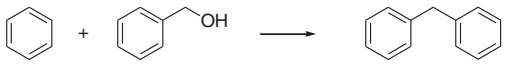

Scheme 2.

In a similar study Kim and co-workers [25] studied the performance of dealuminated mordenite in the ethylation of biphenyl. Here, only moderate selectivity towards the para isomer could be observed and the authors attribute this to the lower steric restriction of the mordenite framework as compared to isopropylation.

Xiao et al. [26] compared a mesoporous zeolite beta prepared by templating with mesoscale cationic polymers to conventional beta with a slightly smaller crystal size in the alkylation of benzene with 2-propanol. They operated the reaction at 473 K with a benzene/2-propanol ratio of 4:1. It was shown that the mesoporous sample exhibited higher activity than the conventional, and that the selectivity towards isopropyl benzene was also significantly higher.

Recently Sun and Prins [27] compared a mesoporous ZSM-5 prepared using amphiphilic organosilane as mesopore directing agent to a conventional ZSM-5 sample in alkylation of benzene with benzyl alcohol (Scheme 2). In this case, the mesoporous ZSM-5 exhibited dramatically improved catalytic activity in comparison with the conventional ZSM-5 sample.

Li et al. [28] also reported the use of a mesoporous zeolite for alkylation of benzene with benzyl alcohol. In this report, mesoporous mordenite was prepared by a combination of acid and base leaching procedures. It was shown that the activity of the mesoporous mordenite was much higher than that of the parent sample. To support the data from the benzene alkylation the authors used the isomerization of 2-methyl-2-pentene as a model reaction. The 2-methyl-2-pentene reaction is commonly used to probe the acidity of solid acids by evaluating the ratio of isomers formed. The model study identified the acid- and base leached mordenite as the most active catalyst as was found to be the case in the benzene alkylation.

Jin et al. [29] compared a mesoporous ZSM-5 sample obtained by desilication with a conventionally prepared ZSM-5 sample and showed that the hierarchical zeolite exhibits higher activity as well as longer lifetime in the alkylation of 2-methyl naphthalene with methanol to 2,6-dimethyl naphthalene. The reactants and products are of a similar size as the channels in the zeolite and therefore a large improvement in activity increasing from 5.3% to 37% after about 10 h at 673 K was seen. The authors argued that the mesoporosity and not a decreasing Si/Al ratio was the deciding factor determining the activity. This was investigated by comparing catalytic performance of the hierarchical ZSM-5 with that of a nanosized ZSM-5 having a significantly lower Si/Al ratio. The selectivity expressed as the ratio of 2,6-dimethyl naphthalene/2,7-dimethyl naphthalene was simultaneously affected. Selectivity towards the desired less sterically hindered product 2,6-dimethyl naphthalene was highest in the parent zeolite. From increasing mesoporosity the limiting mass transport was gradually relieved and the selectivity decreased for the most strongly desilicated samples. This example also illustrates that the activity of the catalyst can come at the cost of the selectivity due to partial loss of the shape selective properties of the zeolite, indicating that a compromise needs to be identified. In this specific case the authors were however able to address this problem using a different subsequent post treatment.

A recent study by Musilova et al. [30] have drawn similar conclusions with respect to selectivities when comparing a reference ZSM-5 with mesoporous samples prepared by carbon templating after catalytic testing of toluene disproportionation as well as toluene and *p*-xylene alkylation with isopropyl alcohol. In this study, thorough FTIR characterization was performed using

Please cite this article in press as: M.S. Holm, et al., Catalysis with hierarchical zeolites, Catal. Today (2011), doi:10.1016/j.cattod.2011.01.007

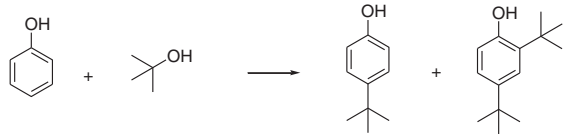

Scheme 3.

deuterated acetonitrile, pyridine and 2,6-di-tert-butyl pyridine as molecular probes. The authors were able to convincingly use a set of parent and mesoporous samples with insignificant differences in acid strength, concentration and type (Brønsted vs. Lewis) while showing that the amount of Brønsted acidic sites located at the external surface increased, correlating well with the introduced mesoporosity.

2.2. Alkylation and acylation of other substrates

Xu and co-workers [31] reported the use of a hierarchical ZSM-5 prepared by templating with polystyrene colloidal spheres in the alkylation of phenol with *t*-butanol. The authors investigated the activity as well as the selectivity towards 4-*tert*-butyl phenol and 2,4-di-*tert*-butyl phenol (Scheme 3). The hierarchical zeolite was much more active than the conventional sample, and apparently, the selectivity towards the highly bulky 2,4-di-*tert*-butyl phenol was also increased.

Nano-sized zeolite beta prepared by confined space synthesis by Derouane et al. was shown to be active for acylation of anisol by acetic anhydride [32]. The authors observed an improved catalytic performance at intermediate conversions when using the nano-crystals. This was attributed to the lowered mean diffusion length allowing for the easier egression of the bulky product *p*-methoxyacetophenone. Recently, nano-sized ZSM-5 was also used for acylation of anisol with acetic anhydride as well as acetyl chloride [33]. Also in this report, the mesoporous zeolite catalyst was more active than the conventional one.

3. Methanol to hydrocarbons and aromatization reactions

The methanol to hydrocarbons reaction (MTH) enables the use of gasified coal or biomass to form hydrocarbons and thus could play an important role in the future. The MTH reaction is an example of a reaction composed of multiple alkylation, cracking and isomerization steps, each catalyzed by the same strong Brønsted acidity sites. The aromatization of olefins resembles the MTH reaction to a great extent and zeolites are active catalysts in both cases. The general finding when using mesoporous zeolites is that an increased catalyst lifetime is observed. This effect could be attributed to an increased resistance towards coking of the mesoporous zeolites, however observations describing lower rates of coke formation as well as coke predominantly forming on the external surface have also been reported.

For the methanol to gasoline reaction Bjørgen et al. [34] and Lietz et al. [35] have tested mesoporous ZSM-5 obtained by desilication. In both studies, an increased lifetime of the mesoporous ZSM-5 zeolite compared to the conventional ZSM-5 is reported. Bjørgen and co-workers calculated the total methanol conversion capacity ($g_{methanol\ converted}/g_{zeolite}$ extrapolated from 50% deactivation) of the parent and the optimally desilicated sample and saw a significant increase by a factor of 3.3 when introducing mesoporosity. The initial activity of the hierarchical zeolite was observed to increase only slightly as a function of the desilication but the selectivity towards the gasoline fraction C_{5+} was on average improved by a factor of 1.7. Another pronounced difference was seen in a higher C_4 hydrogen transfer index (HTI-index) for the mesoporous samples which identify a more pronounced production of paraffinic and aromatic compounds. Presumably the high content of alkyl benzenes in the effluent is related to the increased ease with which these large compounds escape the mesoporous zeolite crystal. Interestingly, the authors also note that the mesopore formation leads to a decreased *p*-xylene selectivity over *o*-xylene which is in good correlation with other findings described in literature and discussed herein [36].

Recently Ryoo and co-workers published a synthesis approach using an elegantly designed bi-functional surfactant as the structure directing agent and were able to produce sheets of crystalline MFI with a thickness of only a single unit cell (2 nm) [37]. This remarkable material proved temperature stabile and contained conventional strong Brønsted acidity and was tested catalytically in several reactions including cracking of high density polyethylene (HDPE) and MTG. The single sheets possess little shape selectivity but exhibited a superior accessibility to the acidic sites seen by a substantially improved cracking performance of the large HDPE as compared to a conventional zeolite with similar Si/Al ratio. Catalytic results from the MTG reaction showed no initial activity difference due to the small size of methanol, but a significant increase in catalyst lifetime was found. The authors attributed this finding, in part to a slower coke deposition on the mesoporous material, together with the coke deposition predominantly taking place on the external surface since coke precursors readily could diffuse out of the zeolite. This study convincingly illustrates how the use of several catalytic reactions can be applied to highlight the different properties of a newly produced material versus a reference.

Another interesting study, published by the same laboratory, also reports how several mesoporous ZSM-5 samples prepared from different protocols were compared catalytically in the MTH reaction [38]. When plotting the external surface area as a function of the lifetime, until 50% conversion is reached, they observe a near linear correlation which highlights that mesoporosity can yield significantly higher conversion capacities for MFI catalysts in the MTH reaction. Further, a pronounced difference between the mesoporous and the purely microporous catalyst was seen in the distribution of the formed coke being located preferentially externally vs. internally, respectively.

For the methanol to propylene reaction, Mei et al. [39] used mesoporous ZSM-5 with the main findings that the important propylene/ethylene ratio as well as the propylene selectivity could be significantly increased by introduction of mesoporosity. The authors prepared mesoporous ZSM-5 by two different protocols, namely desilication and starch templating. Interestingly, they observe only an improved catalytic performance when using the desilicated zeolite. In part the authors attribute this to differences in the connectivity and location of the mesopores. In the case of desilication the mesopores are accessible from the external surface in contrast to starch templating where the mesopores are randomly distributed and occluded within the crystals. A mesoporous ZSM-5 reported by Sun et al. was also tested in the MTP reaction [40]. The material was prepared by carbonization of a precursor within the pores of SBA-15 followed by dissolution of the SBA-15 material and subsequently using the nanosized carbon as a hard template. In this study no initial selectivity improvement towards propylene was observed; however, a significant lifetime increase could be seen. In a recent study by Sommer et al., [41] SSZ-13 and desilicated SSZ-13 were compared in the methanol to olefins process. Here it was found that the desilicated SSZ-13 had a significantly shorter lifetime and contained less coke upon deactivation compared to conventional SSZ-13. The authors suggested that the cause behind this behavior were alterations in the acidity and surface area which illustrates that while the introduction of mesoporosity might be beneficial in some cases, side effects can have detrimental effects in the catalysis.

Please cite this article in press as: M.S. Holm, et al., Catalysis with hierarchical zeolites, Catal. Today (2011), doi:10.1016/j.cattod.2011.01.007

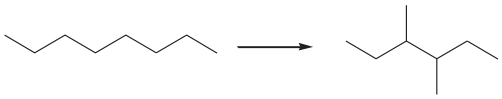

Scheme 4.

Furthermore, mesoporous ZSM-5 has been tested in butene [42] and 1-hexene [43] aromatization. Song et al. [44] investigated butene aromatization and the major finding was that the stability on stream was dramatically improved in the mesoporous zeolite obtained by desilication. As the catalysts deactivate, the xylene composition changes towards increased *p*-xylene selectivity in the case of the parent zeolite, whereas a continual composition close to the thermodynamic equilibrium was seen for the alkali treated samples. The coke deposited onto the zeolites was investigated and it was concluded that an equal amount of coke having similar properties was formed on the mesoporous as well as the conventional sample. Accessibility to the micropores was maintained in the mesoporous system which was explained by a significant amount of the coke being located in the mesopores where it is less detrimental to mass transport. In addition, the authors found that coke located in the mesopores was combusted at a lower temperature compared to coke situated in the micropores, as revealed by temperature programmed oxidation experiments.

In line with the previous report a similar improvement in the resistance towards deactivation by coking was reported in the case of 1-hexene isomerization and aromatization tested over a mesoporous ZSM-5 zeolite also obtained by desilication. Simultaneously, the relative amount of cracking over the mesoporous zeolite is observed to deteriorate which is explained by an unhindered access to the active sites in the micropores and good mass transport, both of which limits the residence time of the products in the micropores. These findings are validated by N_2 sorption–desorption measured on samples containing an equal amount of coke. It is seen that the accessible micropore volume decreases to a much larger extend in the conventional zeolite as compared to the mesoporous.

Upgrading of pyrolysis oil over a zeolite is one way to deoxygenate it and convert low value oxygenates into hydrocarbons and water. Park and co-workers have compared the use of ZSM-5 and hierarchical ZSM-5 prepared using organosilane templates for the upgrading of pyrolysis oil vapors [45]. It was found here that the mesoporous ZSM-5 was more active than the conventional catalyst. The authors ascribe this to the synergetic effect of the high acidity and high porosity of the mesoporous zeolite.

4. Isomerization reactions

Zeolites are often used to isomerize hydrocarbon substrates into more valuable products. An important application of this is the upgrading of straight chained naphtha into highly branched products with high octane numbers and thus better gasoline properties (Scheme 4).

More than three decades ago, before the field of mesoporosity had matured in a field of its own, dealumination [46,47] was a known procedure to improve the performance of zeolite catalysts. An example is the use of dealuminated mordenite as a catalyst in the hydroisomerization of small paraffins into their branched isomers. In an early study by Koradia et al. [48] a series of Pt-loaded mordenite samples were prepared and dealuminated at varying levels and tested in *n*-pentane isomerization at 533 K. The authors identified an optimum dealumination level going from a parent SiO_2/Al_2O_3 ratio of 10.8–17.1. The authors discuss the effects of lower acid density and possible interaction of the loaded metal with the acidic site without addressing porosity. None the less, a large difference in the product selectivity is apparent and the optimal selectivity was found to coincide with the highest activity level.

Interestingly, with the standardization of characterization techniques such as TEM and N_2-physisorption, a new level of understanding could be obtained from analyzing dealuminated mordenite. In relation to the previous report Tromp et al. [49] studied dealuminated mordenite treated to a similar level. The Pt loaded mordenite samples were tested in *n*-hexane hydroisomerisation and the acid leaching increased the activity and shifted the selectivity towards primary products, i.e. mono-branched isomers while suppressing cracking. Results from TEM and N_2-physisorption showed that mesopores and/or cracks in the crystals were indeed formed and decomposition reactions using *n*- and isopropyl-amine showed an increased accessibility as a function of the dealumination treatment. Calculating the Thiele modulus concluded that the reaction was diffusion controlled in the parent sample. It was thus rationalized that the introduced mesoporosity effectively reducing residence time of the products on the catalyst along with better acid site accessibility were the reasons for the improved catalyst performance. Further, a thorough study regarding the diffusivity in dealumnated samples similar to the ones just described under "live" catalytic conditions have been made by van Donk et al. [50]. Using a tapered element oscillating microbalance (TEOM) the authors were able to obtain steady state diffusivities and uptake rates in untreated and dealuminated mordenite. Catalytic experiments showed a superior performance of the mesoporous sample and this activity increase could be assigned partly to decreased diffusion restrains arising from shorter intracrystal diffusion lengths as well as an improved intrinsic activity of the individual sites as aluminum is extracted from the framework.

In a recent study by Chao et al. mesoporous MFI was prepared using a procedure involving base treatment and re-crystallization [51]. This mesoporous MFI material was found to have decreased *n*-hexane and 2-methylpentane sorption capacity while the sorption capacity for 2,2-dimethylbutane was increased. This higher capacity for bulky hydrocarbons is also reflected in a higher selectivity of the bulky isomers for the isomerisation of *n*-hexane at 600 K when using the platinum modified versions. For the hydroisomerisation of *n*-heptane Moushey and Smirniotis [52] compared the activity of ZSM-12 and Beta with those of their mesoporous analogues prepared by carbon templating. In this study, the mesoporous ZMS-12 material was found to exhibit a four times higher activity than the conventional ZSM-12 zeolite at 533 K. A comparison of the product selectivity at 593 K shows that the mesoporous ZSM-12 gives 86% isomerisation product as compared to 72% for the conventional ZSM-12 zeolite. A similar trend was observed for the Beta zeolite. The increased selectivity towards the isomerisation products is attributed by the authors to the shorter residence time of the substrate in the mesoporous zeolite crystal. In a similar study, the hydroisomerisation of *n*-octane using Pt/MOR and Pt/Beta as well as their mesoporous analogues was examined at 503–523 K [53]. The mesoporosity was introduced by partially destroying the parent mordenite and Beta zeolites using sodium hydroxide, followed by a hydrothermal treatment in the presence of cetyltrimethylammonium bromide. Varying degrees of mesoporosity are introduced in this way by changing the amount of sodium hydroxide. The study shows that the mesoporous zeolites in all cases exhibit higher activity than their parent samples (1.3-2 fold increase).

Isomerisation of larger hydrocarbons has also been studied. Delamination of layered zeolite precursors with the FER-type structure can lead to the ITQ-6 material which contains mesoporosity. In a study by Corma and co-workers, this material was used for the hydroisomerisation of *n*-hexadecane at 673 K and compared to ferrierite [54]. Here it was found that ITQ-6 is more active than ferrierite and gives a higher isomerisation to cracking ratio. In addi-

Please cite this article in press as: M.S. Holm, et al., Catalysis with hierarchical zeolites, Catal. Today (2011), doi:10.1016/j.cattod.2011.01.007

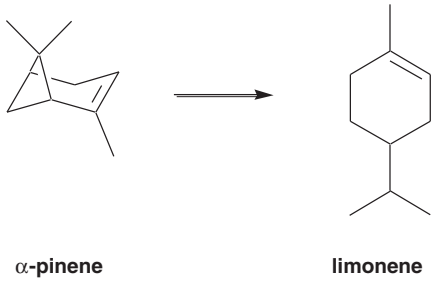

Scheme 5.

tion, the isomerisation products are more highly branched than the isomerisation products formed from using ferrierite.

A comparison of various commercial Beta zeolites for the isomerisation of fatty acids (C_{18}) at 523 K has been carried out by Zhang and Zhang [55]. In this study, zeolites having different Si/Al ratios and mesoporosities are compared. It was found that the mesopore surface area is the most important parameter for increasing the conversion of fatty acids. This observation is well rationalized by the large size of the reactants presumably only allowing the isomerisation reactions to take place on the external/mesopore surface.

The isomerisation of *o*-xylene to *p*-xylene has been studied by Fernandez et al. using a mesoporous ZSM-5 prepared by desilication [36]. The finding here was that the mesoporous ZSM-5 displayed higher activity than the parent ZSM-5, resulting in a higher conversion of *o*-xylene. However, the improved activity comes at the cost of a loss in shape selectivity and more *m*-xylene is formed. This negative side effect was reduced by an acid wash treatment of the desilicated zeolite, removing some of the aluminum in the mesopores that caused the non-shape selective isomerisation reaction.

Hydrocarbons such as monoterpenes are known to readily isomerize. Thus, these have also been studied using hierarchical zeolites [56,57]. Here, ZSM-12 was desilicated using sodium hydroxide to produce a mesoporous ZSM-12 zeolite. This mesoporous material was found to have enhanced activity relative to the conventional ZSM-12 zeolite for the isomerisation of α-pinene as presented in Scheme 5.

A similar result was obtained for the desilication of ZSM-5. In terms of product selectivity, however, the difference between the desilicated and the parent zeolites is less pronounced as a mixture of various monoterpenes with a similar composition is formed in all cases.

5. Cracking reactions

Cracking reactions constitute one of the most important uses of zeolites due to their strong Brønsted acidity. Since mesoporous zeolites combine benefits of strong acidity, high thermal stability and enhanced surface area they have been studied for the cracking of hydrocarbons of sizes ranging from C_6 to hydrocarbons containing thousands of carbon atoms, which is the case for substrates such as polyethylene. Particularly, the fluid catalytic cracking (FCC) and hydrocracking processes are extremely important industrially since huge amounts of heavy hydrocarbon feedstocks are cracked into more valuable fractions on a daily basis in refineries all over the world. These processes apply mesoporous zeolite Y as the catalyst, and the effect of mesopore modification on this zeolite is well known and has been reviewed earlier [1,58]. One particular important point regarding the use of zeolite Y as a cracking catalyst is made by Kung et al. [59]. It is well known that dealumination by steaming or acid treatment enhances the cracking activity of zeolite Y; however, as a function of dealumination a substantial modification of the acidic properties occur, creating entirely new types of acidic sites and the exact origin of the improved activity can thus be rather hard to pinpoint. Interestingly, the authors argue that minimizing diffusion restraints by the introduction of mesoporosity could be critical with respect to increasing rates of bimolecular and oligomeric cracking reactions and thus serve as an alternative explanation to highly active single sites. This example illustrates a major challenge which lies in separating the effects of acid site modification vs. porosity introduction which is of relevance in most of the hierarchical zeolite material described throughout this review. Concerning exactly this Haag et al. [60] have previously demonstrated the ability to isolate catalytic effects from mass transport limitations in ZSM-5 by using crystallites with increasing sizes in the cracking of numerous either linear or branched paraffins.

Recenly, also other zeolites have been studied in various types of hydrocarbon cracking reactions. The general finding here is that mesoporous zeolites are comparable in activity to conventional zeolites for the cracking of small substrates (C_8). However, the mesopores lead to a tremendous activity increase due to the enhanced accessible surface area for larger substrates.

5.1. Naphtha

The cracking of naphtha over mesoporous zeolites has been studied by several groups. Jung et al. prepared mesoporous MFI zeolites by alkali treatment and studied their activity for the cracking of *n*-octane at 773 K [61]. Here it was found that the mesoporous MFI displays a lower activity than the conventional MFI while the product selectivity remains largely unaffected. This decrease in activity is ascribed to the decrease in the number of highly acidic sites due to the alkaline treatment. The effect of mesopores thus does not seem to affect this type of cracking reaction particularly. In a similar study by Niwa and co-workers, mesoporous ZSM-5 synthesized by the use of organosilane templates was used for the cracking of *n*-octane and compared to conventional ZSM-5 [62]. These cracking experiments were also carried out at 773 K and the activity of the mesoporous zeolites was found to be comparable to or slightly lower than the activity of the conventional zeolites. Unfortunately, the product composition was not investigated in this study. A feed of refinery derived naphta was cracked over carbon templated ZSM-5 by Bari Siddiqui et al. [63]. Comparable activities for non-mesoporous references were reported but significantly higher propene and ethylene yields were found from the mesoporous sample attributed to a shorter residence time suppressing secondary reactions. Mesoporous ZSM-5 has also been studied for the cracking of 1-hexene by Xu and co-workers [43]. In this study the mesoporosity is introduced by alkali treatment to produce zeolites containing varying degrees of mesoporosity. Here, the alkaline treated zeolites were found to display a slightly higher activity than the parent ZSM-5 zeolite. The largest difference here is the product selectivity, as the alkaline treated zeolites are reported to be more selective towards aromatics (15–20%) than the parent ZSM-5 zeolite (5%) whereas the latter shows a higher selectivity for C_4–C_{10} olefins (623 K). A biphasic zeolite composite consisting of a core of Y zeolite and an outer layer of Beta nano-crystals was prepared by Zheng et al. and tested for the cracking of *n*-octane [64]. This composite material has a micropore volume comparable to the two parent zeolites (0.19 ml/g), and also a mesopore volume of 0.13 ml/g that is much larger than that of a physical mixture of Y and Beta. For the cracking of *n*-octane at 773 K the composite was found to be more active than pure H-Y (6% conversion) and a physical mixture of H-Y and H-Beta (48% conversion) giving a conversion of 76%. The cracking products were not identified in this study.

It thus appears that for the cracking of small substrates, the acidity of the zeolite is the dominant factor in determining the overall catalyst activity. This observation indicates that only minor, if any,

Please cite this article in press as: M.S. Holm, et al., Catalysis with hierarchical zeolites, Catal. Today (2011), doi:10.1016/j.cattod.2011.01.007

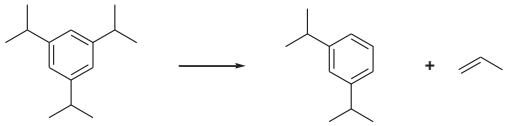

Scheme 6.

mass transport limitations exist at the high temperatures typically employed for hydrocarbon cracking.

5.2. Aromatic compounds

Hierarchical ZSM-5 prepared from a macroporous silica gel has been used for the cracking of triisopropylbenzene (Scheme 6) [65].

Since triisopropylbenzene is too large to enter the microporous system of the ZSM-5 it is not surprising that the hierarchical zeolite achieves a much higher conversion (98%) compared to the conventional zeolite (14%). For the cracking/isomerisation of 1,2,4-trimethylbenzene, mesoporous Beta and ZSM-11, synthesized by the use of polyvinylbutyral as the mesopore directing agent, have been tested and compared [66]. The authors showed that the mesoporous ZSM-11 is more active and *e.g.* shows the same activity at 623 K as the conventional ZSM-11 shows at 663 K. The product selectivity is quite different in the two cases, though. While the conventional ZSM-11 zeolite exhibited a 31% selectivity to xylenes, the selectivity for the mesoporous analogue was only 12%. Instead, the mesoporous ZSM-11 primarily leads to mesitylene isomerisation (79% selectivity) which is lower for the conventional zeolite (57%). This selectivity difference can be explained by the slow diffusion of the bulky mesitylenes in the conventional zeolite leading to increased retention times and also an increased chance of cracking to form smaller products that can easily diffuse out of the zeolite crystal. The mesopores have the opposite effect and serve to reduce the substrate retention time in the zeolite and thus minimizes the chance for cracking.

A study from Weiss and co-workers [67] (and references therein) presents early work using dealuminated mordenite in cracking of cumene into benzene and propylene. Acid leaching is seen to deplete the active sites within the catalyst and the intrinsic activity is lowered but a substantial lifetime increase is simultaneously observed making the dealuminated catalyst superior after prolonged reaction times. This is attributed to an increased rate of product desorption, effectively lowering the tendency to form high molecular weight condensates.

5.3. Hexadecane

The cracking of hexadecane using mesoporous zeolites has also received a lot of attention. In one study, mesoporous HZSM-5 zeolite prepared by carbon templating was compared to conventional HZSM-5 [68]. Here it was found that the mesoporous HZSM-5 had a significantly increased activity, leading to 52% *n*-hexadecane conversion compared to 17% for the conventional zeolite. When the zeolites were impregnated with platinum their cracking activity increased significantly and the mesoporous HZSM-5 was again found to display higher activity. In addition to this, a fourfold increase in *n*-hexadecane isomerisation was achieved for the mesoporous zeolites. This large difference in product selectivity was explained in terms of shorter retention time of the substrates in the zeolite crystals, leading to less cracking and more isomerisation. In a different study, mesoporous silicalite-2 and HZSM-11, both of MEL structure type, were compared to conventional HZSM-5 for the cracking of *n*-hexadecane at 553 K [69]. Here a large difference in *n*-hexadecane conversion was observed. Whereas mesoporous silicalite-2 is almost inactive due to its lack of acidity, mesoporous

Scheme 7.

HZSM-11 gave almost complete (94%) conversion, while the conventional HZSM-5 gave a modest 38% conversion under identical conditions. It should be noted that the mesoporous HZSM-11 used in this study has a lower acid density than the conventional HZSM-5, thus illustrating that the mesopores play a crucial role in the catalyst activity. In a similar study, mesoporous and conventional HZSM-12 are compared and the diffusion of *n*-hexadecane out of the zeolite was studied as well as the effect of coking [70]. For the cracking of *n*-hexadecane the mesoporous zeolite again exhibited superior activity compared to the conventional HZSM-12 zeolite. The mesoporous HZSM-12 was found to contain more coke deposits than the conventional zeolite and yet it maintains a higher activity. The coking resistance phenomena was explained by the effect of the mesopores to increase the number of entry points to the microporous system as well as the overall surface area, and thereby increase the amount of coking needed to restrict its accessibility.

5.4. Vacuum gas–oil

Cracking of VGO is an important refinery process. Recently, Triantafyllidis and co-workers have studied the cracking of VGO using hierarchical MFI zeolites synthesized using organosilane templates [71]. This procedure results in a material having a very narrow set of mesopores, depending on the size of the template used (2.2 nm or 5.2 nm). These two hierarchical zeolites were compared to conventional ZSM5 and found to display much higher activity and selectivity towards gasoline. The gasoline yield improved from 12% to 19% when using the mesoporous zeolites at one set of conditions (823 K) where the VGO conversion also was improved from 33% to 48%.

5.5. Polyethylene/polypropylene

The recycling of plastic waste such as polyethylene and polypropylene is a challenging task since the carbon chain length is typically in the range of tens of thousands. Cracking over a zeolite catalyst to produce light olefins is one option (Scheme 7).

Obviously, the large polymer molecules cannot enter the microporous system of a zeolite. As a consequence, zeolites containing large mesopores and a large external surface area have been studied intensively in the recent years. Serrano et al. have synthesized ZSM-5 nano-crystals (~10 nm) by the addition of an organosilane compound during the zeolite synthesis [72]. This material has a very large external surface area (314 m^2/g) and total surface area (586 m^2/g). In the cracking of polypropylene at 633 K (50/50 wt% of catalyst and polypropylene), this material achieves complete conversion in 3 h compared to 27% for the conventional ZSM-5 zeolite. A similar catalyst was also used by the same group to crack actual agricultural plastic film waste consisting of LDPE (low density polyethylene) and ethylene-vinyl acetate co-polymer [73]. Here the nanocrystalline HZSM-5 again proved to be superior to other zeolites and mesoporous materials. Using a similar approach, hierarchical Beta zeolite having a large external surface area (145 m^2/g) and total surface area (857 m^2/g) was synthesized and used for the cracking of LDPE [74]. Here it was shown that the TOF increases by a factor of 18 when compared to a conventional Beta zeolite. Additionally, while the conventional zeolite exclusively leads to the formation of C_1–C_5 products the hierarchical zeolite only has 50% selectivity to these small products while forming 50% of the larger C_6–C_{40} compounds. This selectivity difference was attributed to the mesoporous nature of the material

Please cite this article in press as: M.S. Holm, et al., Catalysis with hierarchical zeolites, Catal. Today (2011), doi:10.1016/j.cattod.2011.01.007

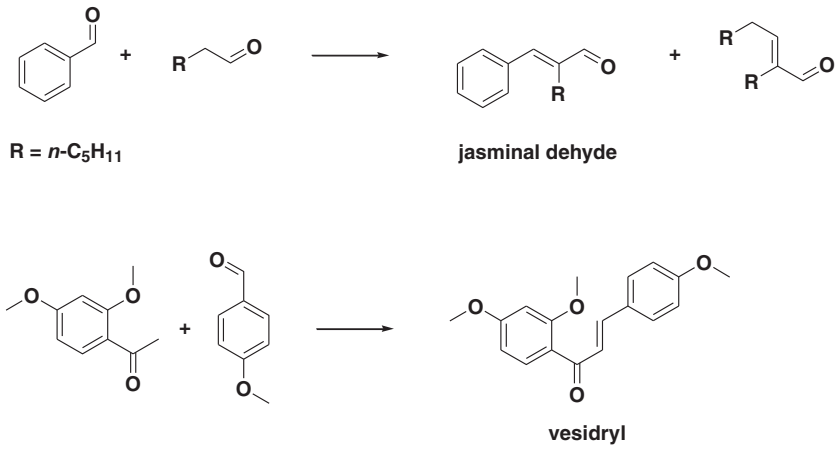

Scheme 8.

which allows the large products to exit the zeolite before they are converted into smaller cracking products. In a separate study by Pérez-Ramírez et al., the mesoporosity was introduced into Beta zeolite by desilication using NaOH [75]. By varying the amount of template still present in the zeolite during desilication, different degrees of mesoporosity can be introduced. In this study, the temperature needed to reach 50% LDPE conversion was compared for the various zeolites and the study shows a good trend between the mesopore volume of the zeolite, and the required temperature. For the conventional Beta zeolite, a temperature of 703 K is required, whereas a temperature of 623 K is required in one case when using a mesoporous sample. This corresponds to a TOF that is ~10 times higher per aluminum for the mesoporous Beta zeolite. MFI containing micro/mesoporosity synthesized by the use of an organosilane surfactant was thoroughly studied by Ryoo and co-workers for the cracking of polyethylene [76]. The hierarchical MFI zeolite was found to display a significantly higher activity than conventional MFI, achieving an 88% PE conversion opposed to 10% for the conventional at 653 K. In order to substantiate that the increase in activity is caused by the mesoporosity of the MFI, selective dealumination of the aluminum in the mesopores was achieved using tartaric acid. Testing of the mesopore-dealuminated MFI zeolite revealed an activity comparable to that of the conventional MFI zeolite (12% conversion), thus supporting the conclusion that the mesopores are the source of the increased activity for the PE cracking reaction.

Catalytic testing showing an improved performance is solid documentation for relevance of a given protocol introducing mesoporosity. It is however often not enough to comprehensively describe the catalyst. Relatively few reports perform actual diffusion or uptake experiments but an example where thorough characterization is coupled with uptake and adsorption data using several probes, as well as catalytic performance is given by Verboekend et al. [77]. The 1-dimensionel zeolite ITQ-4 was desilicated and increasing levels of mesoporosity were introduced as a function of desilication strength. Cracking of LDPE was chosen as test reaction and indeed an optimally desilicated sample was able to operate at lower temperatures; the temperature where a 10% conversion was reached was lowered by 353 K compared to the parent sample. Elution studies using *n*-butane and neopentane reveals a faster desorption from the mesoporous crystals indicating a faster molecular transport within this sample. Interestingly, when adsorbing selected molecules from the gas phase, a pronounced difference between the adsorption behavior of propane and propene is seen. The authors correlate this observation with the introduction of Lewis acidity evidenced by infrared spectroscopy (using pyridine and collidine) and are thus able to discuss the mesoporosity and acidity changes in the proper context.

6. Condensation reactions

Hierarchical zeolites have found application as catalysts for several different types of acid catalyzed condensation reactions. These range from aldol-type reactions, over esterications to protection of aldehydes and ketones by acetalization. These reactions represent illustrative examples of how hierarchical zeolites can be applied in reactions which are traditionally beyond the scope of purely microporous zeolites due to the large molecular size of the reactants or products compared to the dimensions of the zeolite channels.

6.1. Aldol condensation reactions

An example of the application of hierarchical zeolites for condensation reactions is in the syntheses of jasminaldehyde and vesidryl reported by Ryoo and co-workers as shown in Scheme 8 [78].

Here the reactants are relatively bulky and therefore have difficulties in penetrating into the bulk of the crystals. This is evidenced by the low conversion of the substrates when using conventional ZSM-5 as the catalyst, namely 4% in the synthesis of jasminaldehyde and 3% in the synthesis of vesidryl. However, when using mesoporous ZSM-5 as the catalyst, conversions of 98% and 60% are observed, respectively. Thus, here it seems that the added mesoporosity serves to enhance the accessible surface area and thereby increase the activity of the zeolite catalyst dramatically.

In a recent work, the same authors have also prepared a series of nano-sized ZSM-5 zeolites by addition of different alkylalkoxysilanes during the synthesis and tested the zeolites in various reactions [79]. One of these reactions, where a positive effect from mesoporosity can be seen in the conversion, is the condensation of benzaldehyde and 2-hydroxyacetophenone yielding a mixture of flavanone and 2-hydroxychalcone (Scheme 9).

6.2. Esterification reactions

Another reaction investigated was the condensation of resorcinol and ethylacetoacetate to give 7-hydroxy-4-methylcoumarin as the bulky condensation product (Scheme 10).

Please cite this article in press as: M.S. Holm, et al., Catalysis with hierarchical zeolites, Catal. Today (2011), doi:10.1016/j.cattod.2011.01.007

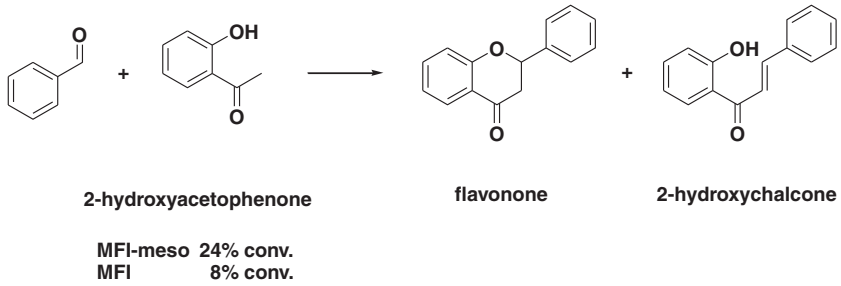

Scheme 9.

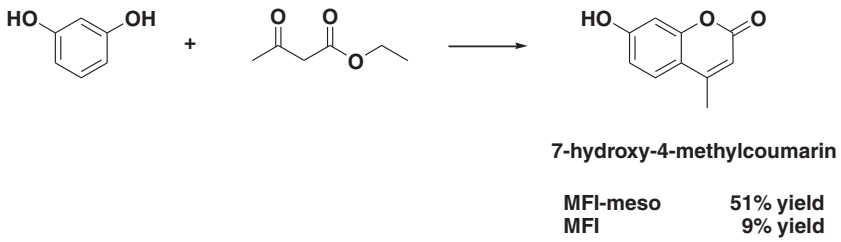

Scheme 10.

Here the product yield was reported to increase from 9% to 51% when using the mesoporous MFI zeolite. Again, this exemplifies that mesoporous zeolites might find application as catalysts for reactions beyond traditional petrochemical industry.

Condensation of a carboxylic acid and an alcohol giving an ester is another type of condensation reaction which has been carried out using mesoporous MFI zeolites (Scheme 11) [76,79].

For this reaction, in terms of hexanoic acid conversion, the hierarchical MFI catalyst is more active than a conventional MFI catalyst as well as an Al-MCM-41-type catalyst. After five experimental runs, the hierarchical MFI catalyst still exhibited 78% benzyl alcohol conversion whereas the other catalysts were completely deactivated. This exemplifies that hierarchical zeolites are more stable than amorphous mesoporous materials even though the initial activities of the catalysts, i.e. conversion after a single run, are comparable. However, this example also illustrates that mesopores can facilitate undesired effects since the benzyl hexanoate selectivity drops from 100% to 79% when using the mesoporous MFI instead of the conventional MFI. This decrease in selectivity is caused by the formation of dibenzylether, a bulky by-product which is too large to be formed in the micropores but which is easily formed in the larger mesopores. Thus, the increased activity in this case again comes at the cost of a decrease in shape selectivity.

6.3. Acetalisation reactions

Reactions involving condensation of aldehydes and ketones with an alcohol yielding an acetal or a ketal, respectively, have also been studied using mesoporous zeolites as the catalyst [76]. These were reported for the condensation of cyclohexanone with methanol forming a relatively small condensation product as well as for the condensation of benzaldehyde with pentaerythritol to give a much bulkier product.

For the condensation of benzaldehyde and pentaerythritol (Scheme 12) using a conventional MFI zeolite, no conversion was observed. In contrast, mesoporous MFI as well as MCM-41 were much more efficient catalysts, leading to near complete conversion under similar conditions (393 K). Both catalysts exhibited high selectivity towards the diacetal product. The reaction was shown to be catalyzed by the exterior acid sites as opposed to the acid sites in the micropores by the observation that no conversion was seen when a catalyst was subjected to preferential dealumination of the exterior acid sites by treatment with tartaric acid. The dealuminated zeolite was inactive for the condensation reaction and it is thus plausible to conclude that the bulky acetal product is preferentially formed in the mesopores of the zeolite and not in the micropores. In contrast, the condensation reaction between cyclohexanone and methanol was found to be much less affected by the use of a catalyst containing mesopores [76]. Here, a 50% yield of 1,1-dimethoxycyclohexane was achieved by the use of a conventional MFI zeolite, while a 58% yield was obtained for the mesoporous analogue under identical conditions. Thus, for this reaction involving small molecules there is not much benefit in applying a mesoporous as opposed to a conventional MFI zeolite.

The use of a hierarchical zeolite obtained by desilication and its use as a catalyst in the Chichibabin condensation of formalde-

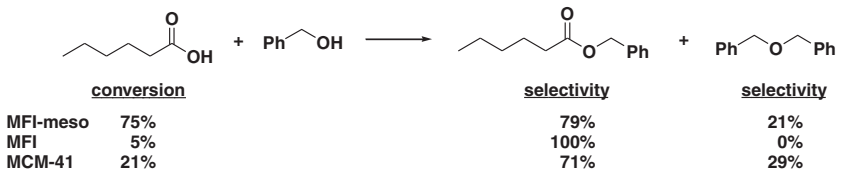

Scheme 11.

Please cite this article in press as: M.S. Holm, et al., Catalysis with hierarchical zeolites, Catal. Today (2011), doi:10.1016/j.cattod.2011.01.007

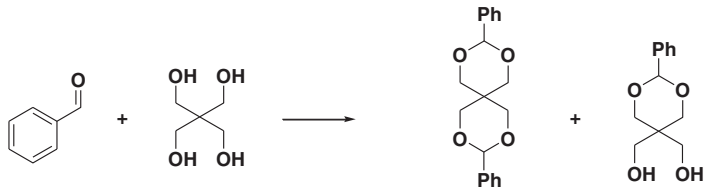

	conversion	selectivity	selectivity
MFI-meso	100%	95%	5%
MFI	0%	-	-
MCM-41	95%	100%	0%

Scheme 12.

hyde, acetaldehyde and ammonia to form pyridine and 3-picoline at 723 K has also been reported [80]. The mesoporous zeolite was found to be slightly more stable than the conventional zeolite. However, the yields of pyridine and 3-picoline were comparable for the parent and desilicated zeolite, suggesting that this reaction involving small reactants and products does not benefit significantly from the use of a mesoporous zeolite. Additionally, it should be noted that the desilication treatment was found by FT-IR studies to lead to the formation of extra framework aluminum species, i.e. the introduction of Lewis acidity. Thus it should be kept in mind that the introduction of mesoporosity by chemical post treatment methods such as desilication inevitably will bring about changes to the zeolite in addition to introducing mesoporosity.

7. Other reactions

Aside from alkylation, isomerisation, cracking and condensation reactions, hierarchical zeolites have also found application as catalysts in several other reactions involving organic substrates. These include the Beckmann rearrangement reaction as well as oxidations and epoxidations. In many of these cases, the reactants are too bulky to penetrate into the interior of the crystals, thus the reaction takes place in the pore mouths or on the external/mesopore surface of the zeolite. Although the specific micropore system of the zeolite for such applications is perhaps not so important, there are still good reasons for choosing a zeolite catalyst as opposed to other types of solid acid catalysts. One of the main reasons is their crystalline nature which makes them more acidic and more stable than amorphous materials of similar chemical compositions.

7.1. Beckmann rearrangement

The use of hierarchical zeolites have been reported for the Beckmann rearrangement reactions of cyclohexanone oxime [81,82] and cyclododecanone oxime [83]. For Beckmann rearrangement of cyclohexanone oxime, silicalite-1 as well as TS-1, i.e. pure silicate MFI and titanosilicate MFI, respectively, were applied as catalysts. The hierarchical silicalite-1 catalyst was made by an approach resembling carbon-templating which involved impregnation of a zeolite gel onto an organic aerogel followed by crystallization and carbonization. The zeolite–carbon material was then calcined to produce a hierarchical zeolite monolith or subjected to a second impregnation and crystallization step. In both cases, the resulting materials were at least twice as active in terms of $(g_{caprolactam})/(g_{catalyst}\cdot h)$ as compared to a hieararchical zeolite reference sample consisting of nanosized crystals. The same reaction was studied using nanosized TS-1 samples prepared in the absence as well as presence of different amounts of crosslinking agent (1,7-dichloro-octamethyl-tetrasiloxane) added to the synthesis gels. After 1 h reaction time at 553 K the caprolactam productivity in terms of $(mmol_{caprolactam})/(g_{catalyst}\cdot h)$ were about the same for the non-crosslinked nanosized catalyst and the catalyst prepared using 0.65 mmol linker. However, after 4 h reaction time, the caprolactam productivity observed for the non-crosslinked sample decreased by 85% whereas it increased by 28% for the sample crosslinked using 0.65 mmol linker. Still more active was the sample prepared using 1.3 mmol linker, and this catalyst did not even exhibit deactivation after 30 h on stream at 633 K. Thus, addition of crosslinker in the synthesis of nanosized TS-1 leads to more active and more stable catalysts.

Also hierarchical ITQ-2 zeolites made by delamination of MCM-22 were reported active in the Beckmann rearrangement reaction [83]. In this reaction, involving rearrangement of cyclododecanone oxime, the lactam yield at 403 K was significantly higher when ITQ-2 was applied as catalysts than when either MCM-41 or conventional zeolite Beta were used. The lower activity and selectivity of the conventional zeolite Beta catalyst was attributed to the substrate being simply too bulky to penetrate into the bulk of the crystal. Thus, the reaction takes place on the surface where no shape selectivity is possible. On the other hand, the lower activity of the MCM-41 catalyst was shown to be caused by the material having fewer sites with weaker acidity.

7.2. Epoxidation and hydroxylation reactions

Hierarchical TS-1 catalysts have also found application as catalysts for epoxidation and hydroxylation reactions. In fact, epoxidation was one of the first reactions reported in which a hierarchical zeolite was used as catalyst [84]. In the report, a carbon-templated TS-1 catalyst was compared to a conventional TS-1 catalyst in the epoxidation of 1-octene and cyclohexene with hydrogen peroxide at a reaction temperature of 313 K. By plotting the product concentration ratios for the mesoporous and conventional catalysts ($C_{mesoporous}/C_{conventional}$) it was shown that epoxidation of 1-octene is not diffusion-limited under the reaction conditions, since $C_{mesoporous}/C_{conventional}$ is close to unity during the entire experiment, whereas for the epoxidation of cyclohexene there is a clearly improved catalytic activity for the mesoporous sample. Very recently, epoxidation of cyclohexene was reported using mesoporous TS-1 prepared by assembly of seeds [85]. Also hierarchical TS-2, i.e. MEL-structured titanosilicate, has been applied for epoxidation reactions [86].

Recently, also nanocrystalline TS-1 was studied as catalyst for the epoxidation of 1-octene using the bulky organic tertbutylhydroperoxide as the oxidant [87]. The hierarchical catalysts were prepared by adding a silanization agent to hinder the growth and agglomeration of zeolitic seeds during crystallization. Comparing the catalytic performance of a small series of samples with decreas-

Please cite this article in press as: M.S. Holm, et al., Catalysis with hierarchical zeolites, Catal. Today (2011), doi:10.1016/j.cattod.2011.01.007

ing crystal size and thus increasing inter-particle porosity it was observed that the epoxide selectivity in all cases was 100%. However, large differences, ranging from 6% to 42% conversion at 373 K after 3 h were observed. The authors argued that the high external surface area and the increased accessibility to the active Ti-sites were the source of the catalytic improvements.

Hydroxylation of benzene with nitrous oxide forming phenol was recently reported using hierarchical ZSM-5 catalysts prepared by desilication [88]. The most pronounced difference seen in the catalytic tests was a dramatic deactivation of the parent zeolite which was avoided in the case of the hierarchical zeolite. ICP-OES and EPR measurements showed that the state and amount of iron in the two samples were similar, thus the improved catalytic performance is most likely due to the interconnected mesopore system, which effectively lowers the average diffusion length for reactants and products. Very recently, also hydroxylation of phenol with hydrogen peroxide was reported using carbon-templated mesoporous TS-1 [89]. The mesoporous TS-1 was almost twice as active as the conventional TS-1.

7.3. Hydrotreating reactions

Hierarchical zeolite supported noble metal catalysts were recently reported as catalysts for hydrogenation of bulky aromatic molecules [90,91] as well as for hydrodesulfurization of 4,6-dimethyldibenzothiophene [91,92]. Concerning hydrogenation of pyrene, ion exchange of $Pd(NH_3)_4^{2+}$ onto mesoporous zeolite Beta afforded a catalyst (Pd/Beta-meso) which was more active than similarly prepared conventional Beta, Al-MCM-41 and γ-Al_2O_3 based catalysts. The improved activity of the Pd/Beta-meso sample in comparison with Pd/Al-MCM-41 and Pd/γ-Al_2O_3 was attributed to the higher amount and strength of acid sites. However, the improved activity of the Pd/Beta-meso sample in comparison with Pd/Beta must be attributable to the additional mesoporosity since the acid amount and strength distribution of these samples are quite similar. In addition to exhibiting higher conversion of pyrene, the content of deep hydrogenation products (hexahydro-, decahydro- and perhydropyrenes) in the reaction liquids was also considerably higher for Pd/Beta-meso than for the other catalysts. This is important, since it is well known that the intermediately hydrogenated products become increasingly refractory towards further hydrogenation. This observation is apparent from a similar hydrogenation study in which it was shown that hydrogenation of naphthalene proceeded with similar activity over Pd/Beta-meso and Pd/Al-MCM-41, but where Pd/Beta-meso was considerably more active than Pd/Al-MCM-41 in the hydrogenation of tetralin [91]. Moreover, the Pd/Beta-meso catalyst showed much greater tolerance than the Pd/Al-MCM-41 sample when carrying out hydrogenation of naphthalene as well as pyrene in the presence of 200 ppm thiophene.

Another hydrotreating reaction which has been studied using hierarchical zeolites recently is hydrodesulfurization of 4,6-dimethyldibenzothiophene [91,92]. This reaction has been studied using the Pd/Beta-meso catalyst mentioned above, as well as with mesoporous Pt/ZSM-5, Pd/ZSM-5 and Pt-Pd/ZSM-5 catalysts. In one of the reports, Pd/Beta-meso was shown to be able to reduce the sulfur content of the reaction liquid more than the Pd/Al-MCM-41 catalyst it was compared to [91]. For instance, the sulfur content after 3 h at 523 K was 165 ppm using the Pd/Beta-meso catalyst in comparison with 226 ppm for the Pd/Al-MCM-41 catalyst. This finding was attributed to the increased acidity of the Beta-meso support in comparison with the Al-MCM-41 support. Concerning the mesoporous ZSM-5 supported catalysts, comparison of Pt and Pd samples on these supports with reference catalysts of the same metals on conventional ZSM-5 and γ-Al_2O_3 showed that mesoporous Pt/ZSM-5 (63%) and, particularly, mesoporous Pd/ZSM-5 (83%) were considerably more active than the reference catalysts [92]. Very recently, mesoporous zeolite L prepared by assembly of zeolite L nanocrystals was reported as support for more classic CoMo and NiMo type catalysts for hydrodesulphurization (HDS) [93] In this report it was shown, that the mesoporous L material was a better support for the active material than purely microporous zeolite L as well as the Al_2O_3. The excellent performances of the mesoporous zeolite L supported catalysts were attributed to high amounts and strengths of acid sites as well as a highly porous structure.

7.4. Reactions involving inorganic substrates

Hierarchical zeolites have also found application as catalysts for conversion of inorganic molecules such as NO and N_2O. Concerning these molecules the application of hierarchical zeolite catalysts has proceeded along two different avenues. One strategy is the selective catalytic reduction (SCR) of NO with NH_3, another is the direct decomposition of NO or N_2O. At any rate, the key issue is the conversion of NO or N_2O to N_2 (and H_2O/O_2).

One strategy for NOx removal in stationary as well as automotive applications is the selective catalytic reduction (SCR) of nitrogen oxides with NH_3. For this application, conventional Fe and Cu zeolites are currently attracting much attention [94]. Also mesoporous iron-containing zeolites have been studied as catalysts for NO SCR with NH_3 [95,96]. It was shown, that mesoporous Fe-ZSM-5 as well as mesoporous Fe-ZSM-12 catalysts were more active than the conventional analogues at all temperatures in the studied interval (573–773 K) and that they were both more active than the reference 3% V_2O_5/TiO_2 catalyst above 723 K [96]. Moreover, it was shown that the NO conversion activity is increased when increasing the iron loading of the samples until a maximum is reached. For the mesoporous Fe-ZSM-5 sample a maximum of ca. 30% conversion at 623 K is achieved at an iron loading of 6–7%, whereas for the conventional Fe-ZSM-5 sample, a maximum of ca. 15% is reached at an iron loading of 2–3% [95]. Similarly, a maximum of ca. 60% conversion at ca. 6% loading is reached over mesoporous Fe/ZSM-12 in comparison with 35% at 4% loading for the conventional Fe/ZSM-12 [96]. This suggests that a better dispersion of the iron species is possible in the mesoporous samples in comparison with the conventional samples.

Another strategy for NO removal is the direct decomposition of this molecule to N_2 and O_2. This reaction has also been studied using mesoporous zeolite catalysts, in this case Cu-ZSM-5 and Cu-ZSM-11 [97]. It was shown that both mesoporous Cu-ZSM-11 and mesoporous Cu-ZSM-5 were more active than their conventional references. These observations were shown to correlate with the accessibilities of the active Cu species in the zeolite samples. Moreover, EPR (electron paramagnetic resonance) investigations revealed that mesoporosity in the zeolites facilitate the formation of dimeric or oligomeric Cu-species in contrast to the monomeric Cu-species dominating in the conventional samples. Another observation apparent from the experimental data was that the mesoporous Cu-ZSM-11 catalyst was twice as active as the mesoporous Cu-ZSM-5 catalyst. This was attributed to preferential formation of active Cu-sites in the straight channels of ZSM-11 rather than in the sinusoidal channels of ZSM-5.

Also decomposition of N_2O has been studied using hierarchical zeolite catalysts [98–100]. In a thorough study, it was shown that steam activation of Fe, Ga and “normal” Al-ZSM-5 samples improved the catalytic activity in N_2O decomposition, whereas merely calcining the samples prior to the catalytic experiments had a detrimental effect on the activity [98]. Moreover, the authors showed that alkaline treatment of the steam-activated samples further increased their catalytic activity. One reason for this was further touched upon in a more recent report, where it was shown

Please cite this article in press as: M.S. Holm, et al., Catalysis with hierarchical zeolites, Catal. Today (2011), doi:10.1016/j.cattod.2011.01.007

that alkaline treatment enhanced the iron uptake capacity during ion exchange [99]. In fact, it was shown that the Fe ion exchange capacity of as-received ZSM-5 was limited to 0.9 wt% whereas the alkaline treated sample could contain up to 1.98 wt% Fe. The increased iron uptake capacity was also evident from the catalytic experiments, however, it appears that only a fraction of the extra Fe becomes active in the reaction, since the activity was only slightly increased. However, this relatively low activity increase might perhaps be explained by the observation that acidity is important for the reaction as was shown earlier [98]. In fact, this might explain why a subsequent NH_4NO_3 ion exchange treatment of alkaline treated ZSM-5 improves the N_2O conversion significantly [100].

8. Summary and discussion

The most important reason for using a mesoporous zeolite is its large external surface area that enables easy diffusion of substrates and products in and out of the zeolite. Unlike mesoporous materials such as MCM-41, mesoporous zeolites are crystalline and thus have much stronger hydrothermal stability and also much higher acidity which often makes them preferable for use in catalysis and also viable alternatives to conventional solid acid catalysts such as clays and solid phosphoric acids. However, introducing mesoporosity in zeolites simultaneously dictates that an increasing portion of the acidity will be available for molecules too large to actually enter the micropore structure. In order to analytically describe this important issue Pérez-Ramírez and co-workers have introduced an accessibility index (ACI) and the hierarchy factor (HF). The accessibility index is a characterization tool using bulky bases (pyridine, 2,6-lutidine and 2,4,6-collidine) in combination with infrared spectroscopy, to directly measure the effective mesoporosity of any zeolite system. It was shown that 2,4-lutidine probes approximately half the Brønsted acidic sites in a commercial ZSM-5 sample vs. all after a strong desilication and 2,4,6-collidine can access only 6% of the Brønsted acidic sites in the reference sample contrasted by almost 40% post desilication. This observation further supports the need to consider non-shape selective reactions in highly mesoporous zeolites in order to fully understand the properties of these materials in which the ACI can be a helpful tool [101]. The hierarchy factor [102] is an analytical tool intended to make comparison of mesoporosities possible independent of sample preparation. If considering a shape selective reaction taking place within the micropores, the micro- and mesopores will serve a distinctly different purpose, i.e. confining the active sites and facilitate mass transport, respectively. The authors thus argue that an optimum between the relative distributions is important in identifying the best catalyst for a given reaction. The hierarchy factor is defined as the product of (V_{micro}/V_{pore}) and (S_{meso}/S_{BET}) and can be conceptualized as a measure of how large a fraction of the micropore volume is advantageous to sacrifice in order to produce mesoporosity while still improving the catalytic performance. A linear correlation between productivity and the HF could be seen for benzene alkylation with ethylene [102] which very interestingly shows that not simply the most mesoporous sample performed best in this reaction but rather a sample having a pronounced mesoporosity as well as a (relatively) preserved microporosity. It must be noted that the HF does not take account for changes in acidity and should thus naturally be used supplemented by additional characterization. It does however, give an improved understanding of the porosity introduced allowing for a discussion of at which point a zeolite is in fact mesoporous enough. Supposedly a high HF is beneficial with respect to catalytic applications but this further depends on the reaction investigated. The same authors [77] have presented an illustrative example where the cracking of LDPE was tested over zeolite ITQ-4 desilicated to increasing levels. As the cracking reaction proceeds on the mesopore surface and pore openings the catalytic optimum was seen after the HF had reached its maximum. On the other hand considering a reaction with only a slight diffusion restraint one could expect the catalytic optimum to occur before a maximum in HF was reached. The HF is nonetheless an excellent tool for analyzing mesoporosity in zeolites, especially if porosity obtained by different protocols is to be compared.

8.1. Effect of mesopores on different reactions

Despite the different conditions and materials reported throughout literature, some generalizations on the effect of mesoporous zeolites in different reaction categories can be made though. Most of these can be classified into one of following two groups: reactions which take place in the micropores of the zeolite and reactions that take place on the external surface or in the pore mouths. For reactions taking place in the micropores, the mesopores effectively enhance the rate of diffusion in the bulk catalyst. For reactions taking place outside the microporous system, the mesopores dramatically increase the external surface area. The overall feature for both groups is that an increased catalytic activity is observed. This is especially the case for the cracking of large molecules such as polyethylene and hexadecane [68–76] but also in the condensation of large molecules and in the alkylation of aromatic compounds [12,76,78].

The effect of mesoporosity on selectivity is often a result of the increased diffusion of products out of the zeolite, thereby reducing the retention time of the product in the zeolite and thus the chance of it undergoing a second reaction. This effect causes an increase in the selectivity of most isomerisation reactions over that of cracking and in some cases an increase in the amount of large products formed in the cracking of *e.g.* polyethylene is seen. However in some cases a loss in selectivity of a desired product is observed. This is often caused by a loss of shape selectivity, leading to the formation of bulky by-products outside of the zeolite micropore system [76]. If a reaction benefits from the shape selective feature of a conventional zeolite, this effect is likely to be diminished using a mesoporous analogue and a decrease in selectivity is thus likely to occur unless measures are taken to deactivate the acid sites of the external surface of the crystals.

8.2. Effect of mesopores on the catalyst

The lifetime of the catalyst has in many cases been shown to increase by the introduction of mesoporosity. The main cause of deactivation in most cases relates to the effects of pore blocking by coke deposition in the zeolite. Numerous reports have argued that the positive effect on lifetime is caused not by a decreased rate of coke formation but rather from an enhanced resistance to the effects of coking. Shorter mean diffusion lengths coupled with more pore entrances in the mesoporous crystals render the crystal harder to block and this could very well account for the decreased effects of coking. This simple argument may however not describe the full picture. Authors have reasoned that as a consequence of the mesoporosity the products formed will have a lower retention time in the micropores which can suppress secondary reactions (coking). Naturally these considerations are very reaction specific but in this way the increased stability would be an effect derived of the improved mass transport.

9. Outlook

There are many methods of introducing mesoporosity into zeolites and these methods allow a high degree of fine-tuning to take place, enabling mesoporous zeolites containing a high degree of complexity to be synthesized. However, this also has the inherent drawback that a vast amount of unique mesoporous materials

Please cite this article in press as: M.S. Holm, et al., Catalysis with hierarchical zeolites, Catal. Today (2011), doi:10.1016/j.cattod.2011.01.007

are reported in the literature, making comparison across research groups a difficult task. Therefore a large proportion of the work effort related to mesoporous zeolites is spent on material preparation, leaving less room for more thorough characterization and catalytic testing. However, the use of mesoporous zeolites in catalysis is certainly gaining momentum and comparison across research groups is now possible as the volume of literature usable for comparison increases and generalized tools such as the ACI and HF have been introduced. The present review is focused on the catalytic use of hierarchical zeolites. The field combines multiple disciplines bringing together advanced material preparation, sophisticated and equipment-demanding characterization, as well as careful catalytic testing. From the reviewed literature it is clear that some of the best scholarly studies come from scientific groups which are well founded within all three categories and have dedicated time to perform in-depth characterization and demonstrate detailed knowledge of the catalytic reactions tested, while following the general recommendations for catalytic testing [103]. Reports preparing exciting materials but lacking the catalytic aspect have thus not been described in this contribution.

At present it is clear that many reactions indeed can benefit from the use of a mesoporous zeolite. A challenge within the field lies in the evaluation of the level and type of mesoporosity introduced into the zeolite crystal. Some of the protocols used for manufacturing the mesoporous zeolites can fairly easily be tuned into generating a series of zeolites with increasing levels of mesoporosity. This is especially true for desilication [104] but has also been shown valid by changing the carbon source in carbon-templating [105], varying the amount of cationic-polymer [26], *etc*. From comparing a series of zeolites with increasing levels of mesoporosity it could prove possible to extrapolate which level of mesoporosity is sufficient for the specific reaction. In this context it is naturally very important to consider whether the reaction is taking place within the micropores, in the pore mouths or solely on the external/mesopore surface. Evidently all three types of reactions will benefit from introducing mesoporosity into the zeolite. However, for a reaction that is proceeding within the micropores the level of mesoporosity at which diffusion is no longer a limiting factor is presumably different from a reaction proceeding in the pore mouths or on the mesopore walls. Further, in cases where a balance between activity and shape selectivity is sought, insight into the catalytic evolution using a series of hierarchical samples could contribute to understanding the reaction and the effect of mesoporosity in the zeolite catalyst.

Another challenge is connected to the need of comparing the hierarchical zeolite to a zeolite with physical-chemical properties differing only in the absence of mesoporosity. Indeed zeolites are complicated materials and often when a reference material is produced it can be problematic to claim that it is representative of a perfect non-mesoporous counterpart with exactly similar Si/Al ratio, crystal size, elementary distribution, defect density, *etc*. This problem can be negligible in most cases but for example in the case of desilication extra-framework aluminum can form on the external surface during the procedure [42,80,106]. The extra-framework aluminum sites thus represent an alien non-shape selective reactivity in the otherwise shape selective catalyst. This exemplifies why caution should be exercised in the interpretation of the catalytic data, since the mesoporosity introduced is presumably the most significant difference between the conventional/parent and the hierarchical sample, but potentially not the only one.

References

[1] S. van Donk, A.H. Janssen, J.H. Bitter, K.P. de Jong, Catal. Rev. 45 (2003) 297.
[2] M. Hartmann, Angew. Chem. Int. Ed. 43 (2004) 5880.
[3] Y. Tao, H. Kanoh, L. Abrams, K. Kaneko, Chem. Rev. 106 (2006) 896.
[4] L. Tosheva, V.P. Valtchev, C. R. Chim. 8 (2005) 475.
[5] J. Cejka, S. Mintova, Catal. Rev. 49 (2007) 1.
[6] K. Egeblad, C.H. Christensen, M. Kustova, C.H. Christensen, Chem. Mater. 20 (2008) 946–960.
[7] J. Perez-Ramirez, C.H. Christensen, K. Egeblad, C.H. Christensen, J.C. Groen, Chem. Soc. Rev. 37 (2008) 2530.
[8] C.D. Chang, C.T.W. Chu, US Patent no 4,594,333 (1986).
[9] C.D. Chang, C.T.W. Chu, P. Chu, R.M. Dessau, W.E. Garwood, G.H. Kuehl, J.N. Miale, D.S. Shibabi, US Patent no 4,876,228 (1989).
[10] J.M. Garces, D.M. Millar, US Patent 6,017,508 (1998).
[11] C.A. Drake, A.H. Wu, US Patent 5,952,259 (1999).
[12] C.H. Christensen, K. Johannsen, I. Schmidt, C.H. Christensen, J. Am. Chem. Soc. 125 (2003) 13370–13371.
[13] C.H. Christensen, K. Johannsen, E. Törnqvist, I. Schmidt, H. Topsoe, C.H. Christensen, Catal. Today 128 (2007) 117–122.
[14] J.C. Groen, T. Sano, J.A. Moulijn, J. Pérez-Ramirez, J. Catal. 251 (2007) 21–27.
[15] A.N.C. van Laak, R.W. Gosselink, S.L. Sagala, J.D. Meeldijk, P.E. de Jongh, K.P. de Jong, Appl. Catal. A 382 (2010) 65–72.
[16] J.C. Groen, J.C. Jansen, J.A. Moulijn, J. Perez-Ramirez, J. Phys. Chem. B 108 (2004) 13062–13065.
[17] A.N.C. van Laak, S.L. Sagala, J. Zecevic, H. Friedrich, P.E. de Jongh, K.P. de Jong, J. Catal. 276 (2010) 170–180.
[18] S.-T. Tsai, C.-H. Chen, T.-C. Tsai, Green Chem. 11 (2009) 1349–1356.
[19] H. Yang, Z. Liu, H. Gao, Z. Xie, Appl. Catal. A 379 (2010) 166–171.
[20] G.-s.J. Lee, J.M. Garces, G.R. Meima, M.J.M. van der Aalst, US Patent 5,243,116 (1993).
[21] G.-s.J. Lee, J.M. Garces, J.J. Maj, US Patent 5,015,797 (1991).
[22] G.-s.J. Lee, J.M. Garces, D.A. Hucul, T.L. Young, K.A. Burdett, US Patent 5,583,268 (1996).
[23] J.M. Garces, M.M. Olken, G.J. Lee, G.R. Meima, P.A. Jacobs, J.A. Martens, Top. Catal. 52 (2009) 1175–1181.
[24] G.S. Lee, J.J. Maj, S.C. Rocke, J.M. Garces, Catal. Lett. 2 (1989) 243–248.
[25] X. Tu, M. Matsumoto, T. Maeda, Y. Sugi, T. Matsuzaki, T. Hanaoka, Y. Kubota, J.-H. Kim, Micropor. Mater. 3 (1995) 593–595.
[26] F.-S. Xiao, L. Wang, C. Yin, K. Lin, Y. Di, J. Li, R. Xu, D.S. Su, R. Schlögl, T. Yokoi, T. Tatsumi, Angew. Chem. Int. Ed. 45 (2006) 3090–3093.
[27] Y. Sun, R. Prins, Appl. Catal. A 336 (2008) 11–16.
[28] X. Li, R. Prins, J.A. van Bokhoven, J. Catal. 262 (2009) 257–265.
[29] L. Jin, X. Zhou, H. Hu, B. Ma, Catal. Commun. 10 (2008) 336–340.
[30] Z. Musilova, N. Zilkova, S.-E. Park, J. Cejka, Top. Catal. 53 (2010) 1457–1469.
[31] L. Xu, S. Wu, J. Guan, H. Wang, Y. Ma, K. Song, H. Xu, H. Xing, Chen, Xu, Z. Wang, Q. Kan, Catal. Commun. 9 (2008) 1272–1276.
[32] E.G. Derouane, I. Schmidt, H. Lachas, C.J.H. Christensen, Catal. Lett. 95 (1–2) (2004) 13–17.
[33] D.P. Serrano, R.A. Garcia, D. Otero, Appl. Catal. A 359 (2009) 67.
[34] M. Bjørgen, F. Joensen, M.S. Holm, U. Olsbye, K.-P. Lillerud, S. Svelle, Appl. Catal. A 345 (2008) 43–50.
[35] G. Lietz, K.H. Schnabel, Ch. Peuker, Th. Gross, W. Storek, J. Völter, J. Catal. 148 (1994) 562–568.
[36] C. Fernandez, I. Stan, J.-P. Gilson, K. Thomas, A. Vicente, A. Bonilla, J. Perez-Ramirez, Chem. Eur. J. 16 (2010) 6224.
[37] M. Choi, K. Na, J. Kim, Y. Sakamoto, O. Terasaki, R. Ryoo, Nature 461 (2009) 246–249.
[38] J. Kim, M. Choi, R. Ryoo, J. Catal. 269 (2010) 219–228.
[39] C. Mei, P. Wen, Z. Liu, H. Liu, Y. Wang, W. Yang, Z. Xie, W. Hua, Z. Gao, J. Catal. 258 (2008) 243–249.
[40] C. Sun, J. Du, J. Liu, Y. Yang, N. Ren, W. Shen, H. Xu, Y. Tang, Chem Commun. 46 (2010) 2671–2673.
[41] L. Sommer, D. Mores, S. Svelle, M. Stöcker, B.M. Weckhuysen, U. Olsbye, Micropor. Mesopor. Mater. 132 (2010) 384–394.
[42] Y. Song, X. Zhu, Yi. Song, Q. Wang, L. Xu, Appl. Catal. A 302 (2006) 69–77.
[43] Y. Li, S. Liu, Z. Zhang, S. Xie, X. Zhu, L. Xu, Appl. Catal. A 338 (2008) 100–113.
[44] Y. Song, X. Zhu, Yi. Song, Q. Wang, L. Xu, Appl. Catal. A 302 (2006) 69.
[45] H.J. Park, H.S. Heo, J.-K. Jeon, J. Kim, R. Ryoo, K.-E. Jeong, Y.-K. Park, Appl. Catal. B 95 (2010) 365.
[46] J.R. Kiovsky, W.J. Goyette, US Patent 4,182,692 (1980).
[47] A. Voorhies, C.N. Kimberlin, E.M. Gladrow, US Patent 3,480,539 (1969).
[48] P.B. Koradia, J.R. Kiovsky, M.Y. Asim, J. Catal. (1980) 290–293.
[49] M. Tromp, J.A. van Bokhoven, M.T.G. Oostenbrink, J.H. Bitter, K.P. de Jong, D.C. Koningsberger, J. Catal. 190 (2000) 209–214.
[50] S. van Donk, A. Broersma, O.L.J. Gijzeman, J.A. van Bokhoven, J.H. Bitter, K.P. de Jong, J. Catal. 204 (2001) 272–280.
[51] P.-H. Chao, S.-T. Tsai, S.-L. Chang, I. Wang, T.-C. Tsai, Top. Catal. 53 (2010) 231.
[52] D.L. Moushey, P.G. Smirniotis, Catal. Lett. 129 (2009) 20–25.
[53] H. Zhu, Z. Liu, D. Kong, Y. Wang, Z. Xie, J. Phys. Chem C 112 (2008) 17257–17264.
[54] A. Chica, U. Diaz, V. Fornéz, A. Corma, Catal. Today (2008), doi:10.1016/j.cattod.2008.10.046.
[55] S. Zhang, Z.C. Zhang, Catal. Lett. 115 (2007) 114–121.
[56] L. Mokrzycki, B. Sulikowski, Z. Olejniczak, Catal. Lett. 127 (2009) 296–303.
[57] Ł. Mokrzycki, B. Sulikowski, Stud. Surf. Sci. Catal. 174B (2008) 1231–1234.
[58] J.A. Rabo, M.W. Schoonover, Appl. Catal. A 222 (2001) 261.
[59] H.H. Kung, S.M. Babitz, J.T. Miller, W.O. Haag, R.Q. Snurr, Top. Catal. 10 (2000) 59–64.
[60] W.O. Haag, R.M. Lago, P.B. Weisz, Faraday Discuss. Chem. Soc. 72 (1981) 317–330.

Please cite this article in press as: M.S. Holm, et al., Catalysis with hierarchical zeolites, Catal. Today (2011), doi:10.1016/j.cattod.2011.01.007

[61] J.S. Jung, J.W. Park, G. Seo, Appl. Catal. A 288 (2005) 149–157.
[62] K. Suzuki, Y. Aoyagi, N. Katada, M. Choi, R. Ryoo, M. Niwa, Catal. Today 132 (2008) 38–45.
[63] M.A. Bari Siddiqui, A.M. Aitani, M.R. Saeed, S. Al-Khattaf, Top. Catal. 53 (2010) 1387–1393.
[64] J. Zheng, X. Zhang, Y. Wang, Y. Bai, W. Sun, R. Li, J. Porous Mater., doi:10.1007/s10934-008-9255-2.
[65] Q. Lei, T. Zhao, F. Li, L. Zhang, Y. Wang, Chem. Commun. (2006) 1769–1771.
[66] H. Zhu, Z. Liu, D. Kong, Y. Wang, Z. Xie, J. Phys. Chem. C 112 (2008) 17257–17264.
[67] H.S. Bierenbaum, S. Chiramongkol, A.H. Weiss, J. Catal. 23 (1971) 61–70.
[68] C.H. Christensen, I. Schmidt, C.H. Christensen, Catal. Commun. 5 (2004) 543–546.
[69] M.Y. Kustova, P. Hasselriis, C.H. Christensen, Catal. Lett. 96 (2004) 205–211.
[70] M. Kustova, K. Egeblad, C.H. Christensen, A.L. Kustov, C.H. Christensen, Stud. Surf. Sci. Catal. (2007) 267–275.
[71] D.H. Park, S.S. Kim, H. Wang, T.J. Pinnavaia, M.C. Papapetrou, A.A. Lappas, K.S. Triantafyllidis, Angew. Chem. Int. Ed. 48 (2009) 7645–7648.
[72] D.P. Serrano, J. Aguado, J.M. Escola, J.M. Rodriguez, A. Peral, Chem. Mater. 18 (2006) 2462–2464.
[73] D.P. Serrano, J. Aguado, J.M. Escola, E. Garagorri, J.M. Rodríguez, L. Morselli, G. Palazzi, R. Orsi, Appl. Catal. B 49 (2004) 257–265.
[74] J. Aguado, D.P. Serrano, J.M. Rodríguez, Micropor. Mesopor. Mater. 115 (2008) 504–513.
[75] J. Pérez-Ramírez, S. Abelló, A. Bonilla, J.C. Groen, Adv. Funct. Mater. 19 (2009) 164–172.
[76] V.N. Shetti, J. Kim, R. Srivastava, M. Choi, R. Ryoo, J. Catal. 245 (2008) 296–303.
[77] D. Verboekend, J.C. Groen, J. Perez-Ramirez, Adv. Funct. Mater. 20 (2010) 1441–1450.
[78] M. Choi, H.S. Cho, R. Srivastava, C. Venkatesan, D.-H. Choi, R. Ryoo, Nat. Mater. 5 (2006) 718.
[79] R. Srivastava, M. Choi, R. Ryoo, Chem. Commun. (2006) 4489.
[80] F. Jin, Y. Cui, Y. Li, Appl. Catal. A 350 (2008) 71.
[81] W.-C. Li, A.-H. Lu, R. Palkovits, W. Schmidt, B. Spliethoff, F. Schüth, J. Am. Chem. Soc. 127 (2005) 12595.
[82] R. Palkovits, W. Schmidt, Y. Ilhan, A. Erdem-Senatalar, F. Schüth, Micropor. Mesopor. Mater. 117 (2009) 228.
[83] P. Botella, A. Corma, S. Iborra, R. Monton, I. Rodriguez, V. Costa, J. Catal. 250 (2007) 161.
[84] I. Schmidt, A. Krogh, K. Wienberg, A. Carlsson, M. Brorson, C.J.H. Jacobsen, Chem. Commun. (2000) 2157.
[85] M. Reichinger, W. Schmidt, M.W.E. Berg, A. Aerts, J.A. Martens, C.E.A. Kirschhock, H. Gies, W. Grünert, J. Catal. 269 (2010) 367.
[86] M.Yu. Kustova, P. Hasselriis, C.H. Christensen, Catal. Lett. 96 (2004) 205.
[87] D. Serrano, R. Sanz, P. Pizarro, I. Moreno, Chem. Commun. 11 (2009) 1407.
[88] S. Gopalakrishnan, A. Zampieri, W. Schwieger, J. Catal. 260 (2008) 193.
[89] H. Xin, J. Zhao, S. Xu, J. Li, W. Zhang, X. Guo, E.J.M. Hensen, Q. Yang, C. Li, J. Phys. Chem. C 114 (2010) 6553.
[90] T. Tang, C. Yin, L. Wang, Y. Ji, F.-S. Xiao, J. Catal. 249 (2007) 111.
[91] T. Tang, C. Yin, L. Wang, Y. Ji, F.-S. Xiao, J. Catal. 257 (2008) 125.
[92] Y. Sun, R. Prins, Angew. Chem. Int. Ed. 47 (2008) 8478.
[93] Q. Huo, T. Dou, Z. Zhao, H. Pan, Appl. Catal. A 381 (2010) 101.
[94] S. Brandenberger, O. Kröcjer, A. Tissler, R. Althoff, Catal. Rev. 50 (2008) 492.
[95] A.L. Kustov, K. Egeblad, M. Kustova, T.W. Hansen, C.H. Christensen, Top. Catal. 45 (2007) 159.
[96] A.L. Kustov, T.W. Hansen, M. Kustova, C.H. Christensen, Appl. Catal. B 76 (2007) 311.
[97] M.Yu. Kustova, S.B. Rasmussen, A.L. Kustov, C.H. Christensen, Appl. Catal. B 67 (2006) 60.
[98] J. Perez-Ramirez, F. Kapteijn, J.C. Groen, A. Domenech, G. Mul, J.A. Moulijn, J. Catal. 214 (2003) 33.
[99] I. Melian-Cabrera, S. Espinosa, J.C. Groen, B. v/d Linden, F. Kapteijn, J.A. Moulijn, J. Catal. 238 (2006) 250.
[100] J.C. Groen, A. Brückner, E. Berrier, L. Maldonado, J.A. Moulijn, J. Perez-Ramirez, J. Catal. 243 (2006) 212.
[101] F. Thibault-Starzyk, I. Stan, S. Abelló, A. Bonilla, K. Thomas, C. Fernandez, J.-P. Gilson, J. Pérez-Ramírez, J. Catal. 264 (2009) 11–14.
[102] J. Perez-Ramirez, D. Verboekend, A. Bonilla, S. Abello, Adv. Funct. Mater. 19 (2009) 3972–3979.
[103] F.M. Dautzenberg, Characterization and Catalyst Development, 1989, pp. 99–119, chap. 11.
[104] M.S. Holm, K. Egeblad, P.N.R. Vennestrøm, C.G. Hartmann, M. Kustova, C.H. Christensen, Eur. J. Inorg. Chem. 33 (2008) 5185–5189.
[105] Z. Kake, K. Egeblad, C.H. Christensen, Stud. Surf. Sci. Catal. 174a (2008) 285–288.
[106] M.S. Holm, S. Svelle, F. Joensen, P. Beato, C.H. Christensen, S. Bordiga, M. Bjørgen, Appl. Catal. A 1 (2009) 23–30.

Please cite this article in press as: M.S. Holm, et al., Catalysis with hierarchical zeolites, Catal. Today (2011), doi:10.1016/j.cattod.2011.01.007

Part 2

2.6 Aim and idea preceding the studies within co-feeding of oxygenates in MTG

Shortly after discovering the MTG process; it was shown that other oxygenates such as acetone, acetic acid or propanal could also be converted into hydrocarbons over zeolite ZSM-5. However, excessive coking of the catalyst compared to methanol conversion occurred.[1,2] Interestingly, decades later researchers that work in 'green and sustainable chemistry' pursue the conversion of similar oxygenates derived from non-edible biomass into hydrocarbon fuels. To facilitate transport and handling of for example straw it is commonly heat-treated. This produces a liquid (or aqueous suspension) called bio-oil that consists of lignocellulosic degradation products. This "oil" contains hundreds of different oxygenated compounds and is not directly usable as a fuel or even to blend with conventional hydrocarbons. Furthermore, it is corrosive, acidic, unstable and highly viscous.[3] Therefore it was proposed that zeolite-catalyzed deoxygenation could be used to produce hydrocarbons; thereby opening a path to a "green" fuel additive. If bio-oil is feed to a ZSM-5 catalyst at MTG-like reaction conditions (or higher temperatures to obtain a reasonable conversion) a rapid deactivation by coking is observed. Due to the very complex composition of bio-oil it is difficult to determine whether specific functionalities, unfavorable cross reactivity within the mixture or whether relatively few compounds are responsible for this deactivation. Yet another possibility could be that the zeolite-based conversion strategy simply is ill suited for the conversion of oxygenate substrates other than mono-alcohols.

Several reports have tried to convert either pure bio-oil or selected model compounds from bio-oil. They have predicted the reactivity of individual oxygenate species based on the formula given in Equation 2.1 below.[4,5,6,7] This equation defines the so-called effective H/C ratio of a compound.

$$\frac{H}{C}effective = \frac{(H - 2O)}{C}$$

Equation 2.1. The effective H/C ratio of a compound is calculated by inserting the number of hydrogen, oxygen and carbon atoms present in the molecule.

The effective H/C ratio is a measure of how much hydrogen compared to carbon is left in a specific molecule after it has dissociated its oxygen via dehydration. It is recognized in the literature that it is very difficult to predict the reactivity of various ketones, acids, diols, and mixtures thereof at the rather harsh reaction conditions of 370 °C catalyzed by a strong Brøndsted acidic zeolite. Therefore the effective H/C ratio is used as a "rule of thumb" to predict that a decreasing H/C ratio correspondingly will diminish the suitability of the given molecule. However, this approach completely neglects the presence of different functionalities in different positions within the molecule by simply narrowing the reactivity down to the *atomic ratio* of the molecule.

We suspected that the nature of the individual functionalities and positions within a molecule could not be ignored when predicting the potential of oxygenate conversion. We therefore chose to convert a variety of model compounds over zeolite ZSM-5 at MTG-like reaction conditions. In general, the catalytic results clearly showed that conversion of all compounds except mono-alcohols resulted in

extremely short catalyst lifetimes. Nevertheless the results presented in **section 2.7** showed that *i*-propanol proved to be a very suitable reactant that gave significant advantages as compared to reacting methanol or ethanol. Propanol is not present in bio-oil but we initially investigated it as part of the full experimental series. However, higher alcohols are produced in small amounts during methanol synthesis from syn gas. This could make it an interesting reactant at least as a co-feed and efforts are being directed towards increasing the yield of higher alcohols through innovative catalyst design.[8]

Section 2.8 includes the results obtained when reacting model oxygenates diluted in methanol. The co-feed model compounds were chosen based on their abundance in bio-oil and supplemented by compounds selected to cover as wide a span of H/C ratios and functionalities as possible. Further, for practical reasons the co-feed molecules were required to be volatile in order to be introduced into the setup.

[1] C. D. Chang, A. J. Silvestri, *J. Catal.*, 47, (**1977**), 249-259.

[2] W. O. Haag, P. G. Rodewald, P. B. Weisz, (**1981**), Mobil Oil Corporation, US. Patent 4.300.009.

[3] D. Mohan, C. U. Pittman Jr., P. H. Steele, *Energ. Fuel.*, 20, (**2006**), 848-889.

[4] N. Y. Chen, T. F. Degan, Jr., L. R. Koenig, *ChemTech*, (**1986**), 506-511.

[5] P. A. Horne, P. T. Williams, *Renew. Energ.*, 7, (**1996**), 131-144.

[6] R. French, S. Czernik, *Fuel Process Technol.*, 91, (**2010**), 25-32.

[7] T. R. Carlson, T. P. Vispute, G. W. Huber, *ChemSusChem*, 1, (**2008**), 397-400.

[8] J. M. Christensen, P. M. Mortensen, R. Trane, P. A. Jensen, A. D. Jensen, *Appl. Catal. A*, 366, (**2009**), 29-43.

J|A|C|S
ARTICLES

Published on Web 10/30/2009

High Yield of Liquid Range Olefins Obtained by Converting *i*-Propanol over Zeolite H-ZSM-5

Uffe V. Mentzel,*,†,‡ Saravanamurugan Shunmugavel,† Sarah L. Hruby,§ Claus H. Christensen,‡ and Martin S. Holm*,†,‡

Department of Chemistry, Technical University of Denmark, DK-2800 Kgs. Lyngby, Haldor Topsøe A/S, 2800 Kgs. Lyngby, and Department of Chemical and Biological Engineering, Iowa State University, Ames, Iowa 50011

Received September 10, 2009; E-mail: uvm@kemi.dtu.dk; msh@kemi.dtu.dk

Abstract: Methanol, ethanol, and *i*-propanol were converted under methanol-to-gasoline (MTH)-like conditions (400 °C, 1−20 bar) over zeolite H-ZSM-5. For methanol and ethanol, the catalyst lifetimes and conversion capacities are comparable, but when *i*-propanol is used as the reactant, the catalyst lifetime is increased dramatically. In fact, the total conversion capacity (calculated as the total amount of alcohol converted before deactivation in $g_{alcohol}/g_{zeolite}$) is more than 25 times higher for *i*-propanol compared to the lower alcohols. Furthermore, when *i*-propanol is used as the reactant, the selectivity toward alkanes and aromatics declines rapidly over time on stream, and at 20 bar of pressure the liquid product mixture consists almost exclusively of C_4-C_{12} alkenes after approximately a third of the full reaction time. This discovery could open a new route to hydrocarbons via *i*-propanol from syn-gas or biobased feedstocks.

Introduction

The methanol-to-hydrocarbons (MTH) reaction was discovered and commercialized more than two decades ago. However, due to the situation on the global oil market, the gasoline synthesis was discontinued.[1,2] Currently, the MTH reaction is receiving renewed attention due to the focus on renewable fuel sources.[3] The level to which this reaction can contribute to a sustainable nonfossil-based energy sector naturally depends on the origin of the methanol.[4] Methanol is traditionally produced from coal or natural gas via syn-gas, but many interesting nonfossil routes for the production of methanol as well as higher alcohols are investigated today.[5] Methods for production of higher alcohols from syn-gas are also under development[6,7] as is the gasification of biomass to syn-gas.[8]

Since the MTH reaction was discovered in the early 1970s and published in 1977,[9] the reaction mechanism has been widely debated.[10] The "hydrocarbon pool mechanism" in which carbonaceous species in the zeolitic pores are part of the catalytic system has become generally accepted. This idea was originally suggested by Mole[11] and Langner,[12] and a decade later Kolboe et al.[13,14] introduced a more general mechanism. Through isotopic labeling experiments Bjørgen et al.[15] uncovered further mechanistic details about the hydrocarbon pool and suggested "the dual cycle mechanism". Recently, mechanistic modeling has also been used to gain insight into the mechanistic details.[16,17]

In the MTH reaction, the zeolite catalyst suffers from deactivation due to coking and frequent regeneration by combustion of the deposited coke is required. It is thus a key research area to improve the catalyst lifetime between regenerations. Another important objective is to suppress the formation of aromatic compounds and shift the selectivity toward the production of olefins (the MTO reaction).[18,19] Numerous approaches have been tried to obtain these goals, most of them dealing with optimization of the catalyst or modifying the reaction conditions.[20−24]

† Technical University of Denmark.
‡ Haldor Topsøe A/S.
§ Iowa State University.

(1) Stöcker, M. *Microporous Mesoporous Mater.* **1999**, *2*, 9–3.
(2) Topp-Jørgensen, J. *Stud. Surf. Sci. Catal.* **1998**, *36*, 293.
(3) Suntana, A. S.; Vogt, K. A.; Turnblom, E. C.; Upadhye, R. *Appl. Energy* **2009**, *86*, 215.
(4) Vogt, K. A.; Vogt, D. J.; Patel-Weynand, T.; Upadhye, R.; Edlund, D.; Edmonds, R. L.; Gordan, J. C.; Suntana, A. S.; Sigurdardottir, R.; Miller, M.; Roads, P. A.; Andreu, M. G. *Renew. Energ.* **2009**, *34*, 233.
(5) Atsumi, S.; Hanai, T.; Liao, J. C. *Nature.* **2008**, 451.
(6) Iranmahboob, J.; Hill, D. O.; Toghiani, H. *Appl. Catal., A* **2002**, *231*, 99.
(7) Spivey, J. J.; Egbebi, A. *Chem. Soc. Rev.* **2007**, *36*, 1514.
(8) Al Arni, S.; Bosio, B.; Arato, E. *Renew. Energ.* **2010**, *35*, 29.
(9) Chang, C. D.; Silvestri, A. J. *J. Catal.* **1977**, *47*, 249.
(10) Haw, J. F.; Song, W.; Marcus, D. M.; Nicholas, J. B. *Acc. Chem. Res.* **2003**, *36*, 317.
(11) Mole, T.; Whiteside, J. A.; Seddon, D. *J. Catal.* **1983**, *82*, 261.
(12) Langner, B. E. *Appl. Catal.* **1982**, *2*, 289.
(13) Dahl, I. M.; Kolboe, S. *Catal. Lett.* **1993**, *20*, 329.
(14) Dahl, I. M.; Kolboe, S. *J. Catal.* **1994**, *149*, 458.
(15) Bjørgen, M.; Svelle, S.; Joensen, F.; Nerlov, J.; Kolboe, S.; Bonino, F.; Bordiga, S.; Olsbye, U. *J. Catal.* **2007**, *249*, 195.
(16) McCann, D. M.; Lesthaeghe, D.; Kletnieks, P. W.; Guenther, D. R.; Hayman, M. J.; Speybroeck, V. V.; Waroquier, M.; Haw, J. F. *Angew. Chem., Int. Ed.* **2008**, *47*, 5179.
(17) Svelle, S.; Tuma, C.; Rozanska, X.; Kerber, T.; Sauer, J. *J. Am. Chem. Soc.* **2009**, *131*, 816.
(18) Haw, J. F.; Marcus, D. M. *Nanotechnology in Catalysis*; Plenum Publishers: New York, 2004; Vol. 1, Chapter 13.
(19) Bjørgen, M.; Joensen, F.; Lillerud, K.-P.; Olsbye, U.; Svelle, S. *Catal. Today* **2009**, *142*, 90.
(20) Chen, J. Q.; Bozzano, A.; Glover, B.; Fuglerud, T.; Kvisle, S. *Catal. Today* **2005**, *106*, 103.
(21) Mokrani, T.; Scurrell, M. *Catal. Rev.* **2009**, *51* (1), 145.

10.1021/ja907692t CCC: $40.75

Table 1. Feed Rates and Observed Conversion Capacities

	P (atm)	WHSV (h^{-1})	feed rate $n_{alcohol}$ (mmol/g_{cat}*h)	feed rate n_{carbon} (mmol/g_{cat}*h)	conv. cap. $mol_{carbon}/g_{zeolite}$	conv. cap. $g_{alcohol}/g_{zeolite}$
methanol	1	8.4	263	263	11	350
ethanol	1	12.1	263	526	22	505
i-propanol	1	15.8	263	789	565	11300

In the literature, many different reactants have been tested under MTH-like reaction conditions. Already in the first article on MTH[9] a number of different oxygen containing reactants (higher alcohols, carbonyl compounds, acids, and esters) were screened in the reaction, all resulting in a mixture of hydrocarbon products. Recently, Gayubo et al.[25,26] did a thorough screening of reactants, including higher alcohols (propanol and butanol) phenols, aldehydes, ketones, and carboxylic acids. In all cases, a mixture of hydrocarbon products containing olefins, paraffins, and aromatics was produced, illustrating that H-ZSM-5 is virtually omnivorous. In an attempt to elucidate mechanistic information, mixtures of methanol and higher alcohols (ethanol, *i*-propanol, and 1-butanol), were reacted over H-ZSM-5 by Tau et al.[27] Through isotopic labeling experiments it was concluded that the carbon atoms from the different alcohols are scrambled and distributed randomly in the products. Lifetime and deactivation of the catalyst however was not addressed in these studies.

Tabak et al. have converted propene and butene to hydrocarbons over ZSM-5.[28] They show that the small alkenes oligomerize and by varying the reaction temperature and pressure they are able to change the reactivity of oligomerization versus cracking and thereby controlling the molecular weight of the products.

In an early study,[29] methanol and ethanol were compared as reactants over H-ZSM-5, and very similar product distributions were obtained. This was confirmed in a recent article from our research group, where the differences in the hydrocarbon pool were also discussed.[30]

Very recently, Gujar et al. studied the conversion of C_1-C_4 alcohols over H-ZSM-5 in a batch reactor. They concluded that the higher alcohols produce more organic liquid than methanol, when allowed to react for the fixed time in the reactor.[31]

Even though several different reactants and cofeeding experiments have been tested in the catalytic conversion over H-ZSM-5, almost no emphasis has been put on the dependence of the reactant on catalyst lifetime and deactivation when using other reactants than methanol or ethanol. In the present study, methanol, ethanol, and *i*-propanol are compared as reactants over H-ZSM-5 and the focus is placed on the beneficial effects observed on product selectivity as well as lifetime of the catalyst when feeding *i*-propanol.

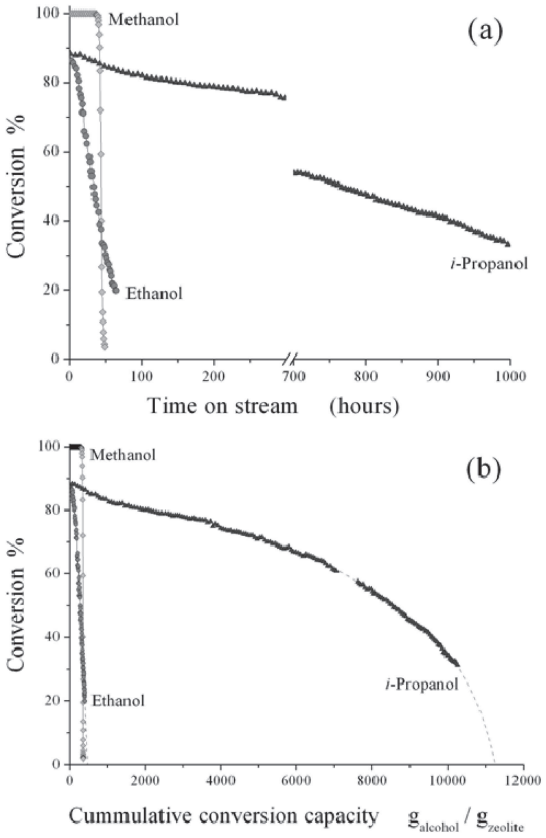

Figure 1. (a) Conversion profiles of methanol, ethanol, and *i*-propanol reacted over H-ZSM-5 at 400 °C. (b) Cumulative conversion capacities in $g_{alcohol}/g_{zeolite}$ given as a function of the alcohol conversion.

Experimental Section

The catalyst used was a commercially available zeolite ZSM-5 (Si/Al = 40) kindly provided by Zeolyst International. The catalytic reactions were performed in a fixed bed reactor at a reaction temperature of 400 °C and a pressure of 1 or 20 bar. In all runs, 300 mg of fractioned (350−500 μm) zeolite catalyst was used. The reactant liquid was introduced by a HPLC pump and evaporated before the catalyst bed. The feed rates of the various alcohols were normalized to introduce an equivalent molar amount of alcohol per unit of time. This resulted in a significantly larger WHSV for the higher alcohols compared to methanol. The feed rates for the different alcohols are listed in Table 1.

For reactions performed at 1 bar, the products were analyzed by an online GC equipped with a flame ionization detector. Helium was used as an inert carrier gas with a flow of 20 mL/min in all nonpressurerized experiments.

When performing the reaction at 20 bar of pressure, the products were condensed at room temperature while still pressurized. The

(22) Bjørgen, M.; Joensen, F.; Holm, M. S.; Olsbye, U.; Lillerud, K. P.; Svelle, S. *Appl. Catal., A* **2008**, *345*, 43.
(23) Christensen, C. H.; Johannsen, K.; Törnqvist, E.; Schmidt, I.; Topsoe, H.; Christensen, C. H. *Catal. Today* **2007**, *128*, 177.
(24) Teketel, S.; Svelle, S.; Lillerud, K. P.; Olsbye, U. *ChemCatChem* **2009**, *1*, 78.
(25) Gayubo, A. G.; Aguayo, A. T.; Atutxa, A.; Aguado, R.; Bilbao, J. *Ind. Eng. Chem. Res.* **2004**, *43*, 2610.
(26) Gayubo, A. G.; Aguayo, A. T.; Atutxa, A.; Aguado, R.; Olazar, M.; Bilbao, J. *Ind. Eng. Chem. Res.* **2004**, *43*, 2619.
(27) Tau, L. M.; Davis, B. H. *Fuel Process. Technol.* **1990**, *26*, 209.
(28) Tabak, S. A.; Krambeck, F. J.; Garwood, W. E. *AIChE J.* **1986**, *64*, 72.
(29) Derouane, E. G.; Nagy, J. B.; Dejaifve, P.; van Hoff, J. H. C.; Spekman, B. P.; Védrine, J. C.; Naccache, C. *J. Catal.* **1978**, *53*, 40.
(30) Johanson, R.; Hruby, S. L.; Rass-Hansen, J.; Christensen, C. H. *Catal. Lett.* **2009**, *127*, 1.
(31) Gujar, A. C.; Guda, V. K.; Nolan, M.; Yan, Q.; Toghiani, H.; White, M. G. *Appl. Catal., A* **2009**, *363*, 115.

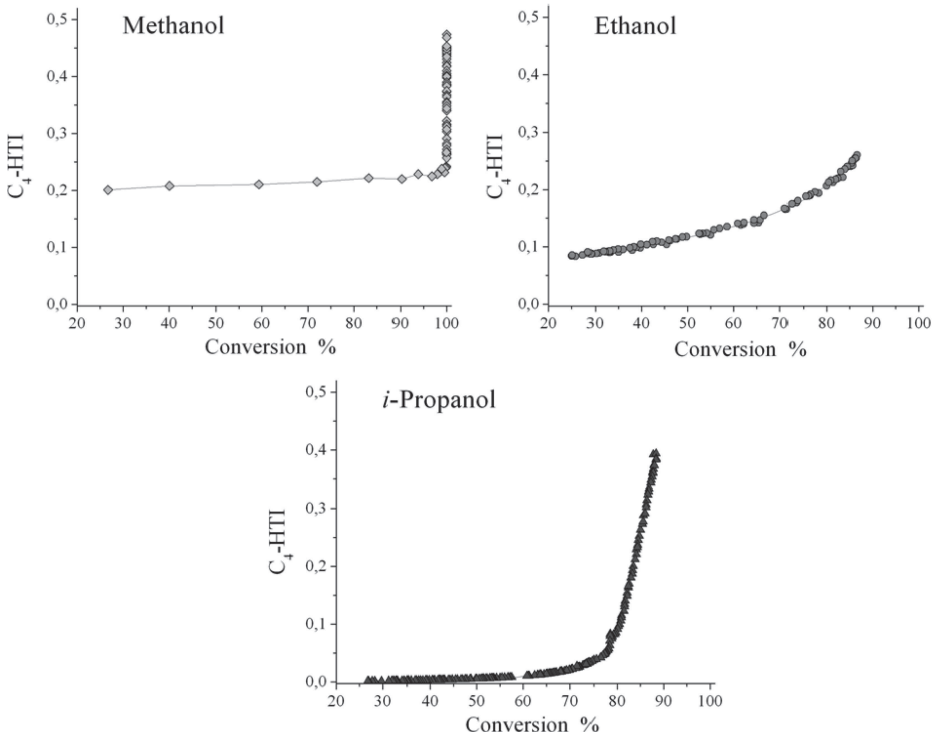

Figure 2. C_4−HTI plotted as a function of the conversion for the three alcohols tested.

gas phase was continuously monitored by an online GC whereas the liquid products were analyzed by offline GC after decompressing the liquid sample to ambient pressure. Helium was used as the carrier gas with a flow of 40 mL/min in all pressurized experiments.

Results and Discussion

The lifetime of the catalyst (conversion vs time on stream) for the different alcohol feeds is illustrated in Figure 1a. When the conversions of the different alcohols are calculated, the direct dehydration products (dimethyl ether, diethyl ether, ethene, dipropyl ether, and propene, respectively) are considered reactants. These dehydration products are still produced over the completely deactivated catalyst, although dipropyl ether was never formed in significant amounts. Initially, we do not observe full conversion in the cases of ethanol and *i*-propanol. This does not mean that the catalyst is not sufficiently active; the (dehydrated) reactants are simply part of the normal products formed during the reaction.

From Figure 1a it is seen that when methanol or ethanol is fed, the catalyst is deactivated within in a few days, but when *i*-propanol is used, the catalyst is still active (>30% conversion) after more than 1000 h on stream.

In addition, the *molar* feed rates are kept constant for the different alcohols, meaning that the catalyst converts three times the amount of carbon/h when *i*-propanol is fed compared to methanol, see Table 1. If *i*-propanol is fed with a WHSV of 8.4 as in the case of methanol, the deactivation of the catalyst scales accordingly, simply making the reaction times required to reach deactivation impractical.

For conversion of methanol, coke is deposited on the catalyst, and a deactivation zone moves through the catalyst bed, resulting in the sudden drop in conversion when the whole catalyst bed is deactivated. This sudden drop in conversion is not observed to the same degree for ethanol and especially not for *i*-propanol.

The cumulative conversion capacity is plotted in Figure 1b, and values showing the total amount (calculated on a weight basis) of alcohol converted over the entire lifetime of the catalyst are summarized in Table 1. When propanol is fed, the catalyst is able to convert more than 25 times the amount of alcohol before reaching complete deactivation, compared to the smaller alcohols.

When the catalytic activity in the MTH reaction is described, the "C_4 hydrogen transfer index" (C_4−HTI) is often used.[22] This is defined as the amount of butanes (iso-butane and *n*-butane) divided by the total amount of C_4-compounds and thus gives a good indication of the development of the hydrogen transfer ability of the working catalyst. When the C_4−HTI is high, the catalyst is able to convert alkenes to aromatics and alkanes. The C_4−HTI as a function of conversion for the three alcohols is presented in Figure 2. For methanol the C_4−HTI is quite high (ca. 0.47) in the beginning and drops steadily as the catalyst deactivates to around 0.22, at which point we observe breakthrough of methanol and the catalyst is completely deactivated. For ethanol and *i*-propanol, the initial values are around 0.26 and 0.38, respectively, and they decline with conversion. Interestingly, for *i*-propanol, the C_4−HTI approaches zero already when the conversion is around 60−70%. This means that the catalyst is no longer able to convert alkenes to aromatics and alkanes, and therefore the product mixture consists almost exclusively of alkenes. A decrease in the C_4−HTI is expected during deactivation due to a decrease in the effective acid site

Table 2. Product Selectivities for Conversion of the Three Alcohols Calculated as Carbon Percentages

	methane	ethane	ethene	propane	propene	C_4-butenes	C_4-butanes	C_{5+}(aliphatics)	aromatics
Methanol									
Initially	0.7	0.2	5.3	6.2	11.8	14.7	12.0	28.3	20.8
~80% conv.	2.4	0.1	8.6	1.1	25.4	14.6	4.0	33.5	10.1
~60% conv.	3.0	0.1	10.9	0.8	24.7	13.2	3.5	33.5	10.0
~40% conv.	4.0	0.1	13.8	0.7	24.2	11.8	3.0	31.1	11.0
Ethanol									
Initially	0.1	0.7	−	5.7	20.6	22.9	7.8	27.3	14.5
~80% conv.	0.1	0.9	−	3.9	23.8	25.2	6.1	27.7	12.4
~60% conv.	<0.1	1.0	−	2.2	27.0	27.8	4.3	29.9	7.8
~40% conv.	<0.1	1.1	−	1.3	29.5	28.5	3.0	30.2	6.5
i-Propanol									
Initially	<0.1	0.1	4.4	7.3	−	19.2	12.4	35.5	21.1
~80% conv.	<0.1	<0.1	2.4	2.2	−	37.1	3.7	50.2	4.4
~60% conv.	<0.1	<0.1	0.7	0.8	−	46.7	0.5	50.8	0.5
~40% conv.	<0.1	<0.1	0.4	0.5	−	38.2	0.1	60.8	<0.1

density present in the catalyst bed.[22,32,33] However, as is the case for the presented methanol experiment, the catalyst will normally be completely deactivated before the C_4−HTI approaches zero. In the case of *i*-propanol this is not true, since the catalyst is still able to perform oligemerization and cracking reactions forming a rich mixture of long branched alkenes when the C_4−HTI is approximately zero.

Product selectivities for the three tested alcohols as a function of the conversion are listed in Table 2. We note that the initial product selectivities are quite similar for all the alcohols, as they all produce a significant amount of aromatics. The selectivity toward aromatics compounds (mainly toluene, xylenes and trimethyl benzene isomers) however decreases significantly for *i*-propanol over time. This is naturally expected from the presented low C_4−HTI of the catalyst at intermediate conversions. Again this observation is in strong contrast to the methanol experiment where the catalyst produces aromatic compounds right up to the point of complete deactivation. Another interesting observation when using *i*-propanol as the reactant is, that the production of ethene also decreases over time. This is in good accordance with conclusions drawn by Svelle et al.,[34] suggesting that the production of ethene is mechanistically linked to the production of aromatics; thus, when a smaller amount of aromatics is produced, a smaller amount of ethene is produced. The fact that the concentration of ethene decreases so dramatically also indicates that only a minor fraction (if any) of the produced ethene is formed from cracking of larger alkenes, since the alkene oligemerization/cracking cycle is still very active at this point. This observation is very important since only small amounts of the lower value products methane, ethane, and ethene are produced.

To confirm the above findings under reaction conditions closer to the industrially used and to push the selectivity toward liquid products, similar experiments with methanol, ethanol and *i*-propanol were performed in a pressure setup operated at 20 bar. The condensed liquid products were periodically withdrawn to atmospheric pressure for GC analysis. The rates of formation of liquid products per gram of zeolite are illustrated in Figure 3 for the three alcohols. Again we observe that the lifetime of the catalyst when feeding *i*-propanol is far superior to the other alcohols. Naturally, the rate of liquid product formation is highly dependent on the WHSV, but in Table 3 the total yields of liquid products before reaching complete deactivation are summarized. Here we see that methanol produces around 160 $mL/g_{zeolite}$ whereas *i*-propanol yields as much as 3550 $mL/g_{zeolite}$.

The dark coloring of the columns in Figure 3(a−c) represents the carbon% present in aromatic compounds. In accordance with the nonpressure experiments *i*-propanol initially produce an aromatic rich liquid but for the latter ~2/3 of the experiment solely C_4−C_{12} alkenes are formed. In Table 3, the total averaged aromatic carbon% of the liquid products is given.

When the reaction is performed at 20 bar, the initial selectivity toward aromatics is higher than at 1 bar, and it declines more rapidly. Furthermore, the lifetime of the catalyst when converting *i*-propanol is around 50% shorter, than at 1 bar. This effect is not observed for methanol and ethanol, where the catalyst shows similar lifetimes at 1 and 20 bar.

Along with the much higher conversion capacity of *i*-propanol, the low aromatic carbon% illustrates the pronounced difference of using *i*-propanol compared to methanol or ethanol as the reactant. GC-MS analysis was used to identify the various compounds formed during the experiment. Figure 4 shows the product distribution in the organic liquid when using *i*-propanol. The sample presented in Figure 4a was obtained after approximately 250 h on stream representing a case from Figure 3c where insignificant amounts of aromatics are formed. Clearly we see that a huge range of different alkene isomers is produced from the reaction. There are no detectable aromatic compounds and only minute traces of alkanes present in the liquid at this point. Alkene contribution ranges from C_4 to C_{12} species. The shape selectivity of the zeolite is clearly affecting the larger products, no bulky products are able to escape the zeolite pores and mainly methylated long chains are present in the products. Interestingly, as the catalyst deactivates further from this point the product distribution changes systematically. In the last hours of operation we observe a pronounced enrichment in the C_6, C_9 and C_{12} alkenes indicating that cracking of the formed alkenes is diminished and we thus mainly observe the direct oligomerization products of propene, see Figure 4b.

Conclusions

It has been shown here that the lifetime and conversion capacity of the zeolite catalyst is increased dramatically when *i*-propanol is used as reactant instead of methanol or ethanol in the catalytic conversion over H-ZSM-5.

Furthermore, when reacting *i*-propanol the C_4−HTI approaches zero after approximately a third of the full experimental

(32) Janssens, T. V. W. *J. Catal.* **2009**, *264*, 130.
(33) Bjørgen, M.; Kolboe, S. *Appl. Catal., A* **2002**, *225*, 285.
(34) Svelle, S.; Joensen, F.; Nerlov, J.; Olsbye, U.; Lillerud, K. P.; Kolboe, S.; Bjørgen, M. *J. Am. Chem. Soc.* **2006**, *128*, 14770.

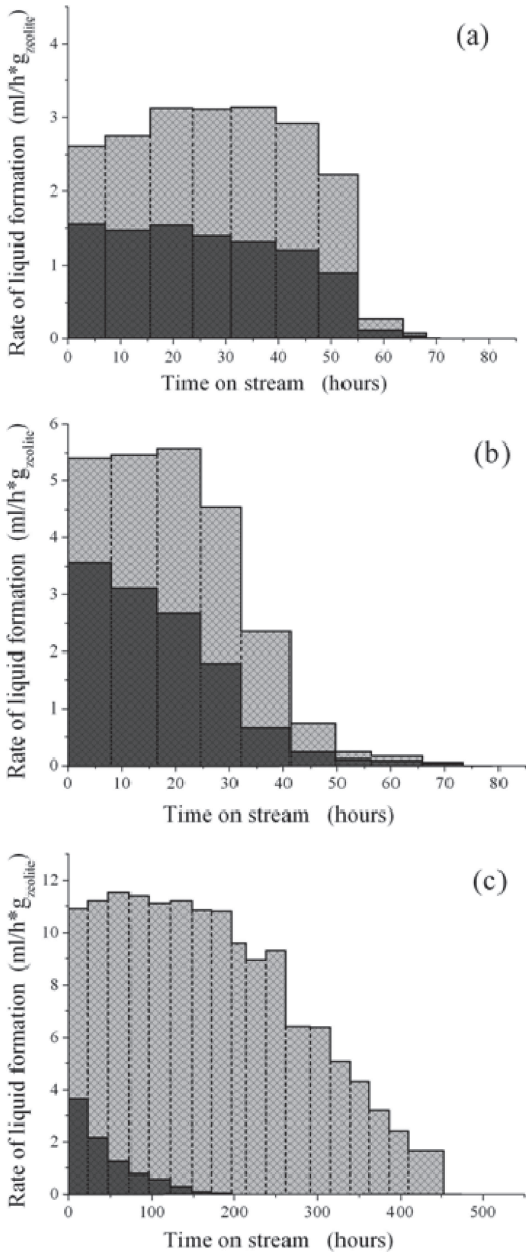

Figure 3. Rate of formation of the organic phase from reacting (a) methanol, (b) ethanol, and (c) *i*-propanol over H-ZSM-5 at 400 °C. The dark coloring represents the carbon% present in aromatics.

run time, meaning that the selectivity is almost exclusively shifted toward the production of alkenes, and only minute amounts of aromatics and alkanes are formed. The resulting alkene rich liquid product which is very low in aromatic content

Table 3. Total Yield and Selectivities at 20 bar

	P bar	WHSV $gg^{-1}h^{-1}$	org. liq. mL/g_{cat}	total carbon in aromatics
Methanol	20	8.4	160	46.9%
Ethanol	20	12	200	49.9%
i-Propanol	20	16	3550	6.1%

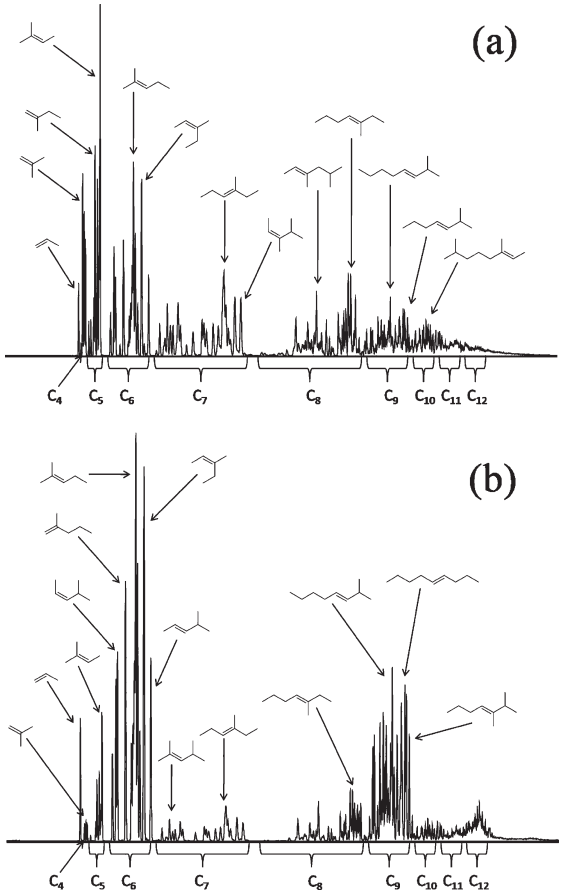

Figure 4. GC-MS analysis of the organic phase feeding *i*-propanol (a) after 250 h on stream and (b) after 425 h on stream. Major compounds are labeled for illustrative reasons.

can serve as an attractive raw material for the chemical industry, or could easily be hydrogenated to produce high quality clean fuel. On the basis of the results presented here, an alternative route from syn-gas or biobased feedstocks to hydrocarbons going via *i*-propanol instead of methanol can be envisaged.

Acknowledgment. The Centre for Catalysis and Sustainable Chemistry is sponsored by the Danish National Research Foundation. S.L.H. acknowledges the National Science Foundation's Partnership for International Research and Education (PIRE) (NSF grant OISE 0730277) for financial support.

JA907692T

G Model
APCATA-13016; No. of Pages 9
ARTICLE IN PRESS

Applied Catalysis A: General xxx (2011) xxx–xxx

Contents lists available at ScienceDirect

Applied Catalysis A: General

journal homepage: www.elsevier.com/locate/apcata

Utilization of biomass: Conversion of model compounds to hydrocarbons over zeolite H-ZSM-5

Uffe V. Mentzel[a,b,*], Martin S. Holm[a,b,*]

[a] Centre for Catalysis and Sustainable Chemistry, Department of Chemistry, Technical University of Denmark, Anker Engelundsvej 1, DK 2800 Kgs. Lyngby, Denmark
[b] Center for Green and Sustainable Chemistry, Department of Chemistry, Technical University of Denmark, Anker Engelundsvej 1, DK 2800 Kgs. Lyngby, Denmark

ARTICLE INFO

Article history:
Received 23 November 2010
Received in revised form 25 January 2011
Accepted 27 January 2011
Available online xxx

Keywords:
Zeolite
ZSM-5
Methanol-to-Hydrocarbons (MTH)
Bio-oil
Biomass-to-liquids (BTL)

ABSTRACT

Zeolite catalyzed deoxygenation of small oxygenates present in bio-oil or selected as model compounds was performed under Methanol-to-Hydrocarbons (MTH) like reaction conditions using H-ZSM-5 as the catalyst. Co-feeding of the oxygenates with methanol generally decreases catalyst lifetime due to coking and results in higher selectivity towards aromatics compared to conversion of pure methanol. The reaction pattern of the different oxygenates did not simply follow the effective H/C ratio of the additives since structural isomers with identical effective H/C ratios showed significant differences with respect to catalyst lifetime and product selectivity. A distinct positive effect on catalyst lifetime was observed for methanol dilution. Thus, the conversion capacity of the catalyst was up to 10 times higher when the reactant was diluted in methanol. We observe that in particular acid/ester functionalities favor oxygen removal through decarbonylation over dehydration which preserves hydrogen in the hydrocarbon product mixture. By employing ^{13}C labeled substrates we confirmed the incorporation of carbon into the hydrocarbon products as well as a pronounced preference of the additive carbon towards incorporation into aromatic compounds.

1. Introduction

The development of a more sustainable and environmentally friendly production of chemicals and transportation fuels is pursued today [1]. The use of a biomass derived fuel additives such as bio-ethanol or bio-diesel represent examples of current strategies towards the employment of "greener" fuels [2,3].

Bio-oil can be produced from numerous types of biomass through a rapid thermal treatment with no or only little oxygen present. Bio-oil represents an abundant and near CO_2 neutral resource which could find application if sufficiently efficient upgrading strategies are identified. Depending on the starting material and the specific treatment conditions, large compositional discrepancies are seen within bio-oils but in general it is a highly complex mixture of oxygenates produced by depolymerization and fragmentation of cellulose, hemi-cellulose, and lignin [4]. Bio-oil is immiscible with hydrocarbons, contains large amounts of water, and is relatively unstable, however the liquid has an advantage over untreated biomass with respect to handling and transportation [5,6]. Transformation of bio-oil into a mixture of hydrocarbons through zeolite catalyzed deoxygenation is highly desired and could ensure compatibility with conventional gasoline [7]. In fact, researchers at Mobil already in the years following the discovery of the Methanol-to-gasoline (MTG) process [8] investigated this idea of converting biomass into hydrocarbons primarily over zeolite ZSM-5 [9,10]. They introduced the effective H/C ratio of a substrate (see Eq. (1)), with H, O, and C being the moles of hydrogen, oxygen, and carbon present in the compound. This is a convenient measure of the hydrogen content left in the products once oxygen is removed as water [11].

$$\frac{H}{C}\text{effective} = \frac{(H-20)}{C} \quad (1)$$

Eq. (1): Definition of the effective H/C ratio, where H, C, and O are the number of hydrogen, carbon, and oxygen atoms present in the specific compound.

Excessive deactivation of the catalyst by coking was discovered as a major problem when reacting compounds with an effective H/C ratio below 2. A carbohydrate with a molecular formula of $C_6H_{12}O_6$ has an effective H/C ratio of 0 and will thus be able to produce only carbon if fully dehydrated. However, if the reactants are deoxygenated by decarbonylation or decarboxylation (formation of CO or CO_2, respectively) hydrogen is retained in the hydrocarbon products. Consequently, if a gasoline product mixture with a similar H/C content as conventional MTH fuel is desired, a hexose would

* Corresponding authors at: Centre for Catalysis and Sustainable Chemistry, Department of Chemistry, Technical University of Denmark, Anker Engelundsvej 1, DK 2800 Kgs. Lyngby, Denmark.
E-mail addresses: uvm@kemi.dtu.dk (U.V. Mentzel), msh@kemi.dtu.dk (M.S. Holm).

0926-860X/$ – see front matter © 2011 Elsevier B.V. All rights reserved.
doi:10.1016/j.apcata.2011.01.040

Please cite this article in press as: U.V. Mentzel, M.S. Holm, Appl. Catal. A: Gen. (2011), doi:10.1016/j.apcata.2011.01.040

need to dissociate 1/3 of its carbon atoms as CO_2 which resembles fermentation where CO_2 and ethanol are formed.

Several authors have reported on zeolite catalyzed conversion of bio-oil/pyrolysis vapors [7,12–17] or selected model compounds present in bio-oil [18–31] over mainly zeolite ZSM-5 at MTH-like reaction conditions. Due to the very complex nature of bio-oil only limited information regarding the reactivity of the individual components is obtained when feeding the highly complex bio-oil mixture which merits the investigation of representative model compounds. Very interestingly the reports show that hydrocarbons can indeed be produced from virtually any oxygenate but generally the catalyst suffers from extremely fast deactivation by coking. The addition of methanol, which has an effective H/C ratio of 2, will increase the combined H/C ratio of the feed and has been reported to have a positive effect e.g. on the conversion of furfural [11,32]. Also dilution of bio-oil with methanol has been reported [33] and recently Bilbao and co-workers showed that methanol addition attenuates the condensation of pyrolytic lignin when the feed is heated prior to introduction to the reactor [34]. Significant improvements were thus achieved in a two-step process where the bio-oil and methanol mixture was volatilized in a separate unit before the catalytic conversion [35,36].

The use of zeolite catalysts for conversion of biomass derived compounds in the high temperature range of FCC have also recently been reported [37–39]. In relation to this, Huber and co-workers used finely dispersed sugar physically blended with the catalyst while applying extremely rapid heating, and were thus able to produce single- and poly-aromatics alongside CO_2 and water although also substantial coking of the catalyst occurs [40–42].

Here we present a study investigating the reactivity of selected oxygenates when co-fed with methanol at MTH reaction conditions over zeolite H-ZSM-5. The additives contain different functionalities and were selected to cover a wide range of H/C ratios. The oxygenates were co-reacted as 10 wt% solutions in methanol to obtain lifetimes between one hour and 2.5 days which made evaluation of their compatibility with MTH possible. The most interesting compounds were further tested in a wt% series intended to quantify the positive effect of methanol dilution with respect to conversion capacity of the additive. Experiments using ^{13}C-labeling of the substrates were performed in order to address whether the carbon atoms from the additives were in fact incorporated into the hydrocarbon products.

2. Experimental

The zeolite catalyst used in this study was a commercially available zeolite ZSM-5 with a Si/Al ratio of 40 kindly supplied by Zeolyst. The NH_4-ZSM-5 was transformed into proton form by calcination at 550 °C for 6 h reached with a heating ramp of 2 °C/min.

Characterization by XRPD, N_2-sorption, and elemental analysis of the commercial ZSM-5 sample is presented in supplementary data. Phase purity, crystallinity, and the nominal Si/Al ratio of 40 are confirmed.

Catalytic experiments were performed with 300 mg of pure zeolite which was crushed and sieved to obtain particle size of 350–500 μm and fixated by quartz wool in a quartz reactor having an internal diameter of 4 mm. During heating to the reaction temperature (370 °C) the catalyst was kept in a flow of helium of 40 ml/min. The reactants were introduced by an HPLC pump at a rate of 0.05 ml/min through a stainless steel tube (1/16 in.) heated to above the boiling point of the respective reactants. The constant feed volume gave a typical WHSV of around 8 h^{-1} depending on the density of the specific feed composition. Conversion capacities reported in $g_{feed}/g_{zeolite}$ for the individual experiments were calculated from the measured WHSV multiplied by the lifetime observed when a conversion of 50% of additive + methanol/DME was reached [44].

The reaction temperature was measured inside the reactor approximately 0.5 cm below the catalyst bed and was stabilized at 370 °C before the experiments. Steel piping (1/4 in.) heated to >200 °C directed the products to analysis by on-line GC equipped with an FID. Response factors of all hydrocarbons were assumed to be 1 while 0.63 and 0.81 was used for DME and methanol, respectively. Response factors for other oxygenates were estimated to be equal to that of DME. The concentrations of CO and CO_2 in the effluent were determined by a BINOS instrument placed after condensation of liquids in a cold trap kept at 0 °C.

In the case of experiments converting ^{13}C enriched reactants; the same setup, scaling and reaction conditions were used. The conversion and product selectivities were monitored by on-line GC in order to verify similarity with conventional runs while additional product samples were frequently withdrawn for GC–MS analyses. Calculation of the ^{13}C content in the products was done based on reference spectra obtained from reacting pure ^{13}C labeled methanol. In a typical ^{13}C experiment enough substrate was used to continue operation for approximately 1 h. In all cases only minor deactivation occurs in this short time range thus giving information on additive carbon incorporation over a "fresh" catalyst.

TPO (temperature programmed oxidation) of the deactivated catalysts was performed on 100 mg of sample. The coked catalyst was heated from RT to 670 °C at a rate of 2.7 °C/min in a flow of 20 ml/min of 5% O_2 in He. The formed CO and CO_2 were continuously detected by a BINOS instrument.

All chemicals are commercially available and were used as purchased without further purification. A full list of chemical compounds is found in supplementary data.

3. Results and discussion

3.1. Additive screening

An initial screening of pure compounds with relatively low effective H/C ratios (≤1.5) was done at MTH reaction conditions (370 °C) over H-ZSM-5. This resulted in catalyst lifetimes in the order of minutes which was in strong contrast to reacting methanol which gives a catalyst lifetime of around 65 h. Clearly, this illustrated that excessive coking of the zeolite catalyst occurred when non-mono alcohols (ethylene glycol, propanediol, glycerol, etc.) were converted. In order to examine all molecules under similar conditions we therefore chose to react the compounds diluted to 10 wt% in methanol. This resulted in catalyst lifetimes spanning from as little as 2% to approximately equal that of pure methanol thus illustrating the "toxicity" of co-converting the individual molecules. Table 1 presents the additives chosen for co-feeding, their effective H/C ratio, the total conversion capacities in $g_{feed}/g_{zeolite}$ and the amounts of CO and CO_2 formed (given as a percentage relative to the molar amount of additive introduced). The initial product distribution is described by grouped selectivities in combination with the C_4-HTI (hydrogen transfer index) which is a descriptor of the hydrogen transfer activity of the catalyst (see Eq. (2)) [43]. The C_4-HTI and the selectivity were both measured approximately 5–10% into the full experiment run time. As is the case in conventional MTH, the product selectivity in the co-feeding experiments shifts from large amounts of aromatic and paraffinic products towards olefins as the catalyst gradually deactivates [44].

$$C_4\text{-HTI} = \sum \frac{\text{Butanes}}{\text{Butanes} + \text{Butenes}} \quad (2)$$

Eq. (2): Definition of the C_4-HTI.

Please cite this article in press as: U.V. Mentzel, M.S. Holm, Appl. Catal. A: Gen. (2011), doi:10.1016/j.apcata.2011.01.040

Table 1
Conversion capacity, initial selectivity, C_4-HTI, and CO/CO_2 production from conversion of various oxygenates as 10% solutions in methanol (T = 370 °C, P = 1 bar, 300 mg H-ZSM-5, WHSV = 8 h^{-1}).

Additive	Eff. H/C (additive)	Conversion capacity[a]	C_4-HTI[c]	CO[b]	CO_2[b]	C_{1-3}[c]	C_4[c]	C_{5+}[c] (aliphatic)	C_{6-10}[c] (aromatic)
H_2O	–	512	0.36	0%	0%	22%	28%	31%	19%
Methanol	2	471	0.38	0%	0%	22%	28%	31%	19%
Formaldehyde dimethyl acetal	1.33	62	0.34	0%	0%	22%	25%	28%	25%
Formic acid	−2	496	0.38	85%	2%	22%	28%	32%	18%
Ethanol	2	487	0.36	0%	0%	24%	27%	31%	18%
Ethyleneglycol	1	131	0.31	4%	0%	23%	24%	25%	28%
Acetaldehyde	1	72	0.29	7%	0%	26%	23%	22%	29%
Acetic acid	0	91	0.26	5%	3%	21%	20%	23%	36%
Glycolaldehyde dimethyl acetal	1	40	0.31	43%	3%	23%	26%	28%	23%
Methyl glycolate	0	86	0.34	91%	0%	23%	25%	26%	26%
2-Propanol	2	578	0.38	0%	0%	21%	28%	32%	19%
1,2-Propanediol	1.33	190	0.32	1%	0%	21%	25%	29%	25%
1,3-Propanediol	1.33	96	0.33	1%	0%	22%	25%	28%	25%
Glycerol	0.67	44	0.33	8%	0%	24%	23%	25%	28%
Acetone[d]	1.33	271	0.29	0%	1%	22%	24%	26%	27%
Propionaldehyde	1.33	138	0.31	3%	0%	22%	24%	26%	28%
Propionic acid	0.67	109	0.30	26%	4%	22%	24%	25%	29%
Methyl lactate	0.5	189	0.33	93%	0%	21%	25%	28%	26%
Methyl acrylate	0.5	27	0.27	26%	10%	24%	22%	25%	29%
1-Butanol	2	679	0.39	0%	0%	20%	27%	32%	21%
1,4-Butanediol	1.5	139	0.33	0%	0%	22%	25%	27%	26%
1,3-Butanediol	1.5	120	0.33	0%	0%	23%	26%	27%	24%
1,2-Butanediol	1.5	166	0.33	n.a.	n.a.	22%	26%	28%	24%
2,3-Butanediol[d]	1.5	320	0.31	0%	0%	22%	25%	29%	24%
Butyraldehyde	1.5	146	0.34	5%	0%	22%	25%	27%	26%
Butanone[d]	1.5	327	0.27	0%	0%	23%	25%	26%	25%
Butyric acid	1	219	0.35	62%	0%	21%	25%	30%	24%
1,5-Pentanediol	1.6	299	0.34	0%	0%	22%	25%	28%	25%
Levulinic acid	0.4	37	0.29	90%	0%	24%	25%	25%	26%
γ-Valerolactone	0.8	82	0.33	78%	7%	22%	26%	28%	24%
2-methyl-tetrahydrofuran	1.6	255	0.36	0%	0%	20%	25%	29%	26%
Toluene	1.14	412	0.33	0%	0%	19%	20%	21%	40%
Anisole	0.86	10	na.	0%	0%	26%	21%	21%	32%
1,2-dimethoxybenzene	0.75	9	na.	0%	0%	28%	20%	26%	26%

[a] $g_{feed}/g_{zeolite}$, [b] $mol/mol_{additive}$, [c] initial, [d] breakthrough of additive before DME/methanol.

From the data in Table 1 we see that any additive leads to lower conversion capacities compared to conversion of pure methanol with the exception of water, formic acid and higher alcohols. The latter is in good correlation with results published recently [45] while water and formic acid (formic acid dissociates predominantly into CO and water) leads to a lower WHSV of methanol with an increased water concentration which presumably suppresses coke formation [29]. Co-feeding a 10 wt% solution of the phenolic species anisole or 1,2-dimethoxybenzene results in conversion capacities of <10 $g_{feed}/g_{zeolite}$. The huge difficulty in converting these species is in good agreement with previous reports where removal of phenolic species prior to bio-oil upgrading was suggested [18,19]. Other compounds which deactivate the catalyst strongly are levulinic acid, glycerol, and formaldehyde dimethyl acetal. These compounds all represent highly hydrogen deficient molecules with critically low effective H/C ratios of 0.4, 0.6 and 1.33, respectively. As expected, compounds which are more compatible do indeed have higher effective H/C ratios, e.g. 1,5-pentanediol. In general, lower conversion capacities are obtained for low H/C ratios of the additives. Illustrative examples of this include hydroxy acetaldehyde (introduced as the dimethyl acetal) which deactivates the catalyst faster than acetaldehyde, glycerol is harder to convert than propanediol and butanoic acid performs better than the lower acids, however several additional features should be noted.

Fig. 1 presents the conversion capacities from Table 1 plotted as a function of the effective H/C ratio of the pure additive. Here it can be seen that compounds which have the same effective H/C ratio do not give identical conversion capacities. This is observed for molecules containing oxygen in different functionalities as well as for positional isomers. A pronounced difference in the conversion capacity between 2,3-butanediol and the other butanediols is observed disregarding that they all have an effective H/C ratio of 1.5 and contain the same functional groups. Interestingly butanone performs similar to 2,3-butanediol whereas butyraldehyde groups with the diols having one or two hydroxyl groups at a terminal carbon. This reactivity correlates with the detection of butanone as the direct dehydration product formed from 2,3-butanediol whereas predominantly butadiene and butyraldehyde

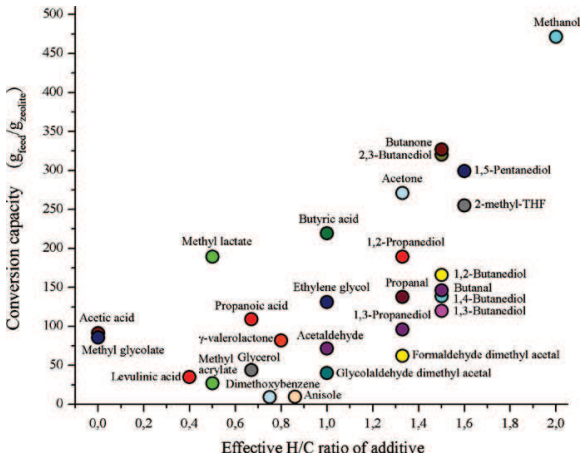

Fig. 1. Total conversion capacity from experiments having 10 wt% of additive in methanol plotted as a function of the effective H/C ratio of the additive (T = 370 °C, P = 1 bar, 300 mg H-ZSM-5, WHSV = 8 h^{-1}).

Please cite this article in press as: U.V. Mentzel, M.S. Holm, Appl. Catal. A: Gen. (2011), doi:10.1016/j.apcata.2011.01.040

are produced from 1,3- and 1,2-butanediol. However, tetrahydrofuran is the main dehydration product of 1,4-butanediol which gives a conversion capacity close to the latter isomers. The same tendency of higher conversion capacities of the ketone over the aldehyde is observed for acetone and propanal, where also 1,2-propanediol is significant better than the corresponding 1,3-propanediol. However breakthrough of butanone and acetone before methanol/DME is observed which indicates a significantly lower reactivity as compared to the corresponding aldehydes. In all other cases the additive (or derivatives thereof) only starts to appear in the reactor outlet alongside unconverted methanol/DME.

Levulinic acid and γ-valerolactone can be derived from biomass [46,47] and represent along with 2-methyl-tetrahydrofuran a series of molecules with an identical carbon backbone which are increasingly hydrogenated. From Fig. 1 (and Table 1) we see that this series does indeed group according to their oxidation state, with the most reduced compounds performing superior, giving conversion capacities of around 10%, 20% and 55% compared to conversion of pure methanol, respectively. This observation can prove important since the use of 1 equivalent of H_2 when going from levulinic acid to γ-valerolactone actually doubles the conversion capacity thus showing that partial hydrogenation could be advantageous.

In conventional MTH the alcohol oxygen is removed by dehydration. When converting higher oxidized compounds it would however be useful to remove oxygen by decarboxylation or decarbonylation in order to preserve hydrogen in the hydrocarbon products. Fig. 1 shows that the acids and in particular methyl lactate performs significantly better than could be expected from their low H/C ratios. Acetic acid forms only minor amounts of CO and CO_2 (5%, 3%) while propanoic acid (26%, 4%) and butyric acid (62%, 0%) produce larger amounts of CO. The high oxidation state of acetic acid in combination with a negligible tendency to dissociate CO and/or CO_2 (at this concentration) leads to a very high initial aromatic carbon percentage of 35% compared to 29% for propanoic acid, 24% for butanoic acid and only 19% for pure methanol.

Fig. 2 shows the initial carbon % located in aromatic products plotted as a function of the effective H/C ratio in the combined feed (methanol + additive) for the compounds in Table 1. The coloring differentiates between molecules able to dissociate significant amounts (>30%) of CO and/or CO_2 (gray) and those unable (dark). Clearly, conversion of compounds deoxygenating through dehydration (dark) results in a relatively high selectivity towards aromatics while compounds which are able to split off CO or CO_2 produce less aromatics. It appears that the intrinsic selectivity of the H-ZSM-5 zeolite forces the product distribution within the gasoline range and preserving hydrogen in the products increases the selectivity towards aliphatic products over the hydrogen deficient aromatic compounds.

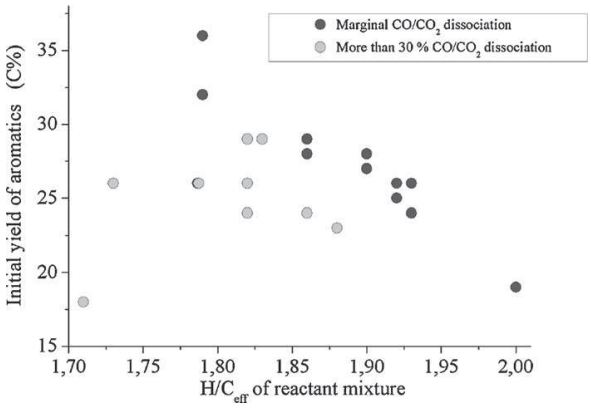

Fig. 2. Initial aromatic carbon % plotted as a function of the effective H/C ratio of the reactant mixture (T = 370 °C, P = 1 bar, 300 mg H-ZSM-5, WHSV = 8 h^{-1}).

Dissociation of CO is also relevant to explain the extraordinary good performance of methyl lactate. More than 90% of the introduced methyl lactate dissociate CO which is in good agreement with very recent results [48]. In fact after complete deactivation of the catalyst we observe a continued formation of mainly CO, acetaldehyde and DME/methanol indicating that acetaldehyde and methanol are the "true" reactants when converting methyl lactate.

Also levulinic acid and γ-valerolactone form large amounts of CO and in the case of γ-valerolactone also small amounts of CO_2 are produced (Table 1). γ-Valerolactone has previously been reported to decompose into CO_2 and butene over a weak solid acid at a similar temperature [49]. However, under MTH conditions butadiene, CO, and water are observed as the primary decomposition products from γ-valerolactone.

3.2. Additive concentration

Based on the data from Table 1 in combination with knowledge of very short lifetimes when reacting the pure compounds we speculated whether the lifetime improvement from dilution in methanol correlated linearly with the wt% of the additives or whether it was possible to convert more of the additive at suitable concentrations. To investigate this, the 4 most interesting compounds from Table 1 (methyl lactate, γ-valerolactone, glycerol, and acetic acid) were converted in different concentrations in methanol. These compounds can potentially be derived from biomass and possessed the ability to dissociate CO/CO_2. Fig. 3 presents the conversion capacities of the additives diluted in methanol. Fig. 3a and b illustrate that reacting pure methyl lactate or pure γ-valerolactone results in very poor conversion capacities. However, looking at the lower levels of methyl lactate in the feed (Fig. 3a) we clearly see that an optimum in the conversion capacity exists at a wt% of 10–25. Conclusively, the dilution of methanol does not only increase the lifetime proportionally to the dilution level but fine tuning the concentration leads to an increased total conversion capacity of methyl lactate before the catalyst is deactivated. The lower limit is rationalized by considering that when only small amounts of methyl lactate is added deactivation from conversion of methanol dominates. This means that even if the catalyst had a similar lifetime as for conversion of pure methanol, a 2.5 wt% solution of methyl lactate would not result in as high additive conversion as a feed in the 10–25 wt% range.

Fig. 3b shows a similar dilution behavior for converting γ-valerolactone as observed for methyl lactate. Also here an optimum exists in the conversion capacity, though it should be noted that the optimum is at a lower wt%, namely around 5–10. In the case of glycerol (Fig. 3c) the experiments revealed an optimum around 2.5–5 wt% and high concentrations (above 50 wt%) deactivate the catalyst so rapidly that we chose not to react pure glycerol under these reaction conditions. Glycerol has a very low effective H/C ratio of 0.67 which correlates well with the low optimum level of addition and the rapid deactivation seen in Table 1. Furthermore, glycerol forms only modest amounts of CO and CO_2 which support the fact that it is one of the most unwanted molecules to co-convert with methanol from a catalyst lifetime perspective.

For acetic acid a somewhat different trend is revealed. Increasing amounts of acetic acid in the feed results in a larger amount of CO_2 which can be explained by increased tendency towards ketonization forming acetone and CO_2 [28]. The conversion capacity of acetic acid thus increases with the concentration correlating with the fact that acetone does not induce massive deactivation (see Table 1). However, very early breakthrough of methyl acetate and acetic acid in the 25 wt% experiment complicates the quantitative interpreta-

Please cite this article in press as: U.V. Mentzel, M.S. Holm, Appl. Catal. A: Gen. (2011), doi:10.1016/j.apcata.2011.01.040

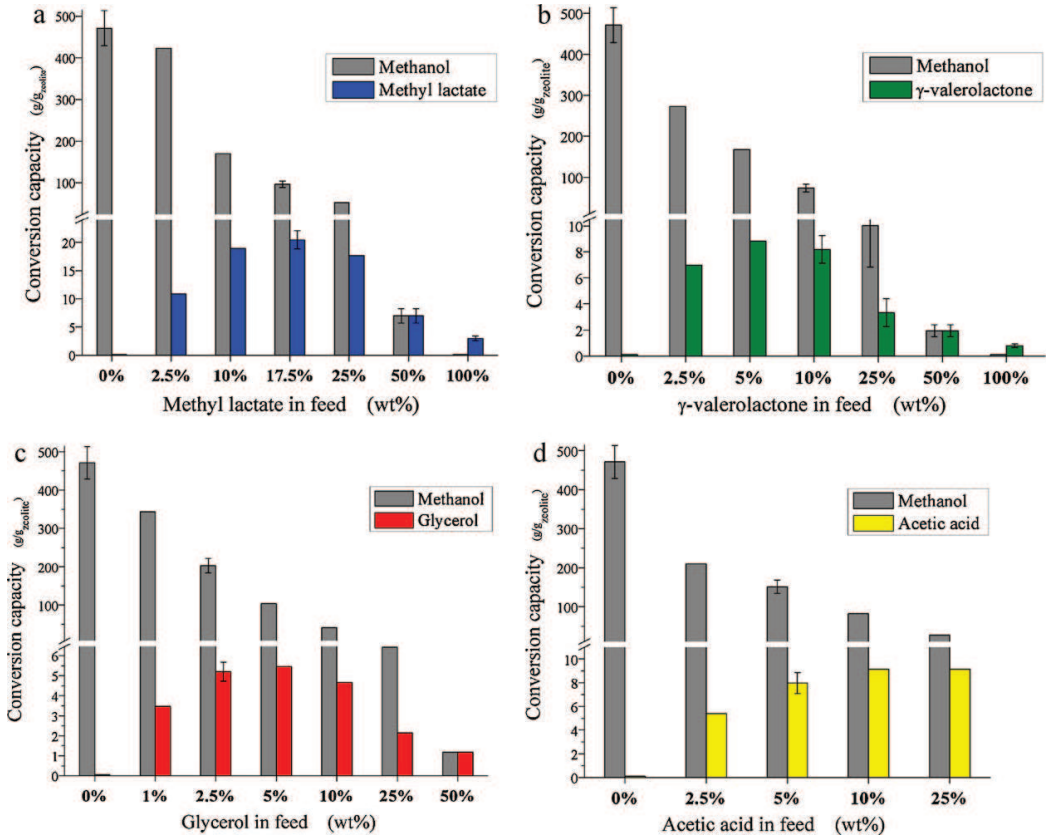

Fig. 3. Conversion capacities plotted at different wt% of additive in the feed. (a) Methyl lactate, (b) γ-valerolactone, (c) glycerol and (d) acetic acid. Error bars represent ±2 standard deviations. Note the different scales below the break (T = 370 °C, P = 1 bar, 300 mg H-ZSM-5, WHSV = 8 h^{-1}).

tion and presumably a higher reaction temperature is required to reach a satisfactory conversion level. Acetic acid and methyl acetate appears alongside methanol and DME in the 10 wt% experiment.

3.3. Product distribution

Not only the conversion capacity but also changes in product selectivity are crucial when co-feeding various compounds. If the deoxygenation proceeds through dehydration and not through decarboxylation and decarbonylation the reaction will inevitably produce a more hydrogen deficient hydrocarbon product mixture. This point is rather important since it has previously been argued that the high aromatic content in MTH derived gasoline limits its implementation [50,51]. Table 2 lists the initial product selectivities as a function of increasing oxygenate addition. We note that reacting small amounts of additive leads to very similar product compositions as observed for pure methanol. However, with increasing amounts of additive a rise in the abundance of aromatics (mainly benzene, toluene, xylenes and tri-methylbenzenes) is observed at the cost of the C_{4+} aliphatic products while no oxygenated aromatic products are detected. This high selectivity towards aromatics at low methanol contents in the feed is supported by a recent report on direct conversion of glycerol over H-ZSM-5, where aromatics are produced in large amounts [25]. Further from Table 2 it is clear that the increasing selectivity towards aromatics comes alongside a decreasing C_4-HTI. The low C_4-HTI could be explained by the possibility of arene production without the necessity of co-production of alkanes due to the low effective H/C ratio of the reaction mixture. It should be noted that in the high concentration experiments (with run times below one hour) the C_4-HTI decreases rapidly with time-on-stream as deactivation is very pronounced.

With respect to the formation of CO and CO_2 in the experiments concerning conversion of glycerol and acetic acid presented in Table 2, high concentration of the additive leads to the production of more CO and CO_2 pr. mole of additive. This indicates that the decarboxylation/decarbonylation routes are favored at low methanol contents, which is in good correlation with a previous report [35]. This is also observed for low concentrations of methyl lactate and γ-valerolactone which indicate that this is a more general trend. Even though the amount of CO and CO_2 produced pr. mole of additive increases at higher concentrations, this is not enough to offset the very low H/C_{eff} ratio at these feed compositions, and the hydrocarbon product mixture is thus very rich in aromatics.

3.4. Isotopic labeling

When CO or CO_2 is formed, some carbon atoms are lost and do not enter the hydrocarbon products. The analysis of the product stream for CO and CO_2 gives an indication of what is occurring but not whether the carbon atoms present in the additive do in fact end up in conventional gasoline products. In order to investigate this issue in detail ^{13}C labeled additives or ^{13}C labeled methanol was

Please cite this article in press as: U.V. Mentzel, M.S. Holm, Appl. Catal. A: Gen. (2011), doi:10.1016/j.apcata.2011.01.040

Table 2
Initial selectivity, C_4-HTI, and CO/CO_2 production from conversion of different concentrations of various oxygenates in methanol (T = 370 °C, P = 1 bar, 300 mg H-ZSM-5, WHSV = 8 h^{-1}).

Additive	wt%	Eff. H/C of feed[a]	C_4-HTI[b]	CO[c]	CO_2[c]	C_{1-3}[b]	C_4[b]	C_{5+}[b] (aliphatic)	C_{6-10}[b] (aromatic)
Methanol	–	2	0.38	0%	0%	22%	28%	31%	19%
Acetic acid	2.5%	1.95	0.34	0%	0%	24%	26%	28%	22%
Acetic acid	5%	1.89	0.31	4%	4%	24%	24%	26%	26%
Acetic acid	10%	1.79	0.27	5%	3%	21%	20%	23%	36%
Acetic acid	25%	1.48	0.19	6%	9%	21%	12%	13%	53%
Glycerol	1%	1.99	0.38	0%	0%	22%	27%	30%	21%
Glycerol	2.5%	1.97	0.36	0%	0%	23%	27%	29%	21%
Glycerol	5%	1.93	0.34	10%	0%	24%	26%	27%	23%
Glycerol	10%	1.86	0.30	11%	0%	24%	23%	25%	28%
Glycerol	25%	1.66	0.23	16%	2%	23%	20%	20%	37%
Glycerol	50%	1.32	na.[d]	21%	3%	24%	15%	16%	45%
Methyl lactate	2.5%	1.95	0.39	70%	0%	21%	26%	30%	23%
Methyl lactate	10%	1.82	0.33	93%	0%	21%	25%	28%	26%
Methyl lactate	17.5%	1.69	0.31	>95%	1%	23%	24%	26%	27%
Methyl lactate	25%	1.56	0.27	>95%	1%	23%	22%	23%	32%
Methyl lactate	50%	1.17	0.20	>95%	1%	25%	17%	17%	41%
Methyl lactate	100%	0.50	na.[d]	na.[d]	na.[d]	26%	7%	6%	61%
γ-Valerolactone	2.5%	1.95	0.39	76%	<2%	24%	27%	28%	21%
γ-Valerolactone	5%	1.91	0.38	78%	6%	22%	27%	29%	22%
γ-Valerolactone	10%	1.82	0.32	78%	7%	22%	26%	28%	24%
γ-Valerolactone	25%	1.58	0.27	73%	9%	23%	23%	25%	29%
γ-Valerolactone	50%	1.26	0.24	72%	11%	21%	20%	19%	40%
γ-Valerolactone	100%	0.80	na.[d]	na.[d]	na.[d]	17%	16%	15%	52%

[a]Calculated from the dehydrated H/C ratios, [b]initial, [c]$mol/mol_{additive}$, [d]too rapid catalyst deactivation to obtain data.

employed and the ^{13}C content in selected main products (butene, butane, pentane, pentene, toluene, xylene and trimethylbenzene) was analyzed in order to trace the carbon atoms from the additives. For labeling experiments we employed the additives investigated in Table 2 and the compounds were reacted in a concentration close to the previously defined optimum. In the case of glycerol and acetic acid, the additives were ^{13}C labeled whereas for methyl lactate and γ-valerolactone we used standard additives and ^{13}C labeled methanol. The experiments were conducted for ~1 h corresponding to less than 1/10 the total reaction time which makes the data representative for the initial product selectivities given in Tables 1 and 2. During this time span no change in the pattern of ^{13}C incorporation was observed.

Fig. 4 presents results from the labeling experiments for glycerol, methyl lactate, acetic acid, and γ-valerolactone, respectively. Fig. 4a shows the ^{13}C content in the products when reacting 5 wt% of ^{13}C labeled glycerol in methanol. The dotted line represents the ^{13}C content in the feed. If all additive carbons were incorporated and distributed evenly in the products, 5.05% ^{13}C would be expected in all products. Interestingly, we see that the aromatic products (toluene, xylene, and trimethylbenzene) actually contain significantly more ^{13}C than the average while the aliphatic products contain less. It thus appears that the reaction path of glycerol favors the formation of aromatics. Carbon atoms present in the aromatics will eventually equilibrate into the remaining products through alkene dissociation as described in detail elsewhere [52]. This observation is in good agreement with a recent report where an increased affinity for aromatization is found for propanal compared to propanol when reacted over HZSM-5 [21], and the authors propose direct production of aromatics from propanal through a series of aldol condensation reactions and dehydrations. In the aliphatic compounds, only a small difference exists between incorporation into saturated and unsaturated compounds, but the longer pentane and pentene have a markedly lower content than their C_4 analogues.

Fig. 4b presents data from conversion of 25 wt% methyl lactate in ^{13}C labeled methanol. From Table 2 it can be seen that methyl lactate splits off CO suggesting a loss of 1/4 of the carbon atoms originally present in the molecule. The dotted lines in Fig. 4b represents the average ^{13}C content in the feed while the dashed line represent the expected ^{13}C content if only 3 of the carbon atoms in methyl lactate are incorporated into the hydrocarbon products. Note that the Y-axis shows the ^{12}C content since ^{13}C labeled methanol is used instead of labeled additive in this experiment. As for glycerol, it is observed that the aromatic products contain more additive carbon compared to the aliphatic products and the C_5 compounds contain less additive carbon than the C_4 compounds. Further, the ^{12}C content of the individual products is located above and below the ^{12}C level for incorporation of 3 carbon atoms in correlation with the fact that one carbon atom from methyl lactate is removed by decarbonylation. At present we are unable to explain the lower incorporation into pentane compared to butane but we note that this trend is also present in the other experiments, though to a smaller extent.

Fig. 4c shows data from the experiment co-reacting 10 wt% of ^{13}C labeled acetic acid in methanol. The pattern of ^{13}C incorporation with high levels in the aromatic compounds and less in the aliphatic is recognized. The total incorporation distributes below and above the ^{13}C content of the feed which means that the vast majority of even the acid carbon from acetic acid is likely incorporated into the hydrocarbon products. This is somewhat surprising since transfer of significant amounts of hydrogen to acetic acid (H/C effective = 0) is required to produce these products. The aliphatic ^{13}C incorporation is somewhat inconsistent with the other experiments which can partly be explained by the reaction path of acetic acid described elsewhere [9,28]. Acetic acid can form acetone and further isobutene in sequence. However only a relatively low amount of CO_2 which would be formed in the ketonization reaction (producing acetone and CO_2) was detected but it could be enough to enrich isobutene above the expected value. Finally in Fig. 4d γ-valerolactone was co-reacted with ^{13}C methanol. The results are very similar to what was observed when converting methyl lactate. Around 4/5 of the carbon from the additive is incorporated into the products (predominantly into the aromatics) which corresponds well with the significant CO and CO_2 formation observed.

From this type of GC–MS analysis it is not possible to analyze the ^{13}C content in the myriad of products formed in the reaction in order to calculate an average ^{13}C content in the gasoline product.

Please cite this article in press as: U.V. Mentzel, M.S. Holm, Appl. Catal. A: Gen. (2011), doi:10.1016/j.apcata.2011.01.040

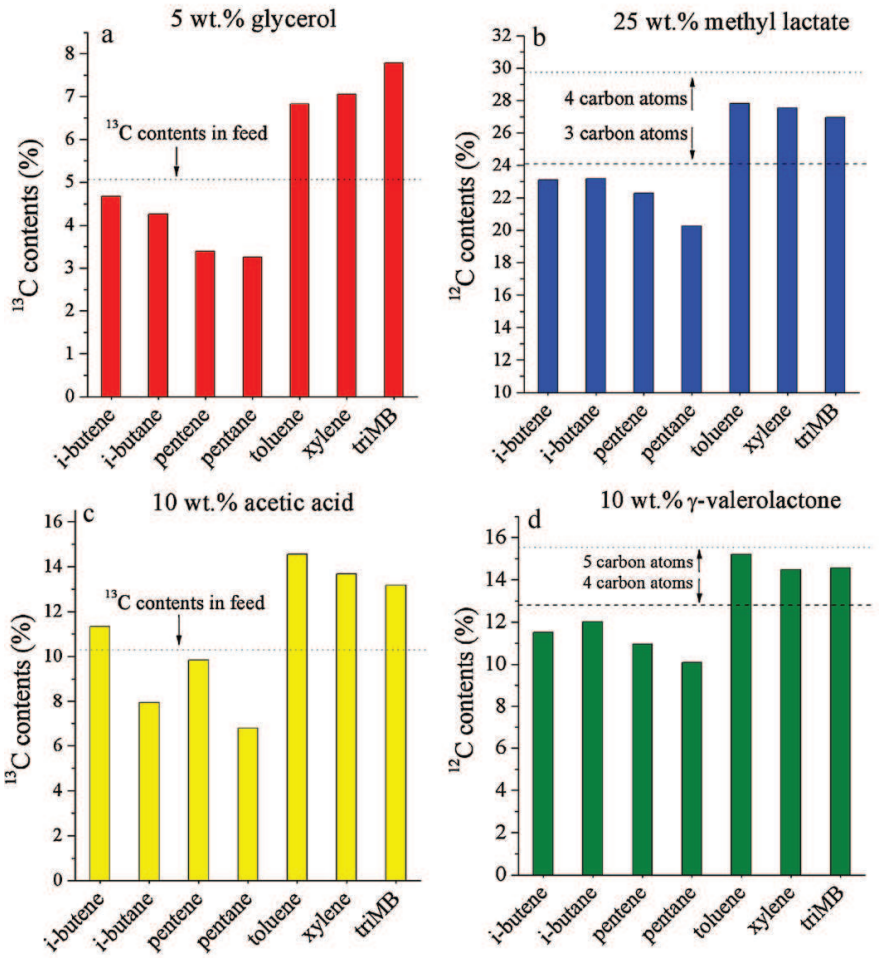

Fig. 4. ^{13}C and ^{12}C content observed in typical main products of MTH. In the case of (a) 5 wt% glycerol and (c) 10 wt% acetic acid ^{13}C labeled additives in unlabeled methanol were used. In the case of (b) 25 wt% methyl lactate and (d) 10 wt% γ-valerolactone ^{13}C methanol was used. The dotted lines correspond to the ^{13}C content in the feed while the dashed lines in (b) and (d) correspond to incorporation of all additive carbon after dissociation of 1 mol of CO or CO_2 (T = 370 °C, P = 1 bar, 300 mg H-ZSM-5, WHSV = 8 h^{-1}).

However, based on the detected levels of CO and CO_2 as well as the presented data on ^{13}C incorporation it seems likely that the majority of the carbon present in the additive, which do not form CO or CO_2, does indeed end up in the hydrocarbon products. Presumably the different additives have individual reaction paths highly dependent on the specific concentration and we are only able to observe the composition after some equilibration (by cracking, isomerization, oligomerization, etc.) over the full catalyst bed has occurred. To address the enrichment of additive carbon in the aromatic products we repeated the experiment with ^{13}C labeled acetic acid with lower amounts of catalyst in order to suppress secondary reactions. The results are given in Fig. 5 and in all cases >99% conversion of methanol/DME and acetic acid was observed.

Fig. 5 reveals that as less catalyst is used, a pronounced decrease in the ^{13}C carbon % of the aliphatics is observed while the content is relatively unchanged in the aromatics products. It is also clear that less additive carbon is present in the saturated aliphatics compared to the corresponding olefins. These results support a reaction path where aliphatic products are not formed directly from acetic acid. Over an active catalyst the initially formed aromatic compounds will subsequently split off alkenes which through hydrogen transfer reactions can produce alkanes and thus distribute the additive carbon into all products.

3.5. Temperature programmed oxidation (TPO)

A catalyst deactivated in methanol conversion is able to catalyze the methanol-DME equilibrium yielding predominantly DME for numerous hours after hydrocarbons are no longer formed in significant amounts. In the case of 10 wt% of γ-valerolactone, methyl lactate, and glycerol in methanol the DME formation decreases rapidly after deactivation whereas DME is continually produced for conversion of acetic acid in methanol. Surprisingly, deactivating the catalyst with 10 wt% of anisole which shows the lowest conversion capacity of all the additives (see Table 1) does however not stop the production of DME. To investigate this observation, TPO on the catalysts used in the concentration series (from Table 2) as well as on selected catalysts from Table 1 was performed in order

Please cite this article in press as: U.V. Mentzel, M.S. Holm, Appl. Catal. A: Gen. (2011), doi:10.1016/j.apcata.2011.01.040

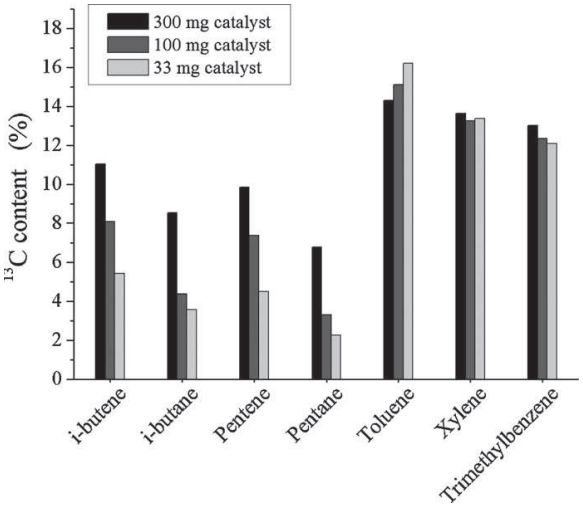

Fig. 5. ^{13}C content in selected products from conversion of 10% ^{13}C labeled acetic acid in methanol over 300 mg (WHSV = 8 h^{-1}), 100 mg (WHSV = 24 h^{-1}), or 33 mg (WHSV = 72 h^{-1}) of catalyst (T = 370 °C, P = 1 bar).

to determine the amount of coke present on the catalyst at full deactivation.

Bilbao and co-workers have done thorough coke analyses for conversion of bio-oil diluted in methanol over H-ZSM-5 and reported a distinction between thermal and catalytic coke. The thermal coke which has a higher H/C ratio was attributed to bio-oil and could be combusted at a lower temperature compared to coke from a conventional methanol experiment [18,34].

Fig. 6 shows the results from TPO experiments of the concentration series from Table 2 and it is clear that the total amount of coke deposited on the deactivated catalyst decreases as the wt% of additive is increased. We were however unable to correlate the combustion temperature to specific types of coke on the catalysts but merely note that a catalyst employed in the conversion of methanol for less than an hour (the lifetime of experiments having ≥50 wt% of additive) contain very small amounts of coke (∼1%) which underline that conversion of the hydrogen deficient additives from Table 1 results in excessive coke formation. No clear trend in levels of coke deposition was observed from the experiments in Table 1 where most catalysts contained approximately 10 wt% carbon although catalysts from conversion of 10 wt% anisole or dimethoxybenzene contained slightly less (∼8 wt%).

4. Conclusions

We have investigated the co-conversion of various model compounds in methanol under MTH reaction conditions which represents an alternative strategy to simply using "green" additives to conventional gasoline. The effective H/C ratio has previously been used as an indicator of whether an oxygenate would lead to rapid deactivation and we confirm the overall tendency of pronounced deactivation for conversion of compounds with low effective H/C ratios. However, the catalytic data also shows that structural isomers can indeed perform very differently with respect to conversion capacity and selectivity. Molecules capable of dissociating CO_2 or CO generally experience higher conversion capacities highlighting that consideration of the specific functionalities present in the additive is crucial in order to understand the reactivity. Converting the pure compounds leads to very short lifetimes of the zeolite catalyst and depending on the molecule an optimal dilution in methanol can result in up to 10 times higher conversion capacities of the additive before deactivation of the catalyst.

Experiments using ^{13}C labeling show that the carbon atoms from the additives are distributed into the hydrocarbon products with a high affinity for the aromatics. We can thus rule out that the additive carbon ends up in single "dead end" hydrocarbons or form new unconvertible oxygenates.

The results presented here give new understanding of the reactivity of different oxygenates when converted to hydrocarbons over H-ZSM-5, and might help pave the road for development of new processes for conversion of biomass to hydrocarbon-based fuels and chemicals.

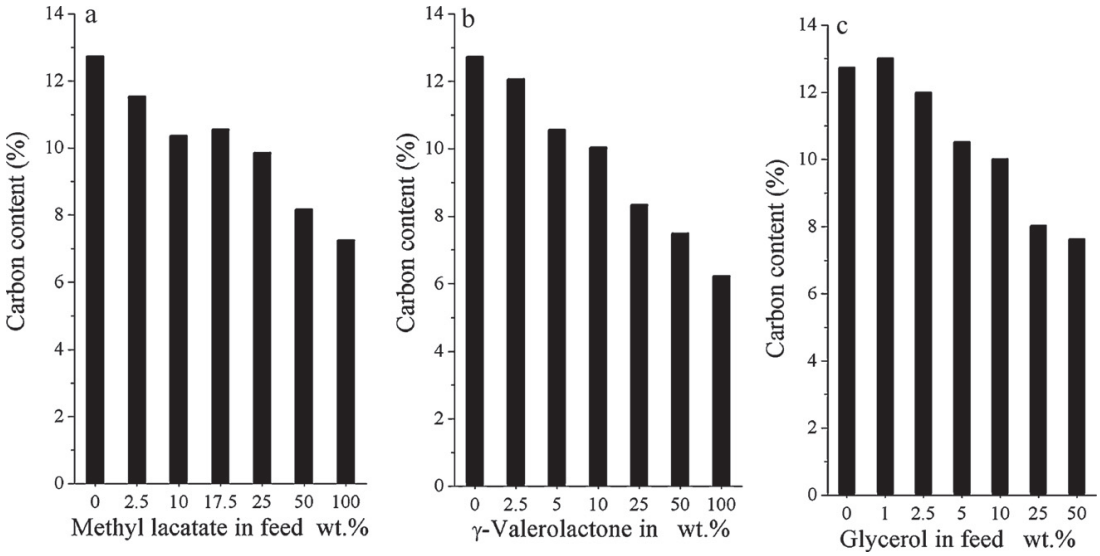

Fig. 6. Data obtained from TPO experiments presenting the amount of carbon deposited on the fully deactivated catalysts upon conversion of different concentrations of additive in methanol. (a) Methyl lactate, (b) γ-valerolactone, and (c) glycerol (T = 370 °C, P = 1 bar, 300 mg H-ZSM-5, WHSV = 8 h^{-1}).

Please cite this article in press as: U.V. Mentzel, M.S. Holm, Appl. Catal. A: Gen. (2011), doi:10.1016/j.apcata.2011.01.040

Acknowledgements

The Center for Sustainable and Green Chemistry is sponsored by the Danish National Research Foundation.

Appendix A. Supplementary data

Supplementary data associated with this article can be found, in the online version, at doi:10.1016/j.apcata.2011.01.040.

References

[1] G.W. Huber, S. Iborra, A. Corma, Chem. Rev. 106 (2006) 4044–4098.
[2] J.R. Regalbuto, Science 325 (2009) 822–824.
[3] A. Demirbas, Energy Convers. Manage. 50 (2009) 2239–2249.
[4] A.V. Bridgewater, M.L. Cottam, Energy Fuels 6 (1992) 113–120.
[5] S. Czernik, A.V. Bridgwater, Energy Fuels 18 (2004) 590–598.
[6] D. Mohan, C.U. Pittman, P.H. Steele, Energy Fuels 20 (2006) 848–889.
[7] R. French, S. Czernik, Fuel Process. Technol. 91 (2010) 25–32.
[8] M. Stöcker, Microporous Mesoporous Mater. 29 (1999) 3–48.
[9] C.D. Chang, A.J. Silvestri, J. Catal. 47 (1977) 249–259.
[10] P.B. Weisz, W.O. Haag, P.G. Rodewald, Science 206 (1979) 57–58.
[11] N.Y. Chen, T.F. Degan Jr., L.R. Koenig, Chemtech 16 (1986) 506–511.
[12] P.D. Chantal, S. Kaliaguine, J.L. Grandmaison, A. Mahay, Appl. Catal. 10 (1984) 317–332.
[13] P.A. Horne, P.T.J. Williams, Anal. Appl. Pyrolysis 34 (1995) 65–85.
[14] J.D. Adjaye, N.N. Bakhshi, Fuel Process. Technol. 45 (1995) 185–202.
[15] R.K. Sharma, N.N. Bakhshi, Fuel Process. Technol. 35 (1993) 201–218.
[16] P.T. Williams, A.J.J. Brindle, Anal. Appl. Pyrolysis 67 (2003) 143–164.
[17] T.P. Vispute, H. Zhang, A. Sanna, R. Xiao, G.W. Huber, Science 330 (2010) 1222–1227.
[18] A.G. Gayubo, A.T. Aguayo, A. Atutxa, B. Valle, J.J. Bilbao, Chem. Technol. Biotechnol. 80 (2005) 1244–1251.
[19] P.A. Horne, P.T. Williams, Renewable Energy 7 (1996) 131–144.
[20] X. Zhu, R.G. Mallinson, D.E. Resasco, Appl. Catal. A 379 (2010) 172–181.
[21] T.Q. Hoang, X. Zhu, T. Sooknoi, D.E. Resasco, R.G. Mallinson, J. Catal. 271 (2010) 201–208.
[22] M.C. Samolada, A. Papafotica, I. Vasalos, Energy Fuels 14 (2000) 1161–1167.
[23] P.D. Chantal, S. Kaliaguine, J.L. Grandmaison, Appl. Catal. 18 (1985) 133–145.
[24] J.L. Grandmaison, P.D. Chantal, S.C. Kaliaguine, Fuel 69 (1990) 1058–1061.
[25] T.Q. Hoang, X. Zhu, T. Danuthai, L.L. Lobban, D.E. Resasco, R.G. Mallinson, Energy Fuels 24 (2010) 3804–3809.
[26] R.J. Evans, T. Milne, ACS Symp. Ser. 376 (1988) 311–327.
[27] T.Q. Hoang, X. Zhu, L.L. Lobban, D.E. Resasco, R.G. Mallinson, Catal. Commun. 11 (2010) 977–981.
[28] G.J. Hutchings, P. Johnston, D.F. Lee, A. Warwick, C.D. Williams, M. Wilkinson, J. Catal. 147 (1994) 177–185.
[29] A.G. Gayubo, A.T. Aguayo, A. Atutxa, R. Aguado, J. Bilbao, Ind. Eng. Chem. Res. 43 (2004) 2610–2618.
[30] A.G. Gayubo, A.T. Aguayo, A. Atutxa, R. Aguado, M. Olazar, J. Bilbao, Ind. Eng. Chem. Res. 43 (2004) 2619–2626.
[31] J.D. Adjaye, N.N. Bakhshi, Biomass Bioenergy 8 (1995) 131–149.
[32] L.H. Dao, M. Haniff, A. Houle, D. Lamothe, 193. National Meeting of the American Chemical Society 32:2 (1987) 308–316.
[33] R.K. Sharma, N.N. Bakhshi, Bioresour. Technol. 35 (1991) 57–66.
[34] A.G. Gayubo, B. Valle, A.T. Aguayo, M. Olazar, J. Bilbao, Energy Fuels 23 (2009) 4129–4136.
[35] A.G. Gayubo, B. Valle, A.T. Aguayo, M. Olazar, J. Bilbao, Ind. Eng. Chem. Res. 49 (2010) 123–131.
[36] B. Valle, A.G. Gayubo, A. Alonso, A.T. Aguayo, J. Bilbao, Appl. Catal. B 100 (2010) 318–327.
[37] A. Corma, G.W. Huber, L. Sauvanaud, P. O'Connor, J. Catal. 247 (2007) 307–327.
[38] A. Corma, G.W. Huber, L. Sauvanaud, P. O'Connor, J. Catal. 257 (2008) 163–171.
[39] I. Graca, F.R. Ribeiro, H.S. Cerqueira, Y.L. Lam, M.B.B. de Almeida, Appl. Catal. B 90 (2009) 556–563.
[40] T.R. Carlson, T.P. Vispute, G.W. Huber, ChemSusChem 1 (2008) 397–400.
[41] T.R. Carlson, G.A. Tompsett, W.C. Conner, G.W. Huber, Top. Catal. 52 (2009) 241–252.
[42] T.R. Carlson, J. Jae, Y.-C. Lin, G.A. Tompsett, G.W. Huber, J. Catal. 270 (2010) 110–124.
[43] M. Bjørgen, F. Joensen, M.S. Holm, U. Olsbye, K.-P. Lillerud, S. Svelle, Appl. Catal. A 345 (2008) 43–50.
[44] T.V.W. Janssens, J. Catal. 264 (2009) 130–137.
[45] U.V. Mentzel, S. Shunmugavel, S.L. Hruby, C.H. Christensen, M.S. Holm, J. Am. Chem. Soc. 131 (2009) 17009–17013.
[46] H. Heeres, R. Handana, D. Chunai, C.B. Rasrendra, B. Girisuta, H.J. Heeres, Green Chem. 11 (2009) 1247–1255.
[47] H. Mehdi, V. Fabos, R. Tuba, A. Bodor, L.T. Mika, I.T. Horvath, Top. Catal. 48 (2008) 49–54.
[48] B. Kartryniok, S. Paul, F. Dumeignil, Green Chem. 12 (2010) 1910–1913.
[49] J.Q. Bond, D.M. Alonso, D. Wang, R.M. West, J.A. Dumesic, Science 327 (2010) 1110–1114.
[50] J.F. Haw, D.M. Marcus, Top. Catal. 34 (2005) 41–48.
[51] J.F. Haw, D.M. Marcus, Nanotechnology in Catalysis, vol. 1, Plenum Publishers, New York, 2004, Chapter 13.
[52] M. Bjørgen, S. Svelle, F. Joensen, J. Nerlov, S. Kolboe, F. Binino, L. Palumbo, S. Bordiga, U. Olsbye, J. Catal. 249 (2007) 195–207.

Please cite this article in press as: U.V. Mentzel, M.S. Holm, Appl. Catal. A: Gen. (2011), doi:10.1016/j.apcata.2011.01.040

Part 3

2.9 Aim and idea preceding the studies within lactic acid formation

Numerous strategies are currently being investigated for upgrading of biomass. Zeolites have been tested in high temperature deoxygenation reactions for hydrocarbon formation as described in detail in part 2 of this thesis. We had the ambition to exploit the attractive characteristics of zeolite catalysts to synthesize commodity chemicals. The target molecules should not be deoxygenated, but instead selectively transformed. Therefore, lower temperatures, alternative active sites and liquid phase reactions were "on the table". To serve as an inspiration was a report by the Sasaki group in Hiroshima, Japan from 2005 where they show that isomerization of triose sugars into methyl lactate occur in alcohol solutions.[1] C_3-sugars are not readily available in nature but they represent an interesting class of compounds and can be produced by for example oxidation of glycerol with air.[2] The Sasaki group showed that the reaction sequence was homogeneously catalyzed by various inorganic halide salts. Particularly, Sn (II) and Sn (IV) chloride proved superior while $CrCl_3$ and $AlCl_3$ were also active. The mechanism presented in Figure 2.1 was proposed.

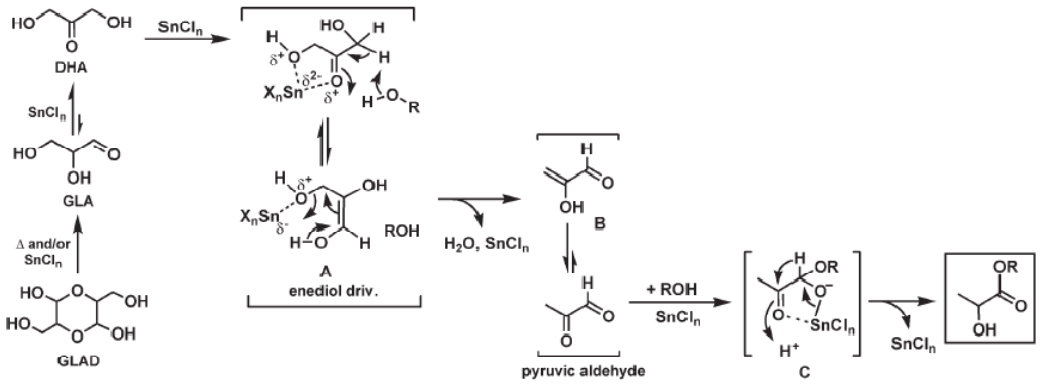

Figure 2.1. Proposed mechanism for the tin halide catalyzed triose isomerization forming alkyl lactate from glycol aldehyde dimer. Figure from Ref. 1.

Of the C_3-sugars, dihydroxy acetone (DHA) has the highest reactivity starting already at room temperature. This indicates that glyceraldehyde (GLA) needs to be converted through the aldose-ketose isomerization into DHA. Coordination of tin to the keto-oxygen and the terminal hydroxyl oxygen catalyzes the formation of the enediol. This isomerization incorporates a hydrogen atom from the solvent into the hydroxyl group on carbon 2. Dehydration could initially form enol-pyruvic aldehyde and then form pyruvic aldehyde by isomerization. This would effectively "land" the solvent hydrogen in the methyl group. This proposed mechanism is based on earlier reports which show that one hydrogen in the methyl group of lactic acid indeed originates from the solvent when the reaction starts from DHA. No incorporation was seen in a control experiment where pyruvic aldehyde was converted.[3,4] Alcohol addition to pyruvic aldehyde and a tin catalyzed 1,2-hydride shift produces the stable alkyl lactate and releases the catalyst.

Interestingly, Esben Taarning (a colleague working on the project) recognized the final step of the sequence resembles an intramolecular Meerwein-Ponndorf-Verley Reduction and Oppenauer oxidation. This step involves the 1,2-hydride shift; scheme 2.1 illustrates a bi-molecular MPVO reaction in which a ketone is reduced and an alcohol correspondingly oxidized.

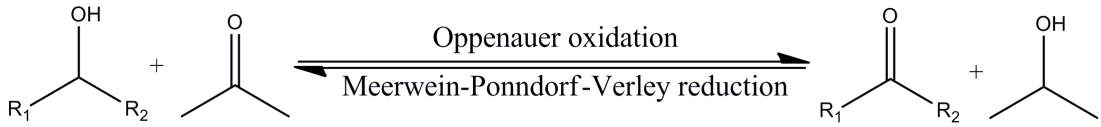

Scheme 2.1. Schematic presentation of an Oppenauer oxidation of a secondary alcohol with acetone and the corresponding Meerwein-Ponndorf-Verley reduction.

This resemblance prompted us to search the literature for heterogeneous catalysts (zeolites) which had been used in MPVO type reactions. Indeed, several zeolite catalysts containing Lewis acidity were in fact reported to be active.[5,6,7] The hypothesis that these zeolite/zeotype materials could be active for GLA/DHA conversion into lactic acid/alkyl lactate became the working hypothesis for the work presented in part 3.

Glycerol oxidation was mentioned above as a potential source of C_3-sugars. Previously, it has been shown that retro aldol condensation of glucose and fructose can occur in (sub) super critical water forming C_3 sugars, glycolaldehyde and eryhtrose as well as a number of different acids.[8] This prompted us to investigate whether the strong affinity for carbonyl functionalities of Sn-Beta could catalyze this fragmentation at elevated temperatures, thus converting hexose sugars directly into lactic acid derivatives.

[1] Y. Hayashi, Y. Sasaki, *Chem. Commun.*, (**2005**), 2716-2718.

[2] E. Taarning, A. T. Madsen, J. M. Marchetti, K. Egeblad, C. H. Christensen, *GreenChem*, 10, (**2008**), 408-414.

[3] E. bang, J. Eriksen, L. Mønsted, O. Mønsted, *Acta Chemica Scandinavia*, 48, (**1994**), 12-19.

[4] J. Eriksen, O. Mønsted, L. Mønsted, *Transition. Met. Chem.*, 23, (**1998**), 783-787.

[5] E. J. Creyghton, S. D. Ganeshie, R. S. Downing, H. van Bekkum, *J. Mol. Catal.* A., 115, (**1997**), 457-472.

[6] A. Corma, M. E. Domine, L. Nemeth, S. Valencia, *J. Am. Chem. Soc.*, 124, (**2002**), 3194-3195.

[7] Y. Zhu, G-K. Chuah, S. Jaenicke., *J. Catal*, 241, (**2006**), 25-33.

[8] M. Sasaki, K. Goto, K. Tajima, T. Adschiri, K. Arai, *GreenChem.*, 4, (**2002**), 285-287.

Journal of Catalysis 269 (2010) 122–130

Contents lists available at ScienceDirect

Journal of Catalysis

journal homepage: www.elsevier.com/locate/jcat

Zeolite H-USY for the production of lactic acid and methyl lactate from C_3-sugars

Ryan M. West [a], Martin Spangsberg Holm [b], Shunmugavel Saravanamurugan [b], Jianmin Xiong [b], Zachary Beversdorf [c], Esben Taarning [d,*], Claus Hviid Christensen [d]

[a] University of Wisconsin-Madison, Department of Chemical and Biological Engineering, Madison, WI 53706, USA
[b] Center for Sustainable and Green Chemistry, Department of Chemistry, Technical University of Denmark, DK-2800 Lyngby, Denmark
[c] Iowa State University, Department of Chemical and Biological Engineering, Ames, IA 50011, USA
[d] Haldor Topsøe A/S, Nymøllevej 55, DK-2800, Denmark

ARTICLE INFO

Article history:
Received 4 June 2009
Revised 21 October 2009
Accepted 24 October 2009
Available online 25 November 2009

Keywords:
Lactic acid
Methyl lactate
H-USY
Zeolite
Dihydroxyacetone
Glyceraldehyde
Triose sugar
Deactivation
Biomass

ABSTRACT

Lactic acid is an interesting platform chemical with many promising applications. This includes the use as a building block for the production of biodegradable plastics and environmentally friendly solvents. A study of the liquid-phase conversion of the triose-sugars, glyceraldehyde and dihydroxyacetone directly to methyl lactate and lactic acid catalyzed by inexpensive commercially available zeolites is presented. One particular zeolite, H-USY (Si/Al = 6) is shown to be quite active with near quantitative yields for this isomerization. Deactivation of the H-USY-zeolite was studied by correlating the catalytic activity to data obtained by TPO, XRD, N_2-sorption, and NH_3-TPD on fresh and used catalysts. Coking and irreversible framework damage occurs when lactic acid is produced under aqueous conditions. In methanol, methyl lactate is produced and catalyst deactivation is suppressed. Additionally, reaction rates for the formation of methyl lactate in methanol are almost an order of magnitude higher as compared to the rate of lactic acid formation in water.

1. Introduction

Lactic acid is currently emerging as a building block in a new generation of materials such as biodegradable plastics and solvents [1–3]. These new materials can be produced from biomass-derived precursors and have the potential to replace existing petroleum-based materials by displaying comparable and even superior properties [4]. Lactic acid also has the potential to become a central chemical feedstock for the chemical industry in the production of acrylic acid, propylene glycol, and different useful condensation products [5–8].

However despite its high potential, the major obstacle in a wider implementation of lactic acid-based materials and a lactic acid platform in the chemical industry is the high cost associated with the expensive and cumbersome manufacturing route of lactic acid. The large-scale production of lactic acid relies on the batch-wise fermentation of aqueous glucose under anaerobic conditions [9,10]. The fermentation reaction typically takes 2–4 days and requires calcium hydroxide to be added continuously to maintain a neutral pH-level in order for the bacteria to function optimally, thereby resulting in the formation of calcium lactate. Crystallization of calcium lactate, followed by acidification with sulfuric acid releases the crude lactic acid and gypsum. Typically, one ton of gypsum is formed for every ton of lactic acid produced [1]. Further purification of lactic acid is done by esterification to methyl lactate followed by distillation and hydrolysis to release pure lactic acid.

Lactic acid is an isomer of the triose sugars dihydroxyacetone (DHA) and glyceraldehyde (GLA). The relative stability of the three isomers are in the order of lactic acid ≫ DHA > GLA. The triose sugars can be formed by aerobic oxidation of glycerol using both homogeneous and heterogeneous catalysts [11–14] or by fermentation of glycerol using the *Gluconobactor suboxydans* strain [15–18].

Homogeneous catalysts such as sulfuric acid and sodium hydroxide are known to catalyze the isomerization of DHA and GLA in very hot water (250–300 °C) to give low yields of lactic acid [19,20]. A more effective isomerization catalyst is zinc sulfate, which is reported to give a 75–86% yield of lactic acid in 300 °C hot water [21]. However, the use of a homogeneous isomerization catalyst is problematic from an environmental point of view and the purification of lactic acid can be problematic. Furthermore, the use of very hot water as the reaction media requires expensive pressure resistant equipment which will make a large-scale process unattractive. Homogeneous metal chlorides are active in this isomerization–esterification reaction. In particular, tin

* Corresponding author.
E-mail address: esta@topsoe.dk (E. Taarning).

0021-9517/$ - see front matter © 2009 Elsevier Inc. All rights reserved.
doi:10.1016/j.jcat.2009.10.023

chloride has been found to be able to form methyl lactate in a high 89% yield [22]. However, a high catalytic amount (10 mol%) of tin chloride is used in this case.

Currently, very limited work has been done using acidic zeolites for the conversion of biomass to value added chemicals. Acidic zeolites have been demonstrated to catalyze the conversion of DHA in ethanol to form ethyl lactate, although in a moderate 65% yield [23]. Very recently Lewis acidic beta zeolites were shown to be highly active in the isomerization reaction of DHA and GLA with excellent selectivity toward methyl lactate/lactic acid [24]. These hydrophobic zeolites were made by incorporating Ti, Zr, and Sn into the framework. In particular the Sn-Beta zeolite appears to be an exceptionally promising catalyst in the DHA/GLA conversion. However, application may be limited due to long synthesis time and to the use of tin. Thus an investigation using commercially available solid acids, mainly zeolites containing only silicon and aluminum and sulfated zirconia was undertaken in batch reactors. The most promising of these catalysts, the proton form of an ultra stable Y-zeolite with a Si/Al = 6 (H-USY-6) showed very good activity with near quantitative yields at appropriate conditions. This zeolite was tested under continuous flow within a plug flow reactor to determine the kinetics of the isomerization network and to study the deactivation of the system. A discussion of the catalytic behavior is coupled to the results from XRD, NH_3-TPD, N_2-sorption, FT-IR, and TPO of the fresh and spent zeolite.

2. Experimental

2.1. Chemicals

Dihydroxyacetone (97%), pyruvic aldehyde dimethyl acetal (PADA) (97%), glyceraldehyde (95%), anhydrous pyridine (99.8%), and methanol (99.9%) were purchased from Sigma-Aldrich. Methyl lactate (97%) was obtained from Fluka. Pyruvic aldehyde (PA) was obtained from SAFC Supply as a 40 wt.% aqueous solution while lactic acid was obtained from Fluka and Riedel-de Haën. All the commercially available zeolites used throughout this study were kindly provided by Zeolyst International. The zeolites are pure and do not contain any binder material. Some of the zeolites were received in the NH_4-form. In these cases the zeolites were calcined at 550 °C in air for 6 h prior to use in order to produce the acidic form.

2.2. Catalytic tests

Batch experiments were performed in an Ace pressure tube with magnetic stirring. In these runs, 80 mg of catalyst, 1.25 mmol of substrate (calculated as monomer), and 4 g of water or methanol were added and mixed in the pressure tube using magnetic stirrer ring. The ace pressure tube was then dipped into an oil bath having a temperature of 140 °C for experiments with water and 120 °C for experiments with methanol. The internal temperature during reaction as recorded with an internal thermocouple was 125 °C and 115 °C, respectively.

In the flow reactor set-up, the feed was introduced into the system by either a Waters 501 HPLC pump, or by a Knauer *K-120* HPLC pump. The catalyst was held in place in a stainless steel reactor tube by quartz wool on both sides of the catalyst. The reactor tube was heated by a Carbolite oven while a type E thermocouple attached to the external surface of the reactor tube was used to monitor the reactor temperature. The effluent was collected in a stainless steel collector tube. The system was pressurized to 20 bar of pressure with Argon before each run. Feeds were created by placing a measured amount of substrate in a volumetric flask and filling to the set volume. For concentrated solutions, the mixtures were heated to 69 °C under stirring for 1–2 h to help dissolve the substrate.

Effluent concentrations for batch and flow experiments were characterized by an Agilent 1200 Series HPLC with an R.I. detector and a Biorad Aminex HPX-87H column and an Agilent 6890N GC with an HP-5column and an FID detector. Species were quantified with standards and confirmed with GC-MS, Agilent 6850 GC system coupled with Agilent 5975 C MSD.

2.3. Zeolite characterization

The degree of carbon deposition on used catalysts was determined using temperature-programed oxidation (TPO). Prior to analysis the used zeolites were dried at 110 °C. The TPO was carried out by heating a premeasured amount of used catalyst to 650 °C at 3.5 °C min^{-1} in a gas flow of 20 mL min^{-1} consisting of 5% oxygen in helium. The release of CO and CO_2 was quantified using a BINOS detector. The TPO data are shown in Table 4 as the weight percent of carbon present on the coked catalyst.

NH_3-TPD, N_2-sorption, and XRD were performed on calcined catalyst samples. The procedures used were either as described for the TPO or calcination at 550 °C for 4 h in static air, heated at a ramp of ~2 °C/min. Nitrogen physisorption was measured on a Micromeretics ASAP 2020 after the samples had been degassed in vacuum at 300 °C for 2 h.

Powder X-ray diffraction (XRD) patterns were recorded on a Bruker AXS powder diffractometer. The XRD data are shown in Table 4 as a relative crystallinity, calculated by integrating the peak area of eight characteristic reflections and comparing to the unused zeolite. The reflections used along with the respective 2θ values given in parenthesis were 331 (15.97), 511 (19.01), 440 (20.71), 533 (24.06), 642 (27.52), 822 (31.29), 555 (31.95), and 664 (34.69) [25].

NH_3-TPD measurements were performed on a Micromeritics Autochem II equipped with a TCD detector. Dry weights of the samples were found after evacuation at 300 °C for 1 h. After saturation with ammonia, the weakly bound ammonia was desorbed prior to measurement at 150 °C for 1 h in a He flow of 25 mL min^{-1}. The desorption curve was then attained at a heating ramp of 15 °C per minute to 550 °C at a He flow rate of 25 mL min^{-1}.

FT-IR operated in transmission mode was used to analyze the zeolites on a BioRad FTS 80 spectrometer equipped with a MCT detector. Self-supporting wafers of the zeolites were pressed and were prior to analysis dehydrated under evacuation at 400 °C for 4 h. The absorbance spectra were obtained after the samples were allowed to cool to RT. Pyridine adsorption was done by saturating the zeolite at RT and subsequently heating the sample to 200 °C for 30 min under evacuation. The sample was once again allowed to cool to RT before the spectrum was recorded.

3. Results and discussion

3.1. Reaction pathway

We have investigated the isomerization of the two three-carbon sugars dihydroxyacetone (DHA) and glyceraldehyde (GLA) into methyl lactate and lactic acid over an acidic zeolite catalyst. When the solvent used is methanol, the resulting product becomes methyl lactate and if water is used, lactic acid is formed. Scheme 1 gives the proposed reaction path of the isomerization reaction in either alcohol or water [22–24]. Pyruvaldehyde (PA) is believed to be an initial product formed by the dehydration of DHA/GLA. After addition of water/methanol the resulting hydrate/hemiacetal can isomerize into lactic acid/methyl lactate (path A). The reaction

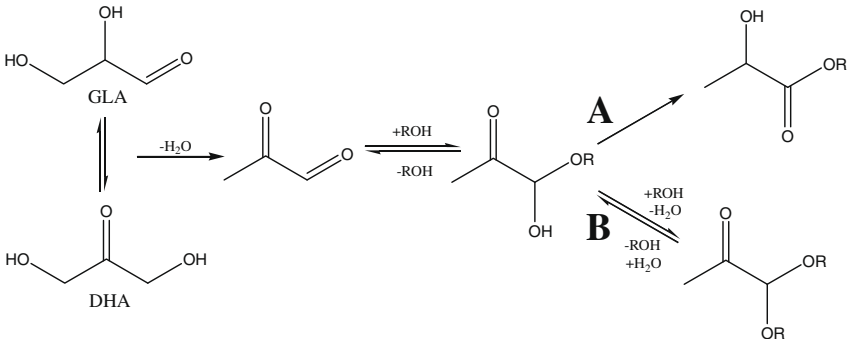

Scheme 1. Reactive pathways of DHA/GLA to lactate/lactic acid (path A) or hydrated/methylated pyruvic aldehyde derivates (path B), in methanol, (R = CH_3) and water (R = H).

path in Scheme 1 will be discussed in detail along with the presentation of the experimental findings.

Product formation in a typical batch experiment was monitored as a function of reaction time. Concentration profiles, based on the carbon balance of the initial triose sugars, are shown in Figs. 1 and 2 for the H-USY-6 zeolite. Fig. 1a and b shows the reaction profiles for DHA and GLA, respectively, in methanol while Fig. 2a and b

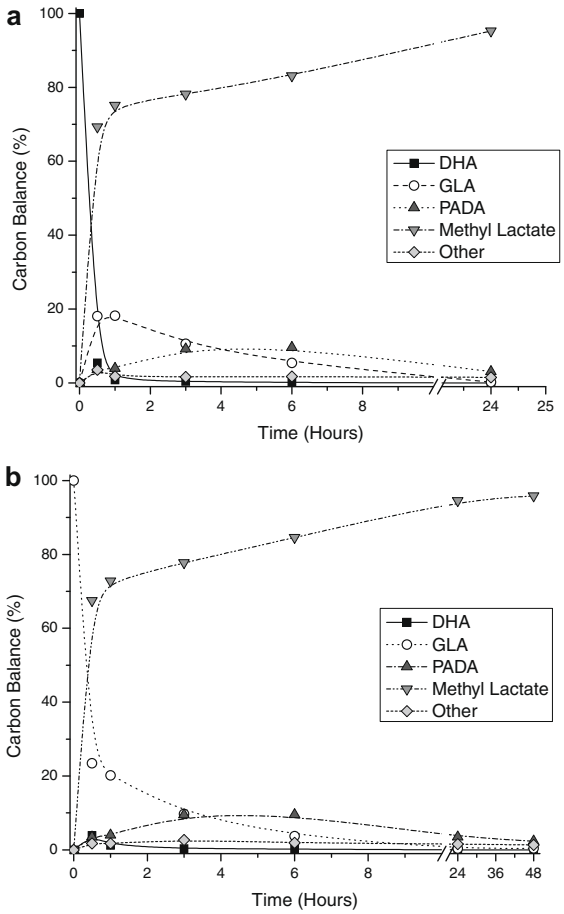

Fig. 1. Batch concentration profiles for DHA and GLA in methanol. Other includes Pyruvic Acid PA, MMP, and TMO. (a) 1.25 mmol DHA in 4.0 g methanol at 115 °C with 80 mg H-USY-6 catalyst; and (b) 1.25 mmol GLA in 4.0 g methanol at 115 °C with 80 mg H-USY-6 catalyst.

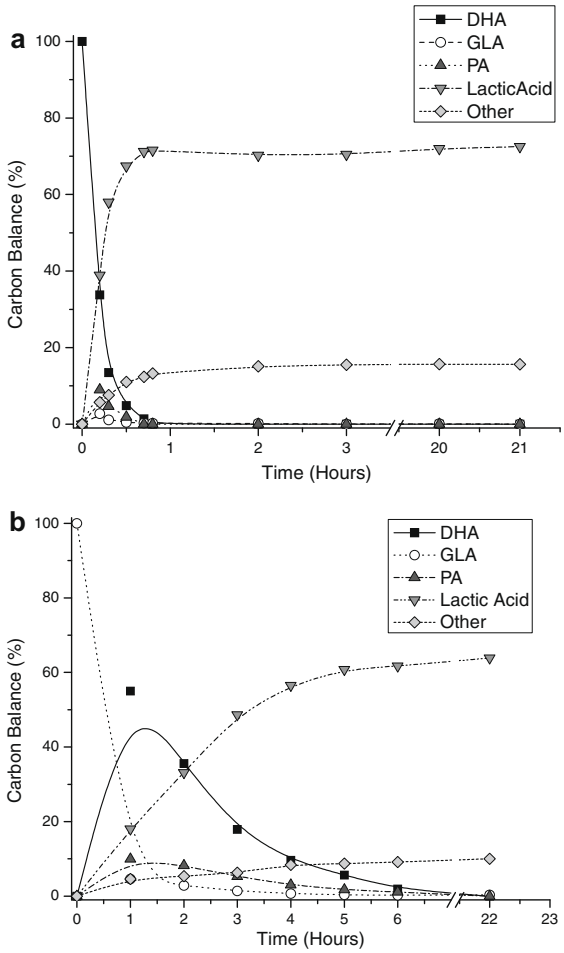

Fig. 2. Batch concentration profiles for DHA and GLA in water. Other includes pyruvic acid, formic acid, acetic acid, levulinic acid, and acetol. (a) 1.25 mmol DHA in 4.0 g water at 125 °C with 80 mg H-USY-6 catalyst; and (b) 1.25 mmol GLA in 4.0 g water at 125 °C with 80 mg H-USY-6 catalyst.

Table 1
Yields obtained from DHA/GLA conversion to lactic acid and methyl lactate over commercial catalysts; 80 mg catalyst, 1.25 mmol substrate (calculated as monomer), 4 g solvent (water or methanol), reaction time 24 h (DHA) or 48 h (GLA), temperature 115 °C (methanol) or 125 °C (water).

Zeolite	Si/Al	Substrate	Water solvent		Methanol solvent	
			Yield of lactic acid (%)	Substrate conversion (%)	Yield of methyl lactate (%)	Substrate conversion (%)
H-USY-6	6	DHA	71	>99	96	99
		GLA	63	>99	98	>99
H-USY-30	30	DHA	47	>99	26	79
		GLA	41	>99	25	64
H-beta	12.5	DHA	63	>99	42	88
		GLA	60	>99	63	90
	19	DHA	37	>99	19	79
		GLA	37	>99	8	64
H-ZSM-5	11.5	DHA	32	>99	17	76
		GLA	30	>99	19	73
	25	DHA	22	>99	7	61
		GLA	23	>99	7	59
H-MOR	10	DHA	39	>99	8	74
		GLA	32	>99	10	28
H-montmorillonite	–	DHA	46	>99	29	44
		GLA	44	>99	30	43
Sulphated zirconia	–	DHA	39	>99	17	96
		GLA	41	>99	37	91
No catalyst	–	DHA	5	>99	0	<0.1
		GLA	4	>99	0	<0.1

shows the profiles in water. The yields of methyl lactate/lactic acid for a variety of solid acids are summarized in Table 1 and are simply the end data point of the individual experiments.

Both GLA and DHA are observed when either substrate is used as a starting reagent as can be seen from Figs. 1a,b and 2a,b. These observations indicate that isomerization between these two sugars occurs and PA is formed as an intermediary product, in accordance with previous reports [26–28]. DHA reacts more quickly than does GLA. In water (Fig. 2b), it is noted that GLA first isomerizes to DHA and the DHA then appears to react. Starting form GLA, the reaction network appears to be dominated by the isomerization and dehydration over the first 6 h. After 6 h, the system approaches the final distribution seen at 22 h. When DHA is instead used as a starting reagent, the final distribution is reached in less than 1 h.

The presence of PA as an intermediate can also be seen in Fig. 2. The concentration of PA is observed to be highest at very short reaction times for both DHA and GLA, thus supporting the hypothesis that PA is an initial intermediate. Addition of either water or methanol forms either hydrated PA or the methyl hemiacetal of PA (PAMA), respectively, both of which can undergo a 1,2-hydride shift and isomerize into lactic acid or methyl lactate (Scheme 1, path A), respectively. The hydrated form of PA can react with an additional water molecule to form the di-hydrated form of PA. It is noted that in water, pyruvaldehyde exists in three forms; aldehyde, hydrated, and di-hydrated with a typical distribution of trace, 56% and 44%, respectively [29]. In the analytical methods used in this study, it was not possible to distinguish these three species, but all are expected to be present. Additionally, the degradation products seen in water consisted of known PA degradation products as seen in commercial sources of pyruvaldehyde, namely pyruvic acid, acetol, and formaldehyde [30].

The same is not true for the methanol case. The PAMA was observed directly as an intermediate species and it can react with another molecule of methanol to form pyruvaldehyde dimethylacetal (PADA), (Scheme 1, path B). PADA has additionally been observed to react further in very small amounts to the methylated form TMP (1,1,2,2-tetramethoxy propane) at low to intermediate conversions. At full conversion, however, PADA, TMP, and PAMA are converted into methyl lactate (Fig. 1) suggesting the back reaction shown in Scheme 1.

3.2. Screening of commercial zeolites

A series of different commercially available zeolites were investigated in the isomerization of the trioses into lactic acid or methyl lactate. Table 1 provides an overview of the yields observed in batch experiments for both GLA and DHA in water and methanol. From Table 1 we conclude that very similar selectivity toward lactic acid/methyl lactate is obtained using either DHA or GLA as the substrate, with only H-beta and sulphated zirconia showing a significant but reproducible selectivity difference with methanol as the solvent.

It is clear from Table 1 that the most effective catalysts for this isomerization–esterification reaction are the proton form of the highly acidic ultra stable Y-zeolite with a Si/Al ratio of 6 (H-USY-6). Indeed, the H-USY-6 zeolite affords methyl lactate yields higher than 95% within the 24 h reaction time which is comparable to the most selective catalysts reported so far in the literature [21–24]. In the absence of a catalyst, DHA and GLA are not converted into methyl lactate/lactic acid in any significant degree. The trioses are stable in pure methanol, but degrade readily in water to form a product mixture consisting of carbonaceous products along with pyruvic aldehyde and some lactic acid. The H-beta zeolite gives moderate yields (DHA 42%/GLA 62%) of methyl lactate, whereas the best H-ZSM-5 catalyst affords only a low yield (<20%) of methyl lactate. In general as the Si/Al ratios are lowered (higher acid density) a higher triose conversion and moderately higher selectivity for methyl lactate is achieved. In a previous work zeolite beta was tested in the isomerization of DHA/GLA to methyl lactate/lactic acid. It was shown that dealumination of zeolite beta by steaming increased the yields of methyl lactate/lactic acid relative to the non-dealuminated catalyst thus indicating that the presence of extra framework aluminum was beneficial for the reaction. However, other factors such as, the effective diffusion rates, acid densities as well as acid strength could also have important roles in determining the activity of the various zeolite structures.

3.3. Characterization by FT-IR

Due to the very large difference in the yield of methyl lactate of the two H-USY samples (98% and 25%, from Table 1) we chose to investigate these two samples by FT-IR using pyridine as a molec-

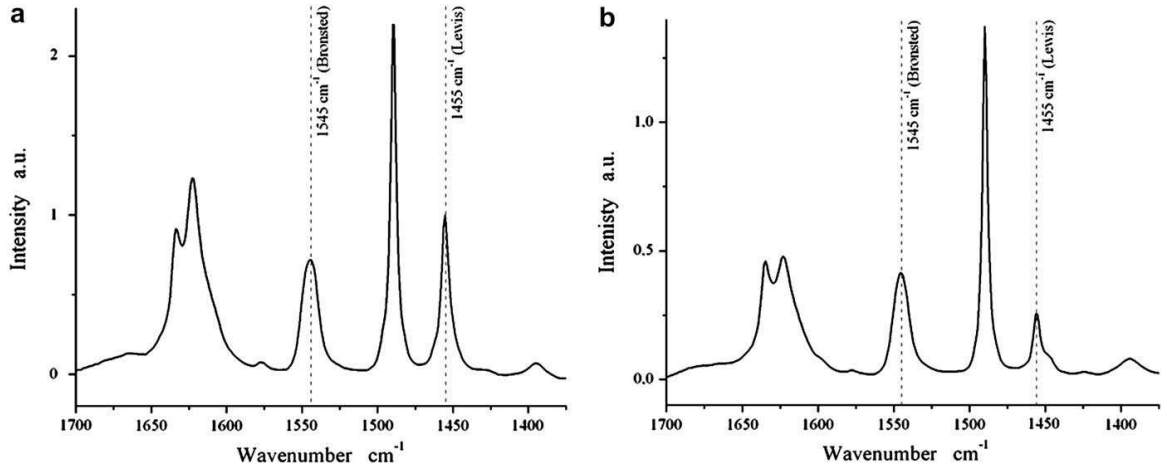

Fig. 3. IR difference spectra after pyridine saturation and subsequent evacuation at 200 °C for 30 min: (a) H-USY-6; and (b) H-USY-30.

ular probe while combined the results with acidity measurements from NH_3-TPD. The dehydrated spectra of the two samples (not shown) reveal the high frequency bridging hydroxyl (HF(OH)) located within the supercage of the zeolite at 3632 cm^{-1}, and the low frequency bridging hydroxyl (LF(OH)) present in the sodalite cage at 3566 cm^{-1} [31]. In addition, contributions at 3602 cm^{-1}, 3526 cm^{-1}, and 3674 cm^{-1} are seen in the case of the H-USY-6 sample. The two former bands located at 3602 cm^{-1} (HF'(OH)) and 3526 cm^{-1} (LF'(OH)) have been reported to occur due to perturbation by extra framework silicoaluminous debris formed upon dealumination of zeolite Y [32,33]. Further, the 3674 cm^{-1} band is said to arise from hydroxyl groups linked to extra framework aluminum (EFAL) species [33]. From pyridine adsorption we were able to differentiate between Lewis and Brønsted acidity while the NH_3-TPD provided a measure of the total acidity. Fig. 3 presents the difference spectra of the pyridine saturated samples after evacuation at 200 cm^{-1} C for 30 min. The relative Brønsted and Lewis acidity ratio could be obtained from integrating the areas under the bands at 1545 cm^{-1} (pyridinium ion) and 1455 cm^{-1} (pyridine) while taking the extinction coefficients into account [34,35]. Using values of $\varepsilon_{Brønsted} = 1.67$ and $\varepsilon_{Lewis} = 2.22$ as reported in Ref. [35], we obtained values of B/L ratio of 1.8 for H-USY-6 and 5.6 for the H-USY-30 zeolite. From NH_3-TPD we found that the total acidity of the H-USY-6 and H-USY-30 samples was 563 $\mu mol/g_{zeolite}$ and 199 $\mu mol/g_{zeolite}$, respectively. Interestingly, these results show that a large fraction of the acidity of the H-USY-6 zeolite actually consists of Lewis acidic sites. Also the total number of Lewis acid sites per gram of zeolite is much larger for H-USY-6 as compared to the H-USY-30 zeolite ($\sim$200 $\mu mol/g_{zeolite}$ and $\sim$30 $\mu mol/g_{zeolite}$, respectively). These findings are in agreement with an earlier report showing that a purely Lewis acidic zeolite beta is highly active for the formation of methyl lactate from triose sugars [24] and they support the hypothesis that the Brønsted and Lewis acidic sites can catalyze two different reaction paths, with only the Lewis acidic sites leading to the formation of lactic acid/methyl lactate in appreciable amounts from DHA/GLA.

3.4. Flow experiments

The high yields obtained when using the H-USY-6 zeolite as catalyst merited further study in continuous flow mode. The stability of the H-USY-6 catalyst at high conversion in water and in methanol was investigated for approximately 45 h on stream. Reaction

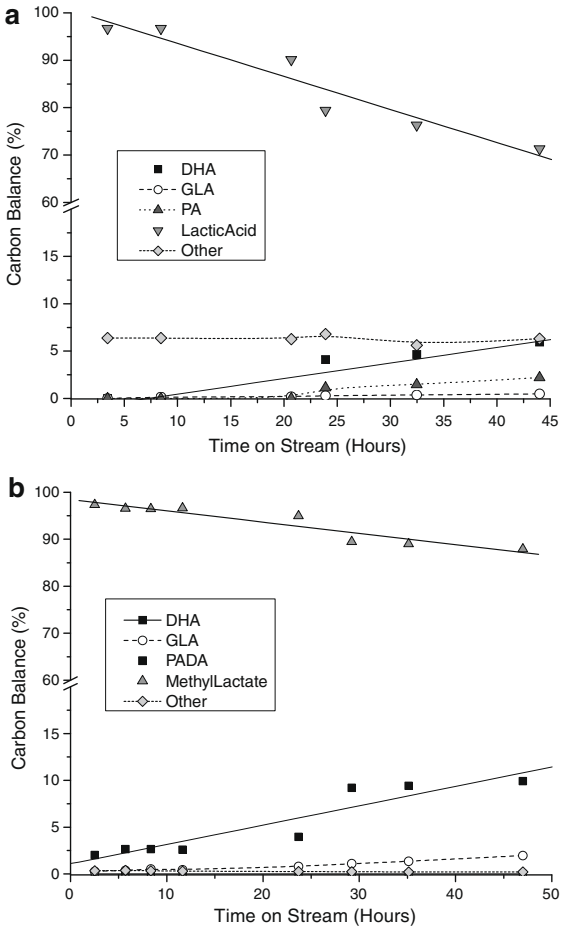

Fig. 4. Concentration profiles vs. time on stream for 0.31M DHA over H-USY-6 catalyst. Other includes pyruvic acid and TMO. (a) DHA conversion in water at 177 °C, WHSV of 0.18 h^{-1}. Other includes pyruvic acid, formic acid, acetic acid, levulinic acid, and acetol; and (b) DHA conversion in methanol at 157 °C, WHSV of 0.16 h^{-1}.

conditions for the two experiments were chosen to achieve full conversion initially, and a high yield of products, i.e. in the case of water, a reaction temperature of 177 °C, concentration of 0.31 M DHA, and a WHSV of 0.18 h^{-1} was chosen, while for methanol a temperature of 157 °C, concentration of 0.31 M DHA, and WHSV of 0.16 h^{-1} was used. Fig. 4 presents the observed product compositions obtained by sampling the effluent as a function of time on stream.

In Fig. 4a while the initial yield of lactic acid in water was quite high, 95%, the sample showed continual deactivation. After around 25 h, the concentration of both unreacted feed and pyruvic aldehyde (PA) increased significantly, while the yield of lactic acid decreased sharply. This deactivation continued for the duration of the run reaching a ~70% yield of lactic acid after 44 h. In the case of methanol as a solvent we observed a much improved stability within the 47 h as shown in Fig. 4b. The yield of methyl lactate remained around or above 90% for the duration of the run. As the yield of methyl lactate drops slowly, the yield of pyruvic aldehyde dimethyl acetal (PADA) increases. Only low concentrations of unreacted triose sugars were observed in the effluent.

3.5. Kinetic study in the flow system

In order to better understand the current system, a simultaneous investigation of the kinetics and deactivation under various reactions conditions were conducted. The temperature, feed concentration, and feed substrates were systematically varied as shown in Table 2 while the catalyst loading was adjusted to keep the initial disappearance of reagent to less than 70% and the yield of lactic acid/methyl lactate to less than 50%. The initial activity and calculated initial activity of the H-USY-6 as a function of systematically altered reaction conditions are shown in Table 2. The initial measured activities are given for the disappearance of triose sugars (total disappearance of GLA and DHA), the appearance of lactic acid/methyl lactate, and for the appearance of intermediate species PA/PAMA (pyruvic aldehyde methyl acetal), and PADA, (depending on the solvents). The calculated values were fit with a simple kinetic model while as described in detail in the modeling section below.

As one would expect, the rates increased as the temperature was increased at otherwise constant conditions, (entries 1–6). The activity of DHA and GLA in water at ~160 °C and 0.31 M (entries 4 and 7) showed quite different results. The total disappearance rate when GLA is the starting reagent is only 305 μmol/(min * g_{cat}), while this value is 425 when DHA is the starting reagent. Likewise, the appearance of lactic acid from GLA is only 120 compared to 355 for DHA at the same conditions. The observation suggests isomerization of GLA to DHA readily occurs with the DHA ultimately reacting as discussed later. When the suspected intermediate species PA is reacted at similar conditions, (entry 8), a higher disappearance of feed of 820 and an appearance of lactic acid of 770 is observed. This observation appears reasonable since the dehydration step is surpassed and the kinetics of isomerization are quite favorable as discussed in a later section.

When the feed concentration of DHA is increased at any temperature, the disappearance of triose sugars is seen to likewise increase (entries 2, 9, and 10 and entries 4, 11, and 13). However, the appearance of lactic acid is not observed to increase correspondingly. In Table 1, it is noted that when given enough time, complete conversion of triose sugars to products other than lactic acid is possible without catalyst in water. It is believed that similar degradation reactions are occurring when the concentration of feeds is increased beyond 0.31 M.

Switching the solvent to methanol (entries 14–19) caused a drastic difference in the observed rates. For a 1.25 M feed solution of DHA, the initial disappearance of triose sugars increased by a factor of ~7 from 775 in water at 160 °C (entry 11) to 5590 in methanol at 150 °C (entry 18), while the appearance increased by a factor of ~8 from 405 for lactic acid to 3315 for methyl lactate. A similar trend is seen at 130 °C where the rate of disappearance increases from 225 to 1305, while the rate of appearance increases from 50 to 1060 (entries 2 and 15, respectively).

Interestingly, using a mixed solvent of methanol and water (entry 17) produced disappearance and production rates between that of pure methanol and water. For a 1.25 M solution of DHA, a 45/55 molar mixture of methanol and water (64.5 wt.% methanol) at 150 °C showed a disappearance rate of 1300, double that of pure water, 775 (entry 11), but much less than that of pure methanol, 5590 (entry 18). The rate of appearance of product, a mixture of lactic acid and methyl lactate for the 45/55 mixture was 860, again about double that of pure water, 405, and much less than that of pure methanol 3315. A mixture of the solvents is indeed an interesting situation since for every one mole of DHA reacted, one mole of water is created in an alcohol solvent meaning that minor

Table 2
Initial rates of reaction under systematically varied conditions using H-USY-6. The total number of acid sites are 563 umol/g based on NH_3-deposition. The number of Brønsted and Lewis acid sites corresponds to 362 μmol/g and 200 μmol/g, respectively (based on pyridine IR-adsorption).

Entry	Conditions of run				Measured initial rate (μmol/(min*g_{cat}))				Calculated rate (μmol/(min*g_{cat}))		
	Temp. (°C)	Reagent	Solvent	Concentration (M)	Triose dissappearance	LA/ML appearance	PA/PAMA appearance	PADA appearance	Triose dissappearance	LA appearance	PA appearance
1	116	DHA	Water	0.31	27	17	2		32	23	8
2	130	DHA	Water	0.31	75	50	8		75	40	35
3	142	DHA	Water	0.31	100	100	15		110	65	35
4	165	DHA	Water	0.31	425	355	40		450	315	90
5	172	DHA	Water	0.31	550	445	25		525	380	75
6	190	DHA	Water	0.31	1530	1055	205		1545	1075	230
7	160	GLA	Water	0.31	305	120	30				
8	160	PA	Water	0.36	–	770	820[a]		–	820	930[a]
9	130	DHA	Water	0.80	180	50	30		210	90	110
10	130	DHA	Water	1.25	225	30	45		260	120	130
11	160	DHA	Water	1.25	775	405	125		710	415	240
12	160	PA	Water	1.25	–	780	865[a]		–	855	975[a]
13	160	DHA	Water	3.44	2475	340	405		2480	1495	785
14	112	DHA	MeOH	1.25	735	620	30	45			
15	130	DHA	MeOH	1.25	1305	1060	35	300			
16	130	GLA	MeOH	1.25	1270	800	25	190			
17	150	DHA	MeOH/water	1.25	920	865	95	150			
18	150	DHA	MeOH	1.25	5590	3315	385	1400			
19	165	DHA	MeOH	1.25	10080	4600	905	2850			

[a] Disappearance of PA.

amounts of water are inevitably present. Further, this situation is important if operating in solvents of only technical grade. Importantly as just outlined above using the mixture of water and methanol did increase the rates with respect to those observed in pure water. However, reaction rates in the solvent mixture are still much closer to the rates seen in water than those in pure methanol.

3.6. Deactivation

The reasons for deactivation were investigated by characterizing fresh and used catalysts. Table 4 demonstrates the surface properties for fresh and selected used catalyst collects from Table 3 as well as H-USY-6 zeolites under modeled deactivating conditions. Table 4 entry 1 represents the fresh, unused H-USY-6 zeolite which is used for comparison. Entries 2–8 contains data for the used catalysts and were chosen as to cover the range of reaction times, temperatures, feeds, concentrations, and solvents used.

Entry 2 was tested at low temperature (116 °C) and short time (6 h) on stream while entry 3A corresponds to the zeolite used in Fig. 3a namely a temperature of 177 °C and time on stream 44 h in water. Entry 3B is the same sample without calcination to show the influence of carbon on the surface area. Characterizing the three used zeolites we note that the adsorption characteristic of entry 2 is very similar to the parent zeolite exemplified by a micropore volume which only decreased from 0.253 ml/g to 0.236 ml/g indicating that the zeolite structure is mostly preserved. This is in strong contrast to the prolonged and high temperature reaction used for entry 3A which resulted in an almost complete loss of crystal integrity. This can be seen by a reduction in the measured surface area and micropore volume of around 80%, a loss of acidity of 46% as well as a final crystallinity calculated to <10%. Furthermore, the catalyst is heavily covered in carbon, containing as much as 9 wt.% carbon.

Entry 4 shows data for the zeolite after a time on stream of 47 h at 157 °C in the conversion of DHA in methanol (Fig. 3b). Ammonia-TPD, porosity measurements, and the estimated crystallinity all shows that less framework deterioration takes place during the reaction in methanol compared to water (entry 3A). However, a modest loss in micropore volume, surface area, and acidity is seen along with a decrease in the calculated crystallinity of around 40% indicating that the catalyst has suffered some structural damage in excess of the deactivation by carbon deposits.

Entries 5 and 6 shows that the highest deposition of carbon takes place when PA is used as the feed, (Table 2 entries 8 and 12, respectively). In 9 h at 160 °C, 5.2% of carbon had deposited onto the H-USY-6 zeolite when using a feed of 0.36 M PA as substrate. Increasing the PA concentration aggravates the deposition of carbon, since 15.7% is deposited in only 5 h when a feed consisting of 1.25 M PA was used. In contrast, after running for 44 h, a 0.31 M DHA solution in water amounted to 9.0% carbon. In addition to the excessive carbon deposits, high surface area and micropore volume losses were also observed (entry 5). It is also noted that the deactivation of the catalyst in the two runs using PA as a feed was also the most rapid among all feeds and conditions tested.

Entries 7 and 8 in Table 4 were created by flushing the H-USY-6 zeolite with either a 0.31 M lactic acid solution in water or a 0.31 M methyl lactate solution in methanol overnight at the specified temperature. The lactic acid and methyl lactate were quantitatively recovered in the effluent indicating that the reverse reactions do not occur. These experiments show that the desired end products in methanol and water, methyl lactate and lactic acid, are not the cause for the excessive carbon deposition onto the zeolite. Importantly, we observe that the product in water, lactic acid, strongly damages the catalyst already after 12 h. Again this is in strong contrast to what is observed in the case of methyl lactate in methanol where more modest changes in the structure of the catalyst were detected for the comparable reaction conditions (entries 4 and 8). Although the XRD show a decrease of 41.2% for this sample the effect on micropore volume, surface area and total acidity of the zeolite is much smaller.

The specific cause of irreversible zeolite destruction was further systematically tested under controlled conditions. Entries 9 through 15 were created by exposing the fresh H-USY-6 zeolite to the specified conditions listed in a sealed teflon container rotated at 20 rpm. The zeolite was subsequently recovered by filtration and washed thoroughly with demineralized water and dried before analysis.

Stirring the zeolite in demineralized water for 24 or 48 h at 140 °C (entries 9 and 10) slightly decreased the surface areas and

Table 3
Modeled kinetic parameters for Scheme 1 on H-USY-6.

	Ea (kJ/mol K)	ln(A) (1/mass)
1	53 ± 13	17.4 ± 8.9
2	61 ± 15	20 ± 13
3	89	26

Table 4
Physical properties of fresh, used, and treated H-USY-6 catalysts.

Entry	Temperature (°C)	Solvent	Feed	Concentration (M)	Time (h)	Location	TPO (% C)	BET (m^2/g)	V_{micro} (mL/g)	V_{meso} (mL/g)	S_{meso} (m^2/g)	NH_3-TPD (umol/g)	XRD, C/C_0 (%)
1	–	–	–	–	–	–	–	725	0.253	0.058	134	563	100
2	116	Water	DHA	0.31	6	Reactor	2.0	674	0.236	0.076	142		
3[A]	177	Water	DHA	0.31	44	Reactor	9.0	182	0.048	0.198	97	306	8.6
3[B]	177	Water	DHA	0.31	44	Reactor		115	0.015	0.188	71		
4	157	MeOH	DHA	0.31	47	Reactor	2.7	619	0.217	0.060	128	461	59
5	160	Water	PA	0.36	9	Reactor	5.2	246	0.076	0.102	79		
6	160	Water	PA	1.25	5	Reactor	15.7						
7	177	Water	LA	0.31	12	Reactor	1.7	405	0.129	0.151	127	394	34
8	137	MeOH	ML	0.31	11	Reactor	1.8	708	0.246	0.071	142	486	56
9	140	Water	–	–	24	Vial		555	0.211	0.089	108	561	80
10	140	Water	–	–	48	Vial		554	0.208	0.108	108		
11	140	Water	LA	0.3	2	Vial		716	0.248	0.094	164		
12	140	Water	LA	0.3	8	Vial		670	0.232	0.106	164		
13	140	Water	LA	0.3	24	Vial		537	0.188	0.118	129	490	71
14	140	Water	LA	1	24	Vial	0.4	238	0.017	0.290	223	158	≈0
15	140	MeOH	–	–	24	Vial		693	0.251	0.057	131	486	93

[A] Calcined
[B] uncalcined.

crystallinity of the sample, however it did not markedly decrease the total acidity of the zeolite.

Carefully repeating the experiment by using a 0.3 M solution of lactic acid and a shorter treatment period caused a more pronounced destruction of the zeolite than pure water. Entries 11–14 show the systematic decrease in surface areas, and micropore volume corresponding to treatment times of 2, 8, and 24 h in 0.3 M lactic acid. At 24 h, the surface areas number of acid sites and crystallinity of the sample subjected to 0.3 M lactic acid (entry 13) were all lower than the corresponding values in pure water (entry 9) at 24 h. Further increasing the concentration of lactic acid to 1.0 M (entry 14) caused a complete destruction of the zeolite with no recognizable diffraction peaks present in the XPRD diffractogram, i.e. the crystallinity of this sample was ≈0%. Results from NH_3-TPD and N_2-sorption analysis support the complete dismantling of the zeolite. Importantly, a concentration of approximately 0.3 M of lactic acid, which is the concentration of final product in either the batch or flow experiments, is sufficient to destroy the zeolite suggesting that it is necessary to work with dilute systems if water is used as the solvent. In entry 8 we used anhydrous methanol for the treatment. It is however clear from the results that the zeolite is extremely stable in pure methanol as the zeolite characteristics are practically identical to the fresh zeolite.

As highlighted from the characterization above it is important to distinguish between the reversible deactivation occurring through coking of the zeolite in contrast to the irreversible deactivation through structural damage of the zeolite. The results indicate that coking originates from decomposition of PA and not from the end products. The conditions that lead to the most rapid loss in activity can be summarized as follows. Higher temperatures and higher concentration of lactic acid (either directly or through the formation from PA) are detrimental to the zeolite structure. Using water compared to methanol as a solvent causes a higher level of irreversible damage. This difference arising from the solvent is further increased as lactic acid also causes far more destruction than does methyl lactate. Minimal deactivation through destruction of the zeolite can therefore be expected when operating at low concentrations, low temperature, and when using an alcohol as the solvent.

3.7. Modeling the reaction path

The initial rate of reaction was modeled as a plug flow reactor with a series of simple first order reactions as shown in Scheme 2 for all runs involving DHA and PA with water as a solvent. The forward rate constants were assumed to be Arrhenius expressions of the form, $k_i = A_i \exp^{\frac{E_{Ai}}{RT}}$. The pre-exponential factor A and activation energy of each step were then estimated by integrating over the mass of catalyst in Matlab using the lsqnonlin function to minimize the differences in calculated and experimental rates for the disappearance of trioses, appearance of pyruvaldehyde, and the appearance of lactic acid. The fit parameters for each step are found in Table 3, while the calculated rates are included in Table 2.

Despite fairly good agreement over the large temperature and concentration range of this study, the confidence intervals seen in Table 3 are quite large. This variance is primarily due to relatively good fit over a range of values; that is similar forward rate constants can be calculated with a range of pre-exponential and activation energies. The initial disappearance of triose sugars was less than 70% while the initial yield was less than 50%, hence the model used incorporated the changing concentrations of the reagents through the reactor. This reaction model is not differential and hence the confidence intervals are quite large. Despite these large intervals, several important conclusions can be made by calculating the forward rate constants at the best fit values for each step in Scheme 2. It is observed that the forward rate constant for isomerization is the largest forward rate constant at all temperatures of this study. The ratio of k_2/k_1 increases as the temperature is increased from a value of 1.1 at 115 °C to 1.7 at 190 °C. This higher value for k_2 implies that the isomerization step occurs more readily than the dehydration step and that the isomerization is relatively more favorable as the temperature is increased. A second trend can be seen by comparing the degradation and isomerization constants, k_2/k_3. At 115 °C this value is 14.6, heavily favoring the isomerization. As the temperature is raised however to 190 °C, this ratio drops swiftly to 3.6 indicating that the degradation reactions become much more favorable at higher temperatures.

The model predicts the initial rates for a variety of concentrations, temperatures, and feeds relatively accurate. The differences between the calculated and observed initial rate of disappearance of triose species and pyruvic aldehyde are less than 20% for concentrations ranging from 0.31 M to 3.44 M and temperatures from 116 to 190 °C indicating the system is well described by the assumptions of first order kinetics and simple activation energies. The estimated production rate of lactic acid is also accurately modeled for the tests at low concentration. Deviations between the model and experimental data are largest at high concentrations with the largest differences between the predicted and observed rates occurring for the production of LA in entries 10 (131 °C 1.25 M) and 13 (159 °C 3.44 M). Since the reaction pathway is believed to be a series of reactions, and since the model does not include surface coverage terms, one possible explanation is that the catalytic sites are covered by either initial species DHA or water, and are blocked from reaction of DHA. A second explanation could include a diffusion limitation at high concentration. The surface blocking explanation is better supported, however, by the close fit between experimental and calculated rates when the intermediate species, PA is used. At higher concentrations of PA (entry 12) the rate of lactic acid production is relatively close to the rate of PA disappearance, while the same is not true of DHA at the same conditions (entry 11). If the system was diffusion limited, one would expect large differences for both cases, however if the initial reactivity of DHA is limited, large deviations would only be expected for the case starting with DHA, as observed.

Previous authors have modeled the degradation of triose sugars under isothermal conditions without a catalyst [26,27]. These studies looked at the isomerization and degradation of GLA and DHA into PA. As in the current case, first-order kinetics were found to appropriately model the disappearances of triose sugars and PA. As expected, the heterogeneously catalyzed activation energy

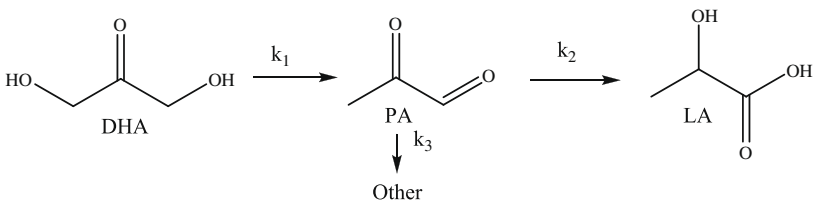

Scheme 2. Modeled reaction scheme for the conversion of DHA into LA.

determined here is much lower than previous reports for the dehydration of triose sugars (53 ± 13 vs. 75–92 kJ/mol, respectively). The degradation/isomerization of PA determined in this report are comparable to previous values, with the isomerization having a lower activation energy (61 ± 15 kJ/mol) and the degradation reaction having similar value (89 kJ/mol) to the other reports (77–94 kJ/mol). It is important to note that due to the aqueous environment of this and previous studies, PA is present as the hydrated and dehydrated forms. This implies that the degradation reactions of PA (as the mono- and di-hydrate) would proceed even in the absence of heterogeneous catalyst and further suggests avoidance by operation at lower temperatures.

From the modeling study, we see that the optimal reactions conditions for the production of a lactic acid derivative are low concentrations in an alcohol solvent such as methanol at low temperatures. The experimental data for the isomerization reactions can despite a relative large confidence interval be described by a series of first-order reaction and the model can be used to gain useful information of the involved rate constants. Specifically, the higher temperatures favor isomerization, k_2 over dehydration k_1, but also favor degradation k_3 over isomerization k_2. To limit degradation to other products, it is therefore suggested that the reaction be run at lower temperatures.

4. Conclusion

It has been demonstrated that the Lewis acidic H-USY-6 zeolite is highly effective for the isomerization of triose sugars to lactic acid and methyl lactate. Indeed, methyl lactate can be formed in almost quantitative yields directly from DHA and GLA, using this inexpensive zeolite. The transformation can be modeled via a series of first order reactions in water. In methanol, the rate of reaction is as much as an order of magnitude higher than in water. The catalyst deactivates both by carbon deposition and by framework degradation. However, deactivation by carbon deposition as well as structural damage can be minimized by using optimized reaction conditions of low concentration and temperature and with an alcohol such as methanol as the solvent. The presented work adds to the pool of information regarding this very interesting process wherein it is possible to produce racemic lactic acid or the corresponding methyl ester from biomass-derived substrates. Furthermore, since methyl lactate is formed directly in this process, purification to form high-grade lactic acid could be facilitated by distillation and hydrolysis, thereby avoiding the cumbersome purification process associated with the current production of lactic acid.

Acknowledgments

Supported by the Danish National Research Foundation, and the National Science Foundation, PIRE Program (Award # 0730277). We also thank Dr. J. Rass-Hansen and R. Johansson for technical assistance.

References

[1] R. Dhatta, M. Henry, J. Chem. Technol. Biotechnol. 81 (2006) 1119.
[2] R.A. Sheldon, Green Chem. 7 (2005) 267.
[3] Y.-J. Wee, J.-N. Kim, H.-W. Ryu, Food Technol. Biotechnol. 44 (2) (2006) 163.
[4] R. Leaversuch, Plast. Technol. 48 (3) (2002) 50.
[5] S. Varadarajan, D.J. Miller, Biotechnol. Prog. 15 (1999) 845.
[6] H.F. Shi, Y.C. Hu, Y. Wang, H. Huang, Chin. Chem. Lett. 18 (2007) 476.
[7] R.D. Cortright, M. Sanchez-Castillo, J.A. Dumesic, Appl. Catal. B: Environ. 39 (2002) 353.
[8] J.C. Serrano-Ruiz, J.A. Dumesic, Chem. Sus. Chem. 2 (6) (2009) 581.
[9] D. Garlotta, J. Polym. Environ. 9 (2) (2001) 63.
[10] R.P. John, K.M. Nampoothiri, A. Pandey, Appl. Microbiol. Biotechnol. 74 (2007) 524.
[11] H. Kimura, K. Tsuto, Appl. Catal. A: Gen. 96 (1993) 217.
[12] H. Kimura, Appl. Catal. A: Gen. 105 (1993) 147.
[13] R. Garcia, M. Besson, P. Gallezot, Appl. Catal. A: Gen. 127 (1995) 165.
[14] E. Farnetti, J. Kaspar, C. Crotti, Green Chem. 11 (2009) 704.
[15] D. Hekmat, R. Bauer, V. Neff, Process Biochem. 42 (2007) 71.
[16] S. Yamada, K. Nabe, N. Izuo, M. Wada, I. Chibata, J. Ferment. Technol. 57 (3) (1979) 215.
[17] K. Nabe, N. Izuo, S. Yamada, I. Chibata, Appl. Environ. Microbiol. 38 (6) (1979) 1056.
[18] M.C. Flickinger, D. Perlman, Appl. Environ. Microbiol. 33 (3) (1977) 706.
[19] M.J. Antal Jr., W.S.L. Mok, G.N. Richards, Carbohydr. Res. 199 (1990) 111.
[20] H. Kishida, F. Jin, X. Yan, T. Moriya, H. Enomoto, Carbohydr. Res. 341 (2006) 2619.
[21] M. Bicker, S. Endres, L. Ott, H. Vogel, J. Mol. Catal. A: Chem. 239 (2005) 151.
[22] Y. Hayashi, Y. Sasaki, Chem. Commun. (2005) 2716.
[23] K.P.F. Janssen, J.S. Paul, B.F. Sels, P.A. Jacobs, Stud. Surf. Sci. Catal. 170B (2007) 1222.
[24] E. Taarning, S. Saravanamurugan, M. Spangsberg Holm, J. Xiong, R.W. West, C.H. Christensen, Chem. Sus. Chem. 2 (7) (2009) 625.
[25] S. Sombatchaisak, P. Praserthdam, C. Chaisuk, J. Panpranot, Ind. Eng. Chem. Res. 43 (2004) 4066.
[26] G. Bonn, M. Rinderer, O. Bobleter, J. Carbohydr. Chem. 4 (1) (1985) 67.
[27] B.M. Kabyemela, T. Adschiri, R. Malaluan, K. Arai, Ind. Eng. Chem. Res. 36 (1997) 2025.
[28] G. Lookhart, M.S. Feather, Carbohydr. Res. 60 (1978) 259.
[29] A.C. McLellan, P.J. Thornalley, Anal. Chim. Acta 263 (1992) 137.
[30] C. Rae, S.J. Berners-Price, B.T. Bulliman, P.W. Kuchel, Eur. J. Biochem. 193 (1990) 83.
[31] F. Wakabayashi, J.N. Kondo, K. Domen, C. Hirose, Microporous Mater. 8 (1997) 29.
[32] O. Cairon, T. Chevreau, J.-C. Lavalley, J. Chem., Soc., Faraday Trans. 94 (1998) 3039.
[33] S. Kotrel, J.H. Lunsford, H. Knözinger, J. Phys. Chem. B 105 (2001) 3917.
[34] T. Barzetti, E. Selli, D. Moscotti, L. Forni, J. Chem. Soc. Faraday Trans. 92 (8) (1996) 1401.
[35] C.A. Emeis, J. Catal. 141 (1993) 347.

DOI: 10.1002/cssc.200900099

Zeolite-Catalyzed Isomerization of Triose Sugars

Esben Taarning,[b] Shunmugavel Saravanamurugan,[b] Martin Spangsberg Holm,[b] Jianmin Xiong,[b] Ryan M. West,[c] and Claus Hviid Christensen*[a]

Lactic acid is an important chemical that is used for production of biodegradable polymers and solvents. The industrial production of lactic acid is based on the anaerobic fermentation of glucose and sucrose using microbial fermentation.[1] The major complications associated with this process are the need to neutralize lactic acid with a stoichiometric amount of base during the fermentation process and the energy-intensive work-up of lactic acid from the aqueous fermentation broth. However, a different route to lactic acid, based on the isomerization of the triose sugars dihydroxyacetone (DHA) and glyceraldehyde (GLA), could be envisioned. Such a process could be based on glycerol as a raw material, which can be converted to GLA and DHA by fermentation[2] or catalytic oxidation,[3] respectively.

Herein, we report that Lewis-acidic zeolites such as Sn-Beta show surprisingly high activities and selectivities for the isomerization of trioses to lactic acid, and for the isomerization–esterification to form lactate esters. This discovery represents one of the most selective zeolite-catalyzed transformations of a biomass substrate. Furthermore, we demonstrate the important role that Lewis and Brønsted acidity have on the product selectivity and we propose that the isomerization reaction involves a Meerwein–Ponndorf–Verley reduction and Oppenauer oxidation (MPVO)-type redox step that is catalyzed only by Lewis acids.

Isomerization of DHA and GLA into lactic acid is energetically favored by 24 and 27 kcal mol^{-1}, respectively (1 cal = 4.184 J).[4] Aqueous acid[5] and base[6] are known to catalyze this isomerization reaction at temperatures of 250–300 °C to give moderate yields of lactic acid, while aqueous zinc sulphate is known to form up to 86% lactic acid under similar conditions.[7] The isomerization reaction has also been reported to occur in alcohol solvents, in which the resulting product is the corresponding lactate ester. In methanol, $SnCl_4 \cdot 5H_2O$ was demonstrated to give up to 82% methyl lactate from DHA at 90 °C,[8] although in this case large amounts of $SnCl_4$ were needed to achieve high yields. Heterogeneous catalysts have also been employed for this reaction. Janssen et al. reported that acidic Y-zeolites catalyze the isomerization–esterification reaction of DHA in ethanol to give moderate yields of ethyl lactate along with some pyruvaldehyde diethylacetal.[9]

The reaction of DHA in alcohols is believed to proceed via dehydration to form pyruvaldehyde,[8–9] followed by conversion to either pyruvaldehyde dimethylacetal (PADA) or methyl lactate (Scheme 1). The formation of methyl lactate (pathway A)

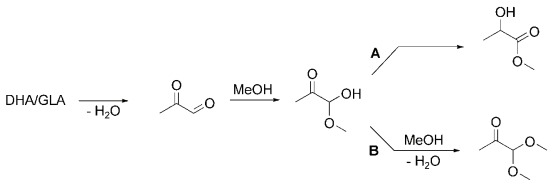

Scheme 1. Conversion of DHA in methanol to form methyl lactate or pyruvaldehyde dimethylacetal (PADA).

necessitates a redox step in the reaction pathway. We therefore hypothesized that a high selectivity towards methyl lactate is favored by zeolites that feature redox activity. This particular redox reaction bears a distinct resemblance to the MPVO-redox reaction, in which a ketone or an aldehyde is reduced by an alcohol in the presence of a Lewis-acidic catalyst.[10] We therefore decided to investigate the activity of zeolites that are known to be highly active MPVO-redox catalysts in the conversion of DHA to methyl lactate and lactic acid. Such catalysts include, amongst others, extra-framework-aluminum (EFAL)-containing zeolites,[11] but more interestingly non-Brønsted-acidic zeolites containing framework titanium,[12] zirconium,[13] and tin[14] have also been reported to be highly active MPVO-redox catalysts.

We synthesized a series of Beta zeolites containing Al, Zr, Ti, and Sn to evaluate their relative activities and selectivities for the reaction of DHA in methanol as well as pure siliceous Beta for comparison (Table 1). In addition, we prepared the corresponding oxides by incipient wetness impregnation to evaluate the importance of framework incorporation of the metals.

Interestingly, tin incorporated into zeolite Beta was found to be highly selective for the formation of methyl lactate from DHA and GLA in methanol. Full conversion of DHA was achieved in water at 125 °C for all zeolites, however, only in the case of Sn-Beta was DHA fully converted in methanol at 80 °C. Sn-Beta could be reused for three consecutive runs without any noticeable loss in activity by simply adding fresh DHA after the 24 h reaction when the reaction was carried out in methanol. However, in water this was not possible because

[a] *Prof. C. H. Christensen*
Haldor Topsøe A/S
Nymøllevej 55, 2800 (Denmark)
Fax: (+45) 4527 2999
E-mail: chc@topsoe.dk

[b] *Dr. E. Taarning, Dr. S. Saravanamurugan, M. S. Holm, Dr. J. Xiong*
Center for Sustainable and Green Chemistry
Department of Chemistry, Technical University of Denmark
2800 (Denmark)

[c] *R. M. West*
Department of Chemistry and Biological Engineering
University of Wisconsin–Madison
Madison, WI 53706 (USA)

Supporting information for this article is available on the WWW under http://dx.doi.org/10.1002/cssc.200900099.

Table 1. Conversion of DHA to methyl lactate in methanol and to lactic acid in water using various catalysts.[a]

Catalyst	Si/Me ratio[b]	Surface area [$m^2\,g^{-1}$]	Micropore volume [$mL\,g^{-1}$]	Methyl lactate [%]	Lactic acid [%]
Al-Beta	65	449	0.19	0	22
Zr-Beta	125	506	0.20	1	44
Ti-Beta	125	492	0.20	2	25
Sn-Beta	125	478	0.19	>99	90
Sn-Beta[c]	125	478	0.19	>99	90
Si-Beta	–	462	0.19	0	3
Al_2O_3/Beta	125	460	0.19	0	8
ZrO_2/Beta	125	453	0.19	0	13
TiO_2/Beta	125	464	0.19	0	11
SnO_2/Beta	125	458	0.19	<1	8
SnO_2[d]	–	19	–	<1	6
Acidic resin[e]	–	–	–	<1	11
No catalyst	–	–	–	0	3

[a] 1.25 mmol DHA in 4 g of methanol (80 °C) or water (125 °C), 80 mg of catalyst was added and the mixture was stirred for 24 h. [b] As-synthesized. [c] GLA used as substrate. [d] As nanopowder. [e] DOWEX 50WX8-100.

large amounts of carbonaceous deposits were formed, resulting in a decrease of the formation of lactic acid, from 90% in the first run to 21% in the second run. This could be a result of the unavoidable presence of a Brønsted acid in the aqueous reaction mixture, as the concentration of lactic acid increased. Indeed, when using a purely Brønsted-acidic catalyst, such as an acidic ion-exchange resin in water, only 11% of lactic acid was formed along with large amounts of carbonaceous deposits.

It is interesting to note that when tin is incorporated into the zeolite framework it becomes more active for the formation of methyl lactate than homogeneous tin in the form of $SnCl_4{\cdot}5H_2O$. Thus, the initial rate of methyl lactate formation when using low loadings of Sn-Beta was found to be approximately 45 $mol\,mol_{Sn}^{-1}\,h^{-1}$ with low yields of methyl lactate (<7% yield from DHA), whereas it was only 4.2 $mol\,mol_{Sn}^{-1}\,h^{-1}$ when using a similar molar amount of $SnCl_4{\cdot}5H_2O$. In addition, SnO_2/Si-Beta as well as large amounts of nanopowdered SnO_2 afforded only trace amounts of methyl lactate, illustrating that tin oxide is not catalytically active.

One of the advantages of single-site heterogeneous catalysis[15] is the possibility to probe and study the active site. The single-site enhancement achieved when incorporating tin into the zeolite framework has been studied by Corma and coworkers.[16] Based on NMR evidence it was found to be possible to fully incorporate tin into the zeolite framework.[17] The catalytically active site is believed to be a partially hydrolyzed framework tin species. The Lewis acid strength of the metal site in the zeolite framework can be evaluated by its ability to shift the carbonyl IR stretching frequency of cyclohexanone. The Sn-Beta catalyst used in this study was synthesized according to a procedure by which tin is known to be fully incorporated into the zeolite framework. We found that the C=O stretch of cyclohexanone shifted by 49 cm^{-1} for the Sn-Beta catalyst, 28 cm^{-1} for Zr-Beta, and 22 cm^{-1} for Ti-Beta. These results clearly indicate that Sn-Beta is a stronger Lewis acid than Ti-Beta and Zr-Beta, which could explain its increased activity relative to the other metals.

In methanol, the acidic ion-exchange resin was found to be highly selective towards PADA. In order to study the selectivity difference for the formation of methyl lactate and PADA, a reaction series was performed at a higher temperature (115 °C), where all the catalysts are appreciably active (Figure 1). Here,

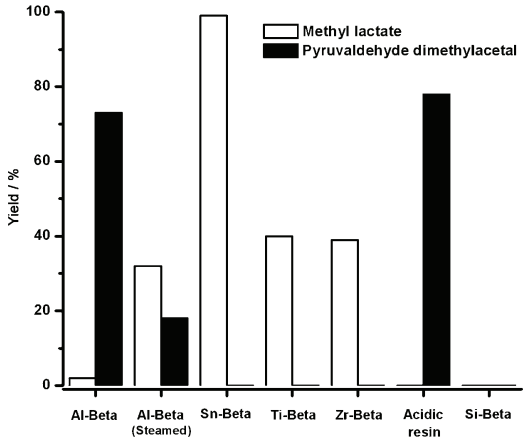

Figure 1. Yield of methyl lactate and PADA for various catalysts. Conditions: DHA (1.25 mmol), methanol (4 g), and catalyst (80 mg) were stirred at 115 °C for 24 h.

the acidic ion-exchange resin is highly selective towards the formation of PADA (pathway B, Scheme 1) whereas Sn-Beta, Zr-Beta, and Ti-Beta are only selective for the formation of methyl lactate (pathway A, Scheme 1). Al-Beta is highly selective towards PADA, suggesting that it mainly contains Brønsted-acidic framework aluminum. In order to substantiate this argument, we decided to steam-dealuminate the Al-Beta zeolite from Table 1 for comparison. Hence, the Al-Beta was steam-calcined at 750 °C for 20 h. The selectivity towards methyl lactate was found to increase significantly, as would be expected from the formation of more EFAL sites.

It is thus clear that for the reaction of triose sugars in methanol, Lewis-acidic catalysts are selective towards the formation of methyl lactate whereas Brønsted-acidic catalysts are selective towards PADA. The zeolite activity correlates with its relative Lewis-acid strength as determined by IR measurements of adsorbed cyclohexanone. The reaction pathway could be thought to involve a MPVO-type redox reaction of the pyruvaldehyde hemiacetal (MeOH) or hydrate (H_2O) in which a 1,2-hydride shift takes place in a concerted fashion, leading to methyl lactate or lactic acid, respectively (Scheme 2).

The strongly Lewis-acidic Sn-Beta catalyst used here is, to the best of our knowledge, the most active catalyst for the conversion of triose sugars to methyl lactate and lactic acid reported until now. It is more active than even homogeneous tin

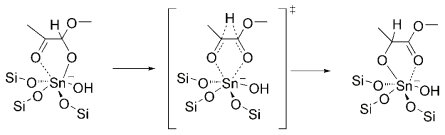

Scheme 2. Tentative MPVO-type redox reaction leading to methyl lactate.

chloride, and because of its ease of reuse it is more attractive from an environmental point of view. The surprising activity, selectivity, and reusability illustrate the important potential that zeolites have in the conversion of biomass to value-added chemicals.

Experimental Section

Sn-Beta, Zr-Beta, Ti-Beta, Al-Beta, and Si-Beta were all synthesized in fluoride media according to known procedures.[17] The metal oxides on Si-Beta were prepared by incipient wetness impregnation using the corresponding metal precursors and then calcined at 450 °C for 4 h.

In a 15 mL ace-vial, 1.25 mmol of triose, 4.0 g of solvent (MeOH or H_2O), and 80 mg of catalyst were added. In the case of MeOH, naphthalene was added as an internal standard. The vials were then heated and stirred for 24 h. Samples were analyzed by GC (MeOH) and HPLC (H_2O).

Experimental details, a time-course study, and details on the catalyst characterization are provided as Supporting Information.

Acknowledgements

The Center for Sustainable and Green Chemistry is sponsored by the Danish National Research Foundation. R.M.W acknowledges funding by PIRE, NSF OISE 0730277.

Keywords: biomass · heterogeneous catalysis · Lewis acids · tin · zeolites

[1] a) Y.-J. Wee, J.-N. Kim, H.-W. Ryu, *Food Technol. Biotechnol.* **2006**, *44*, 163; b) R. Datta, M. Henry, *J. Chem. Technol. Biotechnol.* **2006**, *81*, 1119.
[2] a) D. Hekmat, R. Bauer, V. Neff, *Process Biochem.* **2007**, *42*, 71; b) S. Yamada, K. Nabe, N. Izuo, M. Wada, I. Chibata, *J. Ferment. Technol.* **1979**, *57*, 215.
[3] a) H. Kimura, K. Tsuto, *Appl. Catal. A* **1993**, *96*, 217; b) H. Kimura, *Appl. Catal. A* **1993**, *105*, 147.
[4] R. M. West, E. L. Kunkes, D. A. Simonetti, J. A. Dumesic, *Catal. Today* **2009**, 10.1016/j.cattod.2009.02.004.
[5] M. J. Antal, Jr., W. S. L. Mok, G. N. Richards, *Carb. Res.* **1990**, *199*, 111.
[6] H. Kishida, F. Jin, X. Yan, T. Moriva, H. Enomoto, *Carb. Res.* **2006**, *341*, 2619.
[7] M. Bicker, S. Endres, L. Ott, H. Vogel, *J. Mol. Catal. A* **2005**, *239*, 151.
[8] Y. Hayashi, Y. Sasaki, *Chem. Commun.* **2005**, 2716.
[9] K. P. F. Janssen, J. S. Paul, B. F. Sels, P. A. Jacobs, *Stud. Surf. Sci. Catal.* **2007**, *170*, 1222.
[10] C. F. de Graauw, J. A. Peters, H. van Bekkum, J. Huskens, *Synthesis* **1994**, *10*, 1007.
[11] P. J. Kunkeler, B. J. Zuurdeeg, J. C. van der Waal, J. A. van Bokhoven, D. C. Koningsberger, H. van Bekkum, *J. Catal.* **1998**, *180*, 234.
[12] J. C. van der Waal, E. J. Creyghton, P. J. Kunkeler, K. Tan, H. van Bekkum, *Top. Catal.* **1997**, *4*, 261.
[13] Y. Zhu, G.-K. Chuah, S. Jaenicke, *J. Catal.* **2006**, *241*, 25.
[14] A. Corma, M. E. Domine, L. Nemeth, S. Valencia, *J. Am. Chem. Soc.* **2002**, *124*, 3194.
[15] J. M. Thomas, R. Raja, D. W. Lewis, *Angew. Chem.* **2005**, *117*, 6614; *Angew. Chem. Int. Ed.* **2005**, *44*, 6456.
[16] a) M. Boronat, A. Corma, M. Renz, P. M. Viruela, *Chem. Eur. J.* **2006**, *12*, 7067; b) M. Boronat, A. Corma, M. Renz, *J. Phys. Chem. B* **2006**, *110*, 21168.
[17] a) Y. Zhu, G. Chuah, S. Jaenicke, *J. Catal.* **2004**, *227*, 1; b) M. Renz, T. Blasco, A. Corma, V. Fornés, R. Jensen, L. Nemeth, *Chem. Eur. J.* **2002**, *8*, 4708; c) T. Blasco, M. A. Camblor, A. Corma, P. Esteve, A. Martínez, C. Prieto, S. Valencia, *Chem. Commun.* **1996**, 2367.

Received: December 30, 2008
Published online on June 27, 2009

Supporting information

Zeolite-catalyzed Isomerisation of Triose Sugars

*Esben Taarning, Shunmugavel Saravanamurugan, Martin Spangsberg Holm, Jianmin Xiong, Ryan M. West, Claus Hviid Christensen**

Reactions with the trioses

Experimental procedure for the triose isomerisation

The triose sugar (DHA or GLA, 112.5 mg, 1.25 mmol) was added to a 15 ml Ace-vial together with 4 g of solvent (H_2O or MeOH) and naphthalene (*ca.* 60 mg, internal standard only for MeOH as solvent). Finally, 80 mg of catalyst was added and the flask was sealed with the Teflon lid and immersed into a preheated oilbath (80 or 120 ºC for MeOH and 140 ºC for H_2O). The internal reaction temperature was measured in a separate control experiment by drilling a hole in the Teflon cap and tightly inserting a thermocouple. This showed that the internal temperature for the experiments with methanol at 120 ºC was 115 ºC and while with water at 140 ºC it was 125 ºC. After the desired reaction time, the flask was cooled to room temperature and a sample was acquired using a syringe with a filter. The sample was then analyzed by GC (MeOH, using internal standard) and HPLC or HPLC only (for H_2O as solvent, using a calibration curve). A time-course study is shown in figure s1. Figure s1.2 compares the yields of methyl lactate as a function of time obtained when using an equivalent amount of tin in either Sn-Beta or $SnCl_4 \cdot 5H_2O$. Catalyst and substrate loadings in Figure s1.2 are chosen as to generate data in the low conversion/low yield regime.

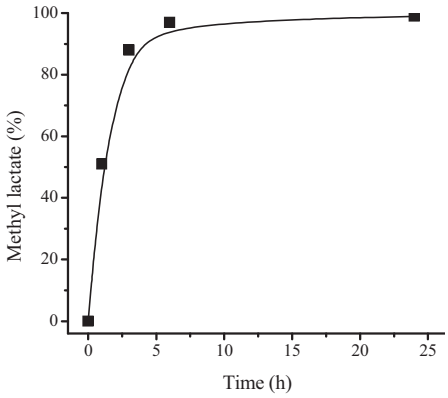

Figure s1. Time-course study on the formation of methyl lactate from DHA at 80 ºC. DHA (1.25 mmol), Sn-Beta (80 mg), methanol (4.0 g) and naphthalene (60mg) were charged in a 15 mL Ace-vial. Small aliquots of the reaction mixture were withdrawn at various time intervals and analyzed by GC. The yield of methyl lactate was 97% at 6 hours reaction time and more than 99% of methyl lactate was observed after 24 hours.

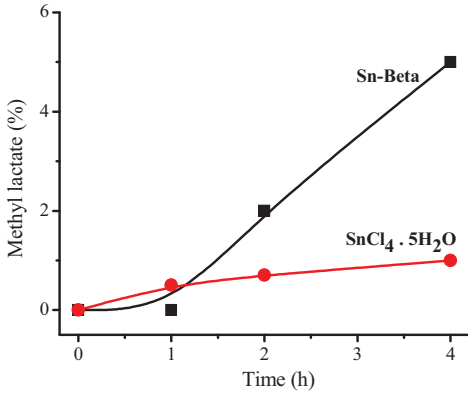

Figure s1.2. Effect of catalysts on the formation of methyl lactate at low conversion. The influence of reaction time was investigated over Sn-beta (0.0080 g) and $SnCl_4.5H_2O$ (3,7 mg) at 80 ºC on the yield of methyl lactate. Dihydroxyacetone (2.5 mmol), methanol (4.0 g) and naphthalene (60mg) were charged in a 15 mL Ace-vial.

Instrumental information
GC-analysis was performed on an Agilent 6890N instrument with an FID-detector. The column equipped was an HP-5 capillary column (30.0 m x 320 µm x 0.25 µm). A helium flow-rate of 6.0 ml/min pressurized at 1.498 bar was used. The oven temperature program is as follows: the initial temperature is 50 ºC (hold 2 min) and then heated to 280 ºC (ramp 20 ºC per min). The retention time of methyl lactate when using these settings is 1.51 min. A GC-MS instrument (Agilent 6850 GC system coupled with an Agilent 5975C mass detector) was also used in some cases for qualitative purposes. HPLC analysis was performed using an Agilent 1200 series instrument equipped with an Aminex® HPX-87H column (30 cm length). The eluent used was in all cases a 0.005 M aqueous sulfuric acid solution.

Chemicals used
All chemicals were used as purchased without further purification.
Dihydroxyacetone dimer (97%, Aldrich), DL-glyceraldehyde (minimum 95%, Aldrich), Naphthalene (99+%, Aldrich), DOWEX® 50WX8-100 ion exchange resin (Aldrich) and methanol (Biotech grade, 99.93%, Aldrich) were all used as received from the chemical companies. Commercial samples of methyl DL-lactate (≥97%, Aldrich), L-(+)-lactic acid (99%, Fluka) and Pyruvaldehyde dimethylacetal (≥97%, Fluka) were used as reference compounds for GC and HPLC analysis.
Tetraethylammonium hydroxide 40 wt.% in water (analytical grade, Fluka) , TEOS ≥99% (Fluka), HF 40 wt.% in water (analytical grade, Fluka), Zirconium(IV) oxychloride octahydrate ≥99% (analytical grade, Fluka), Tin(IV) chloride pentahydrate 98 % (Aldrich), Aluminum nitrate nonahydrate ≥98% (Sigma-Aldrich), Aluminum chloride hexahydrate ≥99% (Fluka), Titanium(IV) ethoxide (analytical grade, Fluka), Hydrogen peroxide 30 wt.% in water (Merck), Nitric acid 69 wt.% (analytical grade, Merck), Ammonium Nitrate ≥98% (Riedel-de-Haën), Cyclohexanone ≥99,9% (Fluka), Demineralized water, Tin(IV) oxide nanopowder (Sigma-Aldrich)

Catalyst synthesis

Synthesis of zeolite Beta seeds
Whenever seeding was applied in the syntheses, beta seeds synthesized and dealuminated in close accordance to US patent 5968473A[s1] were used. 1.85 g. $AlCl_3$*$6H_2O$ was dissolved in 4.33 g. water. To this solution 45.24 g. TEAOH (35 wt.%) was added followed by 40 g. of TEOS. The gel was aged under stirring for 8 hours before being transferred to a Teflon cup with lid and fitted into a stainless steel autoclave for crystallization. Crystallization took place for 3 days at 140 °C while rotated at 20 rpm. The product was isolated and then washed using centrifugation and subsequently dried at 110 °C overnight. The dealumination step was done by suspending the "as synthesized" zeolite in 65 wt.% HNO_3 and heating to 80 °C for 24 hours while stirring. A ratio of approximately 1 g. of zeolite per 50 g. HNO_3 was used. The dealuminated zeolite was isolated by suction filtration and washed thoroughly with demineralized water.

Synthesis of Ti-Beta
Synthesis of unseeded Ti-Beta was done according to a previous published procedure[s2] introducing minor modifications described here. A molar oxide ratio in the gel before aging of 0.008 TiO_2: 1 SiO_2: 27.5 $(TEA)_2O$: 0.55 HF: 0.33 H_2O_2: 9 H_2O was aimed for. 30.0 g. of TEOS and 29,0 g. of TEAOH (40%) was mixed and stirred for a few minutes. 5.3 g. of H_2O_2 (30%) was added and after an additional 5 minutes 0.26 g. TEOT was added slowly. The gel was allowed to age for

s2

approximately 7 hours allowing for the evaporation of ethanol produced by hydrolysis of TEOS. This produced a homogeneous and slightly yellow paste. 3.9 g. HF (40%) was then added drop wise under rapid stirring. The rigid gel obtained was manually homogenized before it was transferred to a Teflon cup with lid which was inserted into a stainless steel autoclave for crystallization. The autoclave was rotated at a speed of 20 rpm. while kept at a temperature of 140 °C for 10 days.

Synthesis of Zr-Beta, Al-Beta and Si-Beta

Synthesis of Zr-Beta was done according to a previous published procedure[s3] introducing minor modifications described here. A molar oxide ratio in the gel before aging of 0.008 ZrO_2: 1 SiO_2: 0.28 $(TEA)_2O$: 0.56 HF: 10 H_2O was aimed for. 30 g. TEOS and 29.7 g. TEAOH (40%) were mixed and stirred for 90 min. A solution of 0.37 g. $ZrOCl_2*8H_2O$ in 3 g. water was added slowly and the gel was subsequently allowed to age for 7 hours while stirred. At this point 4.04 g. HF (40%) was added under stirring which produced a white rigid gel. An aqueous suspension of 0.36 g. dealuminated beta seeds in 2.5 g. demineralized water was sonicated for 5 minutes and then added to the gel while mixing. The gel was manually homogenized before it was transferred to a Teflon cup with lid which was inserted into a stainless steel autoclave for crystallization. The autoclave was rotated at a speed of 20 rpm. while kept at a temperature of 140 °C for 20 days.
The pure siliceous and the aluminum containing zeolite Beta from Table 1 were synthesized using an identical procedure as the one described for the Zr-Beta. Though with the exception of either excluding the addition of the metal salt or replacing the zirconium salt with 0.83 g. of $Al(NO_3)_3*5H_2O$, respectively. The crystallization times in both these syntheses were 10 days.

Synthesis of Sn-Beta

Synthesis of Sn-Beta was done according to a previous published procedure[s1,s4] introducing minor modifications described here. A molar oxide ratio in the gel before aging of 0.008 SnO_2: 1 SiO_2: 0.27 $(TEA)_2O$: 0.54 HF: 11 H_2O was aimed for. 30 g TEOS was mixed with 33 g. TEAOH (35%) while stirring. After 90 minutes a solution of 0.42 g. $SnCl_4*5H_2O$ in 2.75 g. water was added. The gel was allowed to age for 10 hours under stirring to allow for ethanol formed by hydrolysis of TEOS to evaporate. 3.86 g. HF (40%) was added drop-wise under stirring which produced a rigid gel. 0.36 g. of dealuminated beta seeds suspended in 1.75 g. of water was sonicated for 5 minutes and then added to the gel while mixing. The gel was manually homogenized before it was transferred to a Teflon cup with lid which was inserted into a stainless steel autoclave for crystallization. The autoclave was rotated at a speed of 20 rpm. while kept at a temperature of 140 °C for 22 days.

Product recovery and ion-exchange procedure

After crystallization the autoclaves were allowed to cool to room temperature. The products were isolated by suction filtration. The zeolites were washed by two fold resuspension in demineralized water and subsequently dried at 110 °C overnight. The dried zeolites were calcined in static air at 550 °C for 6 hours using a ramp of 2 °C/min to remove the structure directing agent.
The zeolite Beta containing aluminum was ion-exchanged into the ammonia form by suspending it in a 1 M. NH_4NO_3 solution at 50 °C for 2 hours. The zeolite was isolated and resuspended two additional times to ensure complete exchange. The proton form of the zeolite was obtained by drying at 110 °C and calcination in static air at 550 °C for 6 hours using a ramp of 2 °C/min.

Incipient wetness impregnation method

The Si-Beta impregnated metal oxides were synthesized by following the procedure: 0.5 ml of an aqueous solution of the appropriate amount of metal precursor (tin(IV) chloride penthydrate, aluminum nitrate nonahydrate, zirconium(IV) oxychloride octahydrate and titanium (IV) ethoxide) was added drop-wise on to appropriate amount of Si-Beta zeolite. The mixture was physically

mixed using a spatula. The solid material was dried at 80 ºC for 2 h and the dried solid material was then calcined at 450 ºC for 4h. In the case of titanium, the titanium source was dissolved in ethanol instead of water. The silicon to metal ratio was 125:1 in all cases.

Catalyst characterization

Table s1 presents an overview of the samples used in this study.

Table s1.

Sample	*Seeded*	*Synthesis time /days*	*Si/Metal**	*Crystal size (SEM)***	S_{BET} (m^2/g)	$V_{micropore}$ (ml/g)	*Cyclohexanone shift (FT-IR)*
Si-Beta	+	10	-	0.5-2 µm	462	0.19	-
Sn-Beta	+	22	125	0.5-2 µm	478	0.19	49 cm^{-1}
Zr-Beta	+	20	125	0.5-2 µm	506	0.20	28 cm^{-1}
Ti-Beta	÷	10	125	2-8 µm	492	0.20	22 cm^{-1}
Al-Beta	+	10	65	0.5-2 µm	449	0.19	n.a
Al-Beta (steamed at 750 °C)			65		450	0.19	n.a
Si-Beta SnO_2-Imp			125		458	0.19	n.a
Si-Beta ZrO_2-Imp			125		453	0.19	n.a
Si-Beta TiO_2-Imp			125		464	0.19	n.a
Si-Beta Al_2O_3-Imp			125		460	0.19	n.a
SnO_2 nanopowder			-	<100 nm***	19	-	n.a

*Si/Metal ratio in the synthesis gel or from impregnation, **Estimated from SEM imaging, ***From BET by supplier

XRD

XRD analyses were performed on a Bruker AXS powder diffractometer. Figure s2 shows the XRD diffractograms of the key materials from Table s1 after calcination. XRD analyses reveals that all samples are phase pure zeolite Beta with a good crystallinity. This is supported by the consistent micropore volumes of 0.19-0.20 ml/g (calculated from the t-plot method) given in Table s1.

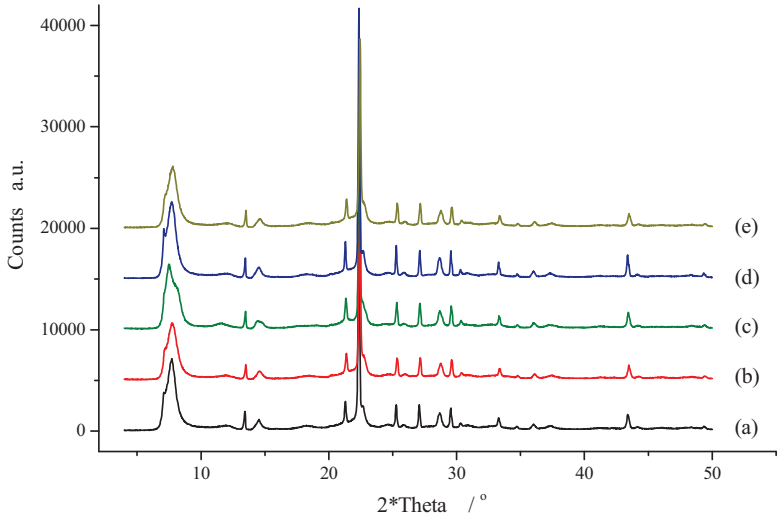

Figure s2. XRPD diffractograms of the key samples from Table s1, Si-Beta (a), Sn-Beta (b), Zr-Beta (c), Ti-Beta (d) and Al-Beta (e). Diffractograms are moved 5000 counts in-between for illustrative reasons.

It is noteworthy, as has previously been observed[s3], that the incorporated of zirconium (c) shifts the relative abundance of the possible polymorphs of zeolite beta. With regard to crystal integrity as a function of the dealumination procedure, Figure s3 shows the XRD diffractograms of the original Al-Beta sample (a) along with the steam dealuminated sample (b). It is apparent from the diffractograms that the dealuminated zeolite has preserved its overall crystallinity which further is supported by the unchanged micropore volume of 0.19 ml/g given in Table s1. Presumably this can be attributed to the relative low aluminum content of the structure.

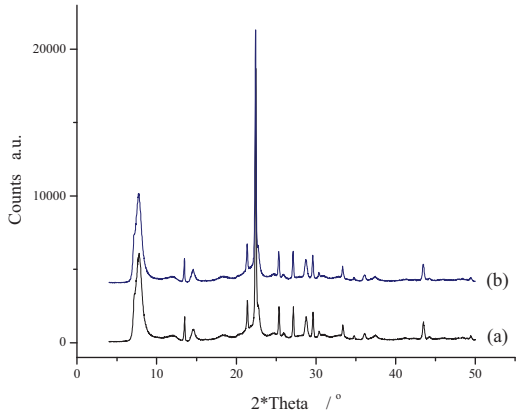

Figure s3. XRD diffractograms of Al-Beta and (a) and steam dealuminated Al-Beta (b). (b) is moved 4000 counts for illustrative reasons.

N_2-sorption experiments

N_2-sorption experiments were performed on a Micromeritics ASAP 2020 apparatus. Prior to sorption analyses samples were outgassed in vacuum at 300 °C for 2 hours. Surface area and micropore volume were calculated by applying the BET and t-plot methods, respectively.

Ammonia-TPD of steam dealuminated Al-Beta

Steam dealumination of zeolite Beta was done at 750 °C in argon. A flow of 35 ml/min was saturated with water at 298 K and lead over the finely dispersed zeolite for 20 hours. The oven temperature of 750 °C was reached from RT within one hour of heating (~12 °C /min).

NH_3-TPD analyses were performed on a Micromeretics Autochem II instrument. Pretreatment was done by first saturating the zeolites with ammonia followed by desorption of weakly bound NH_3 at either 100 °C or 150 °C for 2 hours. Subsequently the actual temperature programmed desorption was performed. Dry weights of the zeolites were measured by outgassing the zeolites in vacuum for 1 hour at 300 °C.

We chose to monitor the acidity of the parent and dealuminated Al-Beta by NH_3-TPD. Figure s4 (a) and (b) shows the NH_3 desorption curves obtained after desorbing weakly adsorbed ammonia at 100 °C and 150 °C, for 2 hours respectively. Clearly the acidity of the samples is affected by the steam treatment. We observe a significant reduction in the band attributed to strong acidity centered at 335 °C as a function of the dealumination. The location of this band correlates well with what we expect arising from strong Brønsted acidity of zeolite Beta. We attribute the reduction of this band to dealumination of the structure. Furthermore, the dealumination could add to desorption in the low or medium temperature regime from NH_3 adsorbed on EFAL species as we observe in (a).

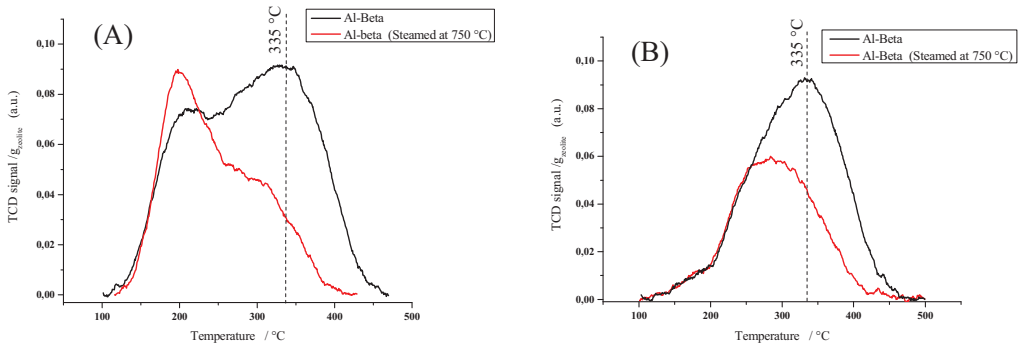

Figure s4. NH_3-TPD of Al-Beta and steam dealuminated Al-Beta. Desorption curves in (A) are obtained after desorbing weakly adsorbed NH_3 at 100 °C for 2 hours prior to measurement and (B) is obtained after a corresponding desorption at 150 °C.

FT-IR using cyclohexanone as a probe

For infrared analysis a BioRad FTS 80 spectrometer equipped with a MCT detector operated in transmission mode was used. The zeolites investigated were pressed into self supporting wafers and mounted in at home-built Pyrex cell equipped with NaCl windows and connected to a vacuum line. Prior to analysis samples were dehydrated at 400 °C for 2 hours, reaching a background pressure of $<5*10^{-5}$ torr. The spectra were recorded after allowing the samples to cool to room temperature. Cyclohexanone was used as a molecular probe in this study. Liquid cyclohexanone was cooled in an ice bath and connected to the IR-cell through a double lock system. Cyclohexanone was dosed by exposing the sample to small aliquots of cyclohexanone vapor. A series of absorbance spectra were recorded in-between the stepwise dosing.

Cyclohexanone was used as a molecular probe to determine the relative Lewis acidic strength of metals isomorphously substituted into the structure of zeolite Beta. It has previously been reported that cyclohexanone coordinated to a strong Lewis acidic site in a zeolite leads to a shift in the stretch frequency of the carbonyl functionality compared to the non-coordinated carbonyl. Further the Lewis acidic strength of the material is thought to correlate with the magnitude of the observed shift[s5,s6,s7]. The zeolites investigated here with infrared spectroscopy possess strong Lewis acidity originating from the non-silicon elements (Ti, Zr and Sn) present in the framework. Importantly this is in contrast to the same elements impregnated onto siliceous zeolite beta which does not possess this strong acidity.[s6] Figure s5 presents the IR region including the zeolite framework overtone as well as the characteristic carbonyl stretch frequencies interesting when probing with cyclohexanone. The pure siliceous zeolite Beta along with the zeolites containing Ti, Zr or Sn from Table s1 were investigated. The absorption spectrum of the dehydrated zeolites corresponds to the lower bold curve in Figure s5 a-d.

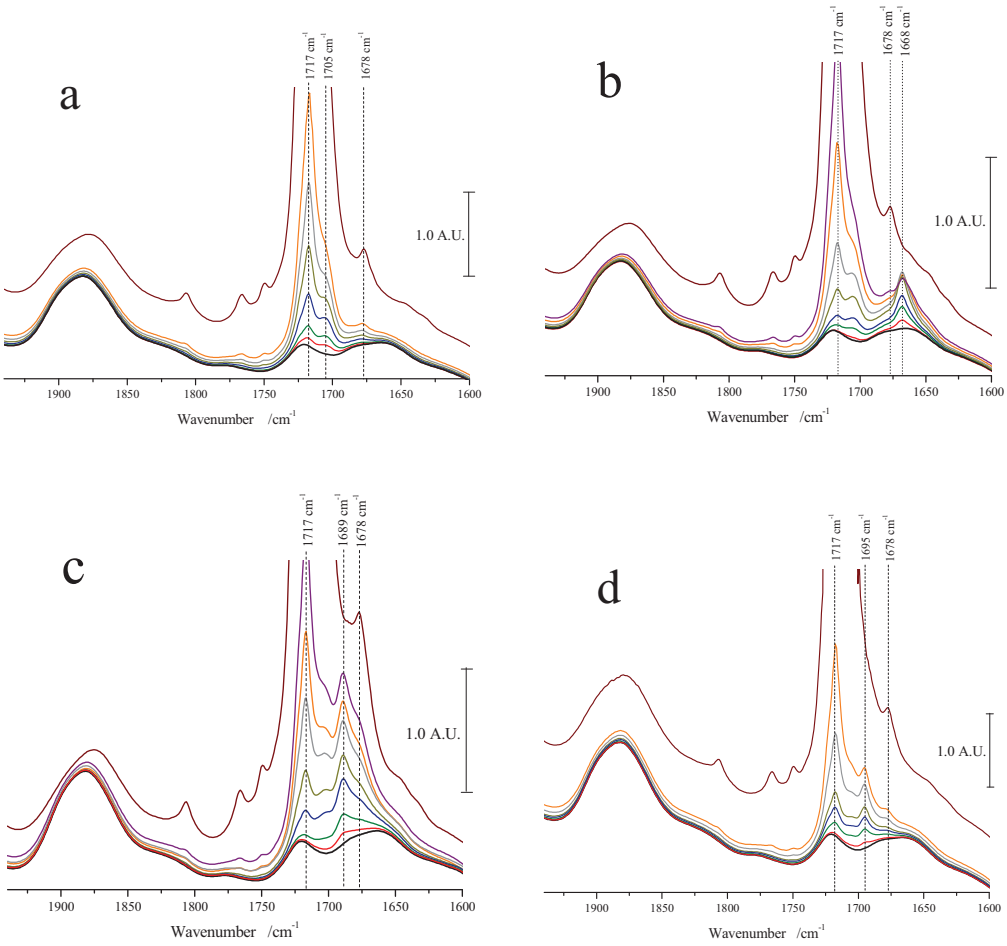

Figure s5. FT-IR spectra recorded in-between aliquot of cyclohexanone dosed to Si-Beta (a), Sn-Beta (b), Zr-Beta (c) and Ti-Beta (d).

From (a) it can be seen that at low cyclohexanone loadings two distinct absorptions are present for the purely siliceous zeolite beta, namely at 1717 cm^{-1} and at 1704 cm^{-1}. However at the high and very high loadings absorption at 1678 cm^{-1} appears. This later absorption is very important since it interferes with the region of the Lewis shifted carbonyl absorptions. Dosing cyclohexanone onto the clean zeolite one would expect cyclohexanone to predominantly adsorb on the strong Lewis acidic sites and the interfering 1678 cm^{-1} absorption to occur only at high cyclohexanone loadings. For this reason we have chosen to perform the IR experiments by dosing very small amounts of cyclohexanone in sequence while recording the absorption spectrum in-between.

In the case of Sn-Beta (b) it is clear from the initial aliquots that a band at 1668 cm^{-1} appears along with the 1717 cm^{-1} and 1704 cm^{-1} absorptions. Further more at higher loadings the 1717 cm^{-1} and 1704 cm^{-1} absorptions increase and finally the 1678 cm^{-1} absorption may be seen. Comparing the shifted 1668 cm^{-1} band to the carbonyl frequency of the physically adsorbed cyclohexanone a shift of 49 cm^{-1} is calculated. A very similar carbonyl shift of 48 cm^{-1} has been reported by Corma *et al.*[s6] for cyclohexanone interacting with Sn-Beta. From the adsorption series in (c) and (d) the induced shift for cyclohexanone adsorbed in Zr-Beta and Ti-beta could be determined to 28 cm^{-1} and 22 cm^{-1}, respectively. Interestingly, this provides an explanation as to

why a much higher catalytic activity for Sn-Beta is observed compared to Zr-Beta and Ti-Beta. Zr-Beta and Ti-Beta are similarly active in the DHA isomerisation reaction, corresponding to them possessing comparable Lewis acidic strengths as measured here by cyclohexanone adsorption. Cyclohexanone adsorption studies using FT-IR is a convenient way to ensure that the metal is incorporated into the zeolite structure since extra framework species do not possess the same Lewis acidic strengths as the framework incorporated samples do.

References used in the supplementary information

[s1] S. Valencia, A. Corma, US 5968473A, **1999**

[s2] T. Blasco, M. A. Camblor, A. Corma, P. Esteve, A. Martínez, C. Prieto, S. Valencia, *Chem. Commun.*, **1996**, 2367.

[s3] Y. Zhu, G. Chuah, S. Jaenicke, *J. Catal*. **2004**, *227*, 1.

[s4] M. Renz, T. Blasco, A. Corma, V. Fornés, R. Jensen, L. Nemeth, *Chem. Eur. J*., **2002**, *8*, 4708.

[s5] A. Corma, M. E. Domaine, S. Valencia, *J. Catal*., **2003**, *215*, 294.

[s6] A. Corma, M. E. Domine, L. Nemeth, S. Valencia, *J. Am. Chem. Soc*., **2002**, *124*, 3194.

[s7] Y. Zhu, G. Chuah, S. Jaenicke, *Chem. Commun*., **2003**, 2734.

2% (*8*). However, they constitute a significant fraction of the supermassive black hole mass density in the universe (*29*). Adding the extra obscured accretion reported here, which lasts as long as the optically bright phase, increases our original estimate of the integrated black hole mass density at $z = 0$ by 4%, to $4.5 \times 10^5\ M_\odot\ \mathrm{Mpc}^{-3}$ (*8*). Including this additional contribution, the integrated black hole growth in the obscured quasar phase is $1.3 \times 10^5\ M_\odot\ \mathrm{Mpc}^{-3}$, or ~ 30% of the total black hole mass density at $z = 0$, in agreement with our conclusion that the obscured quasar phase can harbor a large fraction of the black hole growth (*30*). Our results are in agreement with recent estimates (*26*) that suggest an average accretion efficiency of ≤10% even accounting for heavily obscured accretion.

References and Notes

1. By quasar, we refer here to the most luminous members of the AGN family, typically $M_B < -23$, $L_X > 10^{44}$ erg/s or $L_{bol} > 10^{45}$ erg/s.
2. M. Schmidt, *Nature* **197**, 1040 (1963).
3. G. T. Richards *et al.*, *Astrophys. J.* **180** (suppl.), 67 (2009).
4. A. J. Barger *et al.*, *Astron. J.* **126**, 632 (2003).
5. N. L. Zakamska *et al.*, *Astron. J.* **126**, 2125 (2003).
6. A. Martínez-Sansigre *et al.*, *Mon. Not. R. Astron. Soc.* **370**, 1479 (2006).
7. R. Gilli, M. Salvati, G. Hasinger, *Astron. Astrophys.* **366**, 407 (2001).
8. E. Treister, C. M. Urry, S. Virani, *Astrophys. J.* **696**, 110 (2009).
9. D. B. Sanders *et al.*, *Astrophys. J.* **325**, 74 (1988).
10. D. B. Sanders, I. F. Mirabel, *Annu. Rev. Astron. Astrophys.* **34**, 749 (1996).
11. J. E. Barnes, L. E. Hernquist, *Astrophys. J.* **370**, L65 (1991).
12. R. Genzel *et al.*, *Astrophys. J.* **498**, 579 (1998).
13. By heavily obscured, we refer here to sources with neutral hydrogen column densities $N_H > 10^{23}\ \mathrm{cm}^{-2}$, enough to hide most of the soft x-rays to optical quasar signatures.
14. P. Tozzi *et al.*, *Astron. Astrophys.* **451**, 457 (2006).
15. D. M. Alexander *et al.*, *Astrophys. J.* **687**, 835 (2008).
16. F. Fiore *et al.*, *Astrophys. J.* **693**, 447 (2009).
17. E. Treister *et al.*, *Astrophys. J.* **706**, 535 (2009).
18. D.-C. Kim, D. B. Sanders, *Astrophys. J.* **119** (suppl.), 41 (1998).
19. P. F. Hopkins, L. Hernquist, T. J. Cox, D. Keres, *Astrophys. J.* **175** (suppl.), 356 (2008).
20. P. F. Hopkins *et al.*, http://arxiv.org/abs/0906.5357 (2009).
21. D. Marchesini *et al.*, *Astrophys. J.* **701**, 1765 (2009).
22. T. Dahlen *et al.*, *Astrophys. J.* **654**, 172 (2007).
23. G. Hasinger, T. Miyaji, M. Schmidt, *Astron. Astrophys.* **441**, 417 (2005).
24. A. J. Barger *et al.*, *Astron. J.* **129**, 578 (2005).
25. G. T. Richards *et al.*, *Astron. J.* **131**, 2766 (2006).
26. A. Martínez-Sansigre, A. M. Taylor, *Astrophys. J.* **692**, 964 (2009).
27. M. Dietrich, S. Mathur, D. Grupe, S. Komossa, *Astrophys. J.* **696**, 1998 (2009).
28. M. Vestergaard, P. S. Osmer, *Astrophys. J.* **699**, 800 (2009).
29. M. G. Haehnelt, P. Natarajan, M. J. Rees, *Mon. Not. R. Astron. Soc.* **300**, 817 (1998).
30. This integrated value was obtained assuming an accretion efficiency of 0.1 and is in very good agreement with observational results (*31*), even after incorporating this additional accretion.
31. A. Marconi *et al.*, *Mon. Not. R. Astron. Soc.* **351**, 169 (2004).

32. R. Della Ceca *et al.*, *Astron. Astrophys.* **487**, 119 (2008).
33. S. H. Teng *et al.*, *Astrophys. J.* **691**, 261 (2009).
34. Support for the work of E.T. and K.S. was provided by the National Aeronautics and Space Administration (NASA) through Chandra/Einstein Postdoctoral Fellowship award numbers PF8-90055 and PF9-00069, respectively, issued by the Chandra X-ray Observatory Center, which is operated by the Smithsonian Astrophysical Observatory for and on behalf of NASA under contract NAS8-03060. P.N. acknowledges the Radcliffe Institute for Advanced Study where this work was started. C.M.U. acknowledges support from NSF grant AST-0407295.

Supporting Online Material

www.sciencemag.org/cgi/content/full/science.1184246/DC1
SOM Text
Figs. S1 and S2
References

4 November 2009; accepted 17 March 2010
Published online 25 March 2010;
10.1126/science.1184246
Include this information when citing this paper.

Conversion of Sugars to Lactic Acid Derivatives Using Heterogeneous Zeotype Catalysts

Martin Spangsberg Holm,[1,2,3]* Shunmugavel Saravanamurugan,[1,2]* Esben Taarning[2,3]†

Presently, very few compounds of commercial interest are directly accessible from carbohydrates by using nonfermentive approaches. We describe here a catalytic process for the direct formation of methyl lactate from common sugars. Lewis acidic zeotypes, such as Sn-Beta, catalyze the conversion of mono- and disaccharides that are dissolved in methanol to methyl lactate at 160°C. With sucrose as the substrate, methyl lactate yield reaches 68%, and the heterogeneous catalyst can be easily recovered by filtration and reused multiple times after calcination without any substantial change in the product selectivity.

Carbohydrates represent the largest fraction of biomass, and various strategies for their efficient use as a commercial chemical feedstock are being established in the interest of supplementing, and ultimately replacing, petroleum (*1*–*4*). The thermal instability of carbohydrates is a major obstacle in this regard, and biochemical processes have proven to be more applicable than catalytic ones, in part because of their ability to operate at low temperatures. On the other hand, catalysis often presents improved process design options, resulting in higher productivity and reduced costs related to product work-up. Indeed, catalysis has proven to be scalable and able to supply numerous low-cost products from petroleum.

In contrast to the case for biochemical processes, relatively few products are directly obtainable from carbohydrates by using catalysis. Gluconic acid and sorbitol can be obtained from glucose by oxidation and hydrogenation, respectively, and acidic catalysts are currently being examined for the direct production of 5-hydroxymethylfurfural (HMF) (*5*–*7*). However, currently the production of fuels and value-added compounds from carbohydrates is dominated by fermentative processes (*8*). An important example is the fermentation of glucose to lactic acid, which is used for the production of biodegradable plastics (*9*, *10*) and solvents (*11*, *12*). Lactic acid has also been investigated as a precursor to the production of a wide range of useful compounds through catalytic transformation (*13*, *14*). However, the future role of lactic acid will largely depend on its production costs. Because the fermentation of glucose to lactic acid

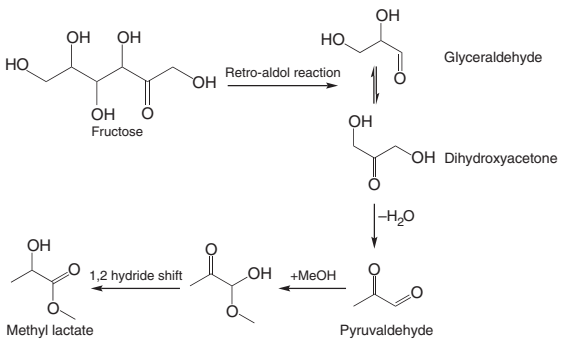

Fig. 1. Proposed reaction pathway for the conversion of fructose to methyl lactate. The reaction formally comprises a retro aldol fragmentation of fructose and isomerization-esterification of the trioses.

[1]Centre for Catalysis and Sustainable Chemistry, Department of Chemistry, Technical University of Denmark, Anker Engelundsvej 1, 2800 Kongens Lyngby, Denmark. [2]Center for Sustainable and Green Chemistry, Department of Chemistry, Technical University of Denmark, Anker Engelundsvej 1, 2800 Kongens Lyngby, Denmark. [3]Haldor Topsøe A/S, Nymøllevej 55, 2800 Kongens Lyngby, Denmark.

*These authors contributed equally to this work.
†To whom correspondence should be addressed. E-mail: esta@topsoe.dk

involves the coproduction of large amounts of salt waste, a less expensive route would be an important step toward a biomass-based chemical industry using lactic acid more widely as a feedstock. Here we show that sucrose, glucose, and fructose dissolved in methanol can be converted directly into racemic methyl lactate in yields up to 68% in a process resembling the alkaline degradation of sugars. Methyl lactate can be purified by distillation, and its one-pot formation offers an advantage over the fermentative route, wherein the esterification of lactic acid to methyl lactate is often necessary.

We recently reported that Lewis acidic zeolites and zeotypes efficiently catalyze the conversion, in methanol, of the two trioses dihydroxyacetone and glyceraldehyde to methyl lactate at moderate temperatures (*15*, *16*). Here we report that while investigating the properties of the Sn-Beta zeolite for fructose transformation, we discovered that, at elevated temperatures, fructose is transformed to methyl lactate in yields of up to 44%. We assume that this reaction proceeds via a retro aldol reaction of fructose forming two trioses (Fig. 1). These trioses are readily converted to the thermodynamically very stable methyl lactate through sequential dehydration and methanol addition, followed by a 1,2-hydride shift as reported previously (*15*–*17*). Indeed, at intermediate reaction times, small amounts of unconverted triose sugars were observed by high-performance liquid chromatography (HPLC), supporting the existence of this reaction pathway.

A retro aldol reaction is favored at high temperatures, and fructose and glucose are known to undergo fragmentation in supercritical water to form C_2 to C_4 carbohydrate products (*18*, *19*). In the presence of aqueous alkali hydroxides, the transformation of the monosaccharides to lactate salts occurs at milder conditions (100° to 260°C) (*20*–*22*). However, to obtain high lactate yields, a stoichiometric amount of base is required because of the acid-base reaction between lactic acid and hydroxide. For the Sn-Beta–catalyzed reaction in methanol, we observed methyl lactate formation from fructose at temperatures as low as 140°C. This observation suggests that the retro aldol reaction is the rate-determining step in the overall transformation of fructose, because methyl lactate is readily formed from trioses at lower temperatures (80°C) (*15*). Glucose and sucrose are less expensive and much more abundant sugars than fructose, and therefore these substrates were also investigated for the production of methyl lactate.

We have synthesized highly crystalline Beta zeolites and zeotypes with the BEA framework topology that differ in the type of metal that is incorporated into the framework according to established procedures (*23*). They can be divided into Lewis acidic (Ti-, Sn-, and Zr-Beta), Brønsted acidic (H-Al-Beta), and nonacidic (Si-Beta) classes. These materials contain well-defined metal single sites that were found to have catalytic activity in various reactions (*24*–*26*). Zeolite Beta has a three-dimensional porous system with 12-ring pores that are sufficiently large to accommodate acyclic monosaccharides (*27*). We tested these materials for the conversion of sugars at 160°C in an autoclave setup (Table 1).

In agreement with previous reports (*28*), we found that the Brønsted acidic zeolite H-Al-Beta catalyzes the dehydration of the sugars, leading to HMF derivatives and methyl levulinate from fructose and predominantly methyl-D-pyranoside from glucose and sucrose (table S1). The Lewis acidic zeolites, on the other hand, were found to induce high selectivities toward methyl lactate. Sn-Beta is the most selective, giving a methyl lactate yield of 64 to 68%, which was calculated on a carbon basis when using sucrose as the substrate. Of the three Lewis acidic zeolites, Sn-Beta has the strongest Lewis acidic sites, which could explain its higher selectivity (*15*, *29*). However, both Zr-Beta and Ti-Beta are capable of producing methyl lactate in moderate yields (31 to 44%). The nonacidic Si-Beta did not improve the yield of methyl lactate over that of the background reaction, indicating that the catalytic ability is related to the Lewis acidity of

Table 1. Conversion of sugars using different zeolite and zeotype materials. Substrate (225 mg), catalyst (160 mg), naphtalene (120 mg), and methanol (8.0 g) were stirred in an autoclave at 160°C for 20 hours. Yields are calculated on a carbon basis and given as mean values. The key experiments converting sucrose using Ti-, Zr-, and Sn-Beta were repeated five times (see table S5 for statistical information). Conversion is calculated based on the amount of unconverted hexoses. Si/M, Si/metal ratio in the synthesis gel.

Catalyst	Si/M	Substrate	Conversion	Yield of methyl lactate
H-(Al)-Beta	125	Glucose	97%	0%
H-(Al)-Beta	125	Fructose	>99%	1%
H-(Al)-Beta	125	Sucrose	99%	0%
Ti-Beta	125	Glucose	99%	31%
Ti-Beta	125	Fructose	>99%	36%
Ti-Beta	125	Sucrose	98%	44%
Zr-Beta	125	Glucose	99%	33%
Zr-Beta	125	Fructose	>99%	33%
Zr-Beta	125	Sucrose	99%	40%
Sn-Beta	125	Glucose	>99%	43%
Sn-Beta	125	Fructose	>99%	44%
Sn-Beta	125	Sucrose	>99%	64%
Si-Beta	—	Glucose	61%	5%
Si-Beta	—	Fructose	79%	9%
Si-Beta	—	Sucrose	63%	6%
No catalyst	—	Glucose	53%	5%
No catalyst	—	Fructose	67%	8%
No catalyst	—	Sucrose	54%	6%
$SnCl_4 \cdot 5H_2O$*	—	Sucrose	99%	31%
SnO_2†	—	Sucrose	81%	4%

*Equivalent molar amount of Sn as for 160-mg Sn-Beta. †160 mg of SnO_2 used.

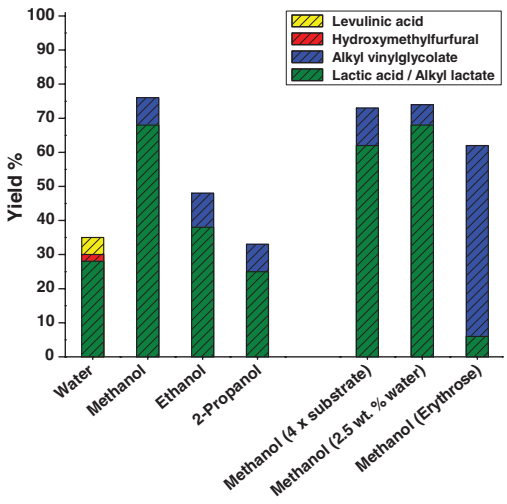

Fig. 2. Comparison of different solvents and reaction conditions for the conversion of sucrose using Sn-Beta (Si:Sn 165). Sucrose (225 mg), Sn-Beta (160 mg), and solvent (8.0 g) were stirred at 160°C for 20 hours.

the metals incorporated into the zeolite structure. Homogeneous $SnCl_4$ as well as nanocrystalline SnO_2, were also tested in the reaction. SnO_2 is inactive, whereas $SnCl_4$ shows moderate selectivity toward methyl lactate.

Glucose conversion proceeds in yields of methyl lactate comparable to those from fructose. We found that the Sn-Beta catalyst is capable of catalyzing Lobry-de Bruyn-van Ekenstein isomerization of glucose to fructose at low temperatures (100°C), which explains the similar yields obtained when using either of the hexoses. In addition, we observed that the disaccharide sucrose gives a substantially higher yield of methyl lactate as compared with fructose and glucose. This trend has also been observed for the alkaline degradation of fructose, glucose, and sucrose in water (*20*, *21*). This result is surprising, because the overall reaction pathway from sucrose to methyl lactate is thought to involve the intermediary formation of glucose and methyl fructoside by methanolysis, from which fructose is then formed via isomerization and hydrolysis, respectively (fig. S1).

Methyl lactate is not the only product formed during the reaction. The largest volatile coproduct is methyl vinylglycolate (methyl 2-hydroxy-3-butenoate), which is formed in yields ranging from 3 to 11% in all cases when using the Lewis acidic catalysts. Retro aldol reaction of glucose will produce erythrose (C_4 sugar) and glycolaldehyde (C_2). Methyl vinylglycolate formation could proceed by a reaction pathway analogous to that forming methyl lactate from trioses (fig. S1). To support this hypothesis, we heated D-erythrose to 160°C in methanol with Sn-Beta as the catalyst, and we observed methyl vinylglycolate formation in a considerably higher yield (56%) than that of methyl lactate (6%). Thus, tetroses appear to be precursors for methyl vinylglycolate (Fig. 2). Other products that were formed in small amounts from the mono- and disaccharides when using Sn-Beta are glycolaldehyde dimethylacetal (<1%), formaldehyde dimethylacetal (<1%), and methyl glycolate (<0.5%). Furthermore, we observed trace amounts of methyl 2-hydroxy butyrate and small amounts of methoxy derivatives of furfural and HMF (table S1 and fig. S2). Many of these products are similar to the saccharinic acids that are formed in the alkaline degradation of sugars, where major products are lactic acid, glycolic acid, 2,4-dihydroxybutanoic acid, as well as higher C_6 acids (*21*). In the case of Sn-Beta, we observed, using HPLC analysis, the presence of a noticeable amount of highly polar products, which could be methyl esters of the higher C_6 saccharinic acids. The combined yields of methyl lactate (68%) and methyl vinylglycolate (8%) exceed 75% for sucrose on a carbon basis when Sn-Beta (Si:Sn 165) is used as the catalyst. When the amount of sucrose and glucose is increased by a factor of four [>10 weight percent (wt %) in methanol], similar combined yields of methyl lactate and methyl vinylglycolate are obtained, and full conversion is still reached within 20 hours (Fig. 2). In this experiment, the average turnover number per Sn atom is >400 for the production of methyl lactate based on the assumed participation of all Sn atoms in the catalyst. A further increase in sucrose concentration to 20 wt % causes a drop in the yields of methyl lactate (47%) and methyl vinylglycolate (12%) in an experiment using twice the amount of Sn-Beta.

Changing the solvent from methanol to higher alcohols or water leads to the formation of the corresponding alkyl lactates and free lactic acid, respectively (Fig. 2 and see table S2 for data for glucose and fructose). Low amounts (<30%) of lactic acid are formed in water together with HMF (1 to 2%) and levulinic acid (~5%). Additionally, temperature-programmed oxidation showed that more carbon is deposited on the catalyst when water is used as the solvent (7.0 wt % of carbon per g catalyst) in place of methanol (1.3 wt %) (table S3). The change in the product composition when using water as the solvent can be explained by the auto-catalytic effect of the organic acids formed. Lactic acid and levulinic acid, being Brønsted acids, will shift the course of the reaction toward that typically seen with Brønsted acid catalysts (HMF, levulinic acid); the result is lower yields of the α-hydroxycarboxylic acid products formed in the pathway catalyzed by Lewis acids. Because small amounts of water are formed during the reaction, we examined the effect of water in methanol. Using a solvent mixture consisting of 2.5 wt % water in methanol, we obtained yields of methyl lactate similar to those obtained in pure methanol (Fig. 2). Changing the solvent to higher alcohols leads to a decrease in alkyl lactate selectivity. In ethanol, 39% of ethyl lactate is formed using sucrose as the substrate and Sn-Beta as the catalyst, whereas 25% of isopropyl lactate is formed in *i*-propyl alcohol.

Long-term stability is a very important characteristic for a heterogeneous catalyst. We therefore explored the prospects for reusing Sn-, Zr-, and Ti-Beta (Fig. 3). Each catalyst was used six times for the conversion of sucrose after calcining between each run to burn away deposited carbon. The catalysts were found to remain active with an almost unchanged selectivity even after the sixth reuse (fig. S5). After the fifth run, the zeotypes were calcined and analyzed by N_2-sorption and x-ray powder diffraction (XRPD) (fig. S6 and table S3). Analysis shows that the BEA structure is preserved and the micropore volumes for Ti-Beta and Zr-Beta remain constant; a very small volume decrease from 0.201 ml/g to 0.197 ml/g was observed for Sn-Beta. These data after >100 hours of catalyst use thus show promising stability characteristics. Further examination of the catalyst stability using a fixed bed reactor shows that Sn-Beta deactivates gradually as a function of time on stream (fig. S7). This indicates that the ability to regenerate the activity by calcination is an important feature of the catalyst. The reusability of Lewis acidic zeolites and zeotypes has also been reported in other reactions (*30*, *31*).

In contrast to the alkaline degradation, acid-catalyzed conversion of mono- and disaccharides does not consume a stoichiometric amount of base. However, the reaction pathway in the acid-catalyzed conversion is highly sensitive to the type of acid used. Whereas Brønsted acids catalyze monosaccharide dehydration reactions, leading primarily to HMF and its decomposition products, Lewis acidic zeotype catalysts lead to retro aldol reaction of the monosaccharides and subsequent transformation to α-hydroxycarboxylic acid derivatives. To achieve a high selectivity in the Lewis acid–catalyzed pathway, it is important to diminish the catalytic effect of Brønsted acids, for example, by using a solvent such as methanol in which esters, rather than free carboxylic acids, are formed.

Unlike the primary product of the Brønsted acid–catalyzed reaction, HMF, a market already exists for lactic acid and its ester derivatives. These compounds are now accessible from sucrose, glucose, and fructose, using non-noble metal–containing catalysts. However, the catalytic process results in a racemic product mixture. This plays no role for solvent or feedstock end-use, but enantiomeric purity is an important parameter in the production of biodegradable plastics.

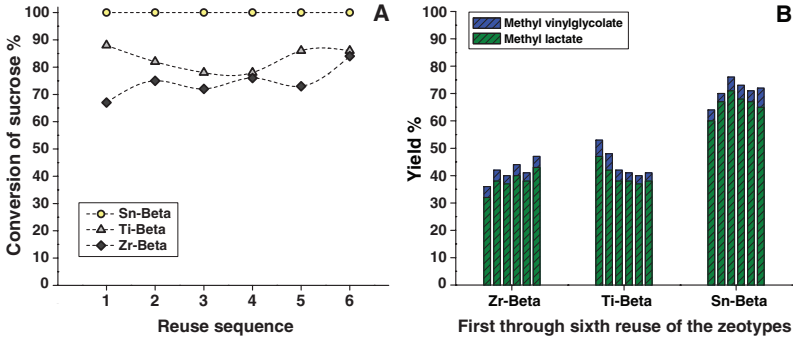

Fig. 3. Reuse of Sn-, Zr-, and Ti-Beta (Si/metal: 125) for the conversion of sucrose in methanol, with calcination of the zeotypes between each experiment. (**A**) Conversion of sucrose and (**B**) yields of methyl lactate and methyl vinylglycolate in the reuse experiments.

References and Notes

1. G. W. Huber, S. Iborra, A. Corma, *Chem. Rev.* **106**, 4044 (2006).
2. H. Danner, R. Braun, *Chem. Soc. Rev.* **28**, 395 (1999).
3. A. Corma, S. Iborra, A. Velty, *Chem. Rev.* **107**, 2411 (2007).
4. C. H. Christensen, J. Rass-Hansen, C. C. Marsden, E. Taarning, K. Egeblad, *Chem. Sus. Chem.* **1**, 283 (2008).
5. H. Zhao, J. E. Holladay, H. Brown, Z. C. Zhang, *Science* **316**, 1597 (2007).
6. Y. Román-Leshkov, J. N. Chheda, J. A. Dumesic, *Science* **312**, 1933 (2006).
7. M. Bicker, J. Hirth, H. Vogel, *Green Chem.* **5**, 280 (2003).
8. M. E. Himmel *et al.*, *Science* **315**, 804 (2007).
9. J. Lunt, *Polym. Degrad. Stabil.* **59**, 145 (1998).
10. E. T. H. Vink, K. R. Ràbago, D. A. Glassner, P. R. Gruber, *Polym. Degrad. Stabil.* **80**, 403 (2003).
11. K. L. Wasewar, A. A. Yawalkar, J. A. Moulijn, V. G. Pangarkar, *Ind. Eng. Chem. Res.* **43**, 5969 (2004).
12. R. Datta, M. Henry, *J. Chem. Technol. Biotechnol.* **81**, 1119 (2006).
13. Y. Fan, C. Zhou, X. Zhu, *Catal. Rev.* **51**, 293 (2009).
14. J. C. Serrano-Ruiz, J. A. Dumesic, *Chem. Sus. Chem* **2**, 581 (2009).
15. E. Taarning *et al.*, *Chem. Sus. Chem* **2**, 625 (2009).
16. R. M. West *et al.*, *J. Catal.* **269**, 122 (2010).
17. Y. Hayashi, Y. Sasaki, *Chem. Commun. (Camb.)* (21): 2716 (2005).
18. T. M. Aida *et al.*, *J. Supercrit. Fluid.* **42**, 110 (2007).
19. M. Sasaki, K. Goto, K. Tajima, T. Adschiri, K. Arai, *Green Chem.* **4**, 285 (2002).
20. R. Montgomery, *Ind. Eng. Chem.* **45**, 1144 (1953).
21. B. Y. Yang, R. Montgomery, *Carbohydr. Res.* **280**, 47 (1996).
22. G. Braun, U.S. patent 2,024,565 (1935).
23. Materials and methods are available as supporting material on *Science* Online.
24. J. M. Thomas, R. Raja, D. W. Lewis, *Angew. Chem. Int. Ed.* **44**, 6456 (2005).
25. M. Boronat, A. Corma, M. Renz, P. M. Viruela, *Chemistry* **12**, 7067 (2006).
26. A. Corma, *J. Catal.* **216**, 298 (2003).
27. J. Jow, G. L. Rorrer, M. C. Hawley, D. T. A. Lamport, *Biomass* **14**, 185 (1987).
28. P. Rivalier, J. Duhamet, C. Moreau, R. Durand, *Catal. Today* **24**, 165 (1995).
29. M. Renz *et al.*, *Chemistry* **8**, 4708 (2002).
30. J. C. van der Waal, E. J. Creyghton, P. J. Kunkeler, K. Tan, H. van Bekkum, *Top. Catal.* **4**, 261 (1997).
31. A. Corma, M. E. Domine, L. Nemeth, S. Valencia, *J. Am. Chem. Soc.* **124**, 3194 (2002).

32. The Catalysis for Sustainable Energy initiative is funded by the Danish Ministry of Science, Technology and Innovation. The Center for Sustainable and Green Chemistry is sponsored by the Danish National Research Foundation. Haldor Topsøe A/S holds patent application EP 090137829 related to the work described in this report. The authors thank C. Hviid Christensen (Haldor Topsøe A/S) for helpful advice.

Supporting Online Material

www.sciencemag.org/cgi/content/full/328/5978/602/DC1
Materials and Methods
Figs. S1 to S8
Tables S1 to S6
References

29 October 2009; accepted 17 March 2010
10.1126/science.1183990

Recent Hotspot Volcanism on Venus from VIRTIS Emissivity Data

Suzanne E. Smrekar,[1]* Ellen R. Stofan,[2] Nils Mueller,[3,6] Allan Treiman,[4] Linda Elkins-Tanton,[5] Joern Helbert,[6] Giuseppe Piccioni,[7] Pierre Drossart[8]

The questions of whether Venus is geologically active and how the planet has resurfaced over the past billion years have major implications for interior dynamics and climate change. Nine "hotspots"—areas analogous to Hawaii, with volcanism, broad topographic rises, and large positive gravity anomalies suggesting mantle plumes at depth—have been identified as possibly active. This study used variations in the thermal emissivity of the surface observed by the Visible and Infrared Thermal Imaging Spectrometer on the European Space Agency's Venus Express spacecraft to identify compositional differences in lava flows at three hotspots. The anomalies are interpreted as a lack of surface weathering. We estimate the flows to be younger than 2.5 million years and probably much younger, about 250,000 years or less, indicating that Venus is actively resurfacing.

Venus' resurfacing record holds important clues to its geological evolution. Venus and Earth are similar in size and in internal heat production, yet Venus is in a stagnant lid convection regime whereas Earth has vigorous plate tectonics. Venus' sparse and largely unmodified crater population has spawned a debate over whether it was resurfaced catastrophically (*1*) or gradually (*2*). These two end members have very different dynamic implications. Catastrophic resurfacing could have been caused by episodic mantle overturn (*3*) or melting in a hot mantle insulated by a stagnant lid (*4*). Gradual resurfacing is consistent with more Earth-like volcanic and interior processes (*5*). The rate and style of resurfacing have important implications for both interior evolution and climate change driven by volatile release from volcanic outgassing.

The Visible and Infrared Thermal Imaging Spectrometer (VIRTIS) on the European Space Agency's Venus Express spacecraft provided a map of thermal emission for much of the southern hemisphere of Venus' surface in the atmospheric window at 1.02 μm (*6*). Surface emissivities in the 1.02-μm band are retrieved from surface brightness by correcting for effects of instrumental stray light, viewing geometry, cloud opacity, and elevation (*7*, *8*). More accurate topographic data (*9*) allowed us to make significantly better maps of surface emissivity (*10*). Absolute surface emissivities are model-dependent (*11*) but are calculated from variations in the emitted fluxes that are up to 12% greater than the average value. These emissivity variations represent differences in material

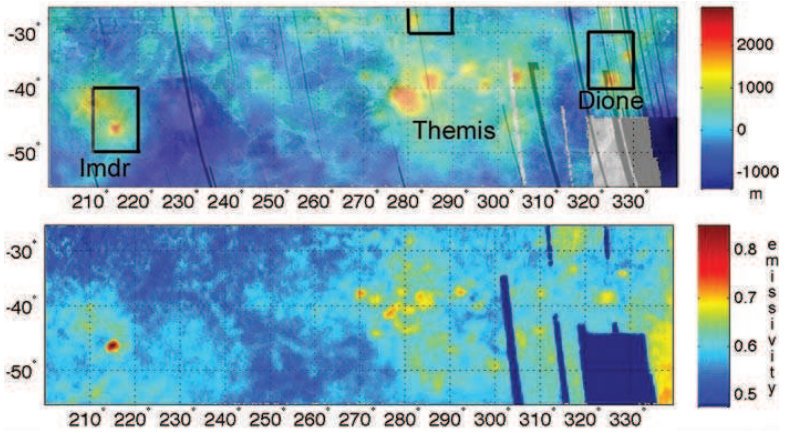

Fig. 1. (Top) Magellan synthetic aperture radar (SAR) image, left looking, overlain on topography. **(Bottom)** Surface emissivity derived from the VIRTIS spectrometer. Regio names are located below the topographic rises. Boxes indicate example sites shown in Fig. 2.

[1]Jet Propulsion Laboratory, Mail Stop 183-501, 4800 Oak Grove Drive, Pasadena, CA 91109, USA. [2]Proxemy Research, 20528 Farcroft Lane, Laytonsville, MD 20882, USA. [3]Institute for Planetology, Westfälische Wilhelms-Universität Münster, Wilhelm-Klemm-Strasse 10, 48149 Münster, Germany. [4]Lunar and Planetary Institute, 3600 Bay Area Boulevard, Houston, TX 77058, USA. [5]Massachusetts Institute of Technology, Earth, Atmospheric, and Planetary Sciences, Building 54-824, 77 Massachusetts Avenue, Cambridge, MA 02139, USA. [6]Institute of Planetary Research, German Aerospace Center, Rutherfordstrasse 2, D-12489 Berlin, Germany. [7]Istituto Nazionale di Astrofisica–Istituto di Astrofisica Spaziale e Fisica Cosmica (INAF-IASF), Via del Fosso del Cavaliere 100, 00133 Rome, Italy. [8]Laboratoire d'Etudes Spatiales et d'Instrumentation en Astrophysique (LESIA), Observatoire de Paris, CNRS, UPMC, Université Paris-Diderot, 5 Place Jules Janssen, 92195 Meudon, France.

*To whom correspondence should be addressed. E-mail: ssmrekar@jpl.nasa.gov

Supporting online material for

Conversion of Sugars to Lactic Acid Derivatives using Heterogeneous Zeotype Catalysts

Martin Spangsberg Holm,[1,2,3]† Shunmugavel Saravanamurugan,[1,2]† Esben Taarning[2,3]*

1) Centre for Catalysis and Sustainable Chemistry, Department of Chemistry, Technical University of Denmark, Anker Engelundsvej 1, 2800 Kgs. Lyngby, Denmark.

2) Center for Sustainable and Green Chemistry, Department of Chemistry, Technical University of Denmark, Anker Engelundsvej 1, 2800 Kgs. Lyngby, Denmark.

3) Haldor Topsøe A/S, Nymøllevej 55, 2800 Kgs. Lyngby, Denmark.

† These authors contributed equally.
*To whom correspondence should be addressed. E-mail: esta@topsoe.dk.

This PDF file includes:

Materials & methods

Catalyst preparation. The zeolite and zeotype catalysts were all synthesized from fluoride media according to known procedures with minor modifications. (*S1,S2,S3,S4*) Tetraethyl orthosilicate (TEOS) and tetraethylammonium hydroxide were mixed and stirred for approximately 90 minutes before the dissolved metal salt (tetraethyl orthotitanate and H_2O_2 in the case of Ti-Beta) was added. The gel was aged while stirring until all ethanol formed by

hydrolysis of TEOS had evaporated. HF was added drop-wise, resulting in a hardened gel, which was homogenized manually. The molar oxide ratio of the resulting gel was as follows: 0.008 MeO_2: 1 SiO_2: 0.27 $(TEA)_2O$: 0.54 HF: 11 H_2O. Dealuminated Beta seeds (~4 wt% compared to the theoretical zeolite amount) were suspended in demineralized water, sonicated and carefully dispersed in the gel (Ti-, Al- and Si-Beta were crystallized unseeded). The gel was transferred to a closed Teflon vessel in a stainless steel autoclave and crystallized at 140 °C with synthesis times varying between 10-20 days. One Sn-Beta zeotype catalyst (Si/Sn ratio of 125) was tumbled at 20 revolutions/minute while the other catalysts were synthesized under static conditions. After crystallization the autoclaves were allowed to cool to room temperature and the products were isolated by suction filtration. The products were carefully washed by two fold resuspension in demineralized water and dried at 110 °C overnight. The dried zeolites were finally calcined in static air at 550 °C for 6 hours using a ramp of 2 °C/min to remove carbonaceous residues. The Al-Beta zeolite was subsequently ion-exchanged into the ammonia form by three times suspending it in a 1.0 M NH_4NO_3 solution at 50 °C. The proton form of the zeolite was obtained by drying at 110 °C followed by calcination in static air at 550 °C.

Catalyst characterization. XRPD data were collected on a Bruker AXS powder diffractometer. N_2-sorption was measured on degassed samples using a Micromeritics ASAP 2020 apparatus. Surface areas and micropore volumes were calculated by applying the BET and t-plot methods, respectively. TPO analysis were performed by heating samples from rt to 700 °C over 4 hours in a flow of 5% oxygen in helium. The formed CO and CO_2 were quantified on a Rosemount Binos 100 apparatus. The metal incorporation was confirmed by FT-IR using cyclohexanone vapor adsorption with spectra recorded on a BioRad FTS 80 spectrometer equipped with an MCT detector. SEM micrographs were obtained on a Philips XL 30 ESEM-FEG instrument.

Carbohydrate conversion and product analysis. A 50 ml autoclave (Microclave reactor from Autoclave Engineers) was charged with carbohydrate (225 mg, 1.25 mmol fructose/glucose or 0.657 mmol sucrose), catalyst (160 mg), naphthalene (internal standard, 120 mg) and solvent (8.0 g) and then pressurised with argon (20 bar). The autoclave was heated to 160 °C and the stirring was started once the temperature reached 100 °C (300 rpm). After 20 hours of stirring, the autoclave was cooled and the reaction mixture analyzed. The undiluted reaction mixture was analyzed on a GC (Agilent 6890N instrument) equipped with an HP-5 capillary column (30.0 m x 320 μm x 0.25 μm) and an FID detector. The reaction mixture was also analyzed on an Agilent 1200 series HPLC (30 cm Aminex© HPX-87H column) with a RI detector using a 0.0050 M aqueous sulphuric acid solution as eluent. An Agilent 6850 GC system coupled with an Agilent 5975C mass detector was used for qualitative analysis. The yields of methyl, ethyl and *i*-propyl lactate and methyl vinylglycolate were calculated from the GC-data, based on the internal standard. All yields were calculated on a carbon-basis, *i.e.* four moles of methyl lactate or three moles of methyl vinylglycolate can be formed from one mole of sucrose. Carbohydrate conversions and lactic acid yield (in water) was determined by HPLC. Sucrose inverts to fructose and glucose on the acidic HPLC-column used, and the conversions were calculated from the monosaccharides fructose, glucose and mannose on a carbon-basis. HPLC standards were made from commercial samples. Yields of methyl-, ethyl- and *i*-propyl lactate, methyl vinylglycolate, formaldehyde dimethylacetal, glycolaldehyde dimethylacetal and methyl glycolate were obtained from GC analysis based on a calibration curve from commercial samples of the compounds. The two compounds ethyl- and *i*-propyl vinylglycolate are not commercially available and they were identified by GC-MS and yields were calculated by using calibration data of the *i*-propyl lactate and *n*-butyl lactate while assuming similar carbon response factors, respectively. Optical rotation

was measured on a product sample obtained by flash distillation of the reaction mixture; the sample containing a mixture of methyl lactate and methyl vinyl glycolate did not display optical rotation (589 nm, 20 ºC, Perkin Elmer-Precisely model 341 polarimeter).

Flow experiments. To illustrate the convenience of using a heterogeneous catalyst Sn-Beta was tested for fructose conversion in a fixed bed reactor. 3.0 g of Sn-Beta (Si:Sn 125) was fractionized (300-600 µm.) and loaded into a stainless steel reactor. Reaction conditions of 164 °C and a flow of 0.50 ml/min of a 5 wt.% fructose solution in methanol was chosen in order to give an initial conversion of approximately 50%. The effluent was collected continuously and analyzed as described above for the batch experiments.

Re-use study. Scaled-up experiments were performed to take catalyst loss during handling into account. After each experiment the catalyst was recovered and calcined at 480 °C for 6 hours in static air before it was reused in a new experiment that was scaled according to the amount of recovered catalyst. Scaling-up the experiments in the autoclave system was found to affect the sucrose conversions slightly when using Zr- and Ti-Beta. Lower sucrose conversions of approximately 80% instead of ~98% were obtained in these cases (Fig. 3) compared to the catalyst screening (Table 1). We believe that this results from small changes in the stirring efficiency when scaling up. In the sixth reuse cycle the scaling of the reactants, solvent and catalyst was similar to that used for the experiments in Table 1 which indicates that a modest loss of activity occurs as a function of reusing the catalyst while the selectivity remains constant (see Fig. S6).

List of Chemicals. All chemicals were used as purchased without further purification.

Sucrose (99.5%, Sigma-Aldrich), D-(-)-Fructose (99%, Sigma-Aldrich), D-(+)-Glucose (99.5%, Sigma-Aldrich), Naphtalene (>99%, Aldrich), D-(-)-Erythrose, (≥75%, Sigma), 2-Propanol

(99.5%, Sigma-Aldrich), Methanol (99.93%, Sigma-Aldrich), Ethanol (99.9 % vol., Kemetyl A/S), (D-L)-2-Hydroxy-3-butenoic acid methyl ester (96%, ABCR), L-(-)-Ethyl lactate (>99%, Fluka), L-(-)-Methyl lactate (98%, Aldrich), Methyl levulinate (≥98%, Aldrich), Levulinic acid (98%, Aldrich), *i*-propyl-L-lactate (≥97%, Sigma-Aldrich), L-(+)-Lactic acid (≥99%, Fluka), 5-(hydroxymethyl)furfural (>99%, Aldrich), TEOS (≥99%, Sigma-Aldrich), Tetraethylammonium hydroxide (40 wt.% in water, Aldrich), Hydrofluoric acid (40 wt.% in water, Fluka), Tetraethyl orthotitanate (97% the rest ~3% is tetraisopropyl orthotitanate, Fluka), Zirconium(IV) oxychloride octa hydrate (>99%, Fluka), Hydrogen peroxide (30 wt.% in water, Merck), Aluminium nitrate nona hydrate (>98%, Sigma-Aldrich), Aluminium chloride hexa hydrate (≥99%, Sigma), Tin(IV) chloride penta hydrate (98%, Sigma), Tin oxide nanopowder (Sigma-Aldrich).

Supporting Figures

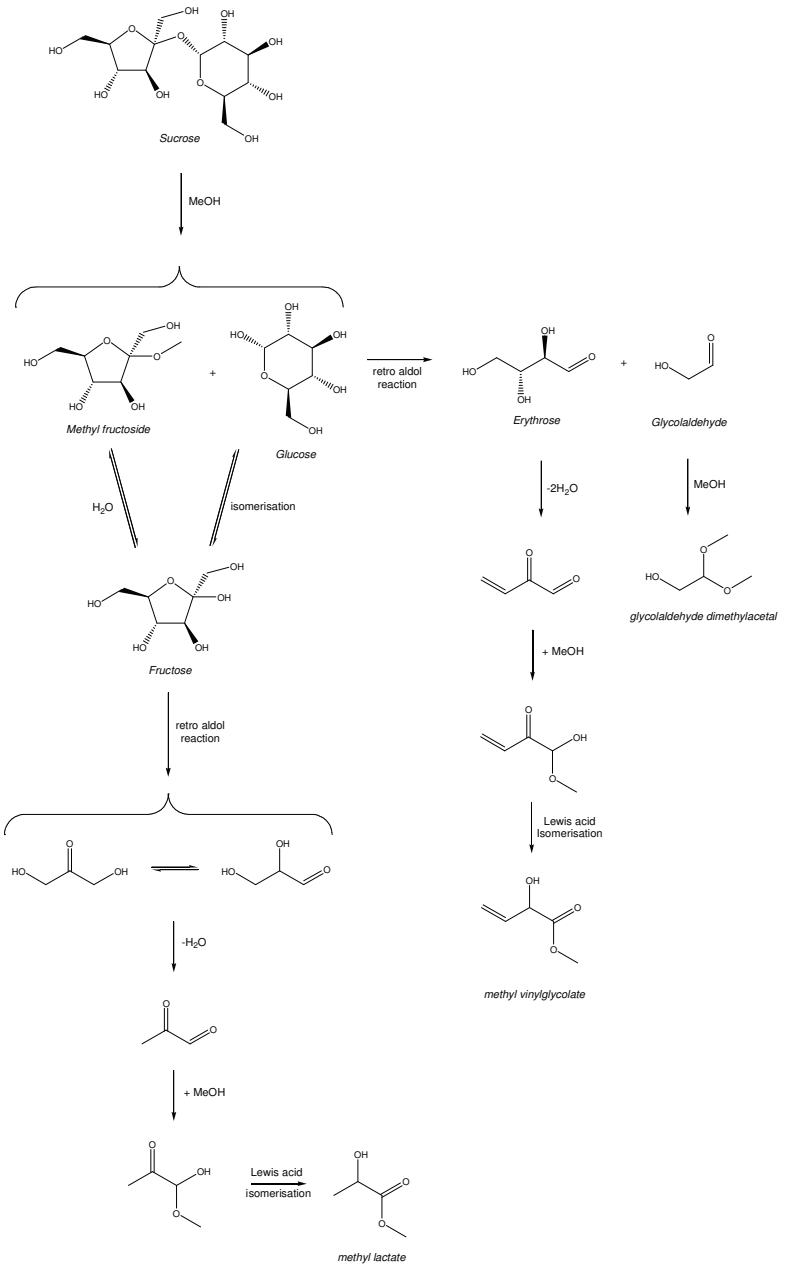

Figure S1. Proposed reaction pathway for the formation of different products from sucrose.

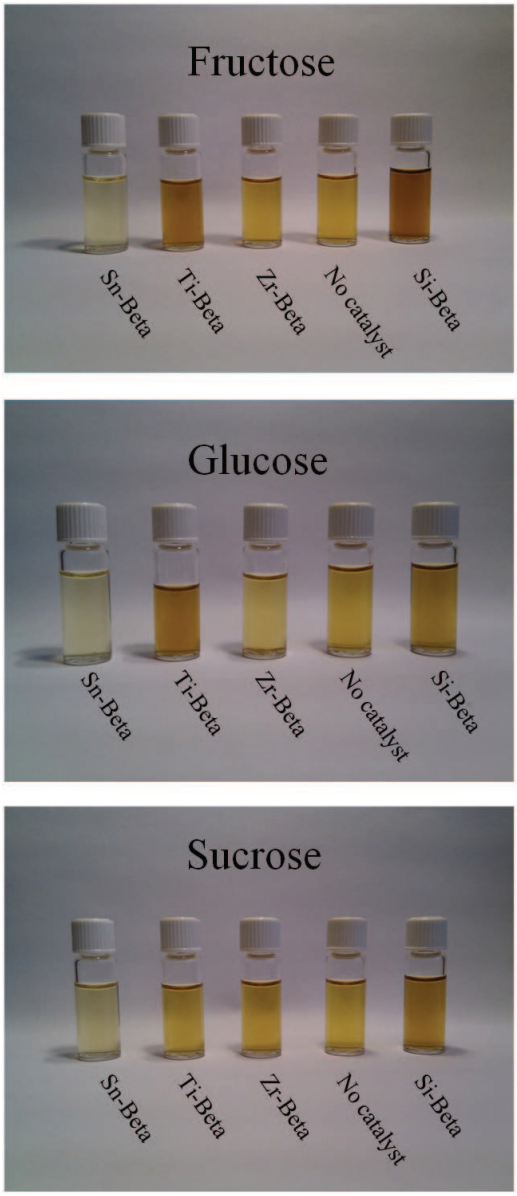

Figure S2. Photographs of the reaction liquids from the experiments in Table 1.

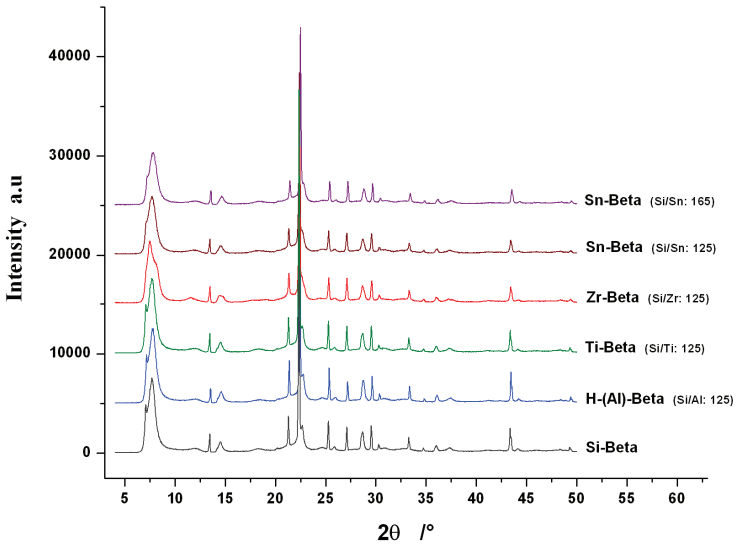

Figure S3. XRPD diffractograms of the calcined zeolite/zeotype catalysts. Individual samples have been moved in steps of 5000 for illustrative purposes.

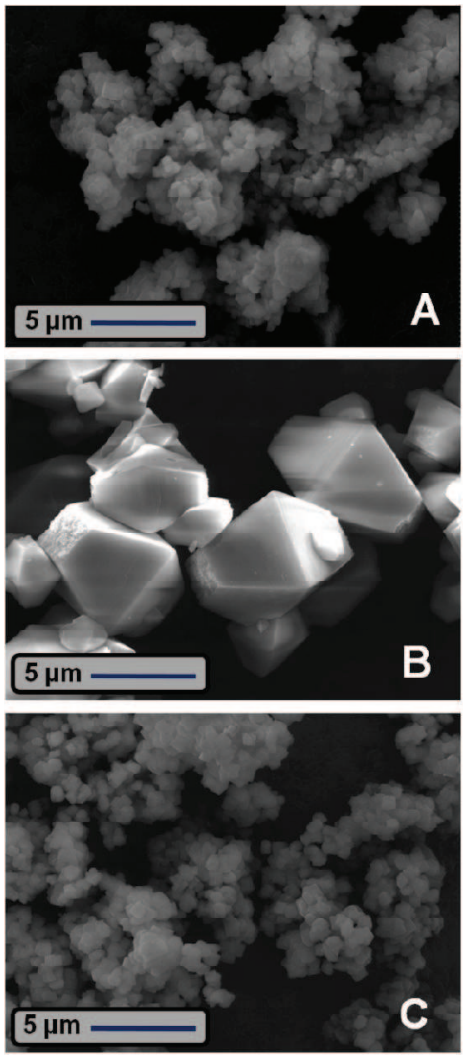

Figure S4. SEM micrographs of the zeotypes (a) Sn-Beta (Si/Sn:125), (b) Ti-Beta and (c) Zr-Beta.

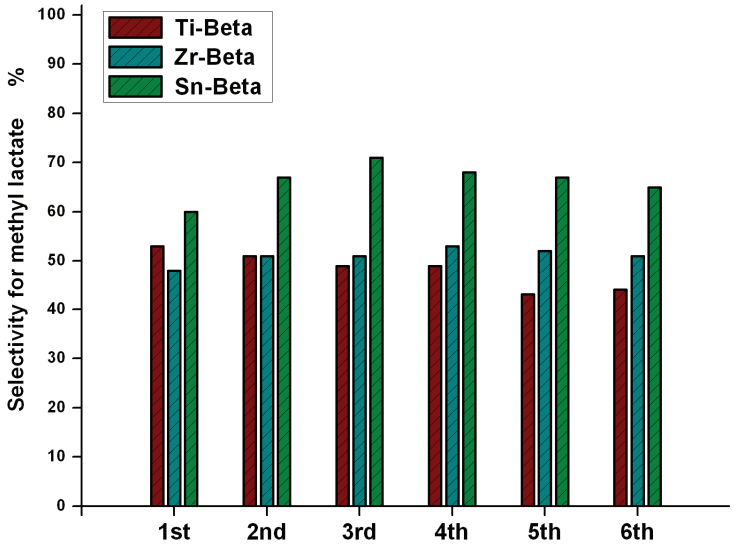

Figure S5. Methyl lactate selectivity during six reuses of the Ti-, Zr- and Sn-Beta catalysts.

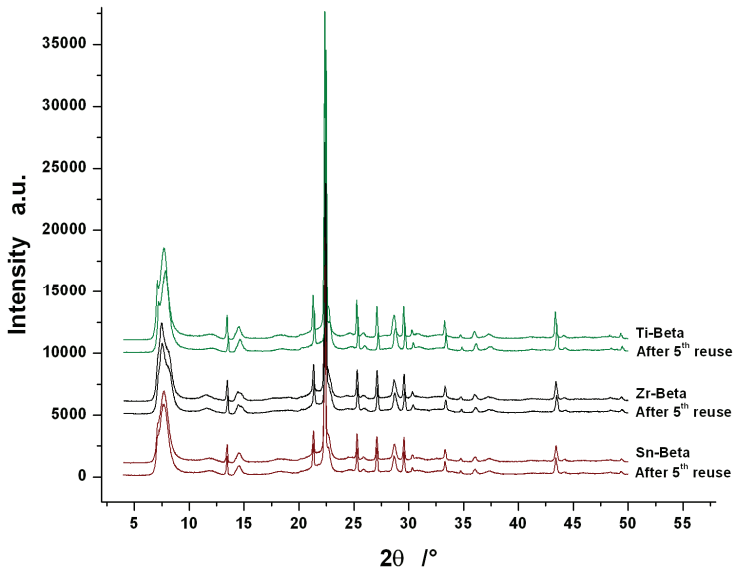

Figure S6. XRPD diffractograms of the Sn-Beta, Zr-Beta and Ti-Beta zeotypes before use (calcined) and after 5 reuses.

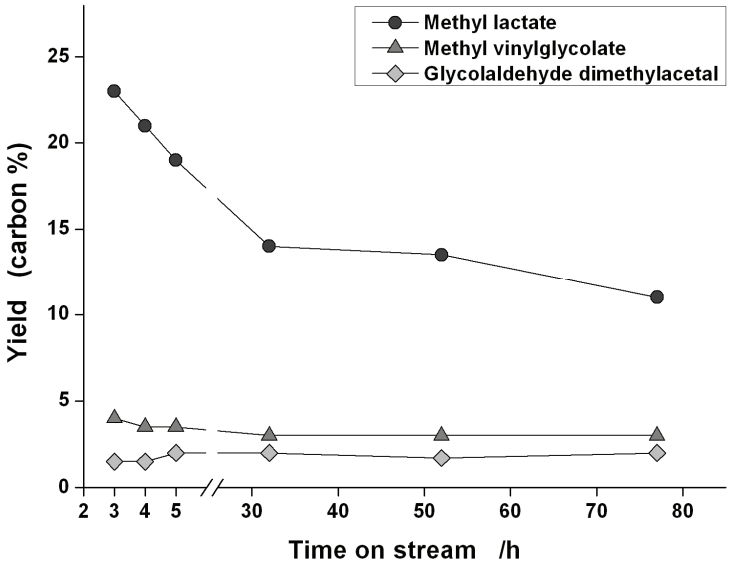

Figure S7. Yield of methyl lactate as a function of time on stream when fructose (5 wt.%) in methanol is converted over Sn-Beta (Si:Sn 125) operated in flow mode at 164 °C.

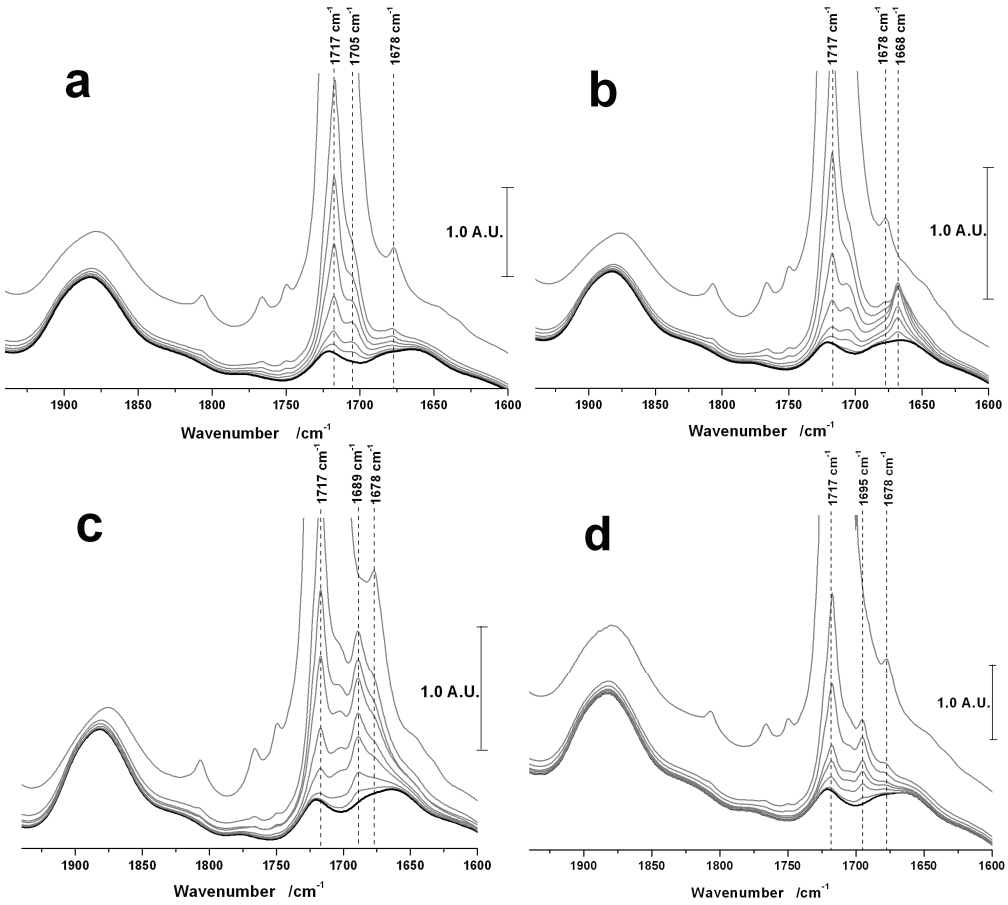

Figure S8. IR absorbance spectra of (a) Si-Beta, (b) Sn-Beta (Si/Sn: 125), (c) Zr-Beta and (d) Ti-Beta during step-wise adsorption of cyclohexanone. Shifts in the carbonyl frequency upon coordination are highlighted.

Supporting Tables

Table S1. Carbon distributions for the experiments in Table 1.

Product	Sn-Beta				Ti-Beta			Zr-Beta			Si-Beta			Al-Beta			No catalyst		
	Fru	Glu	Sucr	Eryth-rose	Fru	Glu	Sucr	Fru	Glu	Sucr	Fru	Glu	Sucr	Fru	Glu	Sucr	Fru	Glu	Sucr
Methyl lactate	44%	43%	68%	6%	36%	31%	44%	33%	33%	40%	9%	5%	6%	1%	<0.1%	<0.1%	8%	5%	6%
Methyl vinylglycolate	9%	10%	8%	56%	2%	4%	4.5%	5%	7%	4%	-	-	-	-	-	-	-	-	-
Formaldehyde dimethylacetal*	1%	1%	1%	1.5%	1%	0.5%	<0.2%	3%	2.5%	2%	<0.5%	0.5%	<0.5%	3%	1%	1.5%	1%	<0.5%	<0.5%
Glycolaldehyde dimethylacetal	0.5%	0.5%	<0.5	0.5%	3%	2.5%	2%	5%	5.5%	5%	0.5%	1.5%	1.5%	-	-	-	0.5%	2%	1%
Unconverted hexoses	<1%	<1%	<1%	<1%	<1%	1%	2%	<1%	1%	1%	21%	39%	37%	<1%	3%	1%	33%	47%	46%
Methyl pyranoside	-	-	-	-	-	-	-	-	-	-	-	-	-	2%	43%	27%	-	-	-
Methyl 2,3-dihydroxy-butanoate*	4%	3.5%	1.5%	16.5%	0.2%	-	0.2%	-	0.1%	-	0.5%	0.1%	-	-	-	-	-	-	-
HMF & furfural derivatives	3%	2.5%	1.5%	<0.2%	4%	3.5%	3%	4%	6%	4.5%	9%	4.5%	5%	7%	1%	1.5%	7%	5%	4.5%
Methyl levulinate	-	-	-	-	-	-	-	-	-	-	-	-	-	40%	5%	23%	-	-	-
Unidentified compounds†	22.5%	27.5%	12.5%	4.5%	6%	5.5%	4.5%	8%	8.5%	8%	16%	10%	11%	17%	6%	11.5%	11.5%	8.5%	8%
Coke	n.d.	n.d.	2.5%	n.d.	n.d.	n.d.	n.d.	n.d.	n.d.	n.d.	n.d.	n.d.	<0.5%	n.d.	n.d.	2.5%	-	-	-
Unaccounted	16%	12%	5%	15%	48%	52%	40%	42%	36.5%	35.5%	44%	39.5%	39.5%	30%	41%	32%	39%	32.5%	34.5%
Carbon balance	**84%**	**88%**	**95%**	**85%**	**52%**	**48%**	**60%**	**58%**	**63.5%**	**64.5%**	**56%**	**60.5%**	**60.5%**	**70%**	**59%**	**68%**	**61%**	**67.5%**	**65.5%**

*Identification is based on the MS fragmentation pattern of the component (*m/z*: *116* 2% [-H_2O]; *91* 6%; *90* 41% [-CH_3CHO or CH_2CHOH]; *89* 46% [-CH_3CHOH]; *87* 3%; *75* 3% [-CH_3O and CO]; *71* 3%; *60* 4%; *59* 26% [$CO(OCH_3)]^+$; *58* 4%; *57* 12%; *56* 4%; *55* 4%; *46* 2%; *45* 100% [$CH_3CHOH]^+$; *44* 4%; *43* 7%). Quantification is based on the FID response factors of methyl vinylglycolate.

† Unidentified compounds that are detectable by HPLC-RI. Quantification is based on the response factor for fructose in the case of highly polar compounds (short elution times) and methyl lactate for less polar compounds (long elution times).

Table S2. Yields of lactic acid/alkyl lactate and alkyl vinylglycolate using various solvents. Reaction conditions are the same as those reported in materials & methods. More than 99% conversion reached in all experiments with Sn-Beta. Tin content in the zeolite used was Si/Sn: 165 (as synthesised, 1.2 wt% of tin).

	Catalyst	Substrate	Lactic acid / alkyl lactate	Alkyl vinyl-glycolate
Water	Sn-Beta	Glucose	26%	n.d.
	Sn-Beta	Fructose	27%	n.d.
	Sn-Beta	Sucrose	28%	n.d.
	No catalyst	Sucrose	1%	n.d.
Methanol	Sn-Beta	Glucose	43%	10%
	Sn-Beta	Fructose	44%	9%
	Sn-Beta	Sucrose	68%	8%
	No catalyst	Sucrose	6%	0%
	Sn-Beta*	Sucrose	62%	11%
	Sn-Beta†	Sucrose	68%	6%
	Sn-Beta‡	Erythrose	6%	56%
Ethanol	Sn-Beta	Glucose	32%	10%
	Sn-Beta	Fructose	35%	10%
	Sn-Beta	Sucrose	39%	8%
	No catalyst	Sucrose	1%	0%
***i*-Propanol**	Sn-Beta	Glucose	18%	8%
	Sn-Beta	Fructose	21%	9%
	Sn-Beta	Sucrose	25%	8%
	No catalyst	Sucrose	3%	0%

*4 times the amount of substrate used.

† Solvent used was 2.5 wt.% H_2O in methanol.

‡ 237 mg erythrose is used as substrate (equivalent carbon amount as is present in 225 mg of sucrose).

Table S3. Porosity and TPO data of the fresh and used zeolite/zeotype catalysts.

Zeolites	Si/Me	Reaction solvent	Surface area (m^2/g)	t-plot (ml/g)	Carbon wt% (from TPO)
Sn-Beta	125		511	0.201	
After 1st use†	-	Methanol	500	0.195	-
After 5th reuse†	-	Methanol	504	0.197	-
Zr-Beta	125		506	0.202	
After 1st use*	-	Methanol	505	0.203	-
After 5th reuse†	-	Methanol	500	0.202	-
Ti-beta	125		492	0.203	
After 1st use*	-	Methanol	491	0.203	-
After 5th reuse†	-	Methanol	490	0.203	-
H-(Al)-Beta	125		501	0.207	
After 1st use*	-	Methanol	494	0.205	1.5%
Si-Beta	∞		487	0.203	
After 1st use*	-	Methanol	486	0.200	<0.1%
Sn-Beta	165		513	0.205	
After 1st use*	-	Water	496	0.192	7.0%
After 1st use*	-	Methanol	499	0.201	1.3%
After 1st use†	-	Ethanol	482	0.196	-
After 1st use*	-	2-Propanol	494	0.195	-

Used catalysts were calcined at 480 °C in static air (ramp of 2 °C/min) for 6 hours before analyzed for porosity.
*Fructose used as substrate
†Sucrose used as substrate

Table S4. Conversion, selectivity and yield for methyl lactate from the 6-fold reuse.

Zeolites	Conversion*	Selectivity to methyl lactate	Yield of methyl lactate	Yield of methyl vinylglycolate
Sn-Beta				
1st use	>99 %	60 %	60 %	4 %
2nd use	>99 %	67 %	67 %	3 %
3rd use	>99 %	71 %	71 %	5 %
4th use	>99 %	68 %	68 %	5 %
5th use	>99 %	67 %	67 %	4 %
6th use	>99 %	65 %	65 %	7 %
Zr-Beta				
1st use	67 %	48 %	32 %	4 %
2nd use	75 %	51 %	38 %	4 %
3rd use	72 %	51 %	37 %	3 %
4th use	76 %	53 %	40 %	4 %
5th use	73 %	52 %	38 %	3 %
6th use	84 %	51 %	43 %	4 %
Ti-Beta				
1st use	88 %	53 %	47 %	6 %
2nd use	82 %	51 %	42 %	6 %
3rd use	78 %	49 %	38 %	4 %
4th use	78 %	49 %	38 %	3 %
5th use	86 %	43 %	37 %	3 %
6th use	86 %	44 %	38 %	3 %

Experiments were performed according to materials & methods. The amount of methanol and sucrose was scaled according to the recovered amount of catalyst.
*Conversion calculated based on unconverted hexoses.

Table S5. Calculations of the mean value and standard deviation for key experiments using sucrose as the substrate.

Catalyst	Yield of methyl lactate (%)					Mean Value (%)	Standard deviation (%)
	1	2	3	4	5		
Sn-Beta_125	62.5	66.4	65.3	66.6	60.6	64.3	2.6
Sn-Beta_165	67.1	68.1	73.1	65.1	68.6	68.4	2.9
Zr-Beta_125	38.3	39.1	37.7	43.4	41.0	39.9	2.3
Ti-Beta_125	39.4	44.9	44.6	46.0	45.3	44.0	2.6

Table S6. Calculations of the mean value and standard deviation for key experiments using sucrose as the substrate.

Catalyst	Yield of methyl vinylglycolate (%)					Mean Value (%)	Standard deviation (%)
	1	2	3	4	5		
Sn-Beta_165	8.4	7.7	7.1	8.5	7.6	7.9	0.6

Supporting References

S1. T. Blasco *et al., Chem. Commun*. 2367-2368 (1996).

S2. M. Renz *et al., Chem. Eur. J*. **8**, 4708-4717 (2002).

S3. S. Valencia, A. Corma, in United States patent 5968473, (1998).

S4. Y. Zhu, G. Chuah, S. Jaenicke, *J. Catal*. **227**, 1-10 (2004).

3.0 Discussion and future perspectives

3.1 Desilication

The work performed within desilication (part 1) was done in the first part of my PhD project. Interestingly, our findings using organic bases as the desilication agent were later expanded on by others. The pore forming abilities of the organic base could, be generalized to other quartenary bases and was useful on an additional zeolite structure (MFI).[1,2] The fact that quartenary ammonium bases are able to produce mesoporosity is indeed interesting. Meanwhile, it is important to evaluate whether they have potential for large-scale application. Speaking against - these chemicals are significantly more expensive than sodium hydroxide and can even pose health problems. But the possibility of circumventing the ion-exchange step represents a simplification of the overall process with an associated cost reduction. However, additional information about zeolite loss during desilication, processing time, effectiveness of the organic desilication, equipment requirements etc. would be needed to make a fair estimate. Reuse of the desilication medium could potentially reduce waste of the expensive base. An alternative strategy would be to use weaker but much cheaper bases. The limitations of desilication with respect to base strength and accessibility of the base to the zeolite interior has not been fully clarified. This could likely be done with bases such as alkyl amines, guanidine, imidazole, bipyridine or 1,8-bisdimethylamino naphthalene (proton sponge).

A very interesting characterization study using alkyl pyridine in combination with FT-IR on desilicated samples was published recently. [3] The findings are in line with what we observe in section 2.3 in that EFAL is formed predominantly located on the external surface or in the newly formed mesopores. The authors further introduce the accessibility index (ACI). The ACI is a generalized concept which is convenient to analytically describe the porosity of a zeolite sample. ACI measures the fraction of acidic sites accessible to substrates of increasing sizes. A thorough description of the accessibility index is given in the review in section 2.5.

3.2 Bio-gasoline production

Part 2 describes our work on the conversion of oxygenates over ZSM-5. The results confirmed that it is indeed possible to form hydrocarbons from most oxygenates at typical laboratory scale MTG reaction conditions (370 °C, WHSV: ~8, He: 40 ml/min, ZSM-5). However, the parameter space for the optimal conversion of each individual additive becomes considerable when one considers the level of methanol dilution, reaction temperature, potential cross reactions, choice of catalyst etc. Nonetheless, the lifetime of the catalyst decreases significantly in almost all cases when reacting a 10 wt.% additive solution compared to pure methanol. We considered this a rather surprising result since 10 wt.% represents a relatively modest additive level. This indicates that the poor performance of bio-oil could be explained by a general problematic conversion of non-methanol oxygenates. Arguably, the methanol conversion could be viewed as exceptionally good, rather than other oxygenates being disastrous. The amount of coke deposited on the catalyst at full deactivation in a methanol experiment corresponds to only about every 2000^{th} carbon atom converted or a hydrocarbon selectivity of ≥99.9.

The differences in lifetime ranging from catastrophic to moderate could thus be an acceptable starting point for oxygenate conversion.

There were exceptions to the general trend that catalyst lifetime dramatically decreased when co-feeding oxygenates. The conversions of 10 wt.% toluene or *i*-propanol were two examples. These compounds (propene in the case of *i*-propanol) are products normally formed in the MTG reaction and appeared to have little or even a positive effect on the lifetime. This observation is quite reasonable. If pronounced deactivation was taking place during the secondary reactions in MTG a strong dependence of catalyst loading (WHSV) on conversion capacity ($g_{converted\ methanol}/g_{zeolite}$) would be seen, which is not the case. Interestingly, toluene has a critically low effective H/C ratio of 1.14. The compatibility of toluene shows that it is not specifically the low H/C ratio of an additive that is the limitation but rather 'poor' selectivity of the additives towards the formation of inert compounds.
Non-MTG products such as tetrahydrofuran, acetaldehyde, and dienes (depending on the additive) were detectable by GC-MS after methanol/DME breakthrough in the 10 wt.% series. Compounds like these are never formed in significant quantities in MTG. It appears that these "alien" compounds initially forms from the additive before they preferentially end up in the aromatics. In order to understand the reactivity and pronounced deactivation of the various oxygenates; knowledge about the favored reaction paths for each intermediate would be required. This would be unrealistic to do so generalizations within the relevant classes of compounds could be a reasonable starting point.

An increased conversion capacity of the additives is seen as a function of optimal methanol dilution. This observation indicates a selectivity change of the additive (decreased tendency towards coke formation). Methanol dilution increases the total effective H/C ratio of the feed. However, the combined H/C ratio of the feed is something very different than the H/C ratio of the individual additive. Similar reactivity from a dilute compound with low H/C and a more concentrated high H/C compound can only be expected if cross-reaction between methanol and the additive is in fact taking place. Methanol/DME is only present in the primary reaction zone of the catalyst bed. Thus, it is important to note if the decreased selectivity towards coking of the additive is due to cross-reactions associated with secondary reactions further down the bed or whether methanol/DME is required to alkylate the oxygenate intermediates (dienes, cyclo compounds, ethers etc.). If alkenes and/or aromatics are responsible for the improvement; then a fraction of the product could simply be recycled to obtain the improved conversion capacity. However, if the presence of methanol/DME is key, we could be registering only a fraction of the positive effect since it would depend on how large a fraction of the additive that is converted simultaneously with methanol/DME. In order to investigate this further; reaction conditions designed to give incomplete methanol conversion could be investigated. Another possibility could be to compare results obtained from a back-mixing reactor with those from plug flow.

We chose to react the additives as 10 wt.% solutions in methanol. The conversion of methyl lactate is an illustrative example of the reactivity and the difficulty in choosing comparable reaction conditions. Upon contact with the catalyst methyl lactate breaks down into acetaldehyde, CO and methanol/DME. A valid interpretation is that that only the acetaldehyde fraction of the additive is in fact the "real" reactant. Converting 10 wt.% acetaldehyde in methanol gives a conversion capacity well below half of that of methyl lactate but this experiment was performed with a higher acetaldehyde concentration in the feed. Acrylic acid ("dehydrated methyl lactate") is slightly more concentrated due to the lower molecular weight but performs catalytically very poor. The large difference between methyl lactate and acrylic acid, despite the same effective H/C ratio, illustrates that the H/C ratio can function as a guideline; but also reveals its limitations in accounting for the chemistry observed. When designing the experiments; we considered how additives could most elegantly be compared and in the end chose

wt.% as the standard. The additives could alternatively have been introduced based on concentration ($mol_{additive}/h$), an equal amount of carbon (mol_{carbon}/h) or calculating an equal carbon concentration while subtracting carbon dissociated as CO/CO_2. The question is: Can carbon from the additive ending up in CO be considered "converted"? This choice depends on whether emphasis is put on catalyst lifetime or strictly on the amount of carbon incorporated into the hydrocarbon products. By comparing additives based on wt.% we focused on catalyst lifetime and it appears reasonable to consider CO a product since it can be utilized further. The effect of minor differences in methanol dilution due to the fact that the additives have different molecular weights is small. Results from section 2.8 (Figure 2.3) showed it was fair to assume that a molecule performing well will continue to do so in a slightly more concentrated or dilute solution.

A peculiar coincidence connected the results from bio-gasoline production in part 2 to part 3 where methyl lactate was synthesized from sugar. Methyl lactate was not an obvious candidate to co-feed in MTG since the unit price of the *pure* compound is significantly higher than gasoline. Lactic acid has the same oxidation state (identical effective H/C ratio) as sugar. A carbohydrate is perhaps the worst type of compound to co-feed in MTG [4,5,6] whereas methyl lactate proved to be a relatively well suited additive when taking the low effective H/C ratio into account. Very recently, R. F. Lobo pointed out how lactic acid (methyl lactate) synthesis from sugar could be viewed as an intramolecular redistribution of oxidation states.[7] Our results in part 2 show exactly that - a redistribution of oxidation states (which functionalities are present where) was the key to tuning reactivity. In all cases the acid/ester functionality favored dissociation of CO (and to a smaller extend CO_2). This occurs to much lower extents from alcohol and carbonyl functionalities. CO can be used to produce H_2 through the water-gas-shift reaction. Then hydrogen could be used to partially hydrogenate either the product mixture or the feed to improve the final energy content (and perhaps lifetime). Interestingly, an improved hydrocarbon yield was recently reported in a study that performed a partial hydrogenation of bio-oil prior to zeolite deoxygenation.[8] This observation is in line with our findings in section 2.8.

Nevertheless, no solution is presented to solve the pronounced deactivation seen when converting phenolic species. Extensive (and selective) hydrogenation can form compounds like cyclohexanol which likely relieves catalyst deactivation but require numerous equivalents of hydrogen. The hydrogen needed could be obtained by reforming a fraction of the biomass. When considering the required amounts of H_2 integration with other renewable energy sources could perhaps be advantageous. A surplus of electricity typically exists outside peak hours. If this energy was used through electrolysis for hydrogenation of bio-oil the extent could depend on the availability of cheap electricity and thus serve as flexible energy storage. Yet another solution would be to separate cellulose and hemi-cellulose from lignin before bio-oil formation. However, the advantage of an easy on-site treatment of the lignocellulosic material would then be (at least partially) lost.[9]

3.3 Synthesis of lactic acid derivatives

The production of lactic acid is today done by fermentation of glucose using lactic acid producing bacteria, but can also be made by fungal species.[10,11] Lactic acid is produced on a relatively large scale (~300.000 t/yr) in a process which has strengths as well as limitations. The fermentation is very selective (~95% selectivity) but the bacteria are highly pH sensitive and the culture supresses lactic acid production at elevated concentrations (product inhibition). Neutralization by calcium hydroxide or carbonate is thus continuously required. Purification of lactic acid from a dilute aqueous medium is challenging. One method is isolating precipitated calcium lactate with a subsequent release of the acid by addition of sulfuric acid. Lactic acid is not volatile and the acid needs to be esterified for

purification by distillation.[12,13] The cost of purification can be as high as 50% of the total production cost while large amounts of lime, equal in weight as the desired lactic acid, are an unfortunate byproduct. Importantly, the purification procedure in a heterogeneously catalyzed reaction where methyl lactate is formed from sugar in methanol would be fundamentally different. Notable differences include the direct formation of volatile methyl lactate and not lactic acid, the solvent is methanol instead of water and the reaction is performed at elevated vs. physiological temperature.

Lactic acid contains a stereo center and fermentation of glucose selectively produces one stereo isomer, whereas the heterogeneously catalyzed route produces a racemic mixture. The prices of these two products (mixtures) are not identical and the optical purity obtained from the biological process is a significant advantage. Polymerization of optically pure or racemic lactic acid into PLA creates polymers with distinctly different properties (e.g. higher melting point).[14] However, as presented in Figure 1.2 (section 1.1) some upgrading routes include elimination of the stereo center and are thus indifferent to the optical purity of the starting material. Furthermore, the use of methyl lactate as a green solvent does not require stereochemically pure lactate. However, it is clear that an alternative route to lactic acid would need to be considerable cheaper than fermentation or have other inherent advantages in substrate utilization, process robustness, higher productivity, decreased investment cost, shut down potential or a good inhibitor resistance to be a realistic competitor to the established lactic acid production.

[1] S. Abello, A. Bonilla, J. Perez-Ramirez, *Appl. Catal. A*, 364, (**2009**), 191-198.

[2] J. Perez-Ramirez, D. Verboekend, A. Bonilla, S. Abello, *Adv. Funct. Mater*., 19, (**2009**), 1-8.

[3] F. Thibault-Starzyk, I. Stan, S. Abello, A. Bonilla, K. Thomas, C. Fernandez, J-P. Gilson, J. Perez-Ramirez, *J. Catal*., 254, (**2009**), 11-14.

[4] N. Y. Chen, T. F. Degnan Jr., L. R. Koenig, *Chemtech*, 16, (**1986**), 506-511.

[5] L. H. Dao, M. Haniff, A. Houle, D. Lamothe, *Prepr. Papr. Am. Chem. Soc. Div. Fuel Chem.*, 32, (**1987**), 308-316.

[6] C. D. Chang, A. J. Silvestri, *J. Catal*., 47, (**1977**), 249-259.

[7] R. F. Lobo, *ChemSusChem*, 3, (**2010**), 1237-1240.

[8] T. P. Vispute, H. Zhang, A. Sanna, R. Xiao, G. W. Huber, *Science*, 330, (**2010**), 1222-1227.

[9] M. G. Adsul, M. S. Singhvi, S. A. Gaikaiwari, D. V. Gokhale, *Bioresource Technol.*, 102, (**2011**), 4304-4312.

[10] E. T. H. Vink, K. R. Rabago, D. A. Glassner, P. R. Gruber, *Polymer Degrad. Stabil.*, 80, (**2003**), 403-419.

[11] Z. Y. Zhang, B. Jin, J. M. Kelly, *Biochem. Eng. J.*, 35, (**2007**), 251-263.

[12] K. L. Wasewar, A. A. Yawalkar, J. A. Moulijn, V. G. Pangarkar, *Ind. Eng. Chem. Res*., 43, (**2004**), 5969-5982.

[13] H. Danner, R. Braun, *Chem. Soc. Rev*., 28, (**1999**), 395-405.

[14] J. Lunt, *Polymer Degrad. Stabil.*, 59, (**1998**), 145-152.

4.0 Appendix

4.1 Publications and patent

Publications relevant for the thesis

M. S. Holm, K. Egeblad, P. N. R. Vennestrøm, C. G. Hartmann, M. Kustova, C. H. Christensen, Enhanching the Porosity of Mesoporous Carbon-Templated ZSM-5 by Desilication, *Eur. J. Inorg. Chem.*, (**2008**), 5185-5185-5189.

M. S. Holm, S. Svelle, F. Joensen, P. Beato, C. H. Christensen, S. Bordiga, M. Bjørgen, Assessing the acid properties of desilicated ZSM-5 by FTIR using CO and 2,4,6-trimethylpyridine (collidine) as molecular probes, *Appl. Catal. A*, (**2009**), 256, 23-30.

M. S. Holm, M. K. Hansen, C. H. Christensen, "One-Pot" Ion-Exchange and Mesopore Formation During Desilication, *Eur. J. Inorg. Chem.*, (**2009**), 1194-1198.

U. V. Mentzel, S. Shunmugavel, S. L. Hruby, C. H. Christensen, **M. S. Holm**, High Yield of Liquid Olefins Obtained by Converting *i*-Propanol over Zeolite H-ZSM-5, *J. Am. Chem. Soc.*, (**2009**), 131, 17009-17013.

E. Taarning, S. Shunmugavel, **M. S. Holm**, J. Xiong, R. M. West, C. H. Christensen, Zeolite-Catalyzed Isomerization of Triose Sugars, *ChemSusChem*, (**2009**), 2, 625-627.

R. M. West, **M. S. Holm**, S. Shunmugavel, J. Xiong, Z. Beversdorf, E. Taarning, C. H. Christensen, Zeolite H-USY for the production of lactic acid and methyl lactate from C_3-sugars, *J. Catal.*, (**2010**), 269, 122-130.

M. S. Holm, S. Shunmugavel, E. Taarning, Conversion of Sugars to Lactic Acid Derivatives Using Heterogeneous Zeotype Catalysts, *Science*, (**2010**), 328, 602-605.

U. V. Mentzel, **M. S. Holm**, Utilization of Biomass: Conversion of Model Compounds to Hydrocarbons over Zeolite H-ZSM-5, *Appl. Catal. A*, (**2011**), accepted, doi: 10.1016/j.apcata.2011.01.040.

Review

M. S. Holm, E. Taarning, K. Egeblad, C. H. Christensen, Catalysis with Hierarchical Zeolites, *Top. Catal*., (**2011**), accepted, doi: 10.1016/j.cattod.2011.01.007.

Patent

E. Taarning, S. Shunmugavel, **M. S. Holm**, Zeolite-catalyzed preparation of alpha-hydroxy carboxylic acid compounds and esters thereof, (**2010**), US 20100121096.

Other publications

K. T. Leth, A. K. Rovik, **M. S. Holm**, M. Brorson, H. J. Jakobsen, J. Skibsted, C. H. Christensen, Synthesis and characterization of conventional and mesoporous Ga-MFI for ethane dehydrogenation, *Appl. Catal. A*, (**2008**), 348, 257-265.

M. Kustova, **M. S. Holm**, C. H. Christensen, Y.-H. Pan, P. Beato, T. V.W. Janssens, F. Joensen, J. Nerlov, Synthesis and characterization of mesoporous ZSM-5 core-shell particles for improved catalytic properties, *Stud. Surf. Sci, Catal.*, (**2008**), 174, 117-122.

4.2 Conference contributions

Sep. 2008	Oral and poster presentation at 2nd EuCheMS Chemistry Congress, Turin, Italy.
Jun. 2009	Poster presentation at inGAP-NanoCat Summerschool, Trondheim, Norway.
Aug. 2009	Poster presentation at EuropaCat-IX, Salamanca, Spain.
Aug. 2010	Oral presentation at Nordic Symposium on Catalysis, Denmark.
2007 - 2010	Oral presentations internally at Haldor Topsoe A/S, Denmark.

4.3 Authorship declarations

Section 2.2 Enhancing the Porosity of Mesoporous Carbon-Templated ZSM-5 by Desilication

Martin S. Holm has made the experiments used in Figure 1-3. He has made the Table and Figures and co-authored the manuscript.

Section 2.3 Assessing the acid properties of desilicated ZSM-5 by FTIR using CO and 2,4,6-trimethylpyridine (collidine) as molecular probes

Martin S. Holm has performed the IR experiments used in Figure 1-5 and he has produced scheme 1.

Section 2.4 "One-Pot" Ion-Exchange and Mesopore Formation During Desilication

Martin S. Holm has made the experiments used in Figure 1-6 in equal collaboration with Martin Kalhmar Hansen. Martin S. Holm has made the Table and Figures and co-authored the manuscript.

Section 2.5 Catalysis with Hierarchical Zeolites

Martin S. Holm has written the section describing alkylation reactions. He has worked with combining the individual contributions and the shaping of the discussion/conclusion part.

Section 2.7 High Yield of Liquid Range Olefins Obtained by Converting i-Propanol over Zeolite H-ZSM-5

Martin S. Holm has made the experiments used in Table 1-2 and Figure 1-4 in equal colaboration with Uffe Vie Mentzel. Martin has been closely involved in preparing the Figures and Tables and has co-authored the manuscript.

Section 2.8 Utilization of Biomass: Conversion of Model Compounds to Hydrocarbons over Zeolite H-ZSM-5

Martin S. Holm has made the experiments used in Table 1-2 and Figure 1-6 in equal colaboration with Uffe Vie Mentzel. Martin has been closely involved in preparing the Figures and Tables and has co-authored the manuscript.

Section 2.10 Zeolite H-USY for the production of lactic acid and methyl lactate from C3-sugars

Martin S. Holm has performed the characterization of the samples e.i. data presented in Figure 3 and Table 4. Martin has co-authored the manuscript.

Section 2.11 Zeolite-Catalyzed Isomerization of Triose Sugars

Martin S. Holm has synthesized, post treated and characterized the samples used (Table 1 and Figure s1-s5). Martin has co-authored the manuscript.

Section 2.12 Conversion of Sugars to Lactic Acid Derivatives Using Heterogeneous Zeotype Catalysts

Martin S. Holm has synthesized and characterized the samples used. Martin has in collaboration with Shunmugavel Saravanamurugan performed the catalytic testing of the materials. Martin has been involved in making the Figures and Tables and has co-authored the manuscript.

4.4 Supporting NMR data

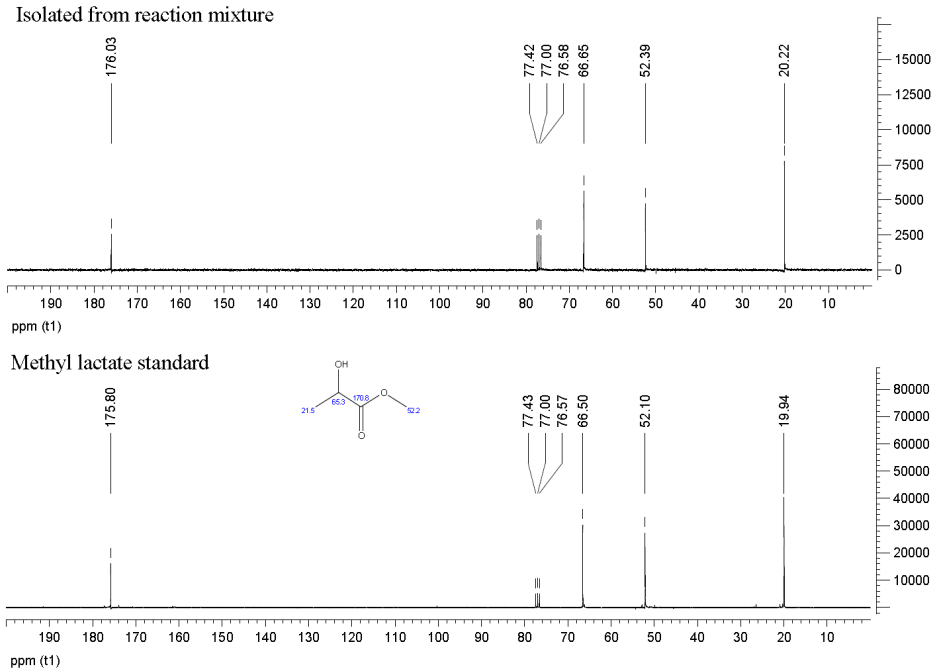

Figure 4.1. Identification of methyl lactate by NMR. Carbon spectrum of methyl lactate isolated from the reaction mixture and a commercial reference sample.

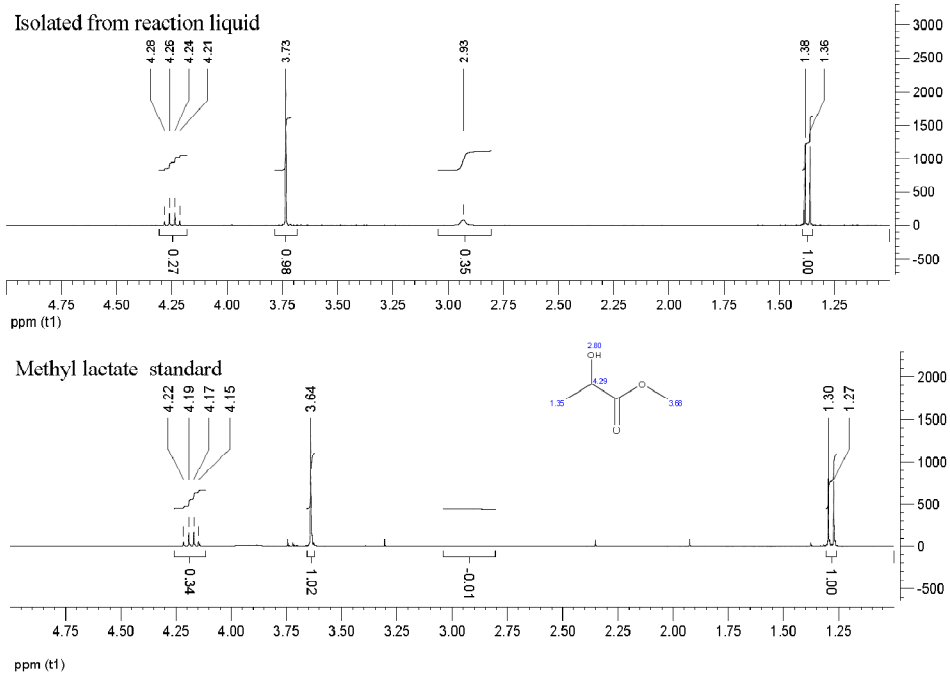

Figure 4.2. Identification of methyl lactate by NMR. Proton spectrum of methyl lactate isolated from the reaction mixture and a commercial reference sample.

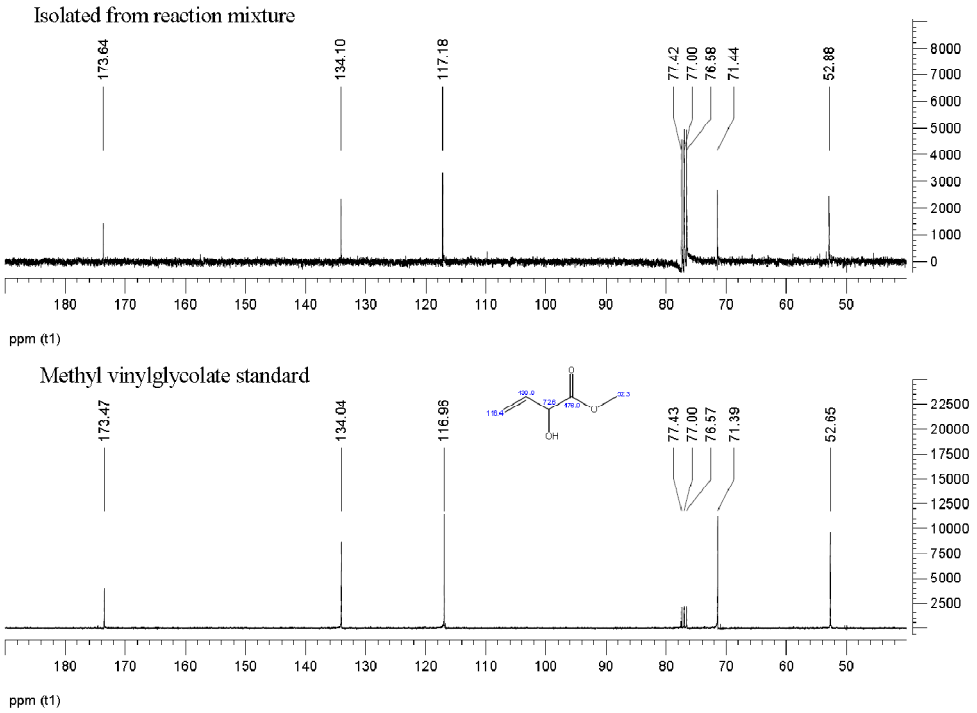

Figure 4.3. Identification of methyl vinyl glycolate by NMR. Carbon spectrum of methyl vinyl glycolate isolated from the reaction mixture and a commercial reference sample.

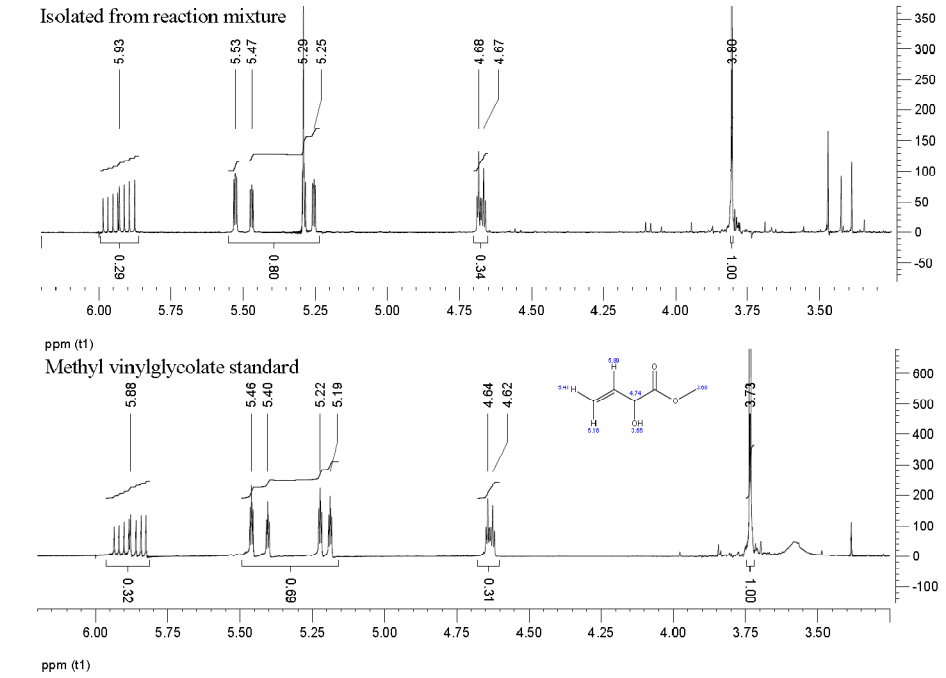

Figure 4.4. Identification of methyl vinyl glycolate by NMR. Proton spectrum of methyl vinyl glycolate isolated from the reaction mixture and a commercial reference sample.

4.5 Supporting FT-IR data

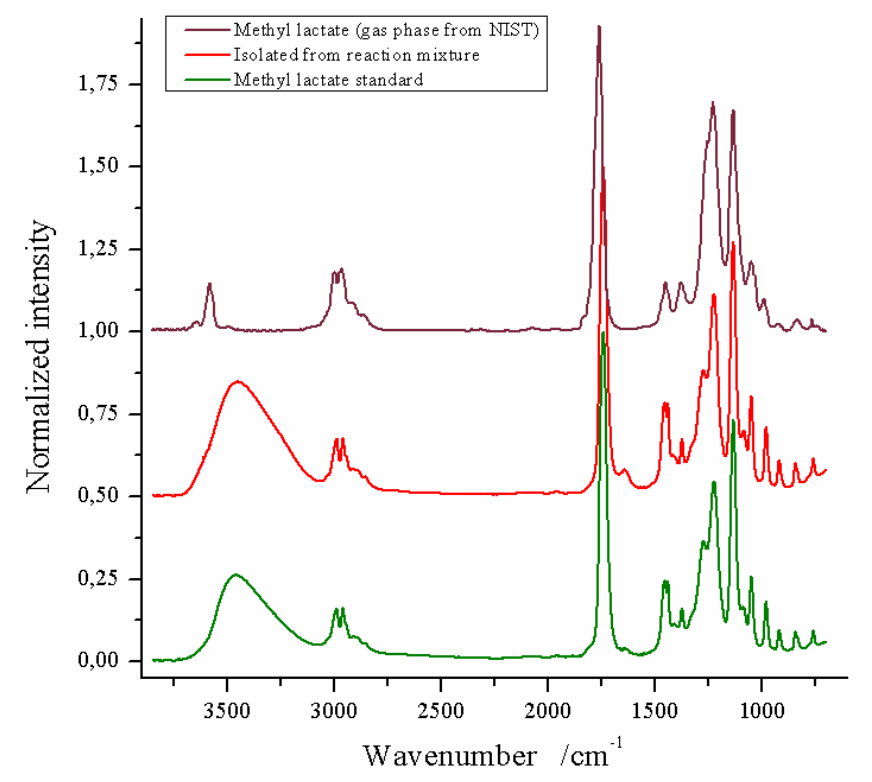

Figure 4.5. Liquid phase FT-IR spectra of methyl lactate isolated from the reaction mixture and a commercial reference sample. Gas phase spectrum downloaded from NIST (http://webbook.nist.gov/chemistry/) is included from comparison. The spectra are offset by 0,5 for illustrative reasons.